



The
University
Of
Sheffield.

**The control of stomatal properties in rice (*Oryza sativa* L.)
and their influence on photosynthetic performance**

By:

MUHAMMAD NAZMIN YAAPAR

A thesis submitted in partial fulfilment of the requirements
for the degree of Doctor of Philosophy

The University of Sheffield
Faculty of Science
Department of Animal and Plant Sciences

July 2017

ABSTRACT

The control of stomatal properties in rice (*Oryza sativa* L.) and their influence on photosynthetic performance

M.N. Yaapar

The earliest stages of leaf development in rice occur without direct exposure to the prevailing light environment, yet the mature leaf shows a number of morphological and physiological adaptations to light. Systemic signals generated in mature leaves are thought to play an important role in controlling the response of the young leaf primordia, but the precise developmental window during which this response can occur requires further characterisation. Stomatal size, density and distribution are likely to be key elements of this response since they play an important role in controlling gas exchange in the mature leaf, yet the cell division processes that control stomata formation are limited to relatively early stages of leaf development.

The work reported here describes the process of stomata formation during rice leaf development and, in particular, identifies the stages up to and including the P3 stage as the phase during which the stomatal differentiation and patterning system is responsive to a shift of the plant from high to low irradiance. Careful staging of the transfer revealed that various aspects of stomatal size could be altered during this early phase of rice leaf development. Variable guard cell width (linked to variation in epidermal cell file width in the rice leaf) was identified as a key variable in this morphological response. Physiological analysis of mature leaves with altered stomatal properties revealed the extent to which biochemical/physiology adaptations could compensate for altered potential parameters of gas exchange. Finally, a whole-mount *in situ* hybridisation (WISH) procedure was optimized and proven to work in a reliable fashion using probes for various genes, thus providing a new tool for the visualisation of gene expression in rice leaves. This paves the way for the analysis of gene expression during the very early stages of leaf development when stomatal differentiation occurs.

The work advances our understanding of the control of stomatal formation in rice and its potential influence on leaf photosynthetic performance. The method developed for the analysis of gene expression will enable future work to characterise the genetic mechanism underlying the environmental control of stomatal properties.

Portions of this thesis have been published in a peer-reviewed journal. The reference for the publications is as follows:

Julia van Campen, Muhammad N Yaapar, Supatthra Narawatthana, Christoph Lehmeier, Samart Wanchana, Vivek Thakur, Caspar Chater, Steven Kelly, Stephen A Rolfe, W Paul Quick, and Andrew J. Fleming. Combined Chlorophyll Fluorescence and Transcriptomic Analysis Identifies the P3/P4 Transition as a Key stage in Rice Leaf Photosynthetic Development. *Plant Physiology* 2016: pp.15.01624v1-pp.01624.2015.

ACKNOWLEDGEMENTS

All praise due to Allah S.W.T for giving me this beautiful opportunity to work and contribute to science. I am indeed a fortunate servant for being able to work with plants which I love immensely in my heart. It has been a great journey destined for me to gain a lot of knowledge and learn many valuable lessons in life which I hope can be learnt by others as well.

My utmost gratitude for having Prof. Andrew J. Fleming as my supervisor. His acumen and astuteness in guiding and dealing with my various needs along this PhD course has definitely made him a great companion any young scientists could have. A good teacher creates a good student and I wish to keep the chain throughout my career.

I would like to thank Universti Putra Malaysia (UPM), The King's Scholarship of Jabatan Perkhidamatan Awam (JPA) and Long-term Research Grant Scheme (LRGS), Food Security Project, Ministry of Higher Education, Malaysia for the financial support to conduct and complete my research and study successfully.

It is an honour to be able to work and learn from various lab members in D59 especially Dr. Christoph Lehmeier for his influential work attitude, helpful lab technicians (Bob Keen, Marion Bauch, Dr. Heather Walker), cheerful and wise lab partners (Dr. Supatthra Narawatthana, Julia V. Campen, Dr. Thomas Harcourt, Dr. Simon Wallace, Dr. Chloe Steels, Dr. Rachel George, Bobby Caine, Sam Amsbury, Alice Bailey, Prof. Mike Burrell, Dr. Mark Burrell, Dr. Marjorie Lundgren and Dr. Casper Chater), Greg Nicholson and Steve from Sir David Read Controlled Environment Facility and Chris Hill & Dr. Darren Robinson from microscopy facility.

Finally endless grateful prayers to my biological parents Zalilah Saad and Yaapar Ramli, the NY brothers; Nuzrin Yaapar, Nizam Yaapar and Nuzmin Yaapar, foster parents: MJ and ZCA, MWHS-USIC brothers and sisters, my apt muses (in order): AZ, YJ, RMG, SN, CL, MZA, MSA and particularly ANZ. Not forgotten Seth Stobus, vivacious Sheffield hiking buddies as well as to all my friends throughout these years who have constantly motivating and showering me with lots of du'as. Oh and not forgotten to my sisters Terong pubescens and Kiyambang rubra for their unconditional love to me.

Jazakumullahu Khairan Kathira

ABBREVIATIONS

¹²C	Carbon-12
¹³C	Carbon-13
A	Net carbon dioxide assimilation
Ace-Pow	Acetone powder
AX	Auxiliary leaf cluster
BCIP	5-bromo-4-chloro-3-indolyl-phosphate
bp	Base pair
BSA	Bovine serum albumin
cDNA	Complementary DNA
CB cycle	Calvin-Benson cycle
C_a	Atmospheric carbon dioxide concentration
C_c	Carbon dioxide concentration at carboxylation site
C_i	Intercellular carbon dioxide concentration
CO₂	Carbon dioxide
DIG	Digoxigenin
DNA	Deoxyribonucleic acid
EDTA	Ethylenediaminetetraacetic acid
GC	Guard cell
GCW	Guard cells width
g_s	Stomatal conductance
HL	High light condition (750 μmol m ⁻² s ⁻¹)
IG	Interveinal Gap
J_{max}	Regeneration of RuBP via the maximum rate of electron transport
kV	Kilovolt
LHC	Light harvesting complex
LL	Low light condition (250 μmol m ⁻² s ⁻¹)
LV	Large vein
mRNA	Messenger RNA
MV	Midvein
NBT	4-nitro blue tetrazolium
O₂	Oxygen
PAR	Photosynthetically active radiation

PBS	Phosphate buffer saline
P_{max}	Maximum photosynthetic rate
PPFD	Photosynthetic photon flux density
PSI and II	Photosystem I and II
P-stages	Plastochron stages
RNA	Ribonucleic acid
ROS	Reactive oxygen species
RPM	Revolutions per minute
Rubisco	Ribulose-1,5-bisphosphate carboxylase/oxygenase
RuBP	Ribulose-1,5-bisphosphate
SAM	Shoot apical meristem
SC	Subsidiary cell
SEM	Scanning electron microscope
SV	Small Vein
TBO	Toluidine Blue-O
TPU	RuBP regeneration via triose phosphate utilization
tRNA	Transfer RNA
VB	Vascular bundle
V_{cmax}	Maximum carboxylation rate by Rubisco
WISH	Whole-mount <i>in-situ</i> hybridisation

CONTENTS

ABSTRACT	II
ACKNOWLEDGEMENTS	IV
ABBREVIATIONS	V
CONTENTS	VI
FIGURE CONTENTS	IX
TABLE CONTENTS	XX
CHAPTER 1: INTRODUCTION	1
1.0 Overview	2
1.1 Rice and people	3
1.1.1 Insufficient rice production	3
1.2 Improved photosynthesis: An approach to enhance rice yield	5
1.2.1 The role of stomata and improvements in photosynthesis	9
1.3 Understanding the rice leaf	12
1.3.1 General morphology	12
1.3.2 Leaf anatomy	14
1.3.3 Leaf development in rice	16
1.3.4 Stomata Development	18
1.4 Environmental signals affect leaf and stomatal developments	22
1.4.1 Light as a stimulus	22
1.4.2 Systemic signalling and stomatal development	24
1.5 Research project outline	25
1.5.1 Aims	25
1.5.2 Overarching hypotheses	26
CHAPTER 2: MATERIALS AND METHODS	27
2.0 Materials and methods	28
2.1 Plant materials and growth conditions	28
2.2 Approximation of leaf developmental stage	30
2.3 Biochemical and physiological analyses	31
2.3.1 Measurements of photosynthesis and stomatal conductance	31
2.3.2 Pigment quantification	32
2.3.3 Carbon isotope analysis	32
2.4 Imaging of leaf primordia using scanning electron microscope	34
2.5 Hand sectioning of leaves for measurements of leaf anatomy	35
2.6 Stomatal and leaf epidermal characteristics	36
2.6.1 Preparation of leaf tissues	36
2.6.2 Measurement of stomatal and leaf epidermal characteristics	37
CHAPTER 3: CHARACTERISATION OF STOMATAL AND LEAF PHYSIOLOGY IN SUN AND SHADE	44

	LEAVES OF RICE	
3.1	Introduction	45
3.2	Aims	52
3.3	Brief methodology	53
	3.3.1 Stomatal and epidermal measurements	53
	3.3.2 Gas exchange measurements and biochemical analyses	53
	3.3.3 Statistical analysis	54
3.4	Results	55
	3.4.1 Comparison of stomatal size and density	55
	3.4.2 Comparison of assimilation rate and stomatal conductance in HL and LL grown plants	62
3.5	Discussion	67
	CHAPTER 4: Characterization of Stomatal Development in Rice	74
4.1	Introduction	75
4.2	Aims	78
4.3	Brief Methodology	79
	4.3.1 Stomatal Measurements	79
	4.3.2 Physiological Measurements and Biochemical Analyses	79
	4.3.3 Statistical Analysis	80
4.4	Results	81
	4.4.1 Effect of transfer of leaves from High Light to Low Light environment at different developmental stages on final stomatal parameters	81
	4.4.2 Effect of transfer of leaves from Low Light to High Light environment at different developmental stages on stomatal parameters	86
	4.4.3 Summary of effect of transfer between high and low light environments at specific leaf developmental stages on stomatal pattern and size	89
	4.4.4 Analysis of the outcome of altered stomatal pattern and size on leaf physiology	91
	4.4.5 Assimilation Rate	91
	4.4.6 Stomatal Conductance (gs)	99
	4.4.7 Intrinsic Water Use Efficiency (iWUE)	104
	4.4.8 Correlation Between Stomatal and Physiological Properties	106
4.5	Discussion	109
	CHAPTER 5: WHOLE-MOUNT <i>IN SITU</i> HYBRIDIZATION IN RICE	116

5.1	Introduction	117
	5.1.1 The principle of WISH	119
5.2	Aim	121
5.3	Methodology	122
	5.3.1 Unmodified WISH method for Arabidopsis performed on rice	123
	5.3.2 Optimization of the blocking reagent to prevent non-specific hybridization and binding	127
	5.3.3 Cutting of transverse samples for better riboprobe penetration into tissues and interpretation of results	129
	5.3.4 Optimised WISH for rice	130
	5.3.4.1 Tissue selection, fixation and permeabilization	130
	5.3.4.2 Post-fixation and pre-hybridization treatments	133
	5.3.4.3 Hybridization and antibody incubations	136
	5.3.4.4 Colorimetric signal detection and imaging	136
5.4	Results	137
5.5	Discussion	149
	CHAPTER 6: GENERAL DISCUSSION	154
6.1	Sun and shades characteristics of rice leaves	155
6.2	Leaf development, stomatal patterning and leaf performance	160
6.3	Optimization of a tool for studying gene expression in rice	167
6.4	Concluding remarks and future work	169
	REFERENCES	171
	PUBLISHED WORK	185

FIGURE CONTENTS

- Figure 1.1** World calories supply and production of the big three crops namely rice, wheat and maize in 2009. Summarized data for (A) obtained at: FAO, Accessed 16 November 2012. <http://faostat.fao.org/site/609/default.aspx#ancor>. Summarized data for (B) obtained at: FAO, Accessed 16 November 2012. <http://faostat.fao.org/site/567/DesktopDefault.aspx?PageID=567#ancor> **4**
- Figure 1.2** Trends in rice production in Asia and globally (A) and regional population growth and projection (B). Both figures are adapted from Elert (2014). **5**
- Figure 1.3** A typical internal structure of a C₃ leaf and a summary of light dependent and independent reactions. (A) shows a typical diffusion path for CO₂ and the association between the light reactions, carbon reduction, and photorespiratory cycles (C, Chloroplast; M, mitochondrion; P, peroxisome). (B) depicts the two important processes that take place in the chloroplast. Light-dependent reactions are the energy-capturing reactions in which chlorophyll within thylakoid membranes absorbs solar energy and energizes electrons. The energized electrons move down the electron transport system and are used for ATP and NADPH production. Both ATP and NADPH are used in the light-independent reactions (or simply Calvin Cycle) which take place in the stroma. These are synthesis reactions that use the products of light dependent reactions to fix CO₂ into carbohydrate (sugar). Figure (A) is adapted from von Caemmerer and Evans (2010) and (B) from Figure 10.5 of Campbell, Neil A., & Jane B. Reece. *Biology*. 7th ed. San Francisco: Pearson/Benjamin Cummings, 2005, p. 185). **7**
- Figure 1.4** Stomatal shape comparison between dumbbell-shaped rice stoma (A- typical of grass) and kidney-shaped stomata in *Aglaonema sp.* (B- typical in other C₃ plant species). Scale bars equal 30µm. (Yaapar, unpublished). **10**
- Figure 1.5** A rice phytomer units comprises one internode, a node, emerged leaf, tiller bud and root primordia. (Based on a drawing by Hoshikawa, 1989). **13**
- Figure 1.6** Rice leaf and its component structures. (A) Culm and leaf sheath; (B) Collar, a pair of auricles and ligule; (C) Sheath pulvinus. **14**
- Figure 1.7** Transverse section of a rice leaf. (LV) large vascular bundle; (SV) small vascular bundle; (BS) bundle sheath cell; (BC) bulliform cell; (TRC) trichome; (STO); substomatal chamber. **15**

- Figure 1.8** Key differences in morphological and developmental pattern between *Arabidopsis thaliana* (dicot) and *Oryza sativa* or rice (monocot) stomata. **(A)** Kidney-shaped stoma of *Arabidopsis* and dumbbell-shaped stoma of rice. **(B)** Stomata distribution and developmental pattern in *Arabidopsis* (top) and rice. GMC (orange oval in *Arabidopsis*, yellow block in rice); SC (small dark blue block in rice); GC (red kidney in *Arabidopsis*, red dumbbell in rice). Figure adapted from Liu *et al.* (2009). **19**
- Figure 1.9** Schematics of comparison between stomatal development in *Arabidopsis* **(A)** and rice **(B)** with proposed sites of expression of three closely related bHLH transcription factors *SPCH*, *MUTE* and *FAMA*. In rice, it is proposed that the action of *SPCH* would occur before the stomatal cell row stage. Figure adapted from Liu *et al.* (2009). **19**
- Figure 1.10** SEM micrograph of a mature stomatal complex cross section in rice and its associated microstructures (Yaapar, unpublished) **21**
- Figure 2.1** **(A)** Image of bottom-cut Eppendorf tubes and **(B)** rice seedlings in hydroponic container. **27**
- Figure 2.2** Leaf sample is sandwiched in between a Styrofoam blocks that has been partially slit. The whole sandwich was always moistened with water while pressing it with index finger. Fine sections are made with sawing motions using razor blade at almost a right angle **36**
- Figure 2.3** A typical structure of a stomatal complex in rice leaves. Each unit comprises four cells where a pair of dumbbell shaped guard cells is sandwiched by two subsidiary cells (SCs). SCA (stomatal complex area is indicated by the blue dotted line); SCL (stomatal complex length); SCW (stomatal complex width) SPA (stomatal pore area) GCW (guard cell width). Scale bar = 5 μ m **38**
- Figure 2.4** SEM micrograph of a partially open stomatal aperture (yellow area) within a stomatal complex on a rice leaf (bar = 10 μ m). The red dotted line shows an approximately elongated-hexagon shaped pore area if the aperture were to open maximally. A stomatal complex comprises a pair of guard cells (GC) being sandwiched by two subsidiary cells (SC). (Yaapar, unpublished). **39**
- Figure 2.5** Description of an elongated hexagon (e-Hex) which is supposed to be the shape of a fully open stomatal pore. Two parameters are measurable **(A)** for any given aperture namely aperture length (A_l) and width (A_w). The formula for an e-Hex area can be derived by first splitting the shape into two producing two equal trapezoids **(B)**. Each trapezoid in turn contains two right-angled triangle whose unknown adjacent lengths can be found using Tangent function ($\text{Tan } \theta = \text{opposite length/adjacent length}$) in trigonometry. **40**

Figure 2.6	Description of angles for a right-angled triangle in either side of a trapezoid. Since the total angle must be 180° for any triangle, the two unknown theta (θ) values must be 45° each.	40
Figure 2.7	Epidermal features and stomatal patterning of a typical interveinal gap (IG). DIC image of an Interveinal Gap (IG) bound by a small vein and a large vein. Each IG comprises a number of cell files where some are pure long epidermal cells (E) and some contain stomata (SF, stomatal file).	43
Figure 3.1	Physical and physiological differences between sun and shade plants. Primary characteristics are highlighted at whole plants, leaves and cells levels. Figure adapted from: Plants In Action, http://plantsinaction.science.uq.edu.au/edition1/?q=content/12-1-1-light-interception-and-utilisation	46
Figure 3.2	Typical response of photosynthesis to different light concentrations for C_3 plant. Dotted lines are extrapolations of initial linear slopes in the light-limited phase of the curve, which also indicates quantum yield (moles of O_2 evolved per mole quanta absorbed). The light-compensation point is the irradiance level required to offset respiration so that net exchange of CO_2 is zero. The P_{max} (light-saturated photosynthesis) of sun leaves is higher than shade leaves in the same species. P_{max} is found in the plateau region of the curve, which reflects carboxylation limitation. Figure obtained at: Plants In Action, http://plantsinaction.science.uq.edu.au/edition1/?q=content/12-1-1-light-interception-and-utilisation	49
Figure 3.3	Modelled rate of net CO_2 assimilation (A) in as a function of chloroplastic CO_2 partial pressure (C_c).	51
Figure 3.4	Vein number and position in a rice leaf. (A) is a DIC image of an interveinal gap (IG) between a large vein (LV) and a small vein (SV) of a control HL leaf where some of the cell files contain at least one stoma (S) or none (E), as indicated on the left hand side of the figure (Scale bar = $50\mu m$). A transverse hand-section (B) shows relative position of the veins, S, E and bulliform cells (BULL). An SEM micrograph (C) further shows a leaf transverse section with the same labelled structures (D) Provides a schematic diagram to show the relative numbers and positions of veins and IGs for a HL leaf (13 SVs, upper diagram) and LL leaf (15 SVs, lower diagram).	56
Figure 3.5	Variation of stomatal properties in each interveinal gap (IG) on the abaxial surface for high light (HL) and low light (LL) grown leaves. The graph shows the mean of (A) stomatal complex area (B) pore area and (C) density for each IG from HL leaves (green lines) and LL leaves (blue lines). Error bars represent standard deviation. Two-tailed pair-wise t-tests between HL and LL in each IG have been performed with significant differences between comparisons being indicated as: $*p < 0.05$,	57

p<0.01 and *p<0.001 (n=5 for each comparison except where stated on the x-axis).

- Figure 3.6** Selected DIC images of stomatal complexes of a high light (HL) grown leaf at IG1 and low light (LL) grown leaf at IG10. Scale bar equals 10 μ m. **58**
- Figure 3.7** Variation in stomatal properties across leaves from midvein towards margin in seven sections of selected IGs. **(A)** Schematic diagram of a leaf to show regions taken for average measurements. Green bands represent IGs and black band is the leaf margin. The middle IG is selected as the position between MV-LV or LV-LV and values from the two IGs bordering an LV are averaged and denoted as 'ab'. When the number of IGs are odd **(B)**, the middle IG taken is always the one closer to the MV. The graphs show the mean values for **(C)** stomatal complex area **(D)** pore area and **(E)** stomatal density, where green lines show values for HL while blue lines are for LL samples. Two-tailed pair-wise t-tests between HL and LL values in each section have been performed with significant differences between comparisons being indicated: *p<0.05, **p<0.01 and ***p<0.001 (n=5). Within each treatment, one-way ANOVA followed by Tukey-Kramer's post-hoc test is performed. Means not sharing the same letter are significantly different (p<0.05). Error bars represent standard deviation. Key: IG, interveinal gap); LV, large vein; MV, midvein and SV, small vein. **61**
- Figure 3.8** Assimilation (A)-light (PAR) response curves of rice leaf no. 5 grown in either a high light (red line) or low light (blue line) environment in Error bars represent standard error of mean for the assimilation where n=3. **62**
- Figure 3.9** Assimilation versus intercellular CO₂ (A-C_i) response curves for high light (HL, **A**) and low light (LL, **B**) grown leaves. Data are pooled from 3 plants for each treatment where each red dot is the average observation for the given A rate and C_i concentration with measurements made at the current CO₂ concentration (C_a= 400ppm) marked on the curves. A_c (dashed blue lines) are CO₂ assimilation rate limited by the amount and activity of Rubisco (enzyme limited/RuBP saturated) while A_j (dashed brown lines) are CO₂ assimilation rate limited by RuBP regeneration (light limited/RuBP limited). Error bars show standard error of mean. **63**
- Figure 3.10** Photosynthetic features of high light (HL) and low light (LL) grown rice leaves at ambient CO₂ (400 ppm) extracted or calculated from the A-C_i curves in Fig. 3.10. **(A)** Assimilation rate (A₄₀₀); **(B)** Rubisco carboxylation rate (V_{cmax400}); **(C)** electron transport rate (J_{max400}); **(D)** stomatal conductance (g_{s400}); **(E)** leaf temperature at 400 and 1600 ppm CO₂; **(F)** percentage stomatal limitation (I_s) to photosynthesis; and **(G)** chlorophyll a/b ratio. Two samples t-tests were performed to compare means with significant differences between comparisons indicated as: * p<0.05; **p< 0.01 and *** p<0.001 (n=3) with error bars to represent standard error of mean. **65**
- Figure 3.11** Water use efficiency **(A)** and carbon isotope ratio ($\delta^{13}C$) is presented on a per mill (‰) basis **(B)**. Two samples t-tests were performed to compare means. Significant differences **66**

between comparisons are indicated as *** $p < 0.001$ ($n=3$). Error bars indicate standard error of mean.

- Figure 4.1** Measurements of stomatal size (**A-E**), epidermal size (**F and H**) and stomatal patterning (**G and I**) in mature L5 grown in HL condition that were transferred to LL condition at different P-stages, as indicated. ANOVA followed by a post hoc Tukey's HSD test (av) was performed on data showing a normal distribution while the non-parametric Kruskal-Wallis multiple comparison test (kw) was performed on data showing non-normal distribution. Each black dot represents a single measurement. Vertical error bars represent standard error of means while the dotted horizontal red lines are the means. Treatments that share same letter in a grouping cannot be statistically distinguished (P -value < 0.05). **82**
- Figure 4.2** Measurements of stomatal size (**A-E**), epidermal size (**F and H**) and stomatal patterning (**G and I**) in mature L5 grown in LL condition that were transferred to HL condition at different P-stages, as indicated. ANOVA followed by a post hoc Tukey's HSD test (av) was performed on data showing a normal distribution while the non-parametric Kruskal-Wallis multiple comparison test (kw) was performed on data showing non-normal distribution. Each black dot represents a single measurement. Vertical error bars represent standard error of means while the dotted horizontal red lines are the means. Treatments that share same letter in a grouping cannot be statistically distinguished (P -value < 0.05). **87**
- Figure 4.3** Summary of possible windows of sensitivity at different plastochron stages (P1 to P5) for the transfer from HL to LL (**A**, based on Fig. 4.3) and LL to HL (**B**, based on Fig. 4.4) for various stomatal and epidermal properties. Each tick (✓) symbol under any P-stage denotes the possibility of altering the corresponding parameter compared to the initial light condition (shaded column on the left). **90**
- Figure 4.4** A-C_i curves in mature rice leaves for the transfer experiment from HL to LL. Rows (i), (ii) and (iii) represent individual curves (total $n=3$) for the corresponding treatment labelled at the top of each column. Row (iv) represents mean A-C_i curve for the particular treatment where the horizontal-vertical bars represent standard error of mean. The blue dotted lines are best fit curves for CO₂ assimilation rate limited by the amount and activity of Rubisco (enzyme limited/RuBP saturated) while the green dotted lines are best fit curves for CO₂ assimilation rate limited by RuBP regeneration (light limited/RuBP limited). Each A-C_i curve is marked with C_a=400ppm to approximately **94**

show assimilation rate at the current ambient CO₂ level while the experiment took place.

- Figure 4.5** Mean assimilation rates measured at 400ppm CO₂ (ambient level, A₄₀₀) (**A**) and maximum assimilation rates (A_{max}) (**B**) achievable for the HL to LL transfer experiment. The measured photosynthetic rates are explained by similar trend in maximum carboxylation (V_{cmax}, **C**) whose capacity depends on CO₂ supply influenced by the relative stomatal limitation (I_s in **D**). The electron transport (J_{max}, **E**) rates also have similar trend to assimilation and the capacity is explained by the ratio of chlorophyll a/b (**F**). All means are extracted from Fig. 4.6iv. One way ANOVA followed by a post hoc Tukey's HSD test where n=3 with groups sharing different letters are significantly different (p<0.05) and error bars represent standard error of mean. **95**
- Figure 4.6** A-C_i curves in mature rice leaves for the transfer experiment from LL to HL. Rows (i), (ii) and (iii) represent individual curves (total n=3) for the corresponding treatment labelled at the top of each column. Row (iv) represents mean A-C_i curve for the particular treatment where the horizontal-vertical bars represent standard error of mean. The blue dotted lines are best fit curves for CO₂ assimilation rate limited by the amount and activity of Rubisco (enzyme limited/RuBP saturated) while the green dotted lines are best fit curves for CO₂ assimilation rate limited by RuBP regeneration (light limited/RuBP limited). Each A-C_i curve is marked with C_a=400ppm to approximately show assimilation rate at the current ambient CO₂ level while the experiment took place. **96**
- Figure 4.7** Mean assimilation rates measured at 400ppm CO₂ (ambient level, A₄₀₀) (**A**) and maximum assimilation rates (A_{max}) (**B**) achievable for the LL to HL transfer experiment. The measured photosynthetic rates are explained by similar trend in maximum carboxylation (V_{cmax}, **C**) whose capacity depends on CO₂ supply influenced by the relative stomatal limitation (I_s in **D**). The electron transport (J_{max}, **E**) rates also have similar trend to assimilation and the capacity is explained by the ratio of chlorophyll a/b (**F**). All means are extracted from Fig. 4.6iv. One way ANOVA followed by a post hoc Tukey's HSD test where n=3 with groups sharing different letters are significantly different (p< 0.05) and error bars represent standard error of mean. **98**
- Figure 4.8** g_s-C_i curves in mature rice leaves for the transfer experiment from HL to LL. Rows (i), (ii) and (iii) represent individual curves (total n=3) for the corresponding treatment labelled at the top of each column. Row (iv) represents mean g_s-C_i curve for the **100**

particular treatment where the horizontal-vertical bars represent standard error of mean. Each g_s - C_i curve is marked with $C_a=400\text{ppm}$ to approximately show assimilation rate at the current ambient CO_2 level while the experiment took place.

- Figure 4.9** Mean stomatal conductance (g_s) rates measured at 400ppm CO_2 (ambient level, g_{s400}) (A) and maximum g_s ($g_{s\text{max}}$) rate (B) achievable for the HL to LL transfer experiment. The means for both g_s conditions were extracted from Fig. 4.10iv. One way ANOVA followed by a post hoc Tukey's HSD test where $n=3$ with groups sharing different letters are significantly different ($p < 0.05$) and error bars represent standard error of mean. **101**
- Figure 4.10** g_s - C_i curves in mature rice leaves for the transfer experiment from LL to HL. Rows (i), (ii) and (iii) represent individual curves (total $n=3$) for the corresponding treatment labelled at the top of each column. Row (iv) represents mean g_s - C_i curve for the particular treatment where the horizontal-vertical bars represent standard error of mean. Each g_s - C_i curve is marked with $C_a=400\text{ppm}$ to approximately show assimilation rate at the current ambient CO_2 level while the experiment took place. **102**
- Figure 4.11** Mean stomatal conductance (g_s) rates measured at 400ppm CO_2 (ambient level, g_{s400}) (A) and maximum g_s ($g_{s\text{max}}$) rate (B) achievable for the LL to HL transfer experiment. The means for both g_s conditions were extracted from Fig. 4.12iv. One way ANOVA followed by a post hoc Tukey's HSD test where $n=3$ with groups sharing different letters are significantly different ($p < 0.05$) and error bars represent standard error of mean. **103**
- Figure 4.12** Mean intrinsic water use efficiency (iWUE) rates measured at 400ppm CO_2 (ambient level, $i\text{WUE}_{400}$) for the HL-LL (A) and LL-HL (C) transfer experiments. The maximum iWUE ($i\text{wue}_{\text{max}}$) for the HL-LL (B) and LL-HL (D) transfer experiments are also calculated. iWUE is the ratio between CO_2 assimilation and stomatal conductance (A/g_s). Carbon isotope ratio ($\delta^{13}\text{C}$) is presented as per mill (‰) basis in (E) for HL-LL and (F) for LL-HL transfer experiments to validate the iWUE analyses. One way ANOVA followed by a post hoc Tukey's HSD test where $n=3$ with groups sharing different letters are significantly different ($p < 0.05$) and error bars represent standard error of mean. **105**
- Figure 4.13** Contour plot of intrinsic water use efficiency at ambient CO_2 level ($i\text{WUE}_{400}$) as a function of guard cells width (GCW) and stomatal density (SD). Note that individual data point for high light (HL) grown leaves are clearly marked. The unit for the colour scale on the top right is $\mu\text{mol CO}_2 \text{ mol H}_2\text{O}^{-1}$. **108**
- Figure 5.1** Overview of steps for *in situ* hybridization method. Tissue is treated to preserve cell structure with enhanced permeability to **120**

allow hybridization with the targeted mRNA in the cytoplasm (A). DIG-labelled riboprobe binds to the complementary mRNA (B) and allowed to react with an anti-DIG antibody that carries the alkaline phosphatase enzyme. Addition of the substrate 5-bromo-4-chloro-3-indolyl-phosphate results in a localized blue-purple precipitation (C). (D) An example of a localized detection of blue-purple precipitate in a developing P4 leaf.

- Figure 5.2** *eEF1A* mRNA expression pattern in rice using the unmodified WISH protocol for *Arabidopsis*. Strong antisense signal (dark purple staining following 36 h staining time) are visible in the young P3 (A) and P4 (B) leaf primordia. In general there is no signal detected for the sense probe (C) except in some interveinal gap (IG) areas (circled) and x-shaped silica bodies located on the veins (arrowheads). For any given IG area there is a vein (V), mesophyll cells (M) and bulliform cells (B) underneath the epidermis. **128**
- Figure 5.3** Staining pattern in P4 leaf tissue using the unmodified WISH protocol except by incorporating either *eEF1A*-sense probe or antibody only. The presence of antibody alone causes positive purple staining in some leaf regions (A) and when magnified (B) reveals staining in some interveinal gap areas and x-shaped silica bodies (arrowheads). When no antibody was added to the hybridized *eEF1A*-sense probe, no signal was obtained (C). V indicates vein. **131**
- Figure 5.4** Background staining pattern in P4 leaf tissue following the introduction of different mixtures of antibody blocking reagents in specific WISH steps. Bovine serum albumin (BSA) solution only prevents x-shaped silica bodies staining on the veins (v) but not in interveinal gap regions (A). Incubation of antibody in acetone powder (Ace-Pow) substantially reduce background staining (B, circled) and the combination of both BSA and Ace-Pow further refines the result (C, circled). The coupling of sheep serum and BSA together with Ace-Pow synergistically prevents background staining, thus producing a completely clear tissue (D). **132**
- Figure 5.5** mRNA expression pattern of the rice *Histone-4* gene in P3 leaf primordia. WISH was performed on the P3 tissue was dissected out. SEM micrograph (A) shows the whole structure of P3. The sense probe yielded no signals (B) and looks clear under magnification. The antisense probe produced signals (C) concentrated near the bottom of primordium and when magnified reveals dotted/speckled staining pattern. **134**
- Figure 5.6** Longitudinal section of a typical rice culm at the base (A), exposing leaf layers of different plastochron (P) stages and shoot apical meristem (SAM). Dashed line indicates a typical cutting level (about 1 cm from the culm base) used for the whole mount *in-situ* to reveal the most number of leaf layers when being viewed from the top. The magnified image is the resultant stub cut (Image by Ahmad Nazrin Zakaria). When the stub is **135**

- viewed from the top (**B**), it always shows leaf no. 3 (L3) as the outermost and oldest leaf layer.
- Figure 5.7** mRNA expression pattern of rice *Histone-4* gene in a transversely cut culm containing a cluster of leaf layers. The outermost and oldest layer is leaf no. 3 (L3) and the leaf layers gets progressively smaller and younger towards the cluster centre. (**A**) shows positive expression pattern (dotted purple stain) for antisense probe in relatively younger leaf layers (L5-7) and the inset image is the magnified centre region of the cluster. No signal is detected anywhere for the sense probe in (**B**). Axillary leaf cluster (AX) that will give rise to a new tiller are also present. Artefact staining (non-purple) is present in lignified dermal layers (arrowheads). **138**
- Figure 5.8** mRNA expression pattern of rice *Cyclin-dependent kinase B2-1 (CDKb2)* gene. The outermost and oldest layer is leaf no. 3 (L3) and the leaf layer gets progressively smaller and younger towards the cluster centre. (**A**) shows positive expression pattern (dotted purplish-crimson stain) for antisense probe in the youngest leaf layers (L6 and 7) and in the axillary leaf clusters (AX). Expression also localized within vascular bundle regions (circled). No equivalent staining is detected anywhere for the sense probe in (**B**). Artefact staining (non-purple) is present in lignified dermal layers (arrowheads). **140**
- Figure 5.9** mRNA expression pattern of rice *Drooping Leaf (DL)* gene. The outermost and oldest layer is leaf no. 3 (L3) and the leaf layer gets progressively smaller and younger towards the cluster centre. (**A**) shows positive expression pattern (dark vertical bands) for antisense probe in the youngest leaf layers (L6 and 7) which localized within presumptive midrib regions. No equivalent staining is detected anywhere for the sense probe in (**B**). Axillary leaf cluster (AX) that will give rise to a new tiller are also present. Artefact staining (non-purple) is present in lignified dermal layers (arrowheads). **141**
- Figure 5.10** mRNA expression pattern of rice *MONOPTEROS (MON4)* gene. The outermost and oldest layer is leaf no. 3 (L3) and the leaf layer gets progressively smaller and younger towards the cluster centre. (**A**) shows positive expression localization for antisense probe in the three youngest leaf layers (L5 - 7) within vascular bundle regions (circled) and in axillary leaf cluster (AX). No equivalent staining is detected anywhere for the sense probe in (**B**). Artefact staining (non-purple) is present in lignified dermal layers (arrowheads). **142**
- Figure 5.11** mRNA expression pattern of rice *CONTINUOUS VASCULAR RING (COV1)* gene. The outermost and oldest layer is leaf no. 3 (L3) and the leaf layers gets progressively smaller and younger towards the cluster centre. (**A**) shows high positive expression (purple stain) for antisense probe in the youngest leaf sheath layer (L4) and also localized in the septum regions between lacuna (circled) in the older sheath layer (L3). No equivalent staining is detected anywhere for the sense probe **143**

- in **(B)**. Artefact staining (non-purple) is present in lignified dermal layers (arrowheads).
- Figure 5.12** mRNA expression pattern of rice *DELTA-7-STEROL-C5 (DWF7)* gene. The outermost and oldest layer is leaf no. 3 (L3) and the leaf layers get progressively smaller and younger towards the cluster centre. **(A)** shows high positive expression (purple stain) for antisense probe in the youngest leaf sheath layer (L4) especially at the edge of lacuna (circled in L4) and also localized in the septum regions between lacuna in the older sheath layer (circled in L3). No equivalent staining is detected anywhere for the sense probe in **(B)**. (AX) is the axillary leaf cluster and non-purple artefact staining is present in lignified dermal layers (arrowheads). **144**
- Figure 5.13** mRNA expression pattern of rice *CHLOROPHYLL A-B (CAB)* gene. The outermost and oldest layer is leaf no. 3 (L3) and the leaf layer gets progressively smaller and younger towards the cluster centre. **(A)** shows high positive expression (purple stain) for antisense probe in the mesophyll areas of developing leaf layers (L5 and L6). Expression is much paler in the presumptive lacuna (circled) and vascular bundle (VB) areas, and this is true for axillary cluster (AX) region as well. No equivalent staining is detected in the youngest L7, the more mature leaf sheath layers (L3 and L4) that contained fully formed lacuna and VB and also for the sense probe in **(B)**. Non-purple artefact staining is present in lignified dermal layers (arrowheads). **145**
- Figure 5.14** mRNA expression pattern of rice *CULLIN-1 (CUL1)* gene. The outermost and oldest layer is leaf no. 3 (L3) and the leaf layer gets progressively smaller and younger towards the cluster centre. **(A)** shows positive expression (slight dark stain) for antisense probe in the youngest leaf sheath layer (L4) especially at the edge of lacuna (circled) . No equivalent staining is detected anywhere for the sense probe in **(B)**. (AX) is the axillary leaf cluster and non-purple artefact staining is present in lignified dermal layers (arrowheads). **146**
- Figure 5.15** False-positive mRNA expression pattern of rice *THYLAKOID FORMATION FACTOR (THF1)* gene. The outermost and oldest layer is leaf no. 3 (L3) and the leaf layer gets progressively smaller and younger towards the cluster centre. **(A)** shows positive staining (purple) for antisense especially in the youngest leaves (L6 and L7) . Similar purple staining is detected in L5 and L6 for the sense probe in **(B)**. (AX) is the axillary leaf cluster and non-purple artefact staining is present in lignified dermal layers (arrowheads). **147**
- Figure 5.16** False-positive mRNA expression pattern of rice *DELTA-14-STEROL REDUCTASE (FACKEL)* gene. The outermost and oldest layer is leaf no. 3 (L3) and the leaf layer gets progressively smaller and younger towards the cluster centre. **(A)** shows positive staining (purple) for antisense especially in the youngest leaves (L5-L7) . Similar purple staining pattern is detected in L5-L7 for the sense probe in **(B)**. (AX) is the axillary **148**

leaf cluster and non-purple artefact staining is present in lignified dermal layers (arrowheads).

Figure 6.1 Relative positions of stomatal files (S) with respect to midvein (MV), small vein (SV) or leaf margin (M). There are usually more than four stomatal files in the interveinal gap (IG) next to a MV (**A**). In IGs in the middle of the leaf width (**B**), stomatal files always follow the 'maximum four rule' The last IG next to margin (**C**) usually has only one stomatal file and a high in stomatal density. **158**

Figure 6.2 Schematic illustration of potential systemic signaling relay system via vascular system perceived by older leaves that influence leaf acclimatization in developing and concealed leaf primordium. **162**

TABLE CONTENTS

Table 1.1	Staging of adult leaf development in rice. I1, Incipient primordium; P1-P6, Plastochron 1-6; (table is adapted from: http://www.shigen.nig.ac.jp/rice/oryzabase/development/search.jsp)	16
Table 2.1	Composition of nutrients used in the hydroponic system. Solutions 1, 2 and 3 were prepared separately before being mixed and diluted with water to the final concentration to prevent precipitation. Each mineral solution was prepared from stock solution kept at room temperature and each preparation for hydroponic solution usage was made fresh and never kept for more than one week. BDH (BDH Merck Ltd.); Fisher (Fisher Scientific UK Ltd.); Fisons (Fisons Plc.); Fluka (Fluka-Sigma-Aldrich Co. LLC).	29
Table 2.2	The approximation of L5 plastochron stages based on the length of L3 blades under high and low light conditions.	30
Table 3.1	Pearson's correlation coefficients (r) between the mean values of stomatal properties from Fig. 3.3 up to IG16. Single asterisks (*) indicate correlations which are significant at the p<0.05 confidence limit. HL (high light); LL (low light); SCA (stomatal complex area); SPA (stomatal pore area); SD (stomatal density).	59
Table 4.1	Pearson's correlation coefficients (r) among the pooled values of stomatal size, patterning and leaf epidermal properties from the transfer experiments (n=11 for each parameter). Single asterisk * indicates correlations which are significant at p<0.05 confidence limit while double asterisks ** indicate correlations which are significant at p<0.01 confidence limit.	83
Table 4.2	Pearson's correlation coefficients (r) among the pooled values of stomatal-epidermal against leaf physiology properties (n=3 for each parameter). Single asterisk * indicates correlations which are significant at p<0.05 confidence limit while double asterisks ** indicate correlations which are significant at p<0.01 confidence limit.	108
Table 5.1	Riboprobes descriptions used for the whole mount in-situ method. Further gene details can be found by entering locus ID at www.rice.plantbiology.msu.edu . All antisense probes were generated using T3 RNA polymerase while T7 RNA polymerase was used for sense probes. cDNAs were cloned into the pBS vector and linearised with Kpn1 or Xho1 for T3 probes or SacI or Xba1 for T7 probes.	124

CHAPTER 1
INTRODUCTION

1.0 Overview

In the first part of the introduction details of global rice production and the need to increase its production will be discussed before summarising what is known about the environmental regulation of leaf development, with specific emphasis on rice and the differentiation of stomata (small pores on the leaf surface with a key role in gas exchange). Primary food for human consumption comes from a limited number of cultivated grasses (rice, wheat, barley) of which rice is globally the most important. However, as global population increases and pressure on agricultural land and resources increases, there is an urgent need to improve grain yield while at the same time using available resources more efficiently, most notably land and water.

The source of all food is the carbon fixed from the atmosphere via photosynthesis. There is an extensive literature on the process of photosynthesis and numerous investigations have explored the possibility of improving the efficiency of this biochemical process and thus theoretically increasing yield (Andrews and Whitney, 2003; Whitney *et al.*, 2011). However, to date this approach has met with little success. An alternative approach to improving the efficiency of photosynthesis is to consider the multicellular organ which has evolved to perform this process- the leaf. A leaf is an organ whose overall form and constituent cells enable the uptake of CO₂ and water and the absorption of light energy so that photosynthesis occurs. The leaf must also facilitate the transport of the products of photosynthesis to other parts of the plant for growth and storage (Evans, 1975; Yoshida, 1972).

A significant body of evidence indicates that the overall form of a leaf and the differentiation of the constituent cells are subject to both an endogenous developmental regulation and influence by external environmental factors. In particular, light quality and intensity are known to influence leaf development with a direct outcome on the photosynthetic capability of the leaf (Pallardy, 2008). Most notably, stomata form and frequency have been identified as potential parameters for optimization which might be exploited to improve crop yield (Schluter *et al.*, 2003; Franks and Beerling, 2009).

1.1 Rice and people

Rice (*Oryza sativa* L.) is touted as being fundamental to life owing to its prominent roles in shaping histories, cultures, diets and economics for half of humanity (Gomez, 2001). Today, rice feeds more than three billion people and more than one billion depend on rice cultivation for their livelihood (Skinner, 2012). Furthermore, it has supported a greater number of people for a very long period of time compared to any other crop since it was domesticated between 8,000 to 10,000 years ago (Greenland, 1997). Unlike maize or wheat, less than five percent of total rice production is traded on world markets, mainly within Asia and from Asia to Africa and Europe. For many Asian countries, rice self-sufficiency and political stability are interdependent issues (Fairhurst and Dobermann, 2002). In Asia two rice sub-species are widely cultivated namely *indica* and *japonica* and they have clear variation in the sequences of genome, physical and physiological properties such as hardiness and yield potential (Oka, 1958; Garris *et al.*, 2005; Huang, X. *et al.*, 2010)

1.1.1 Insufficient rice production

Together with wheat and maize, rice is regarded as one of the 'Big Three Crops' that feed the world. In fact, as a cereal grain, rice is grown on 6 continents and in more than 100 countries. Therefore, it is the staple food for more than half of the world population (more than 3 billion people globally, (IRRRRI, 2015)). In terms of human consumption, especially in supplying calories, rice is by far the most important (Fig. 1.1A). Despite this, rice production is not the highest globally among the three crops mentioned (Fig. 1.1B). This worrying fact is indeed a problem as world population is increasing exponentially and over the next 40 years in Asia alone the population will increase by about 1.5 billion, more than a third of the present population (DESA, 2004).

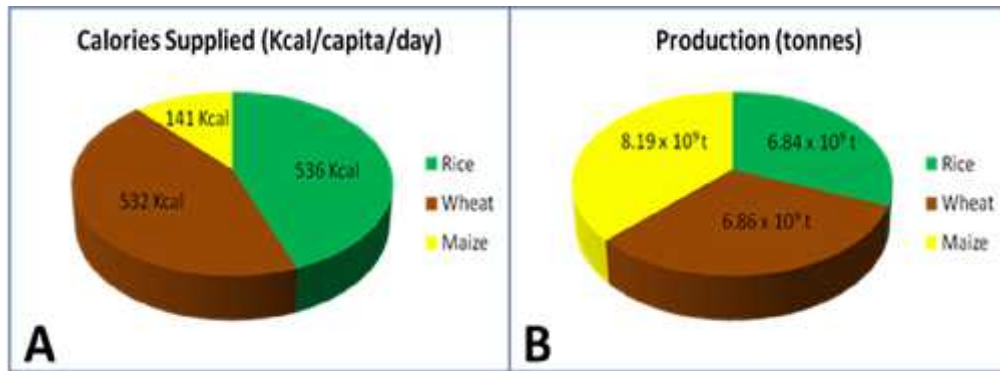


Figure 1.1:

World calories supply and production of the big three crops namely rice, wheat and maize in 2009. Summarized data for (A) obtained at: FAO, Accessed 16 November 2012. <http://faostat.fao.org/site/609/default.aspx#ancor>
 Summarized data for (B) obtained at: FAO, Accessed 16 November 2012. <http://faostat.fao.org/site/567/DesktopDefault.aspx?PageID=567#ancor>

Despite the modern age that we are living in now, about 854 million people are hungry and each day about 25,000 people die from hunger-related causes. Sixty percent of the world's population lives in Asia, where each hectare of land used for rice production currently provides food for 27 people, but by 2050 that land will have to support at least 43 people (Sheehy *et al.*, 2008). Looking at a global picture, world population is expected to grow by over a third, or 2.3 billion people, between 2009 and 2050. Nearly all of this growth is forecast to take place in the developing countries. Meanwhile, urbanization is expected to progress at an accelerating rate with urban areas to account for 70 % of world population in 2050 (49 % increment from present time) and rural population, after peaking sometime in the next decade, is actually declining (FAO, 2009).

By looking at the rice production graph in Fig. 1.2 A, in the last 50 years until recently (2013), rice production has steadily kept pace with the population growth rate, mainly due to the gains from the technologies of the green revolution era such as semi-dwarf and fertilizer responsive varieties, as well as other associated agronomic technologies.

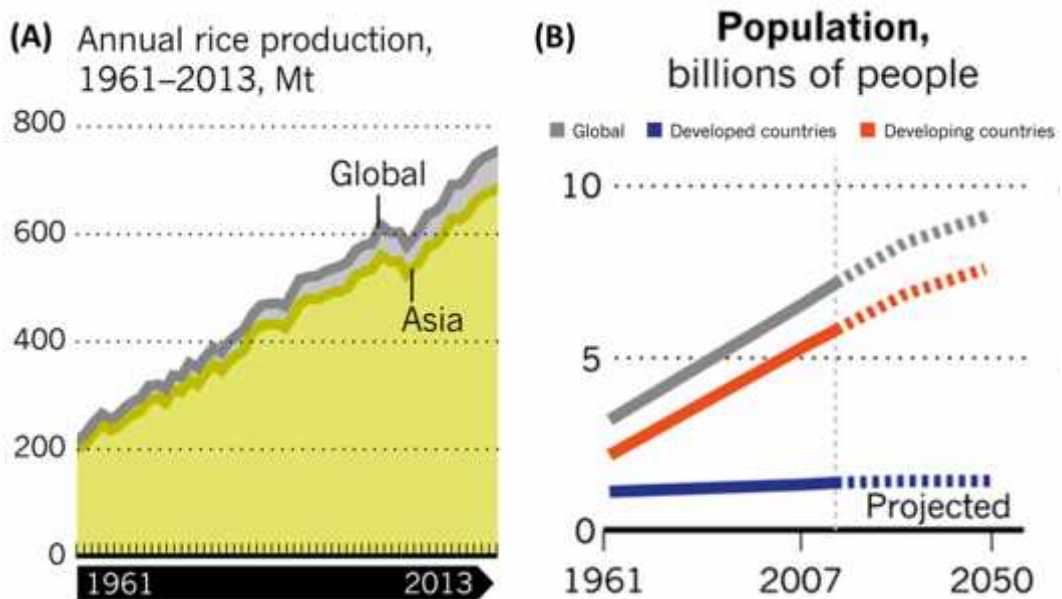


Figure 1.2:

Trends in rice production in Asia and globally (A) and regional population growth and projection (B). Both figures are adapted from Elert (2014).

However about a decade ago, rice yield growth had not increased tremendously compared to what had been obtained before the new millennium. In contrast, the same trend is not seen in the population growth (Fig. 1.2 B). World population constantly grows and is expected to further increase by over a third, or about 2.3 billion people, between 2009 and 2050. This imbalance between food supply and population growth has triggered concern globally and many endeavours are being attempted, such as precision farming and international trade in order to prevent havoc in the future. Therefore, increasing and improving rice production is indeed one of the important efforts that must be worked on for the sake of human sustenance.

1.2 Improved photosynthesis: An approach to enhance rice yield

Photosynthesis is the fundamental process in which plants synthesize carbohydrate and generate oxygen from carbon dioxide (CO₂) and water by using light energy. Carbohydrate acts as a store of energy that serves as a resource to power cellular processes for all forms of life and to provide the carbon skeletons for a vast array of cellular products. However, photosynthesis is not a perfect process. It is the product of an evolutionary path which has set

various constraints on its efficiency. Moreover, although people use plants as a source of food and energy (mainly via the investment of the products of photosynthesis into seed development), plant development is not primarily evolved toward a theoretical maximum to enhance seed yield (Gust *et al.*, 2008). Due to these various constraints, reflecting both basic biochemical inefficiency in the process of CO₂ fixation and the conflicting source and sink relationships within a plant, the efficiency of solar energy conversion into biomass for most crops typically does not exceed 1% (Zhu *et al.*, 2010; Walker, 2009). As a consequence, improving the efficiency of photosynthesis has been identified as a reasonable aim to improve crop yield.

Being the basic organ of photosynthesis, the leaf is constructed in such a way that its orientation and anatomy have a major role in controlling the absorption of light for photosynthesis (Figure 1.3 A). Thus, anatomically, the leaf is highly specialized for light absorption (Terashima and Hikosaka, 1995). For example the epidermis is typically transparent to visible light with convex epidermal cells that act as lenses to focus and intensify the ambient light that reaches the chloroplasts in the lower mesophyll cells. The mesophyll cells themselves are organized to optimize both the capture of light and to enable the influx and efflux of the substrates and products of photosynthesis.

Chloroplasts contain grana are which made up of layers thylakoid membranes (Fig. 1.3 B) that are the sites of light capture by a group of light-harvesting complexes associated with photosystem (PS) II and I. The excitation of special chlorophyll molecules in PSII initiates a series of electron transfers through a number of electron acceptors including plastoquinone, cytochrome *b₆f* complex, plastocyanin and finally to the next PSI (Sacksteder *et al.*, 2000). PSI

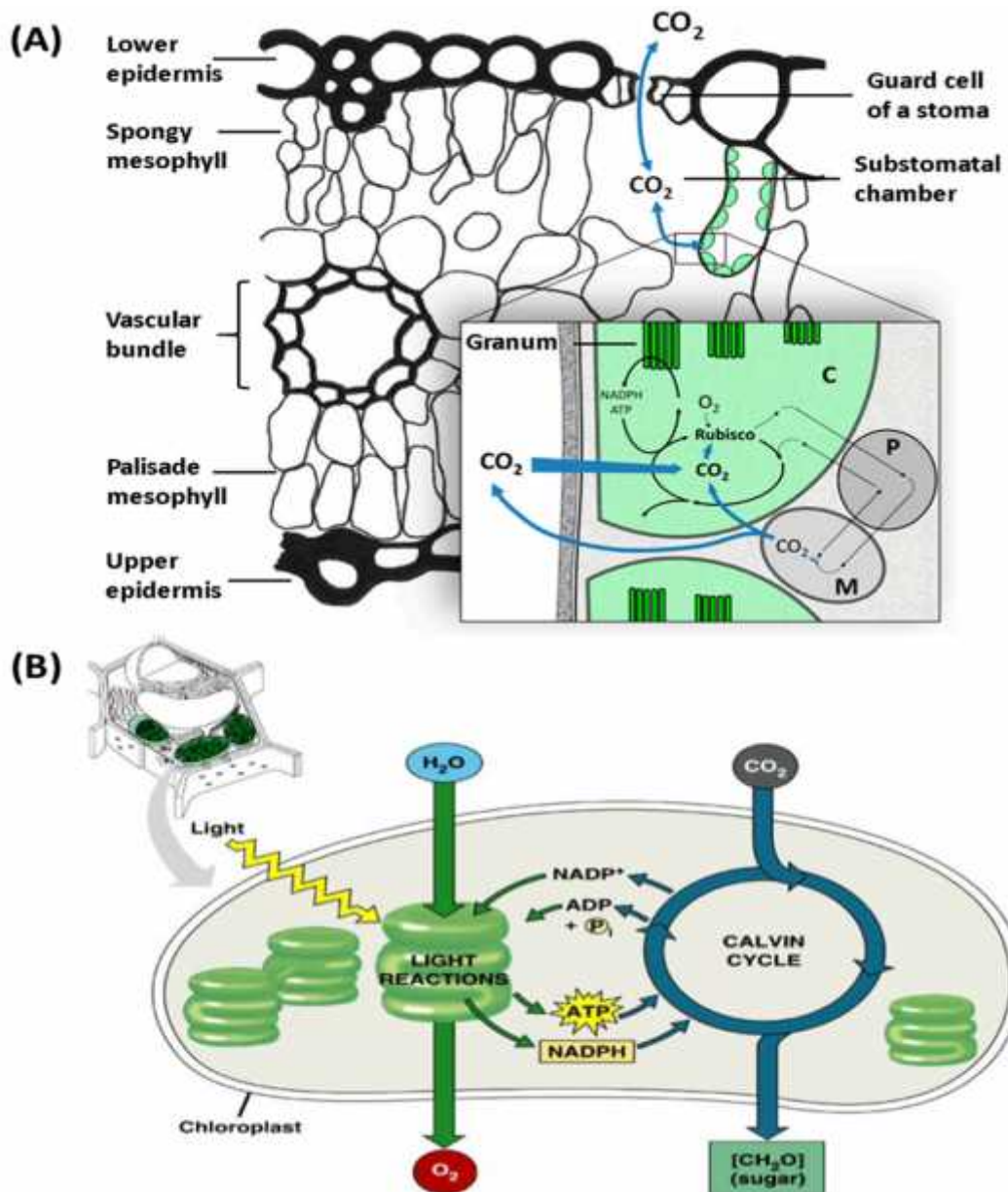


Figure 1.3:

A typical internal structure of a C₃ leaf and a summary of light dependent and independent reactions. **(A)** shows a typical diffusion path for CO₂ and the association between the light reactions, carbon reduction, and photorespiratory cycles (C, Chloroplast; M, mitochondrion; P, peroxisome). **(B)** depicts the two important processes that take place in the chloroplast. Light-dependent reactions are the energy-capturing reactions in which chlorophyll within thylakoid membranes absorbs solar energy and energizes electrons. The energized electrons move down the electron transport system and are used for ATP and NADPH production. Both ATP and NADPH are used in the light-independent reactions (or simply Calvin Cycle) which take place in the stroma. These are synthesis reactions that use the products of light dependent reactions to fix CO₂ into carbohydrate (sugar). Figure **(A)** is adapted from von Caemmerer and Evans (2010) and **(B)** from Figure 10.5 of Campbell, Neil A., & Jane B. Reece. *Biology*. 7th ed. San Francisco: Pearson/Benjamin Cummings, 2005, p. 185).

reduces NADP^+ to NADPH through the action of ferredoxin and the flavoprotein ferredoxin-NADP reductase. PSII contributes to the electrochemical proton gradient that results in the generation of ATPs by the action of ATP synthase enzyme. Both products of these light-dependent reactions namely ATP and NADPH will be used in the Calvin-Benson (CB) cycle to reduce CO_2 .

The CB cycle is a light-independent process located in the stroma of the chloroplast and in general comprises three stages namely, carboxylation, reduction and regeneration (Bassham *et al.*, 1950). CO_2 diffuses through the stomata and makes its journey all the way to the stroma of chloroplast in order to react with ribulose 1,5-bisphosphate (RuBP) which is catalyzed by Rubisco to generate the 3-carbon intermediate 3-phosphoglycerate. This intermediate will be reduced to 3-carbon triose phosphates by enzymatic reactions driven by the photochemically generated ATP and NADPH from the light-dependent reactions. Finally the cycle regenerates RuBP molecules to start the carboxylation process all over again. Since Rubisco can have both carboxylase and oxygenase activities (Farquhar *et al.*, 1980), it is crucial to maintain a high CO_2 concentration around it to promote carboxylation and this is generally achieved through stomata aperture control (Casson and Hetherington, 2010) and mesophyll conductance (Evans *et al.*, 2009). Otherwise the oxygenase reaction of Rubisco will initiate the undesirable (in terms of crop production) photorespiratory pathway involving two other organelles namely peroxisomes and mitochondria (Fig. 1.3 A).

Photosynthesis occurs at the cellular level and involves a number of biochemical processes. However, despite developing an increasingly detailed picture of photosynthetic mechanisms, research has so far failed to deliver any real gains via improving the basic machinery that have given increased crop yields (Fereres and Connor, 2004). One of the most obvious targets to enhance photosynthesis is by engineering Rubisco, the key photosynthetic enzyme responsible for CO_2 fixation. The photosynthetic rate of many C_3 crops (such as rice) is limited by the activity of Rubisco which also has an affinity to oxygen that initiates the apparently wasteful photorespiration process (Sharkey, 1988). Various attempts to improve photosynthetic efficiency through

Rubisco optimization have shown little progress so far (Andrews and Whitney, 2003; Whitney *et al.*, 2011).

Undoubtedly photosynthesis is influenced by a range of environmental factors such as light, ambient CO₂ concentrations and temperature, as well as indirect influences (mediated through stomatal control) to other environmental factors such as humidity and soil moisture (Taiz and Zeiger, 2010a). The dependence of photosynthesis on environmental factors is very significant to farmers and agronomists because crop yield depends strongly on prevailing photosynthetic rates in an ever changing environment. On the other hand, the efficiency of photosynthesis in response to the environment is strongly influenced by leaf physical components such as stomata and the constituent cellular architecture, which are themselves responsive to these same environmental factors.

1.2.1 The role of stomata and improvements in photosynthesis

The major focus of this study is stomata, microscopic pores on the aerial part of terrestrial plant surfaces. The movement of stomata (opening and closing) regulates the exchange of external CO₂ for internal O₂ and water evaporation (transpiration). Fundamentally, a stoma comprises two guard cells, a pore and underlying airspace (sub-stomatal chamber). The morphology of guard cells are used to classify stomata into two broad classes (Evert, 2006) namely dumbbell-shaped stomata (typical of grasses such as rice, Fig. 1.4 A) and kidney-shaped stomata (in other C₃ species, Fig. 1.4 B). Stomata have a very important role in leaf physiology in balancing the need for photosynthetic CO₂ uptake against the need to control water loss through transpiration. Evaporation of water from stomata promotes leaf cooling thus transpiration is thought to be important in maintaining leaf temperature within an optimal range (Mahan and Upchurch, 1988) This is important for photosynthesis to take place efficiently because this greatly affects the enzymatically catalysed reactions, as well as membrane processes in photosynthesis (Lambers *et al.*, 2008). Particularly in C₃ plant species such as rice, high temperature has a significant effect on the kinetic properties of Rubisco whereby the affinity for CO₂ decreases more rapidly than that for O₂ (Atkin *et al.*, 2006). Furthermore,

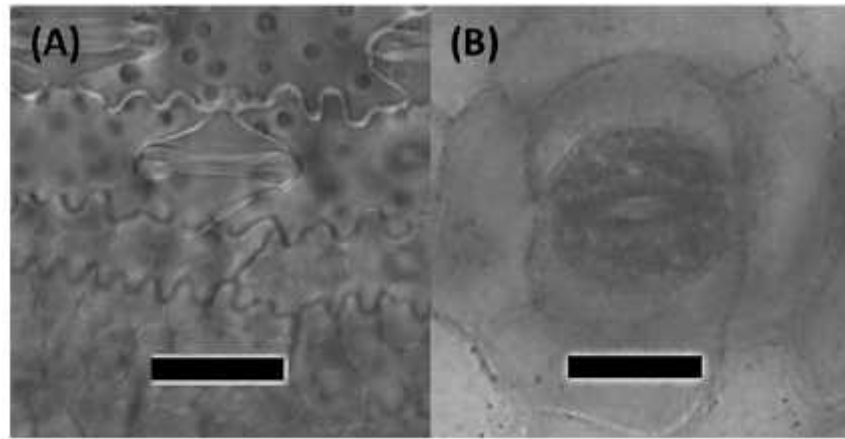


Figure 1.4: Stomatal shape comparison between dumbbell-shaped rice stoma (**A**- typical of grass) and kidney-shaped stomata in *Aglaonema sp.* (**B**- typical in other C₃ plant species). Scale bars equal 30 μ m. (Yaapar, unpublished).

at high temperature the solubility of CO₂ declines more strongly than does that of O₂ (Warren 2007).

The combined elevated temperature effects on CO₂ solubility and Rubisco affinity lead to the increase in photorespiration, a process that reduces the efficiency of photosynthesis in C₃ plants such as rice. Even so, photorespiration at the same time protects the photosynthetic apparatus under stress conditions. Reactive oxygen species (ROS) molecules are generated to regulate acclimation response to stress (Apel & Hirt 2004). Photorespiration helps minimise ROS production by directly or indirectly using ATP and NADPH. CO₂ limitation in the CB cycle (to use excess ATP) and lack of NADP⁺ or other acceptors in photosystem I (PSI) will lead to generation and accumulation of ROS that must be discarded (Spinola *et al.*, 2008).

In addition, net photosynthesis has been conventionally analysed in terms of stomatal and non-stomatal limitations (Jones, 1985; Ni and Pallardy, 1992). Stomatal limitation results from the resistance to CO₂ diffusion into intercellular spaces while the non-stomatal limitation is often assumed as a metabolic constraint. Farquhar and Sharkey (1982) proposed an analysis of the response between the net CO₂ assimilation rate and internal CO₂ concentration (C_i) in order to study these two limitations separately. In this concept, stomatal conductance (g_s) is a useful parameter in studying C₃ plant photosynthesis. g_s

(the inverse of stomatal resistance) is a measurement of the flux of H₂O and CO₂ through the stomata, in and out of the leaf (Farquhar and Sharkey, 1982). Since CO₂ and water share the same stomatal entry pathway, this presents the plant with a functional dilemma, optimizing CO₂ uptake while minimizing substantial water loss. After diffusing through the boundary layer on the leaf surface, the stomatal pore is the main port of entry for CO₂ into the leaf's interior. At this point, stomatal conductance/resistance will determine the amount of CO₂ that diffuses into the leaf. The relationship between stomatal size and density can be expressed in terms of g_s . and can be mathematically obtained (for maximum possible g_s) from a model by Franks and Farquhar (2001):

$$g_s = \frac{S_{density} \cdot D \cdot S_{pore}}{V(S_{depth} + \frac{\pi}{4} \sqrt{\frac{S_{pore}}{\pi}})}$$

Equation 1.1

Where g_s is stomatal conductance to water vapour (minus boundary layer), $S_{density}$ = stomatal density (m⁻²), D = diffusivity of water in air (m²s⁻¹), S_{pore} = stomatal pore area, V = molar air volume (m³ mol⁻¹), S_{depth} = stomatal pore depth (m) and π = 3.142. From this, Franks and Beerling (2009) further proved using fossil samples that high densities of small stomata were the only way to attain the highest g_{smax} values required in order to counter two major drops in ancient atmospheric CO₂ concentrations (from about 3000ppm to 1000ppm) which occurred during Permo-Carboniferous (300-350 million years ago) and Cenozoic glaciations (100 million years ago). This is possible because stomatal diffusivity is inversely proportional to the distance a gas has to travel through the S_{pore} . This value increases with guard cells pair length as they inflate forming an approximately circular aperture.

Interestingly, it has been shown in rice that stomatal conductance is strongly correlated with leaf photosynthesis (Hirasawa *et al.*, 1988). For instance, the *indica* rice variety Takanari is known for its higher grain yield and dry matter

accumulation (Xu *et al.*, 1997). Taylaran *et al.* (2011) reported that the high-yielding capacity possessed by Takanari was linked to a higher stomatal conductance that was responsible for a high leaf photosynthetic performance. However, it is still unclear whether stomatal conductance alone is the dominant factor that limits photosynthetic rate since other forms of conductance such as boundary layer, intercellular air space and mesophyll are also present (Kusumi *et al.*, 2012).

It is worth noting that getting CO₂ into the leaf via improved conductances (stomata, mesophyll *etc.*) only partially influences photosynthesis since other factors such as leaf nitrogen and Rubisco enzyme content are more dominating (Makino, 2003; Makino 2011) thus g_s can be thought of as a co-dominating factor that correlates to photosynthesis. In fact Rubisco specific activity is significantly different between rice and wheat. In wheat, Rubisco K_{cat} is greater than rice (about 50% higher V_{max} for carboxylation) but rice has lower K_m (about 20% lower K_m for CO₂) (Makino *et al.*, 1988). Moreover the specific activity of Rubisco in rice is significantly lower than many other higher plants as well (Table 1 in Makino, 2003). However Rubisco kinetic properties cannot be a target for classic breeding among rice cultivars because no variability has been found among old and modern rice cultivars (Makino *et al.*, 1987).

1.3 Understanding the rice leaf

1.3.1 General Morphology

In rice, the phytomer concept is used to describe repeating units of vegetative growth. A phytomer comprises a leaf subtended by an internode. A tiller bud is present at the lower end of the internode and a root band is present at both the upper and lower end of the internode (Fig. 1.5). A rice node includes the nodal plate as well as the base of the internode above it that bears the next higher leaf.

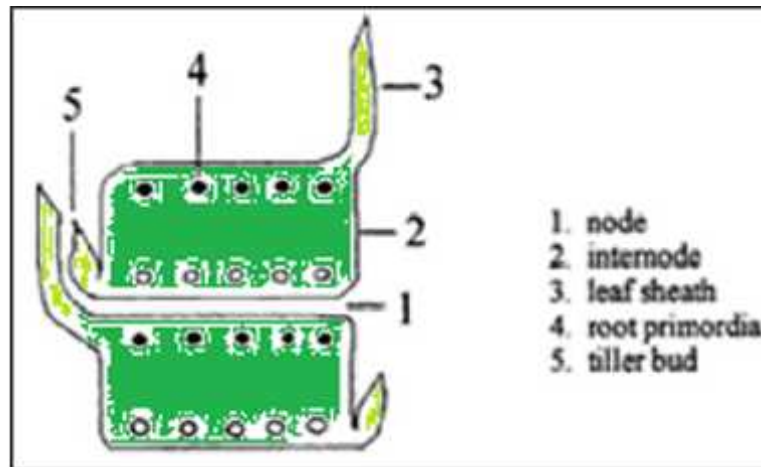


Figure 1.5:

A rice phytomer unit comprises one internode, a node, emerged leaf, tiller bud and root primordia. (Based on a drawing by Hoshikawa, 1989).

On a rice stem or culm, rice leaves are borne alternately on opposite sides. Each leaf consists of two parts, a lower leaf sheath and an upper lamina (leaf blade) (Fig. 1.6 A). These regions are connected by a joint known as the collar. The collar bears a pair of auricles (ears) and a ligule (tongue), protrusions from the leaf surface (Fig. 1.6 B). These structures at the joint are commonly used to distinguish between rice varieties and other grasses (Moldenhauer and Gibbons, 2003). For example, the ligule of *O. sativa* is long and soft but it is short and tough in *O. glaberrima* (OECD, 2006).

The leaf sheath is attached to the nodal plate. It wraps around the culm and has a slight swelling just above the node referred to as the sheath pulvinus (Fig. 1.6 C). The sheath is photosynthetically active and encloses both the developing new leaves and the panicle (the terminal shoot of a rice plant that produces grain). During vegetative growth the sheath provides support to the plant and acts as a storage site for starch and sugar (Moldenhauer and Gibbons, 2003). During the reproductive stage of development it mechanically supports the stem by contributing 30-60% toward shoot breaking strength (Chang, 1964).

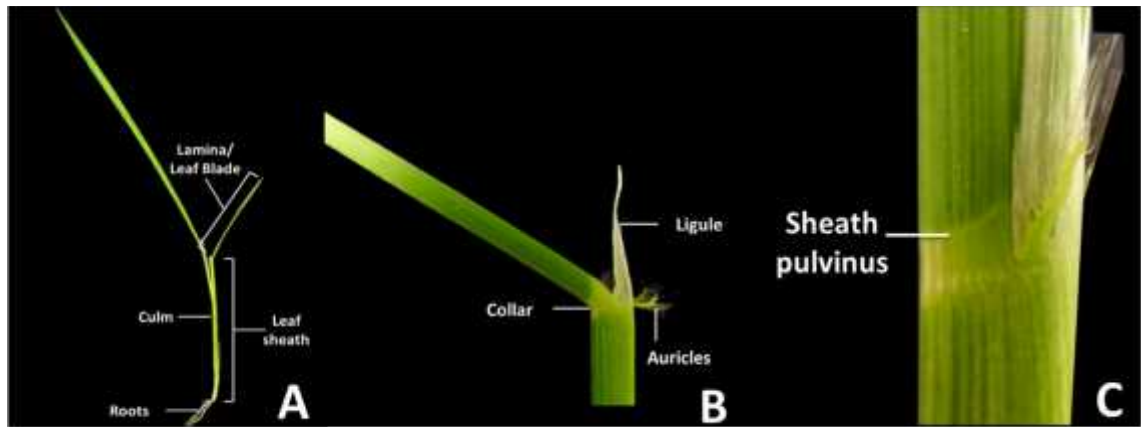


Figure 1.6: Rice leaf and its component structures. **(A)** Culm and leaf sheath; **(B)** Collar, a pair of auricles and ligule; **(C)** Sheath pulvinus.

The lamina in general is flat and lanceolate in shape and provides the main area for light absorption and photosynthesis. Many parallel veins run along the upper surface of the blade with a prominent midrib on the underside of the leaf. Different rice varieties vary in terms of blade length, width, thickness, area, color, angle and pubescence (the presence of cover with fine, soft and short hairs). Some of these characters have been selected by the breeders to ease work in rice fields. Genetically, there is variation for leaf length and width among cultivars (Jennings *et al.*, 1979). The length of the entire leaf (sheath and lamina) also increases with successively higher position on the main culm (Hoshikawa, 1989).

1.3.2 Leaf anatomy

The rice leaf has a classic arrangement of a monocot leaf in which a regular array of parallel veins occurs. A transverse section of a rice leaf shows that it has both small (SV) and large vascular bundles (LV), with the latter occurring approximately once for every six smaller bundles. Each vein is enclosed in a well-defined bundle sheath (BS) that is linked to both the upper and lower epidermis by fibrous bundle cells (Evans and Caemmerer, 2000).

The rice leaf possesses a specialized type of epidermal cell called bulliform or motor cells (BC). Located between the vascular bundles on the adaxial epidermis, they function to control the rolling of the lamina (Fig. 1.7). Under

conditions of water deficit they lose turgor and constrict, causing the lamina to fold or roll inward (Dickison, 2000). They have large vacuoles and little or no chlorophyll (Mishra, 2009). Stomatal files in rice are located next to the veins on the leaf surface. In addition, the rice leaf has two kinds of trichomes, namely micro and macro hairs. Micro hairs are located along the stomatal files or besides bulliform cells while macro hairs are located on silica cells over a thin vascular bundle (Kobayashi *et al.*, 1997).

The rice leaf is generally thinner (about 75µm for IR64 when grown under high-light condition, Narawatthana, 2013) compared to *Arabidopsis* (about 210µm for Col-0 when grown under high-light conditions, Wuyts *et al.*, 2012). There is no mesophyll cell differentiation into palisade and spongy parenchyma, thus there is no remarkable distinction between the adaxial and abaxial sides (Lafitte and Bennett, 2002). In dicots the internal mesophyll cells are polarized in which the closely packed palisade cells are below the adaxial epidermis and loosely packed spongy cells border the abaxial epidermis (McConnell and Barton, 1998). In rice and some grasses like maize, there is a uniform configuration without polarization, which is termed isobilateral mesophyll (Fahn, 1990).

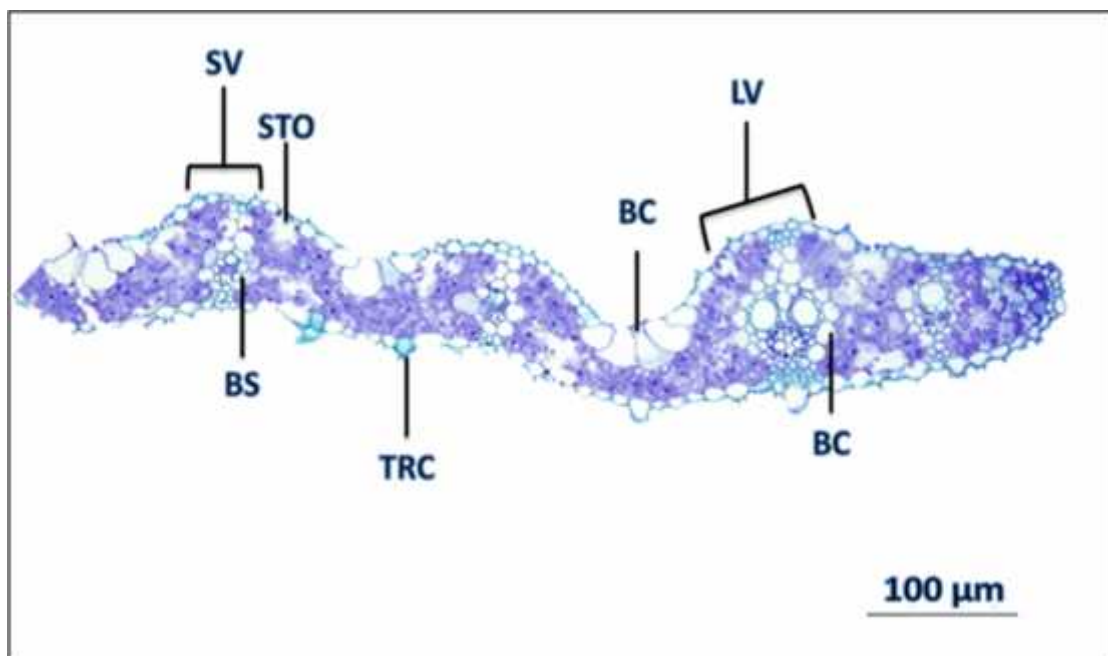





Figure 1.7: Transverse section of a rice leaf. (LV) large vascular bundle; (SV) small vascular bundle; (BS) bundle sheath cell; (BC) bulliform cell; (TRC) trichome; (STO); substomatal chamber.







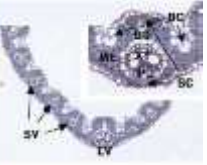
1.3.3 Leaf development in rice

The staging of rice leaf development is mainly described by Itoh *et al.* (2005) and this is summarized below. In defining leaf development it is common to use the plastochron as a unit of developmental time. A plastochron is defined as the interval between two successive leaf initiation events at the shoot apical meristem (SAM). This allows leaves to be allocated a plastochron number (Pi) which defines a specific developmental stage. Table 1 summarizes the staging of adult leaf development in rice.

Table 1.1:

Staging of adult leaf development in rice. I1, Incipient primordium; P1-P6, Plastochron 1-6; (Table is adapted from: <http://www.shigen.nig.ac.jp/rice/orzabase/development/search.jsp>)

Stage	Name	Events and Descriptions	Figures
I1	Formation of leaf founder cells	Recruitment of leaf founder cells to become leaf primordium but not distinguishable morphologically from other cells in the SAM. Can be detected with the expression of gene <i>OsPNH1</i> (<i>OryzasativaHOMEBOX1</i>) (Nishimura <i>et al.</i> 2002). Leaf founder cells are distributed in a half-ring fashion around the SAM.	 <p>Blue region (left) and arrowhead (right) indicate a group of founder cells.</p>
P1	Formation of leaf primordium	Protrusion of primordium on the flank of the SAM or crescent-shaped primordium. Elongation of leaf margin around SAM.	 <p>Crescent-shaped primordium (left) and P1 is marked with a blue.</p>
P2	Hood-shaped primordium	Hood-like shape. Overlapping of two margins. Differentiation of vascular bundle.	 <p>P2 is marked with blue (left). SA, shoot apical meristem.</p>

P3	Formation of ligule primordium	<p>Formation of ligule primordia and (mainly) leaf blade/sheath boundary.</p> <p>The leaf margins overlap and completely enclose the SAM.</p> <p>Differentiation of sclerenchymatous cells.</p> <p>Initiation of epidermal specific cells and small vascular bundle formation occur basipetally.</p>	  <p>Arrow indicates blade sheath boundary</p>
P4	Rapid elongation of leaf blade	<p>Differentiation of epidermal specific cells (bulliform cells, silica cells, cork cells and stomata).</p> <p>Elongation of leaf blade due to the high activity of intercalary meristem at the base of lamina (Kaufman, 1959).</p>	 
P5	Rapid elongation of leaf sheath	<p>Elongation of leaf sheath.</p> <p>Emergence of leaf blade from the sheath of preceding leaf.</p> <p>Formation of lacunae and the maturation of leaf epidermal cells</p>	 <p>Cross section around shoot apex; asterisk, lacuna.</p>
P6	Maturation	<p>Bending of leaf blade at the lamina joint (collar) signifies leaf maturity and complete growth.</p>	  <p>Mature leaf (left); Cross-section of a leaf (right); LB, leaf blade; LG, ligule; AU, auricle; LJ, lamina joint; LS, leaf sheath; LV, large vascular bundle; SV, small vascular bundle; SC, sclerenchymatous cell; phloem; XY, xylem; BS, bundle sheath cell; BC, bulliform cell;</p>

1.3.4 Stomatal development

As mentioned in Fig. 1.4, stomata occur in two classes namely dumbbell (as in rice) and kidney-shaped (as in *Arabidopsis*). Each form follows a unique developmental series and distribution pattern. Despite this, in general both systems involve asymmetric and symmetric cell divisions of specialized epidermal cells. In both types the process is initiated by the asymmetric division of a protodermal cell (Fig. 1.8B), that gives rise to a meristemoid, which is a transient cell state of the stomatal lineage. A meristemoid then proceeds to differentiate into a guard mother cell (GMC) that eventually undergoes a single symmetric division to produce a pair of guard cells (GCs). This is only a simplified explanation for both stomatal developmental systems, with each having its own elaborate characteristics for every transitional state until maturity (reviewed by Bergmann and Sack, 2007 and described below). Even though both systems share a basic common ground in stomatal development, the leaf in *Arabidopsis* is not clearly zoned. The more mature stomata are located within the tip region but this is not absolute since sister cells of a stomata precursor can undergo division later in time. This intercalates newly formed stomata among stomata that have been previously formed. In rice, the leaf is strongly zoned so that the base is the youngest and in this cell proliferation zone the epidermal files that can later form stomata are established (Liu *et al.*, 2009).

Much of our understanding about stomatal development comes from the studies using the model dicot plant *Arabidopsis thaliana*. In this plant, the stomatal lineage begins with a subset of protodermal cells becoming a meristemoid mother cell (MMC – Fig. 1.8B- light blue). The MMC undergoes an asymmetric division, producing a small meristemoid (Fig. 1.8B- yellow oval) within a large sister cell (irregular white shapes) called a stomatal-lineage sister cell. The meristemoid undergoes a cell-state transition to produce a GMC and it divides once symmetrically to produce a pair of GCs. Specialized GCs work in concert to control stomatal opening and they cease division. Liu *et al.* (2009) also proposed the sites of action of three important regulators that direct sequential stomatal development steps seen in *Arabidopsis* (Fig. 1.9A).

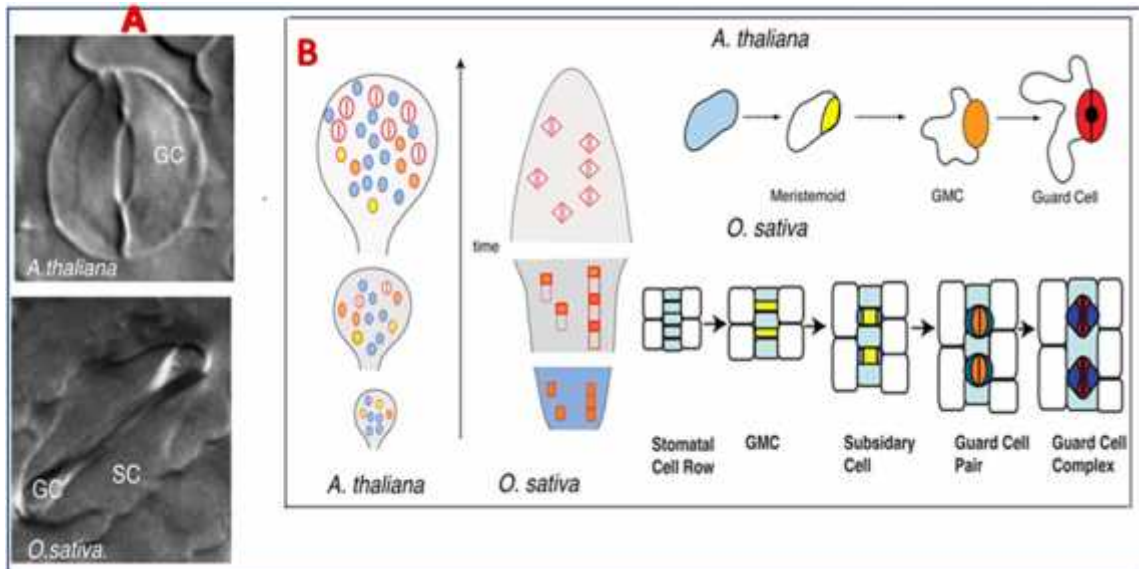


Figure 1.8:

Key differences in morphological and developmental pattern between *Arabidopsis thaliana* (dicot) and *Oryza sativa* or rice (monocot) stomata. **(A)** Kidney-shaped stoma of *Arabidopsis* and dumbbell-shaped stoma of rice. **(B)** Stomata distribution and developmental pattern in *Arabidopsis* (top) and rice. GMC (orange oval in *Arabidopsis*, yellow block in rice); SC (small dark blue block in rice); GC (red kidney in *Arabidopsis*, red dumbbell in rice). Figure adapted from Liu *et al.* (2009).

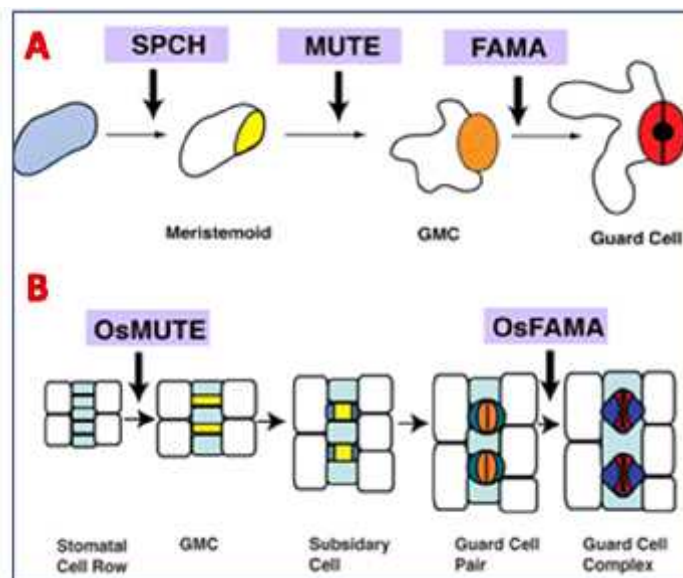


Figure 1.9:

Schematics of comparison between stomatal development in *Arabidopsis* **(A)** and rice **(B)** with proposed sites of expression of three closely related bHLH transcription factors *SPCH*, *MUTE* and *FAMA*. In rice, it is proposed that the action of *SPCH* would occur before the stomatal cell row stage. Figure adapted from Liu *et al.* (2009).

These three positive regulators are the closely related basic helix-loop-helix (bHLH) domain transcription factors namely *SPCH* (*SPEECHLESS*), *MUTE* and *FAMA* (MacAlister *et al.*, 2007). *SPCH* controls the initial asymmetric division of protodermal cells, giving rise to the stomatal lineage namely meristemoid. Later, *MUTE* is required to set GMC fate from the meristemoid stem cell. Eventually, *FAMA* controls the symmetric division of the GMC into a pair of guard cells (Ohashi-Ito and Bergmann, 2006).

In rice, stomatal development occurs in a more fixed manner (specific epidermal files) compared to the scattered patterning seen in *Arabidopsis*. Generally, stomatal development in rice can be divided into five stages (Stebbins, 1960) and the stomata in rice start as a row of cells, known as a stomatal cell row (Fig. 1.8B- light blue shading). These rows can be adjacent but are normally separated by non-stomatal epidermal cell rows. This stomatal cell row undergoes cell division to produce stomatal precursors, which undergo asymmetric division to produce GMCs (Fig. 1.8B- yellow blocks). GMCs induce the neighboring cells to produce subsidiary cells (SCs) (Fig. 1.8B- small dark blue blocks). Later GMCs divide symmetrically to produce a pair of GCs that undergo extensive elongation and morphogenetic changes as they mature (Fig. 1.8B, small red dumbbells). Each stomatal complex (Fig. 1.10) comprises two GCs that are narrow with thickened walls and two subsidiary cells flanking the guard cells.

Even though morphology and ontogeny between *Arabidopsis* and rice stomata are reasonably different, the protein sequences of the switches (*SPCH*, *MUTE* and *FAMA*) that control major cell fate transition during stomatal development are highly conserved between these two angiosperms groups. However, their functions, especially for *MUTE*, *SPCH1* and *SPCH2*, are somewhat divergent (Liu *et al.*, 2009). In *Arabidopsis*, the functions of *SPCH* and *MUTE* are largely tied to the initiation and termination of the stem cell-like division in meristemoids but in grasses it is hypothesized that the activity of *OsMUTE*

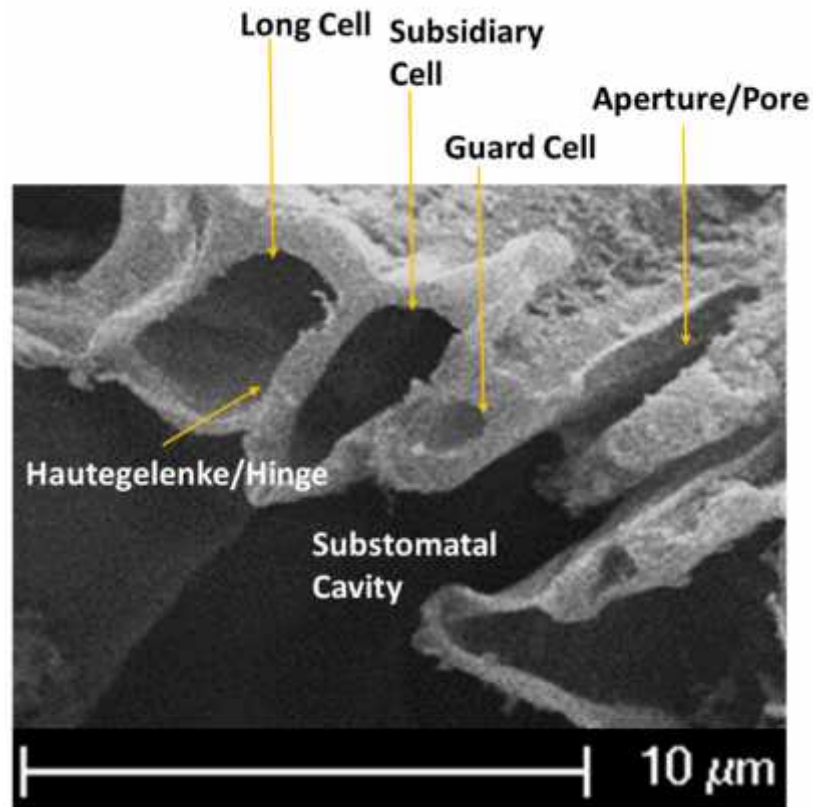


Figure 1.10: SEM micrograph of a mature stomatal complex cross section in rice and its associated microstructures (Yaapar, unpublished)

could be a hybrid between that of *Arabidopsis* SPCH and MUTE (Fig 1.9B). There is evidence that OsMUTE is expressed during early stages in which stomatal files are forming (MUTE in *Arabidopsis* is expressed in later stages where meristemoids have formed). On the other hand, FAMA function is conserved between dicots and monocots despite their different stomatal morphologies.

Despite the progress made in elucidating the molecular control of stomatal differentiation, there are still many blanks to be filled in, especially involving rice, the C₃ model as well as *Setaria* sp. the C₄ model for monocot plants. For example, it is still unknown when SPCH is expressed in rice, although it has been proposed by Liu *et al.* (2009) that the action of SPCH would occur before the stomatal cell row stage (Fig. 1.9). Furthermore, research in *Arabidopsis* has confirmed the presence of integrators SCREAM (SCRM) and SCRM2, two bHLH proteins that work along with SPCH, MUTE and FAMA by promoting all three cell-state transitions (Hunt and Gray, 2009). The current model suggests

that the heterodimerization of SCRM/SPCH enhances activation of stomatal lineage entry but the specific mechanism underlying heterodimer stabilization still remains unclear, even in *Arabidopsis* (Kanaoka *et al*, 2008). This shows that much more extensive work is required to also elucidate the stomatal three-cell state transitions in grasses.

1.4 Environmental signals affect leaf and stomatal development

Many of the key developmental events of a plant's life cycle such as germination and leaf formation, are regulated by environmental signals such as temperature and light. Undoubtedly genetic control plays the most important role in determining leaf size, structure and shape but these parameters are flexible to a certain degree. This is because leaves are able to tailor their growth based on environmental conditions (Tsukaya, 2006).

1.4.1 Light as a stimulus

Light is one of the most important environmental factors that regulates the development of the photosynthetic apparatus in vascular plants. In a high light or low light environment, plants develop sun or shade leaves, respectively (Boardman, 1977). The extent to which a particular species can alter its phenotype in response to growth in different environments, or respond to a change in environment is known as phenotypic plasticity and the processes by which this occurs is known as acclimation. Generally, high-light responses occur to maximize light-saturated rate of photosynthesis whilst low-light responses occur to optimize photon capture. This is reflected in the general fact that sun leaves are thicker, smaller, with more developed palisade tissue and higher stomatal density on both adaxial and abaxial surfaces when compared with shade leaves (Anderson and Osmond, 1987; Murchie and Horton, 1997). (A more detailed discussion of the characteristics of sun and shade leaves is provided in Chapter 3.)

In addition, irradiance levels also affect stomatal density. It has been shown in *Arabidopsis* that a high light environment received by the older leaves will

result in greater stomatal density on both adaxial and abaxial sides of a newly formed leaf (Coupe *et al.*, 2006). This phenomenon shows that stomatal density is one of the contributing factors that explains why high-light grown leaves possess higher photosynthetic capacity. In a recent experiment, Tanaka *et al.* (2013) demonstrated that increased stomatal density in *STOMAGEN*-overexpressing *Arabidopsis*, enhanced the photosynthetic rate by 30%. The *STOMAGEN* gene encodes a small peptide with a putative secretory signal sequence at its N-terminus and is expressed preferentially in mesophyll cells and is a positive regulator of stomatal development in *Arabidopsis*. Even though higher photosynthesis generally results from higher g_s , this is not translated into efficient water use because *STOMAGEN* overexpression did not increase whole plant biomass, although its silencing did cause a reduction in biomass. In their work, Tanaka *et al.* (2013) showed that improved photosynthetic capacity, through higher stomatal density, can be achieved by modulating the gas diffusion process in the leaf. This is regarded as a potential trait for plant engineering in order to improve photosynthesis.

Despite these promising findings, the relationship between stomatal characteristics, photosynthesis and yield for rice has yet to be established (Kundu and Tigerstedt, 1999; Miskin *et al.*, 1972). Low stomatal density in rice has been shown to be attainable only when low irradiance level is coupled with elevated CO₂ but low-irradiance conditions alone, is adequate to produce small stomata (Hubbart *et al.*, 2003). Moreover, the effect is more prominent on the adaxial surface thus validating a previous publication (Zhang *et al.* 2009) and such specific abaxial-adaxial-stomatal response has been shown in *Arabidopsis* (Lake *et al.*, 2002) and common bean (Wentworth *et al.*, 2006) as well. Since high and low light-grown rice leaves will produce sun and shade leaves respectively, it is hypothesized that stomatal distribution and size should vary accordingly to photosynthetic capacity. These stomatal characters are believed to be set during development by the irradiance level received by older leaves, although the exact developmental stages at which these characters are determined is still unknown. Nevertheless it is worthwhile mentioning that developmental and dynamic acclimation are distinct processes (Athanasidou *et al.*, 2009). Dynamic acclimation is especially important in determining the fitness of plants growing in changing environments, for

example, their ability to change the photosynthetic capacity of developed leaves. Developmental acclimation involves changes in leaf morphology and composition (for example stomata which are the focus in this study) being optimized for the conditions (for example low or high light) experienced by plants. Thus measurements made reflect conditions experienced as the leaves develop.

1.4.2 Systemic signalling and stomatal development

Ferjani *et al.* (2008) summarized in their review, that leaf differentiation into sun or shade types is regulated remotely by mature leaves via long-distance signaling. They also highlighted that light quantity is the major stimulus, triggering a systemic signal that controls leaf development. They suggest that the known photoreceptors such as phytochromes, cytochromes and phototropins are probably not involved in the signal perception leading to sun and shade leaves. The exact light sensory mechanism is still unknown but several candidate signals have been considered (Karpinski, 1999; Koch, 2000, 2004). The work by Murchie *et al.* (2005), using the fifth leaf in rice as a model system, showed that rice grown in a low irradiance ($200 \mu\text{mol m}^{-2} \text{s}^{-1}$) environment and a high irradiance ($1000 \mu\text{mol m}^{-2} \text{s}^{-1}$) environment would produce sun/shade leaves respectively whereby sun-type rice leaves had thicker leaves, higher light-saturated rates of photosynthesis (P_{max}), higher amounts of Rubisco protein, and a lower chlorophyll a/b ratio. However, photosynthetic acclimation is limited by leaf age. For instance transfer from low to high light during full leaf extension only altered chlorophyll a/b but not Rubisco protein content.

The development of stomata relies on many exogenous and endogenous signals including light, CO_2 , temperature, water availability, abscisic acid content and the activities of cellular regulatory proteins and RNAs (Bergmann and Sack, 2007; Kwak *et al.*, 2008;). However, much of the work done has used *Arabidopsis* as the model plant, thus detailed information in rice or grass for that matter is still lacking. For example, a stomatal density study by Coupe *et al.* (2006) demonstrated that when mature *Arabidopsis* leaves were given

high or low light treatment, the young, developing leaves that were not receiving the treatment grew with stomatal density as if they were exposed to the treatment. They found that mature leaves that received high light treatment resulted in a newly formed leaf with higher stomatal density on both adaxial and abaxial surfaces. *Arabidopsis* leaf stomatal density is lower on the adaxial surface but in rice the stomatal density is believed to be about the same on both sides of the leaf since the leaf grows in an erect position. Moreover it has been shown in rice that the alteration of stomatal properties (size and density) is one of the strategies in acquiring photoacclimation through systematic signalling generated in mature leaves (Hubbart *et al.*, 2013). Interestingly, both irradiance levels and CO₂ concentrations affect stomata differently in rice where low-light condition produces smaller stomata than high-light condition but when coupled with higher CO₂ environment this effect is attenuated. Similarly for stomatal density where under low-light condition it is lower than high condition only when higher CO₂ environment is introduced. This suggests that there is a complex interactions at play to confer the most beneficial stomatal morphology in rice acclimation.

1.5 Research project outline

1.5.1 Aims

1. Characterise the pattern of stomatal differentiation in rice leaves grown under different levels of irradiance.
2. Investigate the outcome of irradiance-induced altered stomatal patterning on rice leaf photosynthetic performance.
3. Identify the stages of rice leaf development during which altered irradiance can influence stomatal patterning.
4. Investigate the outcome of developmental-stage specific altered stomatal patterning on rice leaf photosynthetic performance
5. Develop a whole mount *in situ* hybridisation method for the analysis of gene expression in rice leaves with the ultimate aim of

characterising stomatal gene expression during early rice leaf development.

1.5.2 Overarching hypotheses

1. There is a specific phase in development when a rice leaf can respond to altered irradiance by altering stomatal patterning, leading to altered stomatal density and size in the mature leaf.
2. Altered stomatal properties in in the mature rice leaf alters leaf photosynthetic performance.
3. Whole-mount *in situ* hybridisation can be used as a rapid and reliable method to study stomatal gene expression.

Chapter 3 Aims

1. Characterise the pattern of stomatal differentiation in rice leaves grown under different levels of irradiance.
2. Investigate the outcome of irradiance-induced altered stomatal patterning on rice leaf photosynthetic performance.

Chapter 4 Aims

1. Identify the stages of rice leaf development during which altered irradiance can influence stomatal patterning.
2. Investigate the outcome of developmental-stage specific altered stomatal patterning on rice leaf photosynthetic performance

Chapter 5 Aims

1. Develop a whole mount *in situ* hybridisation method for the analysis of gene expression in rice leaves with the ultimate aim of characterising stomatal gene expression during early rice leaf development.

CHAPTER 2

MATERIALS AND METHODS

2.0 Materials and Methods

The basic methods used throughout this thesis are described below. The experimental design (replication, randomization variation in conditions and statistical analysis) of individual experiments is given in each chapter.

2.1 Plant materials and growth conditions

Seeds of *Oryza sativa* L spp *indica* variety IR64 were grown in either a high irradiance (HL, 750 $\mu\text{mol m}^{-2} \text{s}^{-1}$) or a low irradiance (LL, 250 $\mu\text{mol m}^{-2} \text{s}^{-1}$) environment in a growth cabinet (Convion Ltd, Winnipeg Manitoba, Canada, model BDR 16) with a 12 h photoperiod. Irradiance was provided by 48 fluorescent bulbs (Master TL5 HO SUPER 80 39W/840 SLV) and 12 tungsten incandescent bulbs (Standard 60W A55 FR 2CT). The relative humidity (RH) and temperature were kept constant at 55% and 28°C respectively with ambient CO₂ (~ 400 ppm). The rice variety IR64 was chosen as part of the work in this thesis was based on that of Narawatthana (2013).

Rice seeds were sown in plastic dishes lined with water-soaked paper towel and sealed with perforated parafilm. After 5 days the seedlings were transferred to a hydroponics system (Figure 2.1). Each seedling was inserted into an eppendorf tube (where the bottom had been removed) to contain and support the rice seedling. The eppendorf tubes were then suspended around the edges of 3 L hydroponic tanks and the centre of which was covered with black plastic sheeting. The hydroponic tanks were filled with nutrient solution following the recipe of Narawatthana (2013) (Table 2.1). The nutrient solution was made up using deionized water and was adjusted to pH 5.9 using 10% KOH. The nutrient solution was topped up every one or two days and completely changed every seven days to maintain the optimum pH environment in the system.

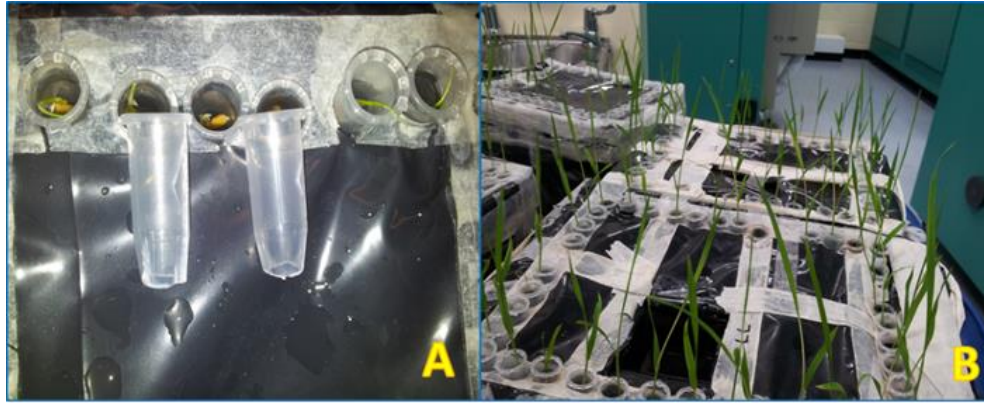


Figure 2.1:

Image of the rice hydroponic system **(A)** Eppendorf tubes with the base removed and **(B)** rice seedlings suspended around the edge of the hydroponic container.

Table 2.1: Composition of the nutrient solution used in the hydroponic system (Narawatthana, 2013). Solutions 1, 2 and 3 were prepared separately before being mixed and diluted with water to the final concentration to prevent precipitation. Each mineral solution was prepared from stock solutions kept at room temperature and each preparation for hydroponic solution usage was made fresh and never kept for more than one week. BDH (BDH Merck Ltd.); Fisher (Fisher Scientific UK Ltd.); Fisons (Fisons Plc.); Fluka (Fluka-Sigma-Aldrich Co. LLC).

Solution	No.	Source	Chemical Formula	Main Elements	Molecular Mass	Final concentration (mM)
1	1	BDH	NH_4NO_3	N	80.04	1.4
	2	Fisher	$\text{NaH}_2\text{PO}_4 \cdot 2\text{H}_2\text{O}$	P	156.01	0.6
	3	Fluka	K_2SO_4	K	174.27	0.5
	4	Fisher	$\text{MgSO}_4 \cdot 7\text{H}_2\text{O}$	Mg, S	246.98	0.8
	5	BDH	$\text{MnCl}_2 \cdot 4\text{H}_2\text{O}$	Mn	197.9	0.009
	6	Fisons	$(\text{NH}_4)_6\text{Mo}_7\text{O}_{24} \cdot 4\text{H}_2\text{O}$	Mo, N	1235.86	0.0001
	7	Fisons	H_3BO_3	B	61.83	0.09366
	8	Fluka	$\text{CuSO}_4 \cdot 5\text{H}_2\text{O}$	Cu, S	249.7	0.003675
	9	Fluka	$\text{ZnSO}_4 \cdot 7\text{H}_2\text{O}$	Zn, S	287.56	0.00075
2	10	Fluka	$\text{CaCl}_2 \cdot 2\text{H}_2\text{O}$	Ca	147.02	0.322
3	11	Fluka	Fe-EDTA	Fe	367.1	0.02

2.2 Approximation of leaf developmental stage

Leaf number 5 (L5) was used as the model leaf for all the experiments conducted in this study. Since the shoot apical meristem and early plastochron stages (P1 to P4) of the rice leaf are concealed in the leaf sheaths, leaf number 3 (L3) was used as a proxy in order to make an approximation of L5 developmental stages (before P5) inside the sheaths. This approximation was based on the work and findings of Narawatthana (2013) detailed in Table 2.2.

Table 2.2:

The approximation of L5 plastochron stages based on the length of L3 blades under high and low light conditions.

High Light ($750 \mu\text{mol m}^{-2} \text{s}^{-1}$)		Low Light ($250 \mu\text{mol m}^{-2} \text{s}^{-1}$)	
<u>Leaf 5 Stage</u>	<u>Leaf 3 Length (mm)</u>	<u>Leaf 5 Stage</u>	<u>Leaf 3 Length (mm)</u>
P1	4-20	P1	10-30
P2	25-70	P2	35-75
P3	75-110	P3	80-160
P4	120-140	P4	170-190

L5 was harvested for measurement and analysis when it had fully expanded (about 21 days after sowing (DAS) for HL and 30 DAS for LL) and the leaf collar (a joint between leaf sheath and leaf blade) was visible and bendable. Length was measured from the cut point of the leaf collar to the blade apex using a ruler. The leaf blade was scanned and area was determined from the scanned image using ImageJ version 1.48 software.

2.3 Biochemical and physiological analyses

2.3.1 Measurements of photosynthesis and stomatal conductance

Measurements of photosynthesis and stomatal conductance were made using a portable photosynthesis system (LI-6400XT from LI-COR Inc.). Irradiance was provided by an LED RGB (Red Green Blue) light source (LI-6400-02B, Li-Cor Inc.) that allows irradiance levels to be changed as required. In all experiments the irradiance was composed of 10% blue light (to promote stomatal opening) with the rest red light. The block temperature within the chamber was maintained at 28°C with ambient humidity (55% relative humidity) where the flow was set at 400 $\mu\text{mol s}^{-1}$. CO₂ was provided by a CO₂ cartridge (Umarex®). A CO₂ injection system allowed the CO₂ to be varied by delivering a precisely controlled stream of pure CO₂ into CO₂-free air.

In all experiments and treatments, at least three replicates of leaf no. 5 were randomly selected and measurements were made on the middle portion of the leaf blade. All measurements were made 1 hour after the light came on in the growth chamber at 8.00 am. The clamped leaf was first left to acclimatize using the settings above at an irradiance of 2000 $\mu\text{mol m}^{-2} \text{s}^{-1}$, for at least 15 min, or until the stomatal conductance readings became stable, before starting the experiments.

Two types of gas exchange measurements experiments were carried out. The first was a light response curve (assimilation versus PAR) (chapter 3) in which the CO₂ was set to 1000 ppm (saturating CO₂) while irradiance (PAR, in $\mu\text{mol m}^{-2} \text{s}^{-1}$) was progressively decreased from 2000 to 0 irradiance as follow: 2000; 1750; 1500; 1250; 1000; 750; 500; 350; 200; 150; 100; 50; 25; 0. Once the leaf had reached steady state photosynthesis the experiment was started. The minimum wait time (the time after each irradiance level change that the system will wait, before checking stability to see if it can log the rate of photosynthesis and stomatal conductance) was set at 180s.

The second experiment was an assimilation versus intercellular CO₂ response curve (A-C_i curve) (chapters 3 and 4). Irradiance was set at 2000 $\mu\text{mol m}^{-2} \text{s}^{-1}$ while the CO₂ concentrations (C_a) were increased from 50 to 1600 ppm in a series as follows: 50; 100; 150; 200; 250; 300; 400; 500; 600; 800; 1000; 1300;

and 1600. Again, the minimum wait time after each CO₂ concentration change that the system will wait before logging photosynthesis and stomatal conductance was set at 180s.

Once measurements were complete for either the light response or A-Ci curves, data were analysed to derive a number of different parameters. Curves were fitted to the data for each replicate leaf using software from Landflux.org. The Photosynthetic Light Response Curve Fitting software (version 1.0) was used to analyse the light response curves where parameter estimates were based on fitting a non-rectangular hyperbola following Marshall and Biscoe (1980) and Thornley and Johnson (1990). The A/Ci Curve Fitting software v10.0 (that provides parameter estimates based on both infinite and optimized mesophyll conductance, the later following Ethier and Livingston (2004)), was used to analyse the A-Ci curves.

The following parameters were measured or derived from the light saturation or A-Ci response curves:

1. Apparent quantum yield of photosynthesis (moles of CO₂ fixed per mole of quanta (photons) absorbed).
2. Maximum net assimilation rate (A_{max})
3. Light compensation point (LCP) (the point at which the rate of Rubisco carboxylation equals the rate of respiration + photorespiratory CO₂ release).
4. J_{max} , maximum light- and CO₂-saturated electron transport rate
5. V_{cmax} maximum Rubisco carboxylation rate
6. g_s : stomatal conductance
7. C_i : intercellular CO₂
8. R_d : dark respiration
9. iWUE: Water Use Efficiency (Rate of photosynthesis/stomatal conductance)
10. Relative stomatal limitation (l_s in %) was calculated based on Farquhar and Sharkey (1982)

$$l_s = 1 - \frac{A_{400}}{A_{Ci400}} \times 100$$

Where A_{400} is the assimilation at $C_a = 400\text{ppm}$ while A_{C_i400} is the assimilation when $C_i = 400\text{ppm}$ and these values were obtained from the A-Ci curve.

2.3.2 Pigment quantification

Chlorophyll and total carotenoids were extracted and quantified using a Lambda 40 UV-VIS spectrometer (PerkinElmer Instruments Inc.) A leaf disc (disk area = 12.57 mm^2) was taken from the middle region of each leaf (L5) using a using a 4.0 mm revolving punch plier supported with a paper towel underneath to prevent leaf breakage. One disk per leaf was used for each extraction. For each treatment five leaves were used ($n = 5$). Each leaf disk was placed in an Eppendorf tube and pigments extracted by incubating in $333\text{ }\mu\text{l}$ of 80% ethanol for 15 min at $70\text{ }^\circ\text{C}$. This treatment was repeated three times. The 3 ethanol aliquots containing extracted pigments were then combined (total = $1000\text{ }\mu\text{l}$) in a $10 \times 10 \times 45\text{ mm}$ disposable cuvette (VWR®, Germany). In order to quantify the pigments, absorption was measured at the wavelengths of 665, 649 and 470nm. Quantification of individual pigments was determined using the following equations from Lichtenthaler and Wellburn (1983). The amount of pigments in the leaf was calculated as $\mu\text{g m}^{-2}$ of leaf.

$$C_a = 13.95 A_{665} - 6.88 A_{649}$$

$$C_b = 24.96 A_{649} - 7.32 A_{665}$$

$$C_{x+c} = (1000 A_{470} - 2.05 C_a - 114.8 C_b) / 245$$

* C_a (chlorophyll-a); C_b (chlorophyll-b); C_{x+c} (total carotenoids xanthophylls + carotenes)

2.3.3 Carbon isotope analysis

Carbon isotope analysis of leaf tissue was carried out to evaluate water use efficiency in rice leaves. For each treatment at least five randomly selected leaf no. 5 were used. Leaves were cut into small pieces and dried in the oven at 37°C for at least a week. Approximately 1 mg of dry leaf was obtained and loaded into a standard weight tin capsule ($6 \times 4\text{mm}$ from Sercon Ltd., Cheshire,

UK). Sample and capsule were rolled together and turned into small balls then dropped into a furnace at 1000°C whilst in an oxygen atmosphere. Complete combustion was guaranteed by passing the combustion products through a bed of chromium oxide at 1000°C using a helium carrier gas. The combustion was completed and any remaining sulfur was removed by a 15 cm layer of copper oxide followed by a layer of silver wool. The products were then passed through a second furnace containing copper at 600 °C in which excess oxygen was absorbed and nitrogen oxide was reduced to elemental nitrogen. Water in the system was removed by a trap containing anhydrous magnesium perchlorate. The gas stream was then passed into a gas chromatograph (GC) in which the components of interest were separated (i.e. N₂ from CO₂) and passed into a mass spectrometer where the isotopic species (i.e. ¹²CO₂ and ¹³CO₂) were ionized and separated by mass using a magnetic field. The isotopes were detected separately and from the ratio the level of ¹³C was calculated using ANCA GSL 20-20 Mass Spectrometer (Sercon Ltd., Cheshire, UK).

The results were reported in delta values which are a difference between sample reading and internationally used standard (delta = 0) namely Pee Dee Belemnite (PDB from Sercon Ltd., Cheshire, UK) which comes from a cretaceous marine fossil, *Belemnitella americana* obtained from the Peedee Formation in South Carolina, USA. This material has a higher ¹³C/¹²C ratio than nearly all other natural carbon-based substances; for convenience it is assigned a delta¹³C (δ¹³C) value of zero, giving almost all other naturally-occurring samples negative delta values. δ¹³C was calculated as follow:

$$\delta^{13}\text{C} (\text{‰}) = \frac{(^{13}\text{C}/^{12}\text{C} \text{ of sample}) - (^{13}\text{C}/^{12}\text{C} \text{ of standard})}{^{13}\text{C}/^{12}\text{C} \text{ of standard}} \times 1000$$

Equation 2.1

2.4 Imaging of leaf primordia using scanning electron microscopy

In order to explore the different developmental stages of rice leaves that were hidden inside the leaf sheaths (especially stage P1 - P4), five primordia were dissected using a single edge razor blade and microlance needles (size: 25G

and 30G). Rice leaf primordia were placed in glass vials in a fixative solution containing 4% v/v paraformaldehyde (Thermo Fisher Scientific Inc.), 2.5% glutaraldehyde v/v (Agar Scientific Ltd), 0.5% v/v Tween-20 (Sigma-Aldrich Co.) and 0.2M Phosphate Buffered Saline (PBS) pH 7.4 (Sigma-Aldrich Co.) for 6 hours at room temperature. The glass vials were placed on an orbital shaker (set at 2 RPM). After this the fixative was replaced with two changes of PBS for 30 minutes each. Samples were then dehydrated in an acetone (Fisher Scientific UK Ltd.) series of 5%, 10%, 25%, 40%, 55%, 70%, 85%, 95% and 2 times 100% for 1 hour each at room temperature. Samples were dried using a Polaron critical point dryer (Agar Scientific, U.K). Liquid CO₂ was let into the chamber and flushed several times to replace the acetone. Samples were left to soak in the liquid CO₂ inside the chamber while maintaining the pressure at 800 psi and left for about 30 minutes. The chamber was heated up using circulating warm water and once the chamber's pressure temperature exceeded 1072 psi and 31°C respectively, CO₂ was immediately drained from the chamber as gas, leaving dry samples without causing the physical destruction. Samples were then mounted onto aluminum stubs using black carbon stickers (Agar Scientific, U.K) and sputter coated with gold (Edwards S150B gold sputter coater) in an argon gas atmosphere. Images were obtained using a SEM (Philips XL-20) at an accelerating voltage of 20 kV and processed with embedded XL-20 software.

2.5 Hand sectioning of leaves for measurements of leaf anatomy

Transverse sections of rice leaves were prepared in order to study aspects of leaf anatomy such as thickness, number of mesophyll cells and the size of the vascular system. A 1 cm in length of the middle portion of the leaf blade was fixed in Carnoy's fixative (ethanol: acetic acid (7:1 v/v), Fisher Scientific UK Ltd.) overnight at 37°C. The solution was replaced with fresh Carnoy's fixative and vacuum infiltrated using a water vacuum pump model MZ 2C NT+AK+EK (Vacuubrand, Germany) for 20 minutes.

Styrofoam blocks were used to sandwich the leaf sample to assist even leaf sectioning using single edge razor blade (Fig. 2.5). Single staining using

Toluidine Blue-O (PBS: 0.1M and pH 7.0, Sigma-Aldrich; 0.1% w/v Toluidine dye salt, Gurr, BDH Ltd.) for 15 seconds was employed for thickness and vascular system observations. For mesophyll and bulliform cell observations, leaf sections were further counterstained with Neutral-red (1% w/v, Sigma Aldrich; 50 mL UHP water; one drop of acetic acid glacial, Fisher) for three minutes at room temperature. The leaf section was then rinsed with water and mounted on a glass slide in a transverse manner. Observations of leaf anatomy were made using a Leica epifluorescence-stereo microscope (LEICA-MZFLIII) and photomicrographs were taken with SPOT RT KE slider camera (Model 7.4) attached to HRD100-NIK 1.0x high-resolution digital camera adapter (Diagnostic Instruments Inc.). Images were captured and processed with SPOT Basic software Version 4.1.

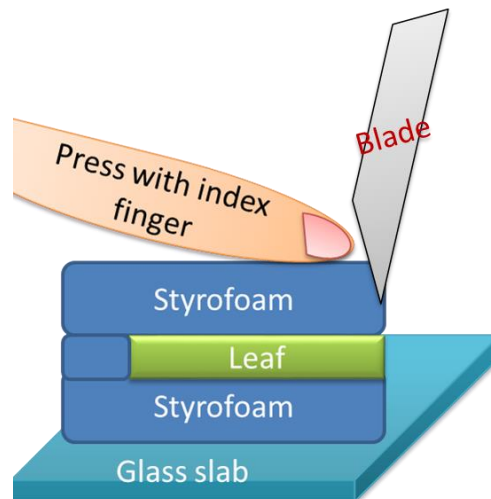


Figure 2.2:

Leaf sample is sandwiched in between a Styrofoam blocks that has been partially slit. The whole sandwich was always moistened with water while pressing it with index finger. Fine sections are made with sawing motions using razor blade at almost a right angle

2.6 Stomatal and leaf epidermal characteristics

2.6.1 Preparation of leaf tissues

One cm from the middle portion of each fully expanded leaf blade (leaf no. 5) was cut and used in all studies. Samples were placed in 24 well microtiter plates containing Carnoy's fixative (ethanol: acetic acid (7:1 v/v)) for 2-3 days

at room temperature and then bleached (25% economic bleach, Ottimo Supplies Ltd.) for another 1 day. Samples were cleared using 2-3 drops of chloral hydrate solution (10gm. chloral hydrate, Riedel-de Haen®; 2.5 mL UHP water; and 1.0 gm glycerol, Sigma-Aldrich Co.) for one hour at room temperature. Leaf sections were then placed on glass slides and mounted in 1 to 2 drops of modified Hoyer's Solution (10gm. chloral hydrate; 1.0 gm glycerol; and 3.0 gm 20% Arabic gum solution, Minerals-Water Ltd.). Leaves were covered with square cover slips (18mm). The epidermal surface of the leaves was observed under an Olympus BX51 light microscope using Nomarski differential interference contrast (DIC) mode.

Photomicrographs were taken with an Olympus camera DP71 (12.5 megapixels) using an Olympus a U-TVO.63XC camera adapter, both mounted on the microscope. Images were captured and processed using CELL-B Version 2.7. Physical measurements of a stomatal complex and its components (Figure 2.3) were made by tracing their outline on the images using a Bamboo® Pen Tablet from Wacom Co., Ltd. ImageJ Version 1.48 software was used to quantify the leaf stomatal and epidermal characteristics described below.

2.6.2 Measurement of stomatal and leaf epidermal characteristics

Stomatal Complex Area (SCA) width (SCW) and length (SCL): A stomatal complex in rice consists of four specialized epidermal cells, a pair of guard cells being sandwiched by two subsidiary cells as indicated by the blue dotted lines (Fig. 2.3). SCA was calculated based on measured values of stomatal complex width (SCW) and length (SCL) (Fig 2.3).

Guard Cell Width (GCW): Guard cell width was measured by drawing lines at the top and bottom of the guard cell and measuring the width (Figure 2.3).

Approximation of Stomatal Pore Area (SPA): Since aperture (pore) area is a likely structure that determines the amount of CO₂ that gets in to the leaf, it is essential to measure pore area to quantify stomatal performance. However with the clearing technique used (in 2.6.1), the aperture is always closed.

Therefore a method was developed to approximate stomatal pore area (SPA) using a simple trigonometric calculation. In a number of stomatal studies, it has been shown that an open stomatal pore (turgid guard cells) in grass species has an elongated hexagon (e-Hex) shape (Willmer and Fricker, 1996 and Taylor *et al.*, 2012). This is also true for rice (Fig. 2.4).

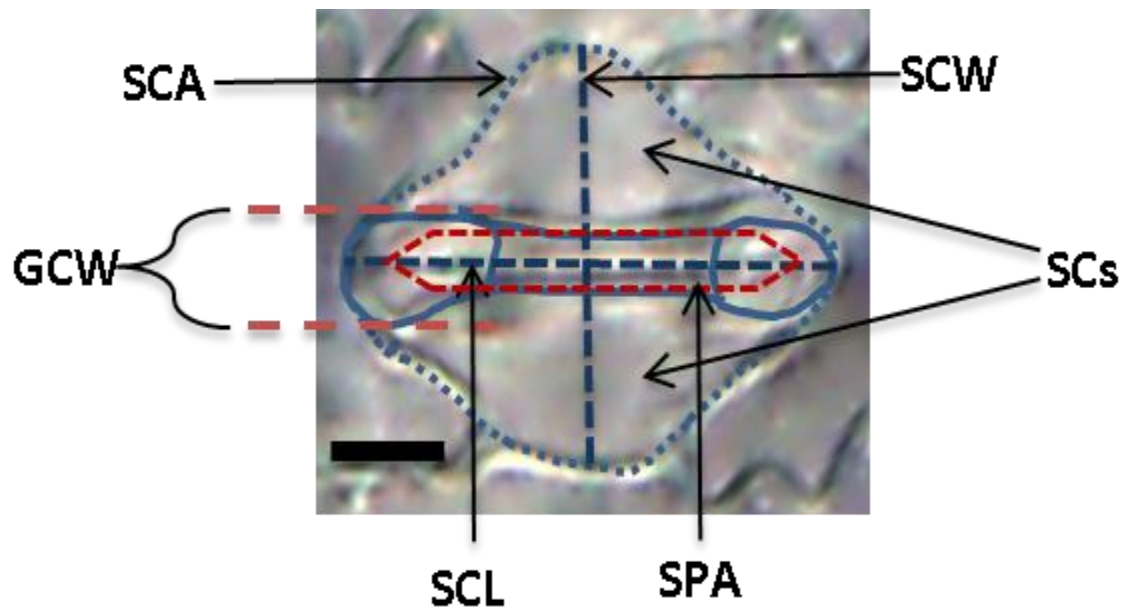


Figure 2.3:

A typical structure of a stomatal complex in rice leaves. Each unit comprises four cells where a pair of dumbbell shaped guard cells is sandwiched by two subsidiary cells (SCs). SCA (stomatal complex area is indicated by the blue dotted line); SCL (stomatal complex length); SCW (stomatal complex width) SPA (stomatal pore area) GCW (guard cell width). Scale bar = 5 μ m

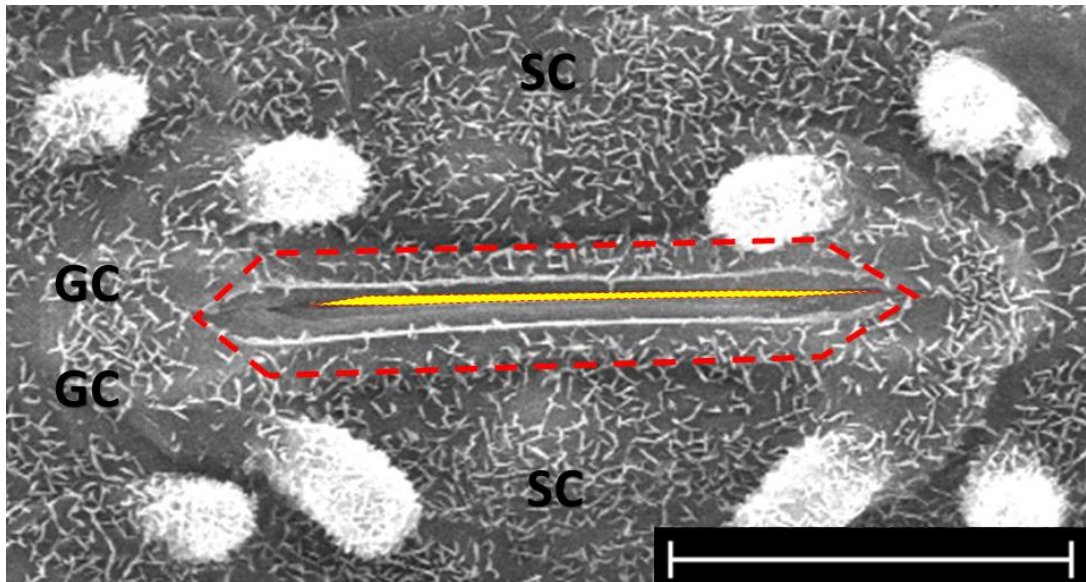


Figure 2.4:

SEM micrograph of a partially open stomatal aperture (yellow area) within a stomatal complex on a rice leaf (bar = 10 μm). The red dotted line shows an approximately elongated-hexagon shaped pore area if the aperture were to open maximally. A stomatal complex comprises a pair of guard cells (GC) being sandwiched by two subsidiary cells (SC). (Yaapar, unpublished).

Since two parameters namely aperture length and guard cells width were measurable, these were used to make an approximation of the maximum stomatal pore area opening in rice. The assumptions are when the stomatal pore is fully open it would occupy the guard cell width and has a perfect e-Hex shape. The e-Hex formula was derived as follows (Thanks to mathematician Yusuf Harun for the advice):

The elongated hexagon (Fig. 2.5A) was split into two identical shapes namely trapezoid. Trapezoid area was determined using the standard formula:

$$\text{Area}_{\text{trapezoid}} = \left[\frac{1}{2} \text{ height i.e. : } \frac{1}{2} (a_w) \right] \times \left[\text{sum of bases i.e. : } (B_s + A_l) \right]$$

Equation 2.2

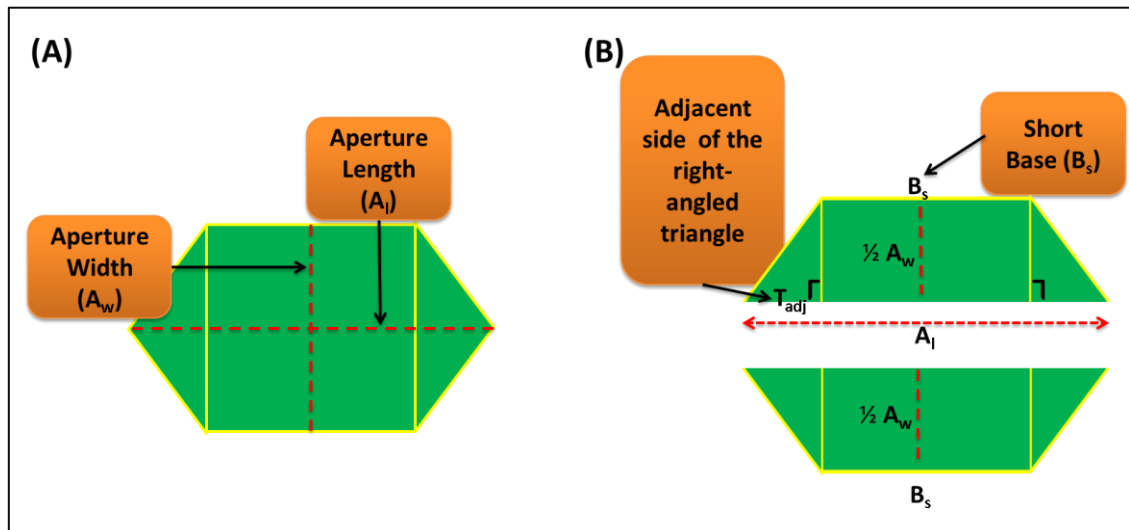


Figure 2.5:

Description of an elongated hexagon (e-Hex) which is supposed to be the shape of a fully open stomatal pore. Two parameters are measurable (**A**) for any given aperture namely aperture length (A_l) and width (A_w). The formula for an e-Hex area can be derived by first splitting the shape into two producing two equal trapezoids (**B**). Each trapezoid in turn contains two right-angled triangles whose unknown adjacent lengths can be found using Tangent function ($\tan \theta = \text{opposite length}/\text{adjacent length}$) in trigonometry.

Each trapezoid has two right-angled triangles (Fig. 2.5 B). This means the two angles in each right-angled triangle must be 45° each because the right angle value is always 90° (Fig. 2.6).

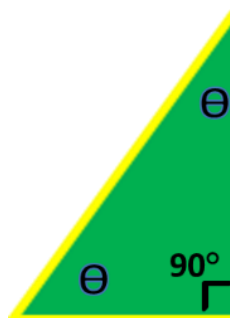


Figure 2.6:

Description of angles for a right-angled triangle in either side of a trapezoid. Since the total angle must be 180° for any triangle, the two unknown theta (θ) values must be 45° each.

To determine the short base (B_s) length, only one of the right-angled triangles in the trapezoid had to be dealt with. From here, the unknown adjacent length of the right-angled triangle (T_{adj}) was calculated using a tangent function in trigonometry:

$\tan \theta = \text{Opposite length} / \text{Adjacent length}$

Since $\theta = 45^\circ$ then $\tan 45^\circ = 1$

Therefore, $\frac{1}{2} A_w = T_{adj}$

Thus, $B_s = A_l - A_w$

Then the new derivation of the trapezoid area is:

$$\text{Area}_{\text{trapezoid}} = \frac{1}{2} (\frac{1}{2} A_w) \times ((A_l - A_w) + A_l)$$

$$= \frac{1}{4} A_w \times (2A_l - A_w)$$

$$= (2A_l A_w - A_w^2) / 4$$

As this was just for one trapezoid (half e-Hex) it was multiplied by 2 to obtain the area of the whole elongated hexagon i.e. the maximum area of fully open stomatal pore is:

$$\text{Stomatal Pore Area}_{\max} = \frac{2A_l A_w - A_w^2}{2}$$

Equation 2.3

Where A_l is the stomatal aperture length while A_w is the aperture width

In general people define maximum the stomatal pore area as an ellipse with major axis equal to the pore length and minor axis equal to half the pore length. This assumption has been widely accepted and employed especially when using diffusive stomatal conductance model (Franks and Farquhar (2001), Eq. 1.1). Thus for rice which has dumbbell guard cells pair that lead to

an e-Hex aperture shape, the ellipsoid definition commonly used for pore area might be incorrect. The approximation method proposed here can be validated by conducting a similar experiment as the one described by Dow *et al.* (2013) who deliberately subjected *Arabidopsis* to conditions that promoted maximal stomatal opening for maximum operational (measured) stomatal conductance. They then compared this value with maximum diffusive (theoretical) conductance obtained by using Eq. 1.1. However the confirmative work was not done in this study.

Stomatal density (SD): In order to calculate stomatal density the number of stomatal complexes was counted in between two interveinal gap areas (Figure 2.6) at 400 X magnification using an Olympus BX51 light microscope. This allowed values to be normalized to express the stomatal density per mm^{-2} of leaf.

Leaf epidermal characteristics:

Figure 2.6 shows the epidermal features and stomatal patterning of a typical interveinal gap (IG). The percentage of files (rows of cells) containing stomata (a cell file row containing at least one stoma) to the total no. of cell files was calculated. Cell file number was obtained by manually counting all cell files in between two parallel veins (Figure. 2.6). Average file cell width was then calculated by dividing the interveinal distance by the cell file number.

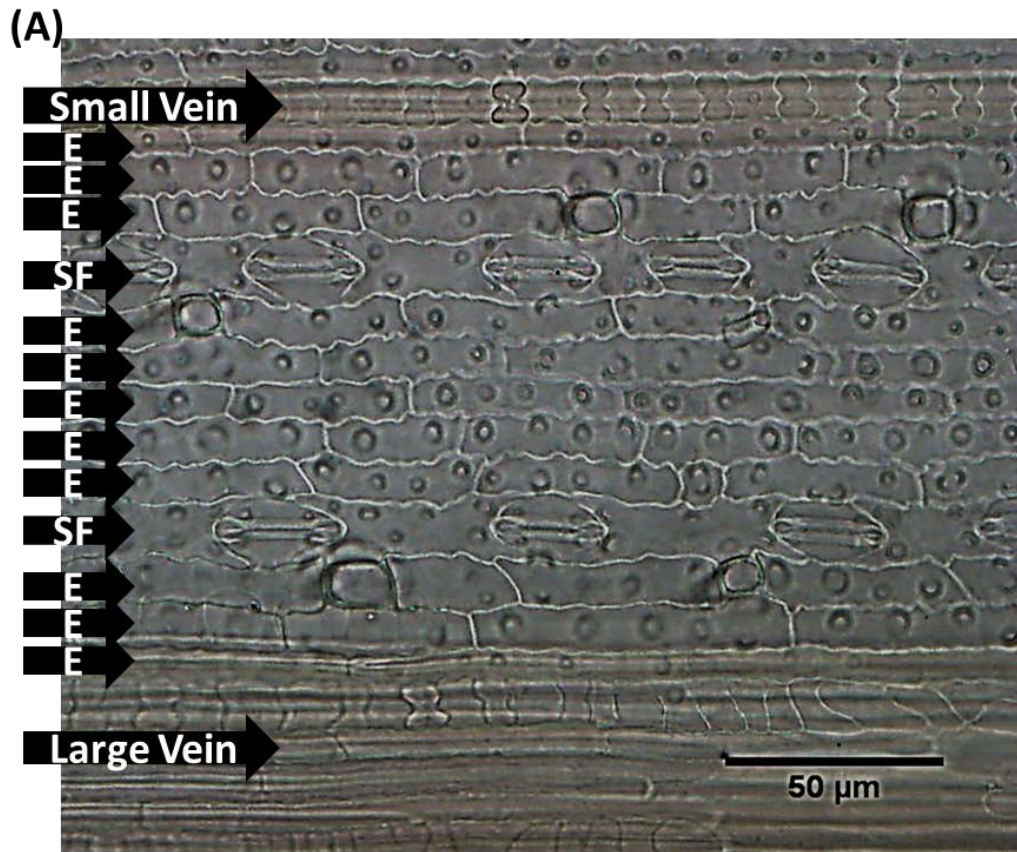


Figure 2.6:

Epidermal features and stomatal patterning of a typical interveinal gap (IG). DIC image of an Interveinal Gap (IG) bound by a small vein and a large vein. Each IG comprises a number of cell files where some are pure long epidermal cells (E) and some contain stomata (SF, stomatal file).

CHAPTER 3

CHARACTERISATION OF STOMATAL AND LEAF PHYSIOLOGY IN RICE LEAVES GROWN IN HIGH AND LOW IRRADIANCE

3.1 Introduction

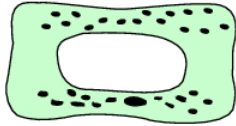
Many comparative studies have demonstrated that leaf development involves responses of plants to environmental cues such as light (Vogelmann and Martin 1993; Strauss-Debenedetti and Berlyn 1994). This developmental plasticity (an ability to adjust to the environment by means of morphological and/or physiological responses) is distinctive to plants (Sultan, 1995). Thus although, for example, photosynthetic responses to changes in light intensity can include short term changes, such as increasing electron transport rate (Bailey *et al.*, 2001), it can also involve more long term changes involving biochemical and morphological acclimation. For example, in high light (HL) conditions many plants generate “sun leaves”, generally characterised by being smaller and thicker than leaves generated under low light (LL) conditions (“shade leaves”). The cellular basis of these changes have been investigated in some plants. For example, Kubinova (1991) showed that barley plants grown in a HL environment produced sun-type leaves which were thicker due to an increase in the number of mesophyll cells and an overall increase in mesophyll volume. However, not all plants show such extreme differences in sun/shade leaf acclimation response. In those that do, the responses are proposed to allow the plant to maintain photosynthesis and minimise stress in a changing environment (Takahashi & Badger, 2011).

The basic concept is that shade leaves acclimate to maximize the light captured while sun leaves need to dissipate excess adsorbed energy to prevent irreversible damage to the photosynthetic machinery. A number of these changes occur at the molecular level, for example modulating PSI and PSII antenna size (Anderson *et al.*, 1995), whereas others alter plant morphology, such as leaf area and thickness (Murchie & Horton 1997). The process thus involves changes at various scales and Figure 3.1 summarizes the functional key differences between sun and shade plants at these various cellular, leaf and plant levels. The study reported in this chapter was performed to highlight/characterise the major differences between sun and shade leaves in rice in our growth conditions, setting the foundations for the experiments reported in Chapter 4 where I investigate how the sensitivity of the response is dependent on leaf developmental stage.

Sun plant

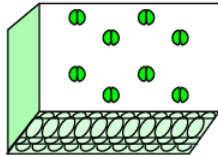
Cells

Large cells
Small chloroplasts
Low chlorophyll/Rubisco ratio
High chlorophyll a/b ratio
High N content
High xanthophyll cycle pigments



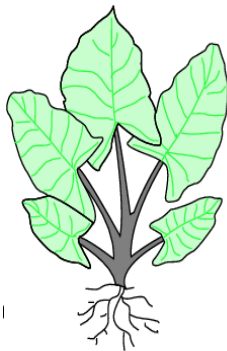
Leaves

Small thick leaves
High stomatal density
High rate of transpiration
High chlorophyll a/b ratio
Low specific leaf area (area per unit mass)
High N content
High xanthophyll cycle pigments



Plants

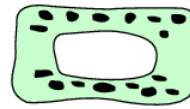
Vertical leaf orientation
Leaf area index higher
More canopy layers
Short leaf lifespan, high turnover
High photosynthetic capacity



Shade plant

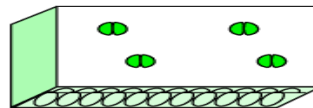
Cells

Small cells
Large chloroplasts
High chlorophyll/Rubisco ratio
Low chlorophyll a/b ratio
Low N content
Low xanthophyll cycle pigments



Leaves

Large thin leaves
Low stomatal density
Low rate of transpiration
Low chlorophyll a/b ratio
High specific leaf area (area per unit mass)
Low N content
Low xanthophyll cycle pigments



Plants

Horizontal leaf orientation
Leaf area index lower
Fewer canopy layers
Long leaf lifespan, low turnover
Low photosynthetic capacity

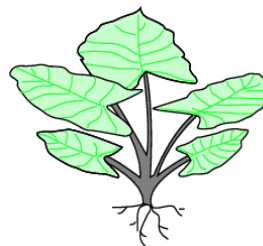


Figure 3.1:

Physical and physiological differences between sun and shade plants. Primary characteristics are highlighted at whole plants, leaves and cells levels.

Figure adapted from: Plants In Action,

<http://plantsinaction.science.uq.edu.au/edition1/?q=content/12-1-1-light-interception-and-utilisation>

A specific aspect of the leaf epidermis of particular relevance to photosynthetic performance, which shows responses to altered light environment, is the stomata. Most of this work has been done on stomata in dicots. For example, *Arabidopsis* stomatal density varies significantly according to the light environment and Fu *et al.* (2010) reported that stomatal density and index (percentage stomata out of the total number of epidermal cells plus stomata) for HL grown *Capsicum* increased, leading to higher values compared to the LL grown plants. However, although such changes may lead to altered gas exchange, the relationship can be complicated. For example, Bussis *et al.* (2006) showed that increased stomatal density was compensated by reduced stomatal aperture, leading to a constant ratio of internal CO₂ concentration in the leaf relative to the ambient CO₂ concentration. Understanding the control of these changes in stomatal properties is complicated by the observation that site of light signal perception and the site of altered stomatal differentiation may be physically remote. Thus, Coupe *et al.* (2006) showed that *Arabidopsis* leaves acquired sun or shade stomatal density via a systemic signalling system, with mature leaves sensing the irradiance level and transmitting (via an as yet unidentified mechanism) the signal to developing leaves. This plasticity of the leaf in changing stomatal characteristics is believed to be an adaptation to improve gas exchange capacity of the leaf in response to altered environmental conditions. Since stomata differentiation generally occurs during relatively early stages of leaf development, systemic signalling allows plants to sense the prevailing environmental conditions and to adjust developing leaves in preparation for the environment they are likely to be exposed to.

Studies on stomatal response in monocot grasses to altered environmental conditions are fewer in number (e.g., Miranda *et al.*, 1981; Weyers and Lawson, 1997; Hubbart *et al.*, 2013). One challenge in comparative studies of stomatal characteristics in grasses is the extent to which sampling stomata from one area of a leaf provides an accurate representation of stomatal properties for the whole leaf. In *Arabidopsis* the stomata are scattered across the leaf and not clearly zoned while in plants such as rice (used in this study) stomata occur orderly in specific cell rows on both leaf surfaces. This non-random distribution raises a number of questions, such as whether stomata at different position relative to the midrib show different properties. Previous

studies of rice stomata have often revealed relatively high variation in parameters of size and density (Miranda *et al.*, 1981; Weyers and Lawson, 1997) and the question arises of the extent to which this reflects real, endogenous variation or variation introduced due to the sampling procedure used (since it is virtually impossible to count all the stomata on one rice leaf). A major aim of the data presented in this chapter was to provide a comprehensive analysis of stomatal characteristics across the entire width of rice leaves at comparable developmental stages. In addition, the variable of HL or LL was introduced to investigate whether any observed response in terms of stomata size or density depended on the position across the leaf surface at which measurements were taken. These results provide the foundation for the experiments reported in Chapter 4 designed to investigate the link between stomatal structural response to altered light regime and the developmental stage of the leaf in which the response is occurring.

As indicated above, an alteration in stomatal size/density is expected to influence photosynthetic performance. Therefore, in addition to the analysis of stomatal patterning, the analysis of gas exchange in HL and LL leaves are reported in the second part of work reported in this chapter. The photosynthetic rate of sun leaves has been shown to be higher compared to shade leaves, for instance in the work on *Alocasia macrorhiza* by Sims and Pearcy (1992). Thicker sun leaves that possess more mesophyll cells increase the mesophyll surfaces occupied by chloroplasts, thus securing the area for CO₂ dissolution and transport. In terms of photosynthetic machinery, sun leaves have been shown to regularly have higher electron transport rate (Yamori *et al.*, 2010) and larger amounts of Calvin-cycle enzymes, especially Rubisco, compared with shade leaves (Timm *et al.*, 2012). In contrast, shade leaves generally have higher levels of *chlorophyll a/b-binding* light harvesting complexes that are essential for them to thrive in low light conditions (Leong and Anderson, 1984). With respect to stomata, various plants, including *Arabidopsis* (Masle *et al.*, 2005) and *Leymus chinensis*, a perennial grass (Xu and Zhou, 2008) show a positive correlation between stomatal density and conductance, thus providing a potential link of altered irradiance response (via stomatal density) and gas exchange.

Sun and shade leaves display distinct photosynthetic properties. These differences are best revealed by the analysis of light response curves (Fig. 3.2) which provides exemplar curves for sun and shade leaves. These curves reveal information on two important limitations at particular irradiance levels, namely the light and carboxylation-limited phases. The light-limited region of the curve provides information on the light compensation point and the quantum yield (light compensation point is the irradiance point when CO₂ uptake (from assimilation) equals CO₂ evolution (from respiration) while the maximum quantum yield is obtained from the slope of the linear portion of the curve). The second phase of the curve, which is relatively flat, reflects the saturating light concentration at which photosynthesis is limited by the carboxylation rate.

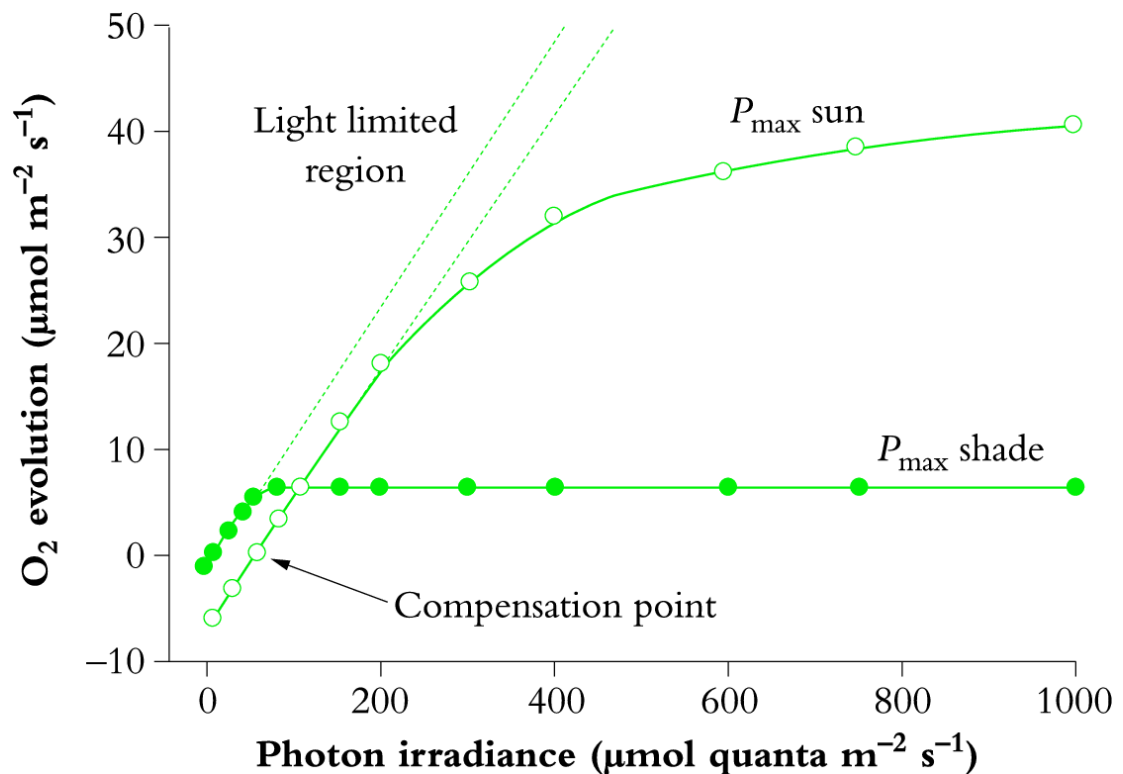


Figure 3.2:

Typical response of photosynthesis to different light concentrations for C₃ plant. Dotted lines are extrapolations of initial linear slopes in the light-limited phase of the curve, which also indicates quantum yield (moles of O₂ evolved per mole quanta absorbed). The light-compensation point is the irradiance level required to offset respiration so that net exchange of CO₂ is zero. The P_{max} (light-saturated photosynthesis) of sun leaves is higher than shade leaves in the same species. P_{max} is found in the plateau region of the curve, which reflects carboxylation limitation. Figure obtained at: Plants In Action, <http://plantsinaction.science.uq.edu.au/edition1/?q=content/12-1-1-light-interception-and-utilisation>

Being a C_3 plant, rice photosynthesis under a light saturating intensity is essentially limited by one or the combination of three parameters, namely (i) the maximum carboxylation rate by Rubisco (V_{cmax}); (ii) the regeneration of RuBP via the maximum rate of electron transport (J_{max}) and (iii) RuBP regeneration via triose phosphate utilization (TPU) (Farquhar *et al.*, 1980 and Bernachi *et al.*, 2009) (Fig. 3.2). These three conditions can be predicted using the C_3 photosynthesis model developed by Farquhar *et al.* (1980) and that has been updated by Sharkey *et al.* (2007).

In the study reported here, modelling of rice photosynthesis was performed using an assimilation versus intercellular CO_2 ($A-C_i$) curve fitting tool from Landflux.org which employs equations from Ethier and Livingston (2003) for theoretical (V_{cmax}) and (J_{max}) estimation. The initial phase or slope of the $A-C_i$ curve provides a measure of the activity of Rubisco in the leaf, as influenced by the amount present (A_c) (Fig. 3.3). Furthermore the curve also provides a means to distinguish between the mesophyll and stomatal limitation of the observed photosynthesis. The second phase of the curve reflects the limitations imposed by RuBP regeneration, which is connected to electron transport rate and ATP synthesis (A_j). The levelling off or decline in assimilation rate at higher CO_2 concentrations can be attributable to the third phase of the $A-C_i$ curve (which is not included in the curve fitting tool from Landflux.org), namely triose phosphate utilization limitation (TPU) (Fig.3.3). TPU happens when triose phosphates accumulate due to the increase in photosynthesis, causing chloroplasts to be starved of phosphates (Sharkey *et al.* 1986). TPU in fact is a collection of events, including the drop in phosphate level, decline in ATP level and, eventually, deactivation of Rubisco (Sharkey 1989, 1990). The $A-C_i$ curves obtained in this study serve as a useful and non-destructive tool to quantify these biochemical components, as well as allowing a separation between stomatal and non-stomatal effects on CO_2 assimilation in rice constantly growing in either HL or LL conditions.

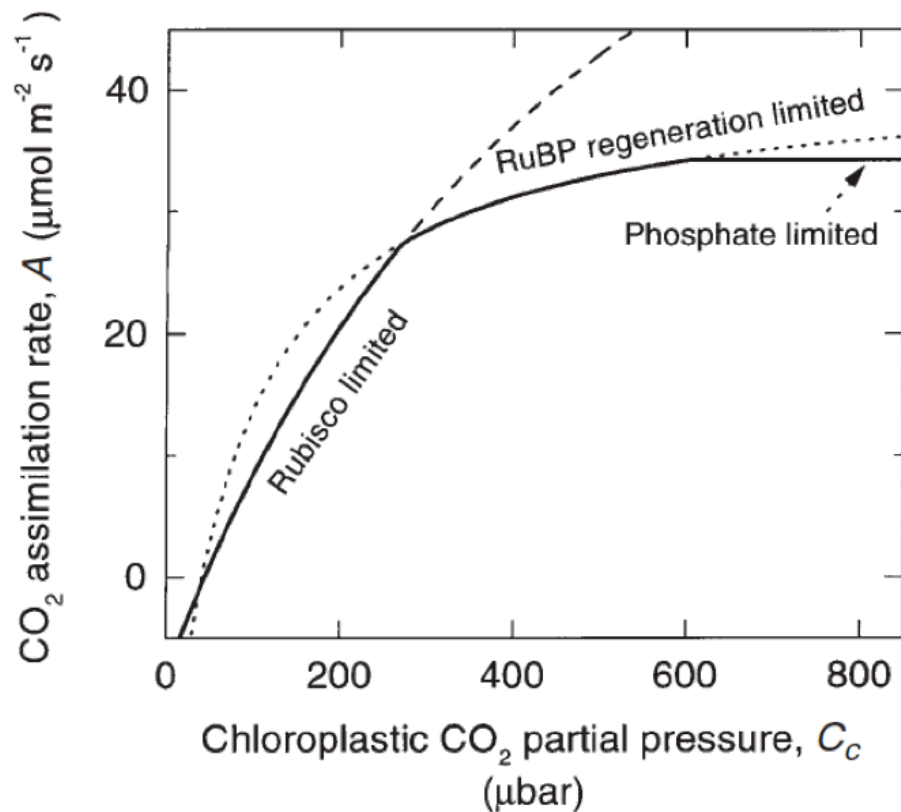


Figure 3.3: Modelled rate of net CO₂ assimilation (A) in as a function of chloroplastic CO₂ partial pressure (C_c).

In general the limitations of photosynthesis in well-watered sun and shade leaves are known, thus this part of the study was performed to establish the techniques to enable the characterisation of the role of stomatal development in limiting rice photosynthesis in HL and LL conditions. The overall aim was to set the foundations for the experiments reported in the next chapter aimed at characterising the effect on final leaf physiology when plants were transferred between HL and LL at specific stages of leaf 5 development, i.e., if transfer between different irradiances at different stages of leaf development leads to different stomatal patterns, what is the outcome on the photosynthetic performance of the mature leaves?

Coupled with the above experiments, biochemical analysis of pigments was also performed to investigate the relationship of photon capture efficiency and the observed assimilation rates. Chlorophyll a/b ratio is an indicator of the light

harvesting capacity of the photosynthetic apparatus and shade leaves generally possess much higher amounts of LHC-II (light-harvesting pigment protein of PSII) than sun leaves and, consequently, their *a/b* ratios are lower than in sun leaves (Lichtenthaler et al., 1982). Finally, the analysis of isotopic composition ($^{13}\text{C}/^{12}\text{C}$ ratio) relative to the standard PeeDee Belemnite is used to compare the photosynthetic discrimination of the heavier carbon isotope ^{13}C in HL and LL grown leaves. Generally, as CO_2 assimilation increases or stomatal conductance decreases, intercellular CO_2 decreases, resulting in decreased discrimination against ^{13}C (Farquhar et al., 1989). These biochemical and isotope discrimination methods facilitate an understanding of the mechanism underpinning any measured change in photosynthetic performance.

3.2 Aims

1. Characterise the pattern of stomatal differentiation in rice leaves grown under different levels of irradiance.
2. Investigate the outcome of irradiance-induced altered stomatal patterning on rice leaf photosynthetic performance.

3.3 Brief methodology

All rice plants were grown hydroponically using growth chamber settings and nutrients solution as described in section 2.1. Plants were grown at HL or LL (section 2.1) until leaf no. 5 was fully expanded. For the HL condition, this was achieved between 21 - 23 days after sowing while for LL-grown plants it was achieved between 25 - 28 days after sowing. Rice was grown at the edge of a hydroponic container (Fig. 2.1) to minimize shading effect among plants. The middle portion of leaf no. 5 blade was used for all measurements.

3.3.1 Stomatal and epidermal measurements

Rice leaves were prepared and photomicrographs obtained using the methods described in sections 2.4, 2.5 and 2.6.1 as required. Measurements of SD, SCA and SPA and IG area were made following the methods described in section 2.6.2. For each parameter five measurements per leaf were taken and averaged to obtain one data point. Eleven replicate leaves were used in total.

3.3.2 Gas exchange measurements and biochemical analyses

Physiological and biochemical measurements were made on the middle section of 3 replicate fully expanded leaf no 5. Gas exchange measurements were carried out to obtain light response curves for both HL and LL-grown rice as described in section 2.3.1. Apparent quantum yield, maximum light saturated rate of photosynthesis and the light compensation point were measured as described in section 2.3.1. Gas exchange measurements were carried out to obtain A-C_i curves as described in section 2.3.1. PAR was maintained at 2000 $\mu\text{mol m}^{-2}\text{s}^{-1}$ with 10% blue light and 90% red light. Stomatal conductance versus intercellular CO₂ concentration curves (g_s-C_i), were also obtained. Intrinsic water use efficiency (iWUE) was computed by taking the ratio between assimilation and stomatal conductance at ambient (400 ppm) CO₂ (C_a) as well as when iWUE was at its maximum (iWUE_{max}), which was always at the last point of A-C_i and g_s-C_i curves. Pigment

quantification and isotopic carbon discrimination determination were performed as described in sections 2.3.2 and 2.3.3 respectively using five replicate leaves for each analysis.

3.3.3 Statistical analysis

In order to compare means two-tailed pair wise t-tests, two sample t-tests or one-way ANOVA followed by Tukey's HSD post-hoc test was carried out as appropriate. Pearson's Correlation Analyses were performed on various HL and LL parameters. Statistical tests used are indicated in each figure legend. All calculations, statistical analyses and graphs were performed and prepared using Microsoft Excel 2016, Minitab 17 and GraphPad Prism 6. All Diagrams were prepared using Microsoft Power Point 2016.

3.4 Results

3.4.1 Comparison of stomatal size and density

The DIC image of a typical interveinal gap of a mature 5th rice leaf (abaxial surface) is presented in Fig. 3.4 A. Rice veins come in three orders where the midvein is central while the large (LV) and small veins (SV) lie parallel along the proximodistal axis of the leaf (Scarpella *et al.*, 2003). Since LV is physically larger than SV (Smillie *et al.*, 2012) it was easy to differentiate from the transverse section but from the aerial view (DIC images), LV could either have two strips of x-shaped silica bodies on it or a single but relatively wider x-shaped silica bodies strip (Fig 3.4 A).

Each IG comprises epidermal cells aligned in parallel to the veins to form a cell file. Some of these files contained only epidermal cells whereas others had at least one stoma. To further understand the top view from the DIC image, 2D transverse hand-section (Fig. 3.4 B) and 3D SEM images (Fig. 3.4 C) were obtained. Each IG from five leaves was analysed for stomatal counts and measurement after two treatments- plants grown under HL or low irradiance LL. It is worth to note that due to natural vein number variations, certain IG had $n \neq 5$ for comparison and this is clearly seen in Fig. 3.5.

Note that all graphs in Fig. 3.5 lack comparison for IG17 and IG18 between the HL and LL treatments because HL leaves always produced fewer small veins than low light leaves, thus decreasing the total number of IGs. The number of large veins was similar between the two treatments (three) but HL leaves in general had fewer small veins (about sixteen) while LL leaves had eighteen IGs (Fig. 3.4 D). At the midpoint of the laminar leaf width for HL and LL leaves was approximately the same (HL = 0.5 ± 0.03 cm; LL = 0.47 ± 0.03 cm), and were not significantly different.

Figure 3.5 shows the variation in stomatal characteristics (SCA, SPA and SD) between the HL and LL treatments in each IG, starting from the mid-vein towards the leaf margin. Pair-wise comparison between HL and LL values for

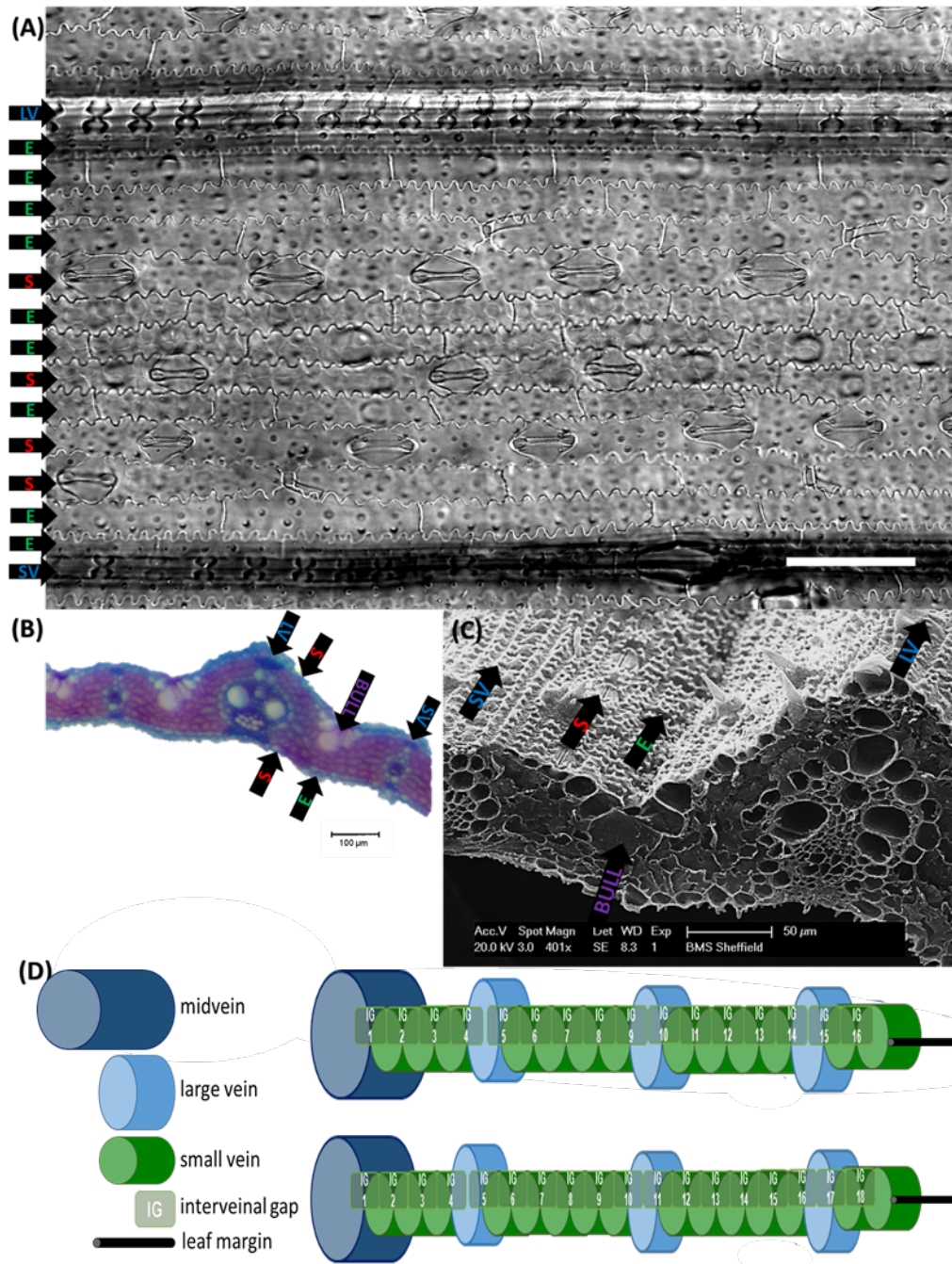


Figure 3.4:

Vein number and position in a rice leaf. **(A)** is a DIC image of an interveinal gap (IG) between a large vein (LV) and a small vein (SV) of a control HL leaf where some of the cell files contain at least one stoma (S) or none (E), as indicated on the left hand side of the figure (Scale bar = 50µm). A transverse hand-section **(B)** shows relative position of the veins, S, E and bulliform cells (BULL). An SEM micrograph **(C)** further shows a leaf transverse section with the same labelled structures **(D)** Provides a schematic diagram to show the relative numbers and positions of veins and IGs for a HL leaf (13 SVs, upper diagram) and LL leaf (15 SVs, lower diagram).

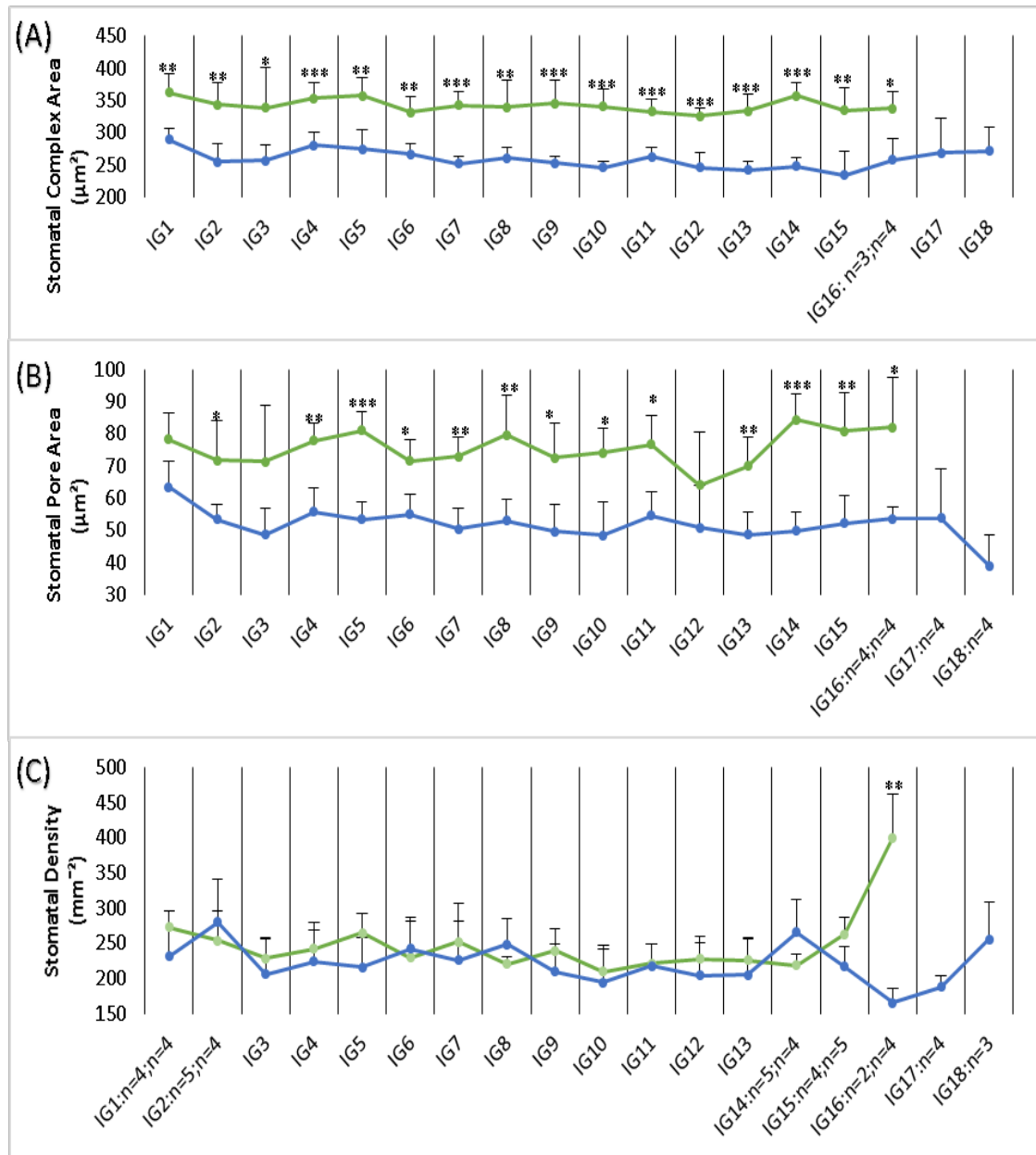


Figure 3.5:

Variation of stomatal properties in each interveinal gap (IG) on the abaxial surface for high light (HL) and low light (LL) grown leaves. The graph shows the mean of (A) stomatal complex area (B) pore area and (C) density for each IG from HL leaves (green lines) and LL leaves (blue lines). Error bars represent standard deviation. Two-tailed pair-wise t-tests between HL and LL in each IG have been performed with significant differences between comparisons being indicated as: * $p < 0.05$, ** $p < 0.01$ and *** $p < 0.001$ ($n=5$ for each comparison except where stated on the x-axis).

each stomatal measurement was made for each IG. Considering the HL and LL treatments, it is clear that for both SCA (Fig. 3.5 A) and SPA (Fig. 3.5 B) the LL treatment led to significantly smaller stomata at most IG positions across the leaf as illustrated in Fig. 3.6.

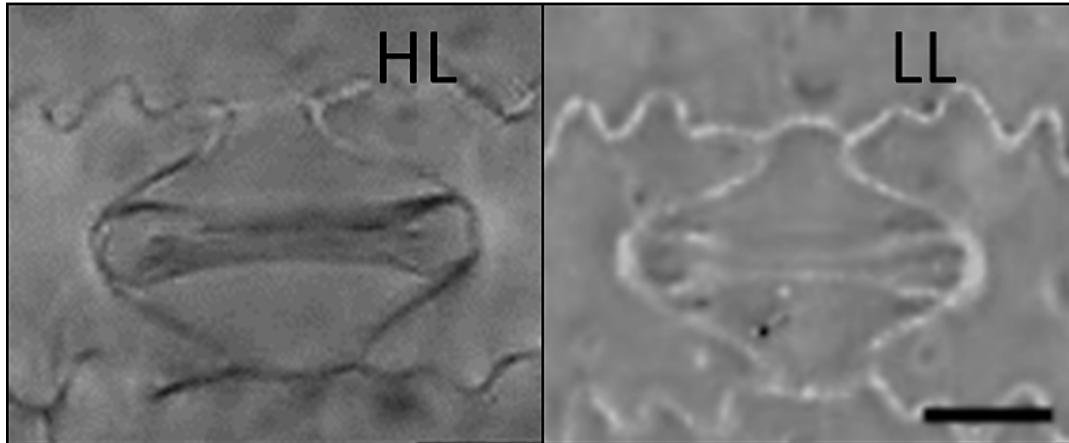


Figure 3.6:

Selected DIC images of stomatal complexes of a high light (HL) grown leaf at IG1 and low light (LL) grown leaf at IG10. Scale bar equals 10 μ m.

However there was a tendency for the mean SCA, SPA and SD values to be slightly higher (or more variable) in IG1 and IGs 14 -17 i.e. at the leaf margins compared to the middle IGs where values were more consistent for both HL and LL leaves. For example, mean SPA values in LL grown leaves were highest in IG1 (about 63 μ m²) with the lowest value being observed in the last IG18 (about 39 μ m²). In HL grown leaves SPA had an extremely low value (about 64 μ m²) in IG12 while SPA was highest (about 80 μ m²) in the last three IGs (IG 14-16). Thus the middle IGs were least variable part of the leaf.

Comparison of SD between HL and LL leaves (Fig. 3.5 C) did not yield any significant differences between the IGs tested except in IG16 (the last IG for HL) where HL leaves had a significantly higher value of stomatal density compared to other IGs in HL leaves. A relatively higher SD was also observed in the last IG in LL leaves although not as high as in HL leaves. IG areas

became progressively smaller towards the leaf margin, yet stomata number per IG did not greatly decrease, resulting in higher frequency per given area.

Table 3.1 shows Pearson's correlation coefficients that were computed to assess the relationship between stomatal properties in HL and LL leaves. Overall, there was a significant positive relationship between stomatal complex and pore areas in all IGs. Increases in SCA were positively correlated with increases in SPA. Stomatal density showed moderate negative correlation ($r = -0.45$) between HL and LL leaves.

Table 3.1:

Pearson's correlation coefficients (r) between the mean values of stomatal properties from Fig. 3.6 up to IG16. Single asterisks (*) indicate correlations which are significant at the $p < 0.05$ confidence limit. HL (high light); LL (low light); SCA (stomatal complex area); SPA (stomatal pore area); SD (stomatal density).

Stomatal properties	HL-SCA	LL-SCA	HL-SPA	LL-SPA	HL-SD
LL-SCA	*0.59				
HL-SPA	*0.58	0.25			
LL-SPA	0.43	*0.80	0.30		
HL-SD	0.09	0.16	0.37	0.30	
LL-SD	0.33	0.14	0.01	0.21	*-0.45

Even though LV number was always three (at least for leaf 5 in this study), SV number (and hence IG number) varied even for the same treatment. This complicates comparison between leaves under different treatments. Thus an alternative approach was taken in order to standardize comparison between the leaves and to see whether fewer sample points could be taken for future leaf comparisons without compromising the analysis, thus decreasing the workload/time required for the analysis of stomatal properties after transfer of leaves from one light environment to another at different stages of leaf development.

In this approach, the IGs starting from MV to the margin were divided into 7 sections as shown in Fig 3.7: (i) MV- IG immediately next to the midvein; (ii) SV1- Middle IG in between MV and first LV; (iii) LV1ab- The average of two IGs bordering with the first LV; (iv) SV2- Middle IG in between the first and second LV; (v) LV2ab- The average of 2 IGs bordering with the second LV; (v) SV3- Middle IG in between the second and third LV and (vii) LV3ab- the average of two IGs bordering with the third LV (Fig. 3.7 A). When the number of IGs did not halve evenly when divided for the middle IG in between MV and LV or LV and LV, the approximate middle IG taken was always the one closer to the MV (Fig. 3.7 B).

Using this approach, it is clear in Fig. 3.7 C and 3.7 D that HL treated leaves had significantly bigger stomatal complex and pore areas (except for the pore area in MV) compared to LL leaves. When values for SCA and SPA were compared within each treatment (HL or LL), there was no significant difference for HL treated leaves with respect to position across the leaf. For LL treated leaves, comparison of SCA indicated some significant differences, with the MV and SV3 positions having higher and lower SCA, respectively. In addition, SPA also showed the same trend as SCA, with SV2 and SV3 positions having significantly SPA than the MV position.

On the other hand when stomatal density data were analysed using this approach (Fig. 3.7 E), although there was a tendency for a higher stomatal density in the HL treated leaves, the large variation in values means that the two data sets cannot be distinguished.

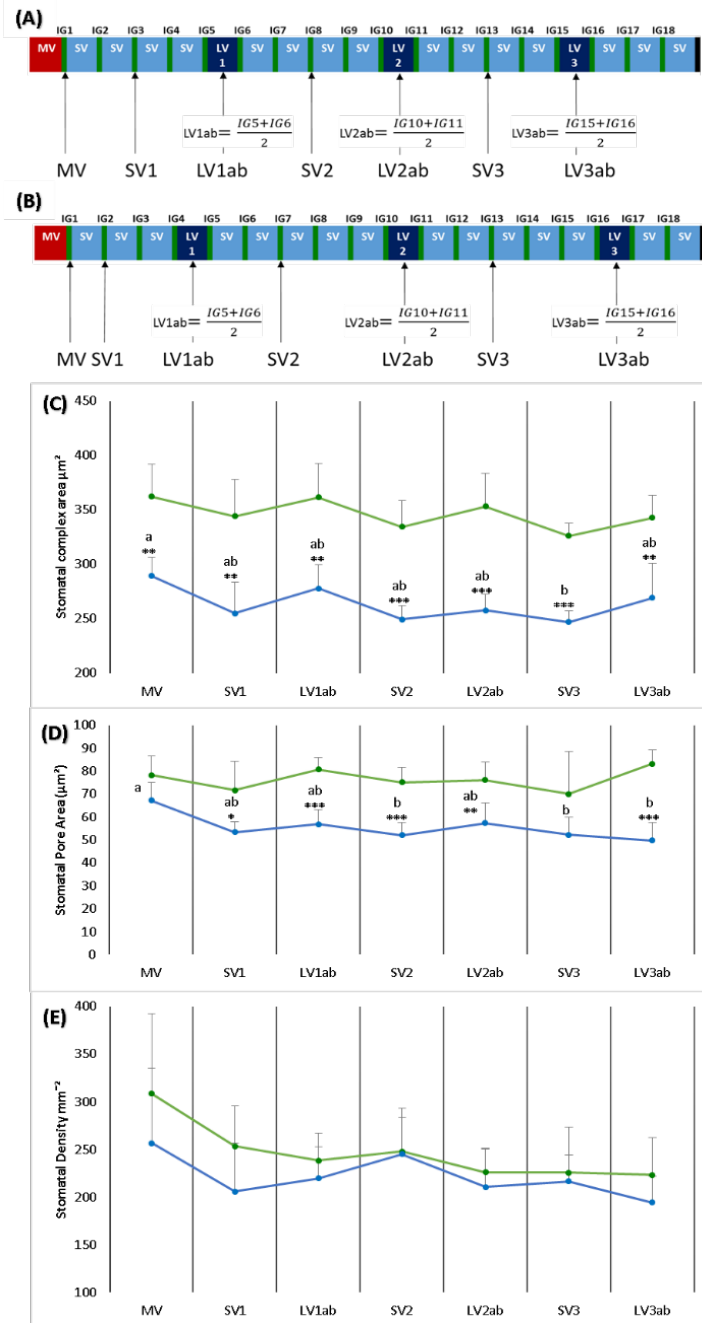


Figure 3.7:

Variation in stomatal properties across leaves from midvein towards margin in seven sections of selected IGs. **(A)** Schematic diagram of a leaf to show regions taken for average measurements. Green bands represent IGs and black band is the leaf margin. The middle IG is selected as the position between MV-LV or LV-LV and values from the two IGs bordering an LV are averaged and denoted as 'ab'. When the number of IGs are odd **(B)**, the middle IG taken is always the one closer to the MV. The graphs show the mean values for **(C)** stomatal complex area **(D)** pore area and **(E)** stomatal density, where green lines show values for HL while blue lines are for LL samples. Two-tailed pair-wise t-tests between HL and LL values in each section have been performed with significant differences between comparisons being indicated: * $p < 0.05$, ** $p < 0.01$ and *** $p < 0.001$ ($n = 5$). Within each treatment, one-way ANOVA followed by Tukey-Kramer's post-hoc test is performed. Means not sharing the same letter are significantly different ($p < 0.05$). Error bars represent standard deviation. Key: IG, interveinal gap; LV, large vein; MV, midvein and SV, small vein.

3.4.2 Comparison of assimilation rate and stomatal conductance in HL and LL grown plants

To investigate the extent to which HL and LL treatments altered the light-saturated rate of photosynthesis, apparent quantum yield and light compensation point a light versus assimilation rate response curve was performed (Fig 3.8).

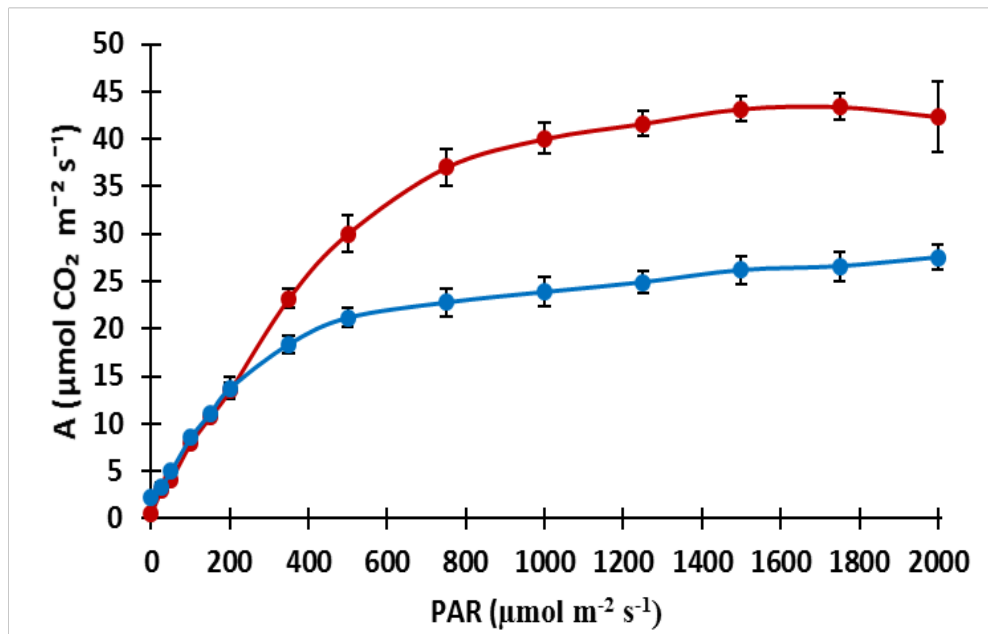


Figure 3.8: Assimilation (A)-light (PAR) response curves of rice leaf no. 5 grown in either a high light (red line) or low light (blue line) environment in Error bars represent standard error of mean for the assimilation where $n=3$.

Leaves grown in either HL or LL had a saturated assimilation rate from an irradiance of $1600 \mu\text{mol m}^{-2} \text{s}^{-1}$ (Fig. 3.8). Thus, for the all the subsequent $A-C_i$ experiments PAR was set to $2000 \mu\text{mol m}^{-2} \text{s}^{-1}$. This was important to eliminate photosynthetic limitation caused by insufficient light quantity as well as to activate Rubisco while studying $A-C_i$ response curves.

The light (and CO_2) saturated rate of photosynthesis was 52% higher in HL grown leaves ($43.9 \pm 2.4 \mu\text{mol m}^{-2} \text{s}^{-1}$) compared to LL leaves ($28.8 \pm 1.4 \mu\text{mol m}^{-2} \text{s}^{-1}$). LL-grown leaves had a slightly higher apparent quantum yield of 0.1 ± 0.007 compared to HL leaves ($0.07 \pm 0.0002 \pm \text{mol/mol}$) but there was no difference in LCP. The later is unusual but may be due to the fact that saturating CO_2 was used in this experiment.

Assimilation versus intercellular CO₂ (A-C_i) response curves for HL and LL-grown plants are shown in Fig 3.9 A and B respectively. In the first phase of the curve, the measured data fitted well with the predicted A_c model (blue dashed lines) for HL leaves (Fig. 3.10 A) but underestimated for LL grown leaves. For the second part of the curve the A_j model (green dashed lines) fitted HL measurements reasonably well but overestimated values for the data points for LL grown leaves. The more parameter values (such as leaf absorptance, mesophyll conductance and day respiration) that could be altered to specifically suit rice, the better curve fitting and prediction for both A_c and A_j models could be.

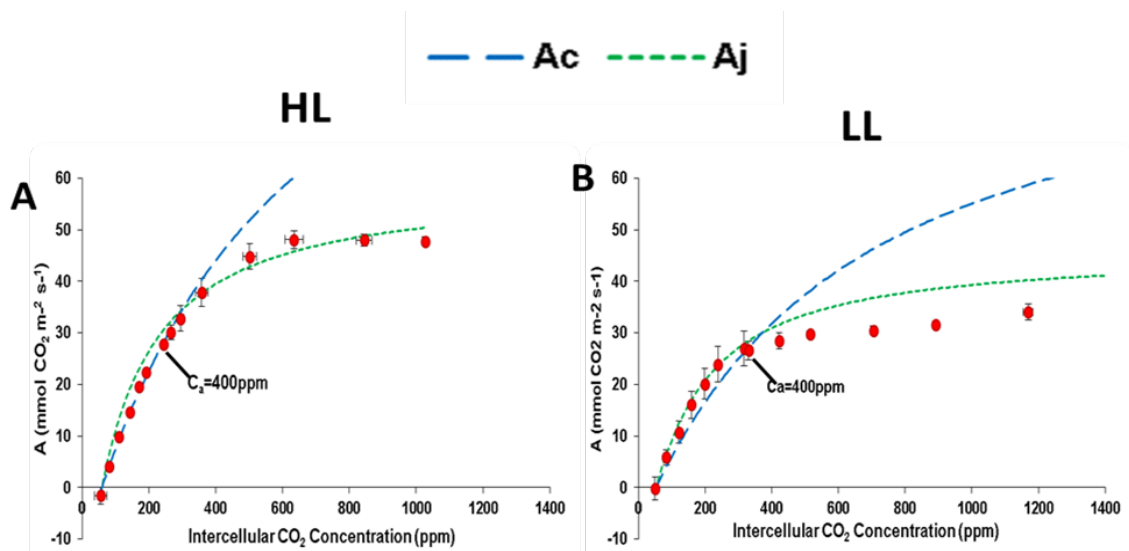


Figure 3.9:

Assimilation versus intercellular CO₂ (A-C_i) response curves for high light (HL, **A**) and low light (LL, **B**) grown leaves. Data are pooled from 3 plants for each treatment where each red dot is the average observation for the given A rate and C_i concentration with measurements made at the current CO₂ concentration (C_a = 400ppm) marked on the curves. A_c (dashed blue lines) are CO₂ assimilation rate limited by the amount and activity of Rubisco (enzyme limited/RuBP saturated) while A_j (dashed brown lines) are CO₂ assimilation rate limited by RuBP regeneration (light limited/RuBP limited). Error bars show standard error of mean.

HL leaves had a significantly higher assimilation rate compared to LL leaves at both saturating (1600 ppm) and ambient (400 ppm) CO₂ (Fig 3.9). At ambient CO₂ HL grown leaves had an assimilation rate of 31 $\mu\text{mol CO}_2 \text{ m}^{-2} \text{ s}^{-1}$ which was 22% higher than that of LL grown leaves (Fig 3.10 A). This difference was

attributable to a significantly higher V_{cmax} and J_{max} in HL grown leaves compared to LL grown leaves (Fig. 3.10 B and C respectively) suggesting that HL grown leaves had higher amounts of Rubisco for carboxylation.

HL leaves had a significantly lower stomatal conductance ($0.34 \text{ mol H}_2\text{O m}^{-2} \text{ s}^{-1}$) than LL leaves ($0.8 \text{ mol H}_2\text{O m}^{-2} \text{ s}^{-1}$) indicating that they were transpiring at a slower rate than LL leaves (Fig 3.10 D). This is consistent with a higher water use efficiency in HL compared to LL leaves (Fig 3.11 A and B). The leaf temperature of HL and LL leaves was not significantly different at ambient CO_2 but was slightly higher in HL leaves at saturating CO_2 (Fig 3.10 E). The stomatal limitation to photosynthesis (I_s) was also significantly higher in HL than LL leaves (Fig. 3.10 F).

Pigment analysis revealed that HL grown leaves had higher chlorophyll a/b ratio compared to LL grown leaves (Fig. 3.10 G), indicating the presence of a larger number of PSII reaction centres and less light harvesting complexes consistent with the higher J_{max} in HL leaves (Fig. 3.10 C). Discrimination against the heavier carbon isotope (^{13}C) was also assessed to validate and understand the relatively higher A_{400} (also higher in iWUE) rate in HL leaves than LL leaves that could be due to stomatal pore (entry) or/and enzymatic preference (Rubisco). LL leaves clearly had a significantly more negative, thus lower, $^{13}\text{C}/^{12}\text{C}$ ratio (about -33.5‰) than HL leaves (-32.5‰) (Fig. 3.11 B), suggesting the effect of high stomatal conductance and/or increased Rubisco discrimination against ^{13}C .

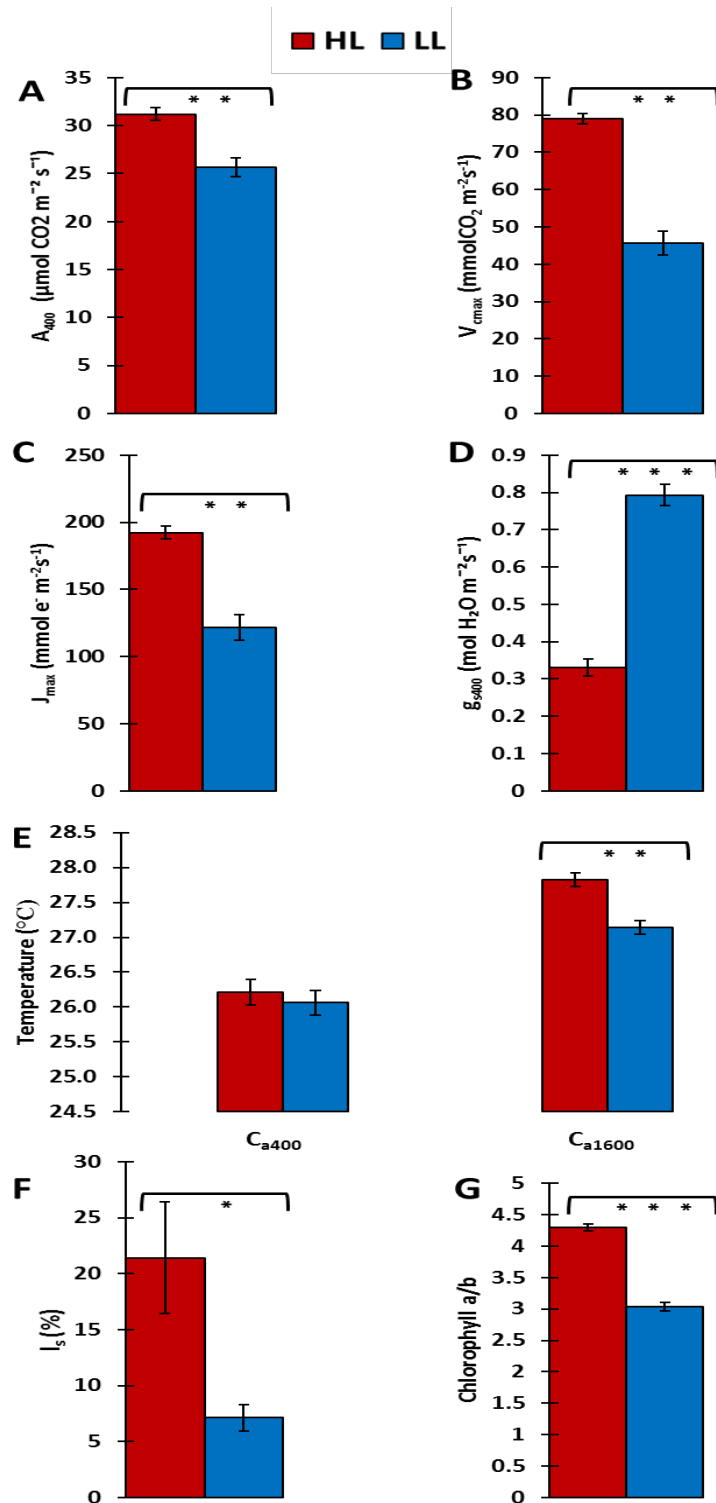


Figure 3.10:

Photosynthetic features of high light (HL) and low light (LL) grown rice leaves at ambient CO_2 (400 ppm) extracted or calculated from the A-C_i curves in Fig. 3.10. (A) Assimilation rate (A_{400}); (B) Rubisco carboxylation rate ($V_{\text{cmax}400}$); (C) electron transport rate ($J_{\text{max}400}$); (D) stomatal conductance (g_{s400}); (E) leaf temperature at 400 and 1600 ppm CO_2 ; (F) percentage stomatal limitation (I_s) to photosynthesis; and (G) chlorophyll a/b ratio. Two samples t-tests were performed to compare means with significant differences between comparisons indicated as: * $p < 0.05$; ** $p < 0.01$ and *** $p < 0.001$ ($n=3$) with error bars to represent standard error of mean.

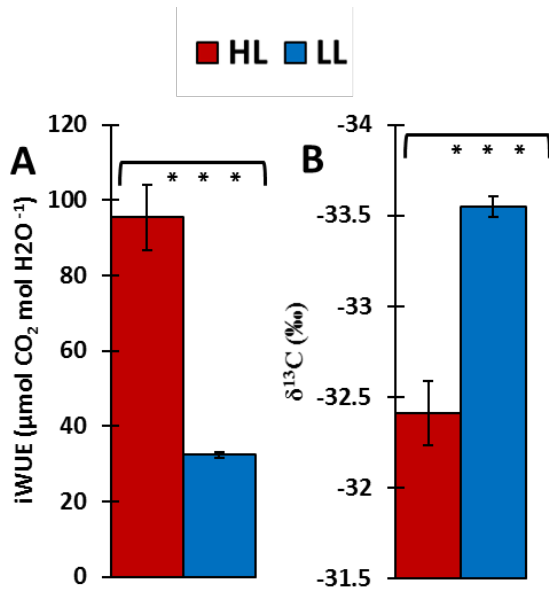


Figure 3.11:

Water use efficiency (**A**) and carbon isotope ratio ($\delta^{13}\text{C}$) is presented on a per mill (‰) basis (**B**). Two samples t-tests were performed to compare means. Significant differences between comparisons are indicated as *** $p < 0.001$ ($n=3$). Error bars indicate standard error of mean.

3.5 Discussion

Results from the first section of this study showed that HL grown rice consistently produce leaf 5 with larger stomatal dimensions (complex and pore areas) across the entire leaf width (Fig. 3.5 A-D). This finding agrees with Hubbart *et al.* (2012) who also reported significantly bigger (longer) stomata on average on the abaxial surface of rice grown under HL conditions but a nonlinear change in stomatal size from the midrib outward. This is probably because they used a different method of sampling where stomata were chosen at four different distances from the midrib compared to the more detailed approach used here using individual IGs. The results from this study suggests that stomatal size measured in any IGs is in general not statistically different from any other, though care must be taken at both the extreme edges of the leaf and in the IGs immediately adjacent to the midvein.

In a related plant, *Muhlenbergia cuspidate*, which is a perennial C₄ grass (Steuter, 1987), individual stomatal characteristics that define size (such as pore length and width) did not necessarily change proportionately under HL or LL. Smith and Martin (1987) reported that when this grass was grown under HL or LL conditions abaxial stomatal length did not change but stomatal width did alter significantly. Meanwhile in C₃ dicot plants, for example *Eucalyptus globulus* and tobacco (*Nicotiana tabacum*), high and low irradiance levels have a clear opposite effect. Thus James and Bell (2000) showed that HL conditions experienced by *E. globulus* resulted in longer stomatal pores compared to LL conditions, but in tobacco there was no significant difference in stomatal pore length between the two light conditions (Thomas *et al.*, 2003). The varying results from different plant groups suggest that the effect of growth in high or low irradiance conditions on stomatal size is species-specific. Stomata, which are vital in photosynthetic gas exchange, are one of the components that plants can modify in order to adapt in a given light condition. Certain plants which lack the ability to alter stomatal size may employ other ways, such as modifying stomatal density and leaf thickness, so that leaf physiological performance can be optimized for the prevailing light conditions during leaf development.

In this study, stomatal density in rice generally did not vary between HL and LL conditions in any of the IG analysed (except in the last IG of HL leaves where stomatal density was significantly higher compared to the same IG position of LL (Fig. 3.5 C). This is one of the noticeable outcomes resulting from comparing stomata 'IG to IG' between different treatments since different light conditions result in different IG number (Fig. 3.4 D). For example, the last IG of HL (IG 16) corresponds to IG16 of the LL that actually is the 3rd last IG for the LL leaf. This partially equivalent IG comparison could be a source for discrepancies for data analysis. Therefore, a simpler system is proposed by basing the comparison on IG's relative distance to the midvein or large vein (Fig. 3.7 A and 3.7 B). It is a more standardized way of picking IGs to be used for stomatal counting and measurement. This method still shows that there is a clear difference in stomatal dimensions between HL and LL (Fig. 3.7 C and 3.7 D). On average, there is a tendency for HL leaves to have higher stomatal density in the selected IGs compared to LL across the leaf but this is statistically not significant (Fig. 3.7 E). IG gap width and epidermal cell file number (other than stomata) vary widely across the leaf and seem not to follow any particular pattern in response to the light conditions given.

The system reported here for selection of the leaf region for comparative analysis of stomatal properties in rice could be useful in other grass species in order to study variation in stomatal characteristics since grass leaves are normally partitioned into IGs and orderly arranged in cell files. Additionally it might also work in other non-grass species, such as *Commelina communis*, which have parallel venation and heterogeneous stomatal characteristics of density and size across the leaf (Smith *et al.*, 1989).

When all stomatal characteristics in this study are taken together, only a few could be used as a proxy for another. For example, correlation analysis suggested that in the same HL or LL leaf stomatal complex area has a significant positive relationship with pore area (Table 3.1), thus measurement of one characteristic is just as good to predict the other. Bearing in mind the way in which stomata are structured in grasses, this is not surprising. Stomatal density did not correlate clearly with any size parameter, which is slightly surprising bearing in mind the proposed linkage of stomatal size and density

(Franks and Beerling, 2009), although this study examined stomatal size over a much larger range of species.

The analysis shows that stomatal density in HL leaves is negatively correlated with stomatal density in LL leaves. This suggests when stomatal density values of either HL or LL leaf are pooled from all IGs and compared with each other, HL and LL leaves do have high and low stomatal density respectively. Thus, the results agree to some extent with those reported by Coupe *et al.* (2005) using *Arabidopsis*, but contrast with Hubbart *et al.* (2012) who also analysed rice. Clearly the sampling and analytical process chosen can influence the conclusions drawn from analysis of stomata.

The plasticity of rice stomatal size in response to either HL or LL conditions raised a question regarding its effect on leaf gas exchange capacity. Measurement of stomatal conductance to water vapour under ambient CO₂ concentration (g_{s400}) which is expressed in mol H₂O m⁻² s⁻¹ was employed to answer this. It is clear from Figure 3.10 D that LL leaves, despite having relatively smaller stomata (Fig. 3.6), still have the ability to regulate aperture opening more than HL leaves thus resulting in higher g_s values. The results are surprising because many investigations using rice, as well as different plants, show that sun leaves have higher g_s values than shade leaves or show no difference. Experiments using the same rice variety IR64 by Narawatthana (2013) showed that at ambient CO₂, the g_s of sun and shade leaves did not differ. In other plant species such as English oak tree (*Quercus robur*, Gross *et al.*, 2008), *Ligustrum vulgare* (Guidi *et al.*, 2008) and rice plants of different variety (*Oryza sativa* cv. F50, Restrepo and Garces, 2013), the sun leaves always had higher g_s than shade leaves. Many factors could contribute to this, for instance Narawatthana (2013) during measurement used a light intensity of 1000 $\mu\text{mol m}^{-2}$ and Restrepo and Garces (2013) used 800 $\mu\text{mol m}^{-2}$, but in this study it was 2000 $\mu\text{mol m}^{-2}$. In other species, like English oak and *Ligustrum vulgare*, direct comparison is fundamentally not equivalent because these two species are dicot plants that have morphologically different stomata. Therefore, the difference in g_s values might be attributable to the mechanics of different stomatal type. Nevertheless, high g_s observed LL leaves is a common protective measure in many shade tolerant species to prevent

damaging temperature at the expense of water use efficiency (Chazdon and Pearcy, 1991; Schymanski *et al.*, 2013).

Equation 1.1 in Chapter 1 is useful to explain mechanistically how higher g_s in a LL grown leaf can be achieved, which is through its smaller pore area and shallower pore depth that leading to a shorter diffusion path distance. This g_s formula was not used in this study because it is only valid when the measuring conditions that promote maximal stomatal opening (high light, high relative humidity and very low CO_2 concentration) are all in place. Small stomata also create more room for extra stomata (Franks and Beerling, 2009) allowing high g_s to be attained, i.e., higher SD. Based on this formula, essentially three stomatal properties control g_s , namely stomatal density, stomatal pore area and stomatal pore depth. By this definition, since stomatal density was not different between the two treatments, HL leaves should have higher g_s than LL leaves simply because they had larger pore area. However the opposite was measured here where LL leaves had a much higher g_s than HL leaves. To explain this, it is important to note that the stomatal pore area formula (Equation 2.1) in this study is the maximum area possible for the given aperture length and guard cells width. It may be that there is a mechanism that enables the stomatal aperture to open differentially, thus affecting the g_s value even when stomatal density does not change.

To put things into perspective, we can compare the theoretical g_s values between the treatments using the equation 1.1. By pooling and averaging all the data from all IGs in each treatment, stomatal pore area for HL leaves is $76 \mu m^2$ and for LL leaves is $52 \mu m^2$. Stomatal density for both treatments is $235 mm^{-2}$ and pore depth is assumed to be the same as guard cell width (taken after Dow *et al.*, 2013), which is approximately $5 \mu m$. By substituting these values into the Equation 1.1, the maximum theoretical values g_s for HL and LL leaves are 4.0 and $3.0 mol H_2O m^{-2}s^{-1}$ respectively. From Fig. 3.10 D, the measured or operational g_s values for HL and LL leaves under ambient oxygen and CO_2 ($C_a = 400ppm$) conditions are about 0.3 and $0.8 mol H_2O m^{-2} s^{-1}$ respectively. This agrees with a number of authors (Williams *et al.*, 2004; Dow *et al.*, 2013) that predicted conductances are often much higher than observation. For HL leaves, the measured g_s is only about 20% of the

calculated g_s . This means, when stomatal density and pore depth are not variable, the pore area was only 8% open, thus accounting for the low measured g_s . For LL leaves, the measured g_s is about 27% of the calculated g_s meaning the pore area was about 26% open, thus resulting in the higher measured g_s than HL leaves. This differential stomatal opening makes it possible for leaves to have variable g_s values even when other stomatal parameters stay the same. Another possible reason why LL leaves had high g_s was due to the shorter distance to travel for water within the leaf as a result of altered vein number and spacing. The higher SV number in LL leaves (Fig. 3.4 D) causes the individual IGs to become narrower. More veins and narrower IGs mean that the leaves have more 'pipes' that provide water and narrow IGs means a smaller tissue area that needs to be filled with water, potentially allowing a greater rate of flow of water to the substomatal chambers.

But why would LL leaves need to transpire a lot of water relative to HL leaves? Since LL leaves have been shown to have relatively lower V_{cmax} and J_{max} (Fig. 3.10 B and C respectively), there is no pressing demand to have more CO_2 into the chloroplasts to satisfy high assimilation rate. Moreover, LL leaves also have relatively lower stomatal limitation (Fig. 3.10 F) thus there is no real need to open the stomata widely just to lose water unnecessarily. One possible explanation is that it is a mechanism employed by LL leaves to prevent damage to the leaves. LL 'shade' grown leaves, have several distinctive characteristics such as thin leaves and low total carotenoid content (Narawatthana, 2013). Such an anatomy and physiology are unsuitable for high light conditions. However, when the gas exchange measurements were being made, the amount of light used throughout the experiment was $2000 \mu\text{mol m}^{-2}\text{s}^{-1}$. For LL plants (which were grown in $250 \mu\text{mol m}^{-2}\text{s}^{-1}$ irradiance), this means the leaves were receiving an excess of light that might result in heat build-up in the leaves. If measuring photosynthesis carried out in the growth environment, the extremely high g_s may not occur.

The excess light condition was more intense in LL than HL leaves due to thinness of the leaves and the low level of total carotenoids (for photoprotection, Yang *et al.*, 2002). The fate of electrons from the excited chlorophyll molecules in PSII can be used to drive photosynthesis, re-emitted

as fluorescence or re-emitted as heat (Murchie and Lawson, 2013), and since J_{\max} is relatively lower in LL leaves thus the other options left are fluorescence and heat re-emittances for excess energy dissipation not used for photochemistry.

Biochemical analyses were also made to validate certain physiological parameters such as V_{cmax} , J_{\max} and $i\text{WUE}$. Since HL leaves must deal with higher irradiance level than LL leaves, it is expected for them to have a high chlorophyll a/b ratio (Kitajima and Hogan, 2003). It is often generalized that lower chlorophyll a/b ratio in LL grown leaves is due to higher chlorophyll-b content in the LHCII (McDonald, 2003; Lichtenthaler and Babani 2004). This shows that for LL acclimated rice larger investment is necessary into making bigger LHCII antenna size increases in to capture more photons to drive photochemistry in PSII. Since relatively lower V_{cmax} is commonly correlated with lower Rubisco content (Adachi *et al.*, 2014), this implies lower overall energy consumption needs for carboxylation thus reflected in relatively lower J_{\max} as well. In terms of electron usage, LL leaves are more efficient than HL leaves since lower J_{\max} means greater CO_2 fixation per electron can be achieved. The simple A/g_s ratio to obtain $i\text{WUE}$ has shown that HL leaves are more efficient than LL leaves (Fig. 3.11 A). This means CO_2 at the site of carboxylation experience fractionation which should be high in HL leaves with relatively higher assimilation rate. This is validated through a more positive value of isotopic carbon discrimination ($\delta^{13}\text{C}$) in HL leaves compared to LL leaves. The abundance of intercellular CO_2 (also means relatively higher C_i/C_a ratio) coupled with the nature of LL leaves that are known to have a relatively lower Rubisco content (Narawatthana, 2013), thus reduced carbon fixation which allows the Rubisco to discriminate more against the heavier ^{13}C isotope. The more positive carbon isotope ratio in HL leaves is thus indicative of a higher water use efficiency (Franks *et al.*, 2015) because a relatively small amount of water is transpired for the high assimilation rates measured compared to LL leaves.

In this section I have shown that the size of stomata in rice leaves is responsive to the light environment. Stomatal plasticity in rice, particularly dimension, has been shown to respond to light where high and low irradiances

produce small and big stomata respectively. Stomatal density is not statistically different in either light condition. A detailed analysis of stomatal properties in each interveinal gap showed that they did not vary significantly, although care has to be taken when considering stomata measured in the interveinal gaps toward the leaf margin. An analysis based on this leaf area alone might lead to spurious conclusions.

Due to the nature of HL and LL leaves that produce inconsistent numbers of interveinal gaps, a simplified method is proposed so that stomatal characteristics across a leaf width can be quantified in a standardized manner. This approach will be used in the subsequent studies of this thesis (Chapter 4) that require analysing stomatal characteristics. The differences in stomatal size in HL and LL leaves are translated into a clearly different g_s and assimilation patterns at different CO_2 concentrations. The relatively high stomatal limitation in HL leaves suggest that big stomata may co-limit assimilation with non-stomatal properties (such as Rubisco and mesophyll conductance) thus can be a point to further improve general photosynthesis capacity without compromising water use efficiency. Predicted g_s values are often much higher than the measured g_s values, thus it is risky employ them unless under certain environmental conditions that promote maximum stomatal aperture opening. Small stomata in LL leaves have higher g_s values than the larger stomata in HL leaves, suggesting a mechanism of differential stomatal opening to promote cooling through high transpiration in response to heat build-up in LL leaves which occurs to dissipate excess energy from the high intensity light in the measuring chamber.

CHAPTER 4

Characterisation of Stomatal Development Following Transfer of Rice From One Light Environment to Another

4.1 Introduction

In Chapter 3 it was shown that rice leaves continuously grown in HL conditions have characteristics typical of sun leaves, for example increased thickness. One of the observations made was that stomata (controllable pores on the leaf epidermis) showed distinct patterns of size depending on the irradiance condition the plant was grown under, with high irradiance leading to larger stomata. This raises the question of when during leaf development stomatal size parameters are set and whether there is a sensitivity window during which environmental conditions, such as irradiance, can influence these parameters.

As outlined in Chapter 1, stomata are the result of patterned cell divisions in the epidermis of leaves. Cell division decreases during leaf development in a progressive manner so that processes dependent on cell division (such as stomatal formation) cease much earlier than growth of the leaf (i.e., mature leaves cannot adjust their number of stomata) (Fleming 2005). This situation is further complicated in grass leaves where their unique cellular organisation means that stomatal differentiation is restricted to particular files of cells. File formation is also controlled by cell division events and the width of stomata will be set by the width of the cell files formed. Stomata size (defined by length and width) will have a strong influence on maximal pore aperture, thus potentially limiting the maximum gas exchange that can occur (Franks and Beerling, 2009). Thus, cell division events during early leaf differentiation will likely define the size and number of mature stomata, determining the limits of stomatal function in gas exchange in mature leaves. Exactly when the events of stomatal cell division terminate in rice, their responsiveness to irradiance level, and to what extent this influences the photosynthetic performance of mature leaves is the focus of this chapter.

Previous work in this area has shown that the ability of plants to acclimate to light is species dependant. For example stomatal density in *Arabidopsis* was reported to be higher in HL than LL conditions (Coupe *et al.*, 2006) but remained approximately the same in rice (Hubbart *et al.*, 2013). It has been demonstrated that the setting of stomatal parameters in young, developing leaves depends on signals from more mature leaves (Lake *et al.*, 2001) and

that this occurs in a range of plants (Coupe *et al.*, 2005). With respect to rice, it has been demonstrated that the ability of a leaf to respond to altered irradiance with respect to photosynthetic acclimation becomes more limited after the leaf has emerged from the sheath of the surrounding, older leaf (Murchie *et al.*, 2005). Overall, published work suggests that stomatal size might be set at a relatively early stage of rice leaf development, but the temporal resolution of previous studies have not allowed a precise resolution of this developmental response window.

Due to the regular generation of leaves by the shoot apical meristem, the time interval between the generation of successive leaves is highly predictable (under controlled growth conditions) and is termed the leaf plastochron (Erickson and Michelini, 1957). A convenient and robust way of defining the developmental stage of any leaf is to define its plastochron stage (P). During the initial events of development as the leaf primordium grows out of the meristem the leaf is defined as being at P1 stage. As soon as the subsequent leaf forms at the meristem, the leaf is defined as entering the P2 stage of development (with the younger leaf being at the P1 stage). Thus, for any plant defining a leaf by its order of formation (leaf 1, leaf 2, leaf 3, and so on) and its P stage (P1, P2, P3 and so on) provides a robust means of identifying and comparing developmentally equivalent leaves. Previous work in our group had already established such a plastochron staging system for rice (Van Campen *et al.*, 2016). A particular advantage of this system in grasses, such as rice, is that it allows the prediction of the developmental stages of very young leaves hidden from view within the surrounding sheaths of older leaves, since (under controlled growth conditions) there is a strong predictive correlation of the P stage of older leaves with the P stage of younger leaves. In the experiments described in this chapter, this plastochron staging system was used to switch rice plants between LL and HL conditions so that leaves at early stages of development (P1, P2, P3, P4) differentiated under different irradiance levels during different phases of their development, allowing me to investigate the outcome on stomatal size and density in the mature leaves. This allowed me to investigate questions such as: if the early stage of a leaf's development occurs in a plant under LL but the later stage under HL, are the stomatal parameters typical of leaves grown continuously under LL or HL (or intermediate)? At

which P stage does the leaf lose its ability to respond to altered external environment?

As highlighted in previous chapters, stomata act as gas exchange regulators for the leaf. By modulating stomatal conductance (g_s) in response to environmental stimuli, they can optimize carbon uptake for photosynthesis while minimizing excessive water loss from transpiration (Farquhar *et al.*, 1980; Kim *et al.*, 2010). Maximal stomatal conductance occurs when stomata are opened to their widest possible aperture and is determined by two physical properties of stomata, namely size (guard cell length multiplied by guard cell pair width) and density (stomata number per unit area) (Franks *et al.*, 2009; Paul *et al.*, 2012). Smaller stomata have the advantage of a faster response time to altered environment (Hetherington and Woodward, 2003; Franks and Farquhar, 2007), thus when coupled with high stomatal density may enable a leaf to achieve high stomatal conductance when plants are in favourable growth conditions and rapidly reduce conductance when conditions are unfavourable (Drake *et al.*, 2013). However, Bussis *et al.* (2006) have shown that increased stomatal density can be compensated by reduced stomatal aperture, leading to the leaf maintaining a constant ratio of internal CO₂ concentration (C_i) to ambient CO₂ concentration (C_a). Thus, changes in stomatal size and density do not necessarily lead to changes in photosynthesis since plants display a high degree of plasticity in their ability to compensate for altered environmental conditions. Moreover, these differences can be species specific. For example, transfer from LL to HL conditions significantly increased photosynthesis in *Betula ermanii* and *Acer rufinerve* but not in *Fagus crenata* and *Alocasia macrorrhiza* (Sims and Percy, 1991; Oguchi *et al.*, 2005). Overall, the relationship between irradiance level and photosynthesis is complicated and stomatal properties represent only one parameter in this relationship. Thus, the extent to which stomatal properties in rice determine or limit photosynthetic performance remains an open question.

The experiments described in this chapter aimed to define the developmental window for stomatal size response to altered irradiance, therefore we expected to generate rice leaves with a range of stomatal parameters. We therefore extended these experiments to include a series of gas exchange analyses on

the mature leaves to examine the outcome of any changes in stomatal properties on photosynthetic performance. To what extent do leaves possess mechanisms that might maintain photosynthetic performance despite variation in stomatal properties arising during leaf development as a result of variation in the environment?

To summarise, in this chapter a series of experiments designed to investigate the influence of the light environment on stomata differentiation at different stages of rice leaf development are reported. Leaves were grown under one irradiance (high light, HL or low light, LL) then transferred to the alternative irradiance (HL to LL or LL to HL) at specific plastochron stages of leaf development (P1 to P5). The leaves were then allowed to grow to maturity and a series of measurements of stomatal size and leaf epidermal characteristics were made. Selected leaves were also analysed for various parameters of photosynthesis to investigate the outcome of any altered stomatal characteristics on these processes.

It should be noted that a portion of this chapter has already been published (van Campen *et al.*, 2016), establishing that the P3-P4 stage transition of the developing rice leaf is the latest phase of a developmental window during which the leaf can respond to altered plant irradiance with respect changes in stomatal properties.

4.2 Aims

1. Identify the stages of rice leaf development during which altered irradiance can influence stomatal patterning.
2. Investigate the outcome of developmental-stage specific altered stomatal patterning on rice leaf photosynthetic performance

4.3 Brief Methodology

All rice plants were grown hydroponically using the growth chamber settings and nutrient solution (described in section 2.1). The plants were grown in either HL or LL conditions (section 2.1) and when they had reached a particular plastochron stage (P1, P3 or P5) they were transferred to the opposite light condition. Since the developing leaf primordia were concealed in layers of leaf sheaths, the length of leaf no. 3 was used as a proxy to approximate leaf no. 5 P-stage (described in 2.2). For plants transferred from HL to LL, leaf 5 was sampled and measured 5 - 6 days after transfer (depending upon the plastochron stage when transfer took place), while for LL to HL transfer the sampling and measurements were made between 3 - 4 days after transfer. Two identical transfer identical experiments were carried out, one to measure stomatal and leaf development characteristics and the other to measure physiological and biochemical leaf parameters.

4.3.1 Stomatal and Epidermal Measurements

Rice leaves were prepared using the methods described in sections 2.4, 2.5 and 2.6.1. Measurements of SD, SCA and SPA, SCW, SCL, GCW, and the percentage of files containing stomata were made following the methods described in section 2.6.2. For each parameter five measurements per leaf were taken and averaged to obtain one data point. Eleven replicate leaves were used.

4.3.2 Physiological Measurements and Biochemical Analyses

Physiological and biochemical measurements were again made on the middle section of the fully expanded leaf 5. Three replicate leaves were used. Gas exchange measurements were carried out to obtain A-C_i curves as described in section 2.3.1. PAR was maintained at 2000 $\mu\text{mol m}^{-2}\text{s}^{-1}$ with 10% blue light and 90% red light. Stomatal conductance versus intercellular CO₂ concentration curves (g_s-C_i) were also obtained. Intrinsic water use efficiency (iWUE) was computed by taking the ratio between assimilation and stomatal

conductance at ambient (400 ppm) CO₂ (C_a) as well as when iWUE was at its maximum (iWUE_{max}), which was always at the last point of A-C_i and gs-C_i curves.

Pigment quantification and isotopic carbon discrimination determination were performed as described in sections 2.3.2 and 2.3.3 respectively using five replicate leaves for each analysis.

4.3.3 Statistical Analysis

For comparison of means, analysis of variance (ANOVA) was employed but when data were non-parametric (according to D'Agostino & Pearson omnibus normality test), Kruskal Wallis multiple comparisons test (add-on macro) was used instead. The relationship between variables was assessed using Pearson's correlation analysis where non-normal data were transformed using the best rounded λ (lambda) values suggested by Box-Cox transformation in Minitab. An F-test was also performed when the variance between two samples needed to be compared for similarity. All statistical analyses, graphs and contour plot were prepared using Microsoft Excel 2016, GraphPad Prism version 6 and Minitab 17 software.

4.4 Results

4.4.1 Effect of transfer of leaves from High Light to Low Light environment at different developmental stages on final stomatal parameters

Considering first Stomatal Complex Area (SCA), the mean value under continuous LL ($262 \mu\text{m}^2$) was significantly lower than observed in mature leaf 5 maintained under continuous HL conditions ($342 \mu\text{m}^2$) (Fig. 4.1A). On transfer from HL to LL at early stages in development (P1, P3) the final mean SCA was similar to those observed in leaves maintained continuously under LL. When plants were transferred at a later stage (P5), mean SCA was intermediate between HL and LL values.

One interesting observation was that although the variances measured in the HL, LL and P5 treatments were relatively small (Coefficient of variation, cv of 6.9%, 10.9% and 9.0% respectively), the values observed in the P3 and especially the P1 transfer experiments were much higher (cv of 13.5% and 26.5% respectively). A two-tailed F-test ($\alpha=0.05$) showed that there was a significant difference in variance ($p=0.01$) between P1 and LL treatments but there was no significantly different in variance between P3 and HL treatments ($p=0.14$).

Measurements of SCA, SCW and SCL are shown in Fig. 4.1 A B and C respectively. Similar tendencies were observed for both SCW and SCL. Stomatal complexes under HL conditions were wider and longer than observed under LL conditions. After transfer at P1 and P3 stages SCW and SCL values were more similar to those measured in leaves kept continuously under LL. Once again, although the SCW variances measured for HL, LL and P5-transfer leaves were relatively small (cv of 7.3%, 5.2% and 5.7% respectively), for leaves transferred at P3 and especially P1 stage the variances measured were much higher (cv of 6.6% and 15.4% respectively).

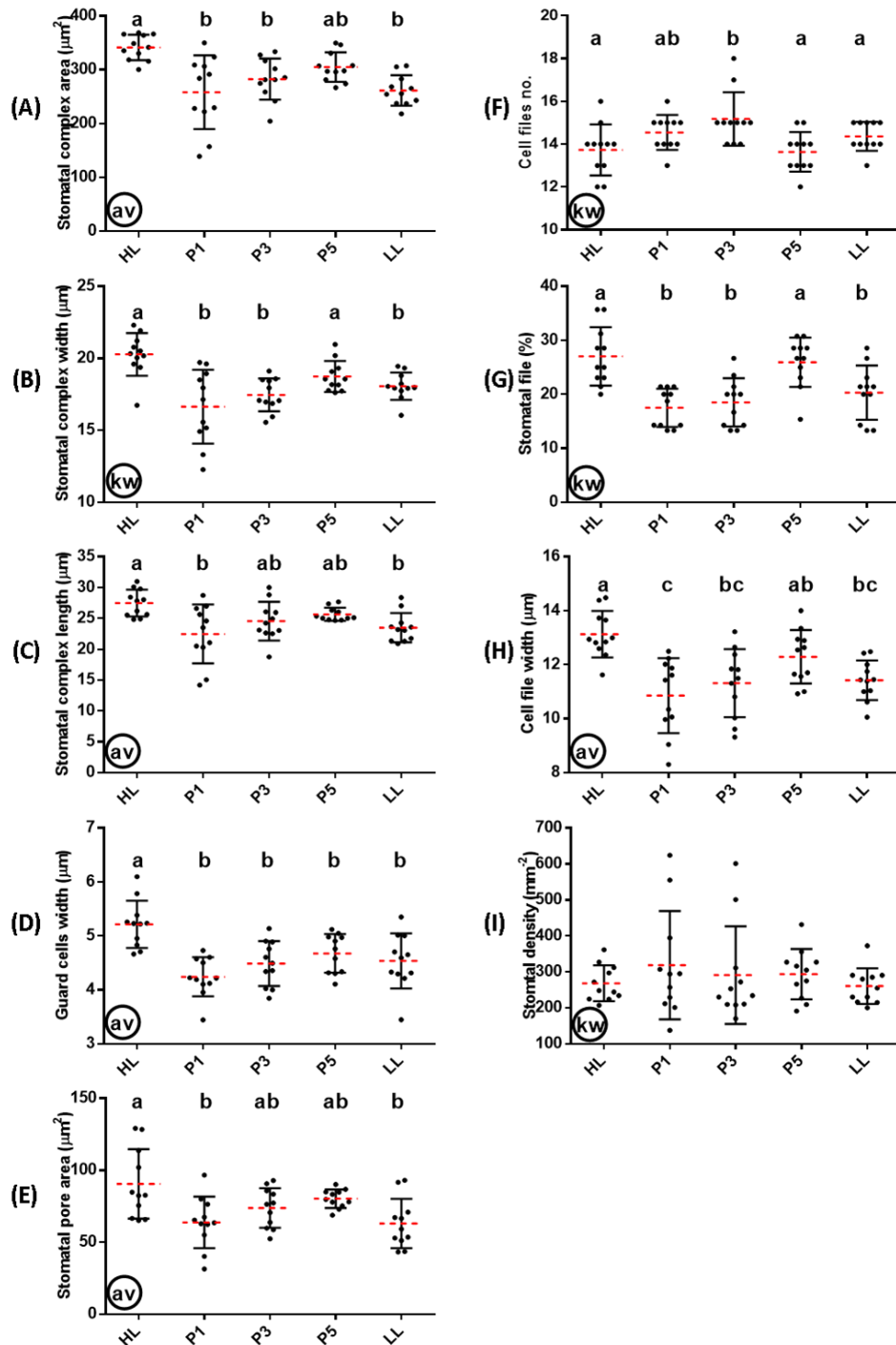


Figure 4.1:

Measurements of stomatal size (**A-E**), epidermal size (**F** and **H**) and stomatal patterning (**G** and **I**) in mature L5 grown in HL condition that were transferred to LL condition at different P-stages, as indicated. ANOVA followed by a post hoc Tukey's HSD test (av) was performed on data showing a normal distribution while the non-parametric Kruskal-Wallis multiple comparison test (kw) was performed on data showing non-normal distribution. Each black dot represents a single measurement. Vertical error bars represent standard error of means while the dotted horizontal red lines are the means. Treatments that share same letter in a grouping cannot be statistically distinguished (P-value <0.05).

Again, the P1 data had a significantly different variance ($p < 0.01$) compared to the LL control but this was not the case for the P3 treatment data. The same trend in variance was also observed for SCL variance analysis, *i.e.*, P1 and P3 transfer value showed a relatively high variance compared to the other data sets in the experiment. Correlation analysis also showed that both SCW and SCL showed a highly significant positive correlation with SCA ($r = 0.72$ and $r = 0.82$ respectively, $p < 0.01$, Table 4.1).

Table 4.1:

Pearson's correlation coefficients (r) among the pooled values of stomatal size, patterning and leaf epidermal properties from the transfer experiments ($n = 11$ for each parameter). Single asterisk * indicates correlations which are significant at $p < 0.05$ confidence limit while double asterisks ** indicate correlations which are significant at $p < 0.01$ confidence limit.

Parameter	SCA	SCW	SCL	GCW	SPA	CFN	SF%	CFW	SD
SCA									
SCW	0.72**								
SCL	0.82**	0.60**							
GCW	0.45**	0.55**	0.34**						
SPA	0.81**	0.46**	0.73**	0.37**					
CFN	-0.16	-0.24*	0.00	-0.23*	-0.14				
SF%	0.26*	0.27*	0.21*	0.10	0.17	-0.16			
CFW	0.67**	0.70**	0.50**	0.51**	0.57**	-0.54**	0.28**		
SD	-0.58**	-0.44**	-0.51**	-0.28**	-0.52**	0.03	0.24*	-0.57**	

Each stomatal complex contains a guard cell pair which forms the actual stomatal pore. To investigate the extent to which measurements of stomatal complex dimension acted as a proxy for guard cell dimension and pore size, these parameters were analysed. As shown in Fig. 4.1D and 4.1E the pattern of guard cell width (GCW) and stomatal pore area (SPA) in leaves after the different treatments was similar. Highest mean values of GCW and SPA were measured in leaves grown continuously under HL ($5.2\mu\text{m}$ and $90.6\mu\text{m}^2$ respectively) and the mean values for these parameters were lower in leaves grown continuously under LL ($4.5\mu\text{m}$ and $63.0\mu\text{m}^2$ respectively). Leaves

transferred at stage P1 from HL to LL showed relatively low means of GCW and SPA whereas leaves transferred at stages P3 and P5 showed mean values either similar to LL samples (for GCW) or intermediate between HL and LL samples (for SPA). GCW and SPA values showed a positive correlation with SCA ($r=0.45$ and $r=0.81$ respectively, $p<0.01$, Table 4.1).

Overall, the data shown in Fig. 4.1A-E suggested that leaves grown under LL had smaller stomatal complexes as well as other size related parameters than those grown under HL, and that transfer from HL to LL resulted in smaller stomatal complexes even when the transfer was performed relatively late in development (P5). For some parameters such as SCA, SCW and SCL, when the transfer was performed at relatively early stages of development (P3 and/or P1) there was a marked variation in the measured values, with some extremely small values observed even when compared to the LL leaves. The correlation analysis in Table 4.1 shows that SCA parameter is a good proxy to estimate other stomatal size related parameters as they all had a highly significant positive correlation with SCA.

To investigate what outcome these shifts in SCA had on stomatal density (SD), this parameter was measured in the same leaves samples analysed in Fig. 4.1A-E. The results of this analysis (shown in Fig. 4.1I) indicated that for leaves maintained under continual LL or HL the differences in the mean SD values were minimal (261 and 269 stomata mm^{-2} respectively). Although mean SD values in leaves transferred from HL to LL at different developmental stages (P1, P3, P5) tended to be slightly higher than those observed in HL and LL, analysis of the data revealed that the transferred leaves were characterised by a massive spread of SD values, with P1 transferred leaves showing SD value as high as 624 stomata mm^{-2} compared with extreme SD values in HL leaves of 362 stomata mm^{-2} and in LL leaves of 373 stomata mm^{-2} . A similar trend in other size parameters was also observed, with variances measured in the HL, LL and HL-LL P5 samples generally being relatively small but large variance being observed when transfer was performed at P1 and P3 stages. Since unequal variance violates the requirements for ANOVA, a non-parametric Kruskal-Wallis test was used to analyse SD. By this analysis the mean SD did not significantly differ between

any of the treatments, but this similarity in mean value obscured a difference in variance depending on leaf stage at transfer from HL to LL.

SD in a rice leaf is likely to reflect both the size of stomatal complexes and the number/size of cell files within which stomata arise. To investigate the potential relationship of stomatal density and size to these parameters epidermal file number within interveinal gaps and the number of cell files within which stomata arose were also studied. As shown in Fig. 4.1F leaves kept under continuous LL had a slightly higher mean number of cell files than HL leaves (about 14 cell files), but the spread of these values was higher under HL than LL conditions (cv of 8.7% and 4.7% respectively). In the P1 and P3-transfer experiments, leaves showed higher mean values for CFN, with P3 transferred leaves having an extreme value of 18 cell files and a minimum of 14 whereas HL leaves had a maximum of 16 cell files and a minimum of 12. Leaves kept under continuous LL had a maximum CFN of 15 and a minimum of 13. CFN showed a significant negative correlation with cell file width (CFW, $r = -0.54$, $p < 0.01$, Table 4.1) but when the number of cell files containing any stomata is considered (Fig. 4.3G) a very weak inverse relationship ($r = -0.16$) to CFN was observed. Thus for leaves maintained continuously under HL the percentage of stomata-containing cell files was significantly higher than for LL leaves and leaves transferred at P1 or P3 stage, suggesting that P3 is the last stage able to initiate additional rows of stomatal or epidermal files in response to altered irradiance. For any given interveinal gap sampled the maximum number of stomatal files was always four.

Since in rice leaves stomata arise in epidermal cell files the width of these files (CFW) is likely to influence the size of the stomatal complexes. To test this idea, the cell file width (CFW) in the transferred and control plants was measured. As shown in Fig. 4.3H there was a similar pattern of CFW and the stomatal complex width (SCW) in Fig. 4.3C ($r = 0.70$, Table 4.1) and a significant inverse correlation with cell file number (Fig. 4.3F) ($r = -0.24$). Thus, mean CFW was significantly high in leaves grown under continuous HL (13.1 μm) and those transferred at P5 from HL to LL (12.3 μm), whereas CFW was significantly smaller in LL (11.4 μm) leaves and those transferred from HL to LL at early stages of P1 and P3 (10.9 μm and 11.3 μm respectively). Once

again, the P1 and P3 transferred leaves were characterised by relatively high variances for the parameter measured, with some extremely narrow cell files measured in the P1 transferred leaves (8.3 μ m).

4.4.2 Effect of transfer of leaves from Low Light to High Light environment at different developmental stages on stomatal parameters

The results described in the previous section described the outcome on stomatal parameters of transferring plants from HL to LL conditions at various stages of leaf development. I also investigated the outcome of the reverse situation where plants were transferred from LL to HL conditions. As shown in Fig. 4.2A, when leaves were transferred at very early stage of development namely P1, the mean value of SCA in the mature leaves was similar to that measured in plants grown continuously under HL. When the transfer occurred later in development (stage P3 and P5), mean SCA remained similar to that measured in plants grown under continuous LL. The variance in the values observed under transfer conditions especially P5 tended to be higher (cv of 17.3%) than those values observed in P1 and P3 transfers and plants maintained under continual HL or LL (cv of 11.4%, 11.4%, 10.9% and 6.9% respectively). To investigate the contribution of change in stomatal complex width (SCW) and length (SCL) to the observed changes in SCA, I measured these parameters in the various treatments. As shown in Fig. 4.2B and 4.2C, similar patterns of change in values were observed in both SCW and SCL, although the absolute value of these differences were often quite small. Thus, after transfer at very early stage of leaf development (P1), there were slight increases both in mean SCW and SCL whereas in the P3 and P5 transferred leaves changes in SCW and SCL were minimal. Correlation analysis in Table 4.1 has shown that there were significant positive relationships between SCA with SCW and SCL, thus showing these parameters are good predictors for each other.

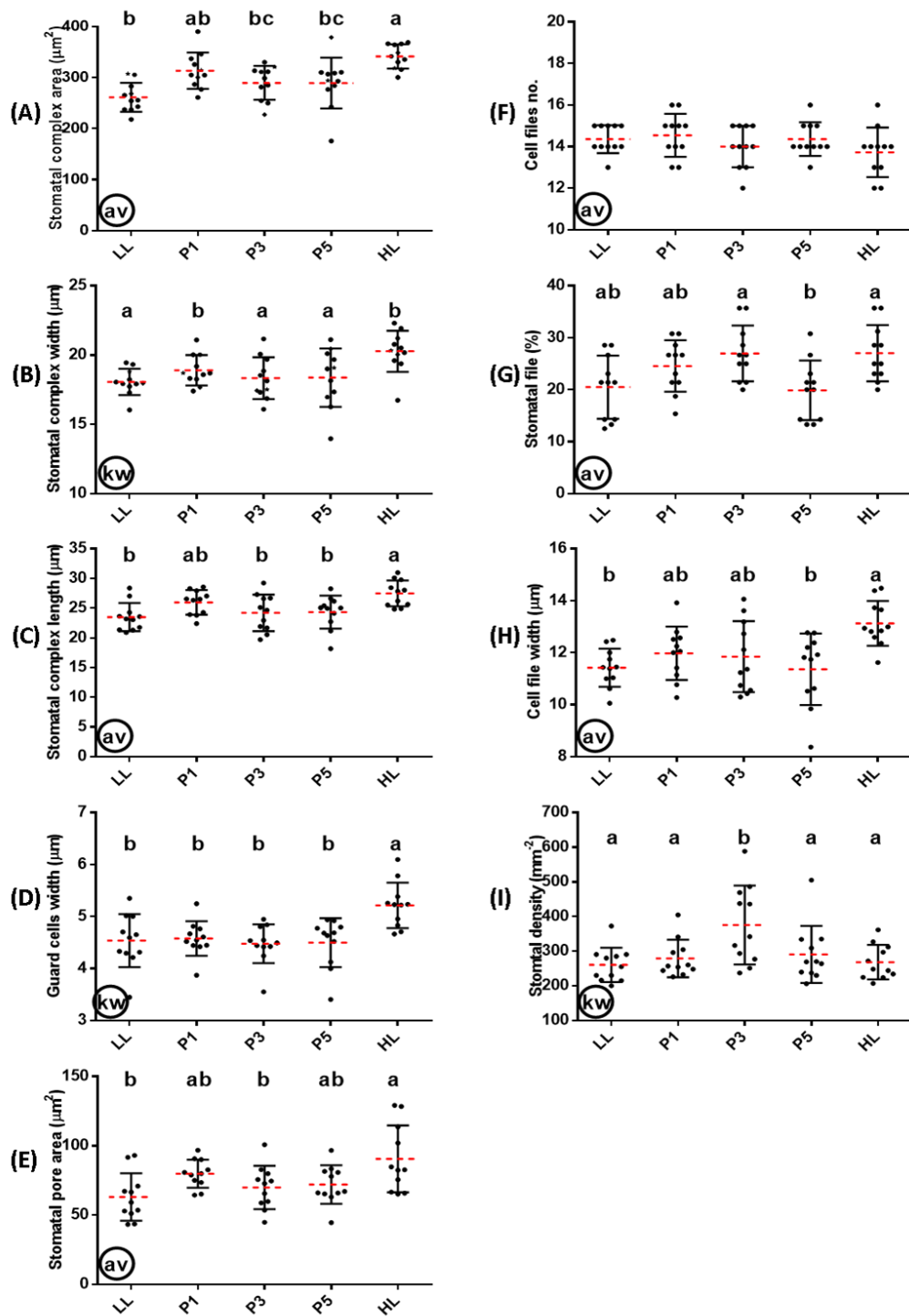


Figure 4.2:

Measurements of stomatal size (**A-E**), epidermal size (**F** and **H**) and stomatal patterning (**G** and **I**) in mature L5 grown in LL condition that were transferred to HL condition at different P-stages, as indicated. ANOVA followed by a post hoc Tukey's HSD test (av) was performed on data showing a normal distribution while the non-parametric Kruskal-Wallis multiple comparison test (kw) was performed on data showing non-normal distribution. Each black dot represents a single measurement. Vertical error bars represent standard error of means while the dotted horizontal red lines are the means. Treatments that share same letter in a grouping cannot be statistically distinguished (P -value < 0.05).

With respect to guard cell width (GCW) and stomatal pore area (SPA), generally mean GCW showed no increase in leaves transferred at any developmental stage, in fact it slightly decreased under P3 and P5 transfers, whereas for plants maintained under continuous HL GCW was significantly higher than in LL-maintained or transferred leaves (Fig. 4.2D). In contrast, estimates of SPA (Fig. 4.2E) indicated that mean values in early transfer (P1) leaves were higher than those measured in P3 and P5 transfer, which were similar to HL leaves. The high variance measured for all of these samples meant that overall there was no significant difference in SPA.

In terms of altered stomatal density (SD), leaves grown under continuous HL and LL and under P1 and P5 transfers had similar SD (Fig. 4.2I). Surprisingly the transfer at P3 resulted in higher mean SD values than the rest of the treatments and this was mainly due to a few leaves in this transfer showing unusually very high densities above 400 stomata mm^{-2} . To investigate whether the differences in SD observed in some transferred samples reflected differences in the number of cell files in the interveinal gap, values of cell file number (CFN), width (CFW) and the number of cell files containing stomata were also measured. With respect to CFN, although there were some differences in mean values for the different treatments, the mean CFN value (about 14) was comparable for all treatments (Fig. 4.2F), although it was noticeable that the P1 transferred samples had the most values of CFN 14 or greater. In terms of CFW, the P5 transferred samples were distinguished by having some extremely narrow cell files ($8.4\mu\text{m}$), leading to a significantly different CFW from leaves maintained under continual HL (Fig. 4.2H). CFN and CFW also showed a significant inverse correlation ($r = -0.54$, Table 4.1) thus can be used as a good predictor for one another. The percentage of cell files containing stomata in the P5 transferred leaves was similar to those maintained under continuous LL, whereas the P3 transferred leaves had mean values very similar to those measured in HL leaves (Fig. 4.2H). P1 transferred leaves however had intermediate values between HL and LL. There was, however, a high variation in percentage of files containing stomata in all treatments. Despite this, there was still a positive significant, although weak, relationship between files containing stomata and CFW ($r = 0.28$).

4.4.3 Summary of effect of transfer between high and low light environments at specific leaf developmental stages on stomatal pattern and size

With respect to the transfer either from HL to LL or LL to HL, the former in general allows significant changes in almost all the parameters after P1 transfer (Fig. 4.3A). Leaves transferred at the later P3 stage showed less ability in significantly changing as many parameters as the transfer at P1, whereas transfer at the later P5 stage did not lead to any significant change in any parameter. The high variation of SCA values, especially in P1 and P3 transfer treatments, implied developmental stages where stomatal phenotypes are highly plastic with respect to environmental signals such as the irradiance intensities used in this experiment. Differences in SCA measurements are determined by both length and width properties of the complex where SCL in general showed a higher degree of positive correlation with SCA. Due to the linear nature of stomatal arrangement in grass leaves, width of SCA is to some extent dependent on cell file width. CFW was most plastic at P1 and P3 stages but by P5 it becomes less responsive to altered irradiance. Similarly, the number of cell files formed (reflecting longitudinal cell divisions during leaf development) is flexible at P1 and P3 but much less flexible at P5 stage.

In rice leaves, it appears that some cell files are stomata-forming while others are not (i.e., stomatal patterning is set by cell file interactions), as evident in Fig. 2.6). It is worth noting that most interveinal gaps in rice leaves contain a maximum of four stomata-containing files while the total number of cell files may vary considerably. This may be connected with stomata position as stomata are always formed over mesophyll cells but not over bulliform cells. Leaves transferred at P1 and P3 stage tend to have many, narrow files but only a small percentage of these form stomata. By P5, the number and width of cell files is set, as well the percentage of cell files containing stomata.

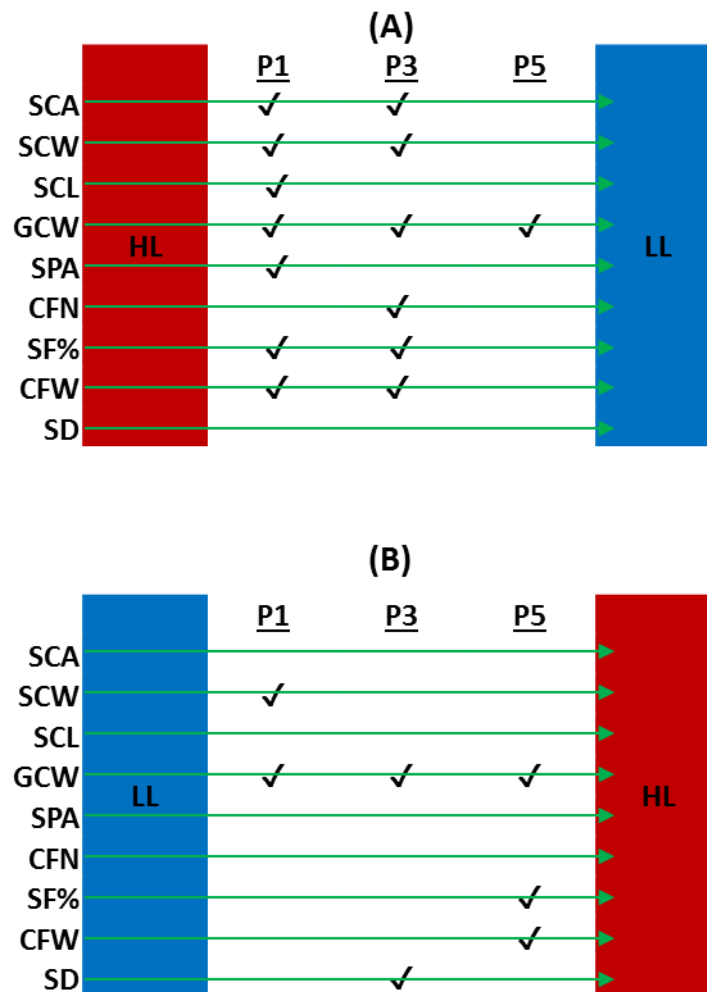


Figure 4.3:

Summary of possible windows of sensitivity at different plastochron stages (P1 to P5) for the transfer from HL to LL (**A**, based on Fig. 4.1) and LL to HL (**B**, based on Fig. 4.2) for various stomatal and epidermal properties. Each tick (✓) symbol under any P-stage denotes the possibility of altering the corresponding parameter compared to the initial light condition (shaded column on the left).

The resultant stomatal patterning shows that there is little major difference between SD in HL and LL leaves but HL leaves have significantly more stomatal containing cell files than LL leaves. The other main difference is stomatal size (SCA), with HL leaves having larger stomata due to an increase in cell file width and the length of the cells formed within a file.

The above points describe the transfer events for transfer from HL to LL. For LL to HL transfer, however, the same ability to significantly change the studied parameters after P1 and P3 transfer was not as clear. This direction of transfer

generally led to less significant alteration in the parameters measured (Fig. 4.3B). Changes are more minor, less pronounced or intermediate. Even at the early P1 and P3 stages the parameters measured seem less plastic and responsive than plants switched from HL to LL conditions. Although the transfer at P3 could significantly alter the SPA, the spread of the data (in Fig. 4.2E) were much larger compared to the transfer at P1 and P3. Nevertheless, it is interesting to note that LL to HL transfer still led to a significant change in guard cell width at each P stage analysed.

4.4.4 Analysis of the outcome of altered stomatal pattern and size on leaf physiology

The results of the analyses in Fig. 4.1 and Fig. 4.2 indicated that by switching rice leaves between different light environments at particular stages of leaf development it was possible to generate leaves with distinct stomatal densities and size. To investigate the outcome of these changes on leaf performance, I performed a series of physiological analyses on some of these leaves (n=3). These leaves described in each subsection below dealing with photosynthetic assimilation, stomatal conductance and intrinsic water use efficiency provided paired data with the measurement of stomatal structure reported in the previous section. This leads to the second hypothesis of this study; that some stomatal or epidermal properties in rice could be a good indicator of important leaf physiological characteristics, thus reflecting overall leaf performance and efficiency.

4.4.5 Assimilation Rate

A series of A-C_i curves was obtained for three plants, each either maintained under continuous HL or LL conditions or transferred from HL to LL at P1, P3 or P5 stage before assessment of physiology at maturity. Measurements were made immediately upon leaf no. 5 maturity (P6) which was marked by the appearance of the collar (joint in between leaf blade and the sheath). From the leaf emergence to this point, the leaf blade had been exposed to the new light

condition (before measurements took place) about 3-4 and 5-6 days for HL and LL conditions, respectively. Measurements were taken very close to full leaf extension, thus ameliorating any potential for reduction in photosynthesis as a consequence of ageing (Murchie *et al.*, 2005).

HL grown leaves in general (Fig. 4.4iv-HL) had higher maximum assimilation rate (A_{\max} , about $46 \text{ mmol CO}_2 \text{ m}^{-2} \text{ s}^{-1}$) than LL grown leaves (about $33 \text{ mmol CO}_2 \text{ m}^{-2} \text{ s}^{-1}$). The first phase (Rubisco limited) of the A- C_i curve for HL grown leaves had a steeper slope than LL grown leaves (Fig. 4.4iv-LL) indicating rapid assimilation of CO_2 suggesting an abundance of Rubisco in the HL leaves. The first phase also ended at lower C_i concentration (about 213 ppm) for HL grown leaves than LL leaves (about 243 ppm), thus a quicker shift to the next phase of the curve (RuBP regeneration limited), marked by a subtle decrease in the curve slope. HL grown leaves had some variance in both A and C_i values measured, especially in the second phase of the curve, whereas LL grown leaves had the same variance trend only for the A values but not C_i values, probably due the lower overall CO_2 assimilation compared to HL grown leaves enabling stomata to more rapidly adjust to maintain a more consistent C_i environment.

It is quite surprising to see that transfer at P1, P3 and P5 stage (Fig. 4.4iv-P1, P3, P5) on average produced similar A- C_i curves and that the A_{\max} and C_i concentration at which the shift into the second phase of the curve occurred was similar to those leaves grown in continuous LL. Further investigation by deriving useful photosynthetic parameters support this claim; the rate for A_{400} (Fig 4.5 A, about $20\text{-}25 \text{ mmol CO}_2 \text{ m}^{-2} \text{ s}^{-1}$) and A_{\max} (Fig. 4.5 B, about $30 \text{ mmol CO}_2 \text{ m}^{-2} \text{ s}^{-1}$) for transfer at P1, P3 and P5 were similar to LL leaves. Such trends were tightly bound to the V_{cmax} (Fig. 4.5C) which also had the same trends as the assimilation rates, where LL leaves had V_{cmax} value of about $40\text{-}50 \text{ mmol CO}_2 \text{ m}^{-2}\text{s}^{-1}$.

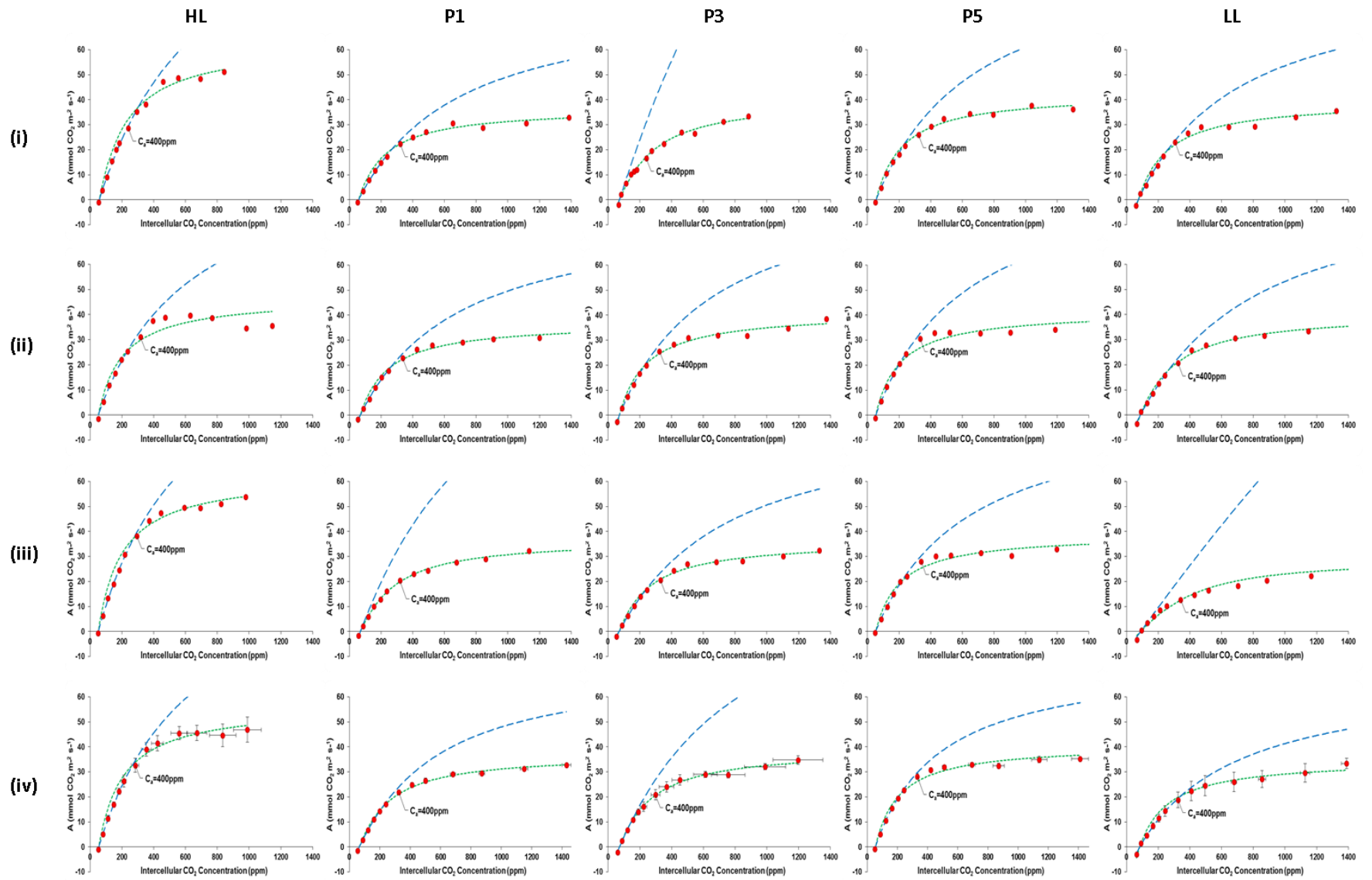


Figure 4.4

A-C_i curves in mature rice leaves for the transfer experiment from HL to LL. Rows (i), (ii) and (iii) represent individual curves (total n=3) for the corresponding treatment labelled at the top of each column. Row (iv) represents mean A- C_i curve for the particular treatment where the horizontal-vertical bars represent standard error of mean. The blue dotted lines are best fit curves for CO₂ assimilation rate limited by the amount and activity of Rubisco (enzyme limited/RuBP saturated) while the green dotted lines are best fit curves for CO₂ assimilation rate limited by RuBP regeneration (light limited/RuBP limited). Each A-C_i curve is marked with C_a=400ppm to approximately show assimilation rate at the current ambient CO₂ level while the experiment took place.

The relative stomatal limitations (*I_s*) for HL (about 20%) and LL (about 15%) leaves were similar to the *V_{cmax}* trend but the P5-transferred leaves showed exceptionally low *I_s* (about 7%) thus partially explaining their relatively higher *V_{cmax}* values compared to P1 and P3 transferred leaves (Fig. 4.5D). *J_{max}* for the transfer at P5 stage (Fig. 4.5E) had an intermediate value between HL (closer) and LL leaves (about 125 mmol e⁻ m⁻²s⁻¹). Pigments analysis for chlorophyll a/b ratio (Fig. 4.5 F) also showed that the P5-transferred leaves had similar ratio (about 4) with HL leaves. thus further explaining their ability to have comparable *A₄₀₀* value with HL leaves. Transfer under all stages produced minimum variation with regard to assimilation rate but on average transfer at P3 produced the largest variation in C_i values, which were similar to HL grown leaves.

When the transfer was performed in the opposite direction from LL to HL condition, leaves transferred at P1 on average (Fig. 4.6iv-P1) had comparable A-C_i curve pattern to HL grown leaves. *A₄₀₀* analysis (Fig. 4.7A) showed that there was a tendency for HL and P1-transferred leaves to have higher *A₄₀₀* (both about 33 mmol CO₂ m⁻² s⁻¹) values than LL leaves while transfer at later P3 and P5 stages resulted in similar *A₄₀₀* to LL leaves (about 18-25 mmol CO₂ m⁻² s⁻¹). But the same trend was not evident in the *A_{max}* analysis (Fig. 4.7B) since transfer at any P-stages would result in comparable values to HL leaves (about 45 mmol CO₂ m⁻² s⁻¹).

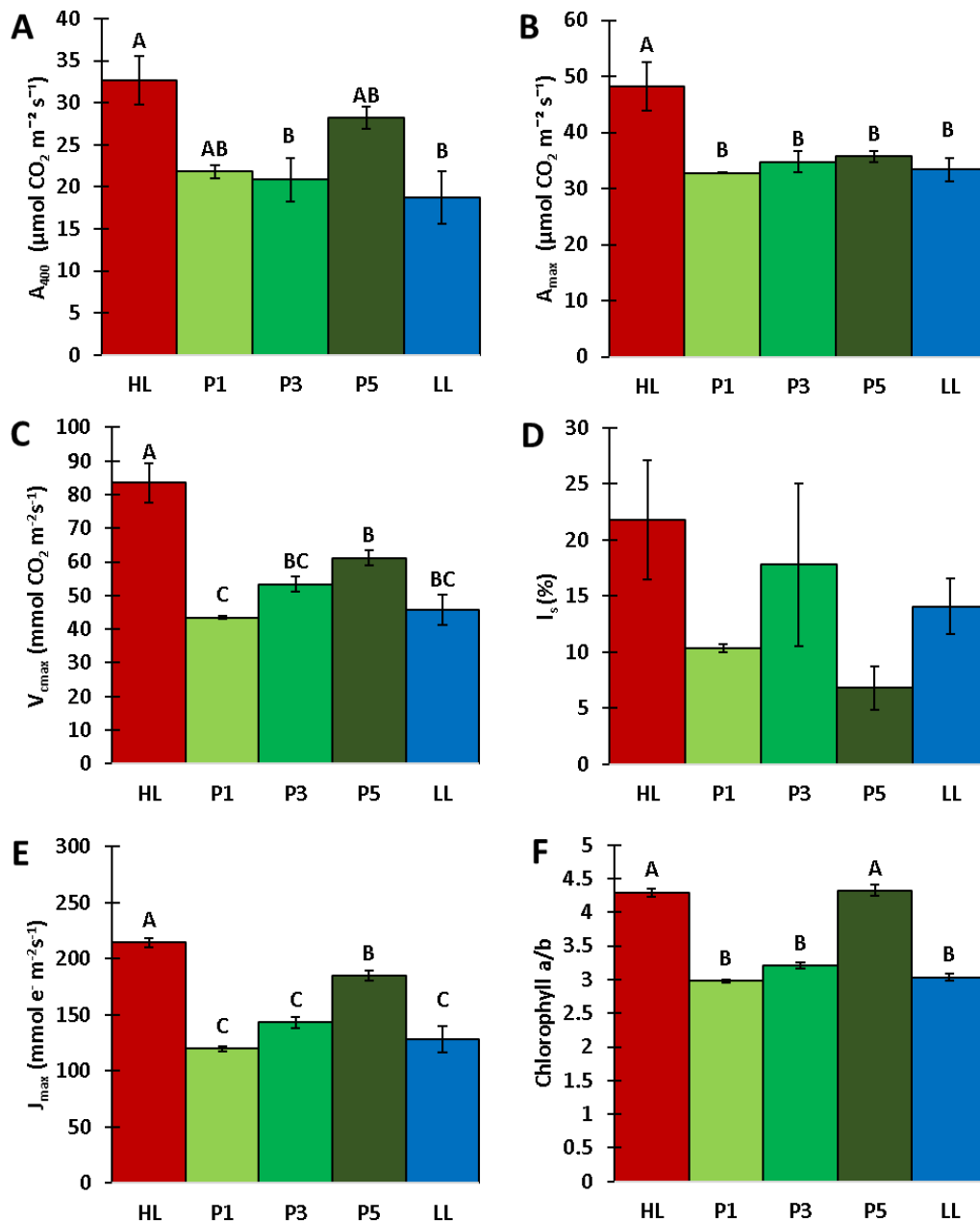


Figure 4.5

Mean assimilation rates measured at 400ppm CO₂ (ambient level, A_{400}) (**A**) and maximum assimilation rates (A_{max}) (**B**) achievable for the HL to LL transfer experiment. The measured photosynthetic rates are explained by similar trend in maximum carboxylation (V_{cmax} , **C**) whose capacity depends on CO₂ supply influenced by the relative stomatal limitation (I_s in **D**). The electron transport (J_{max} , **E**) rates also have similar trend to assimilation and the capacity is explained by the ratio of chlorophyll a/b (**F**). All means are extracted from Fig. 4.4iv. One way ANOVA followed by a post hoc Tukey's HSD test where $n=3$ with groups sharing different letters are significantly different ($p < 0.05$) and error bars represent standard error of mean.

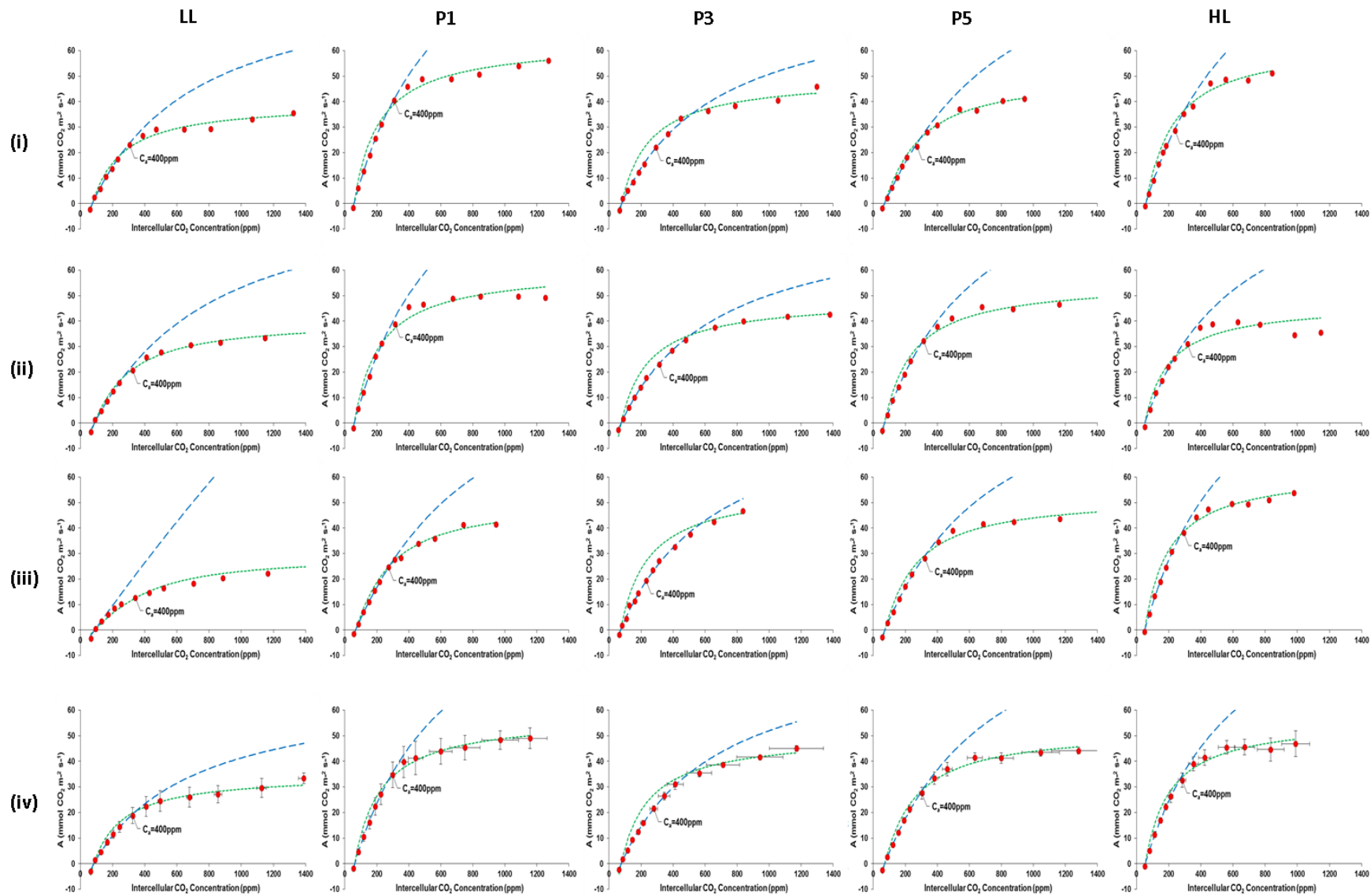


Figure 4.6

A-C_i curves in mature rice leaves for the transfer experiment from LL to HL. Rows (i), (ii) and (iii) represent individual curves (total n=3) for the corresponding treatment labelled at the top of each column. Row (iv) represents mean A-C_i curve for the particular treatment where the horizontal-vertical bars represent standard error of mean. The blue dotted lines are best fit curves for CO₂ assimilation rate limited by the amount and activity of Rubisco (enzyme limited/RuBP saturated) while the green dotted lines are best fit curves for CO₂ assimilation rate limited by RuBP regeneration (light limited/RuBP limited). Each A-C_i curve is marked with C_a=400ppm to approximately show assimilation rate at the current ambient CO₂ level while the experiment took place.

Transfer at later P3 and P5 stages decreased the A_{max} value to around 40 mmol CO₂ m⁻² s⁻¹ but still much higher than those of LL grown leaves. Interestingly variations seen in P1 transferred leaves were also similar to those of HL grown leaves, while for transfer at P3 and P5 the variations were more pronounced in C_i values, especially in the second phase of the curve. These C_i variations could be explained by some odd individual curves (Fig.4.6iii-P3 and 4.6i-P5) where they looked steep in the first phase of the curve with a short lived second phase, suggesting rapid CO₂ influx regulation as well as high assimilation rate. V_{cmax} analysis (Fig. 4.7C) showed that transfer at any P-stages would result in V_{cmax} value similar to HL leaves (80 mmol CO₂ m⁻²s⁻¹) where P1-transferred leaves had exceptionally high V_{cmax} value among all treatments of about 85 mmol CO₂ m⁻²s⁻¹. This indicates a comparable amount of Rubisco between HL and P1-transferred leaves as well as less obstructed CO₂ diffusion, which was evident by a relatively lower (similar to LL leaves) stomatal limitation of about 15% (Fig. 4.7D). J_{max} had the same trend as the A_{max} analysis earlier (Fig. 4.7 E) where HL leaves and the P-transferred leaves had comparable J_{max} values around 200-250 mmol e⁻ m⁻²s⁻¹. Interestingly, all P-transferred leaves had similar chlorophyll a/b ratio (about 3.5, Fig. 4.7F) while LL grown leaves had the ratio of 3, indicating less investment in making chlorophyll-b for LHCII to capture more photons.

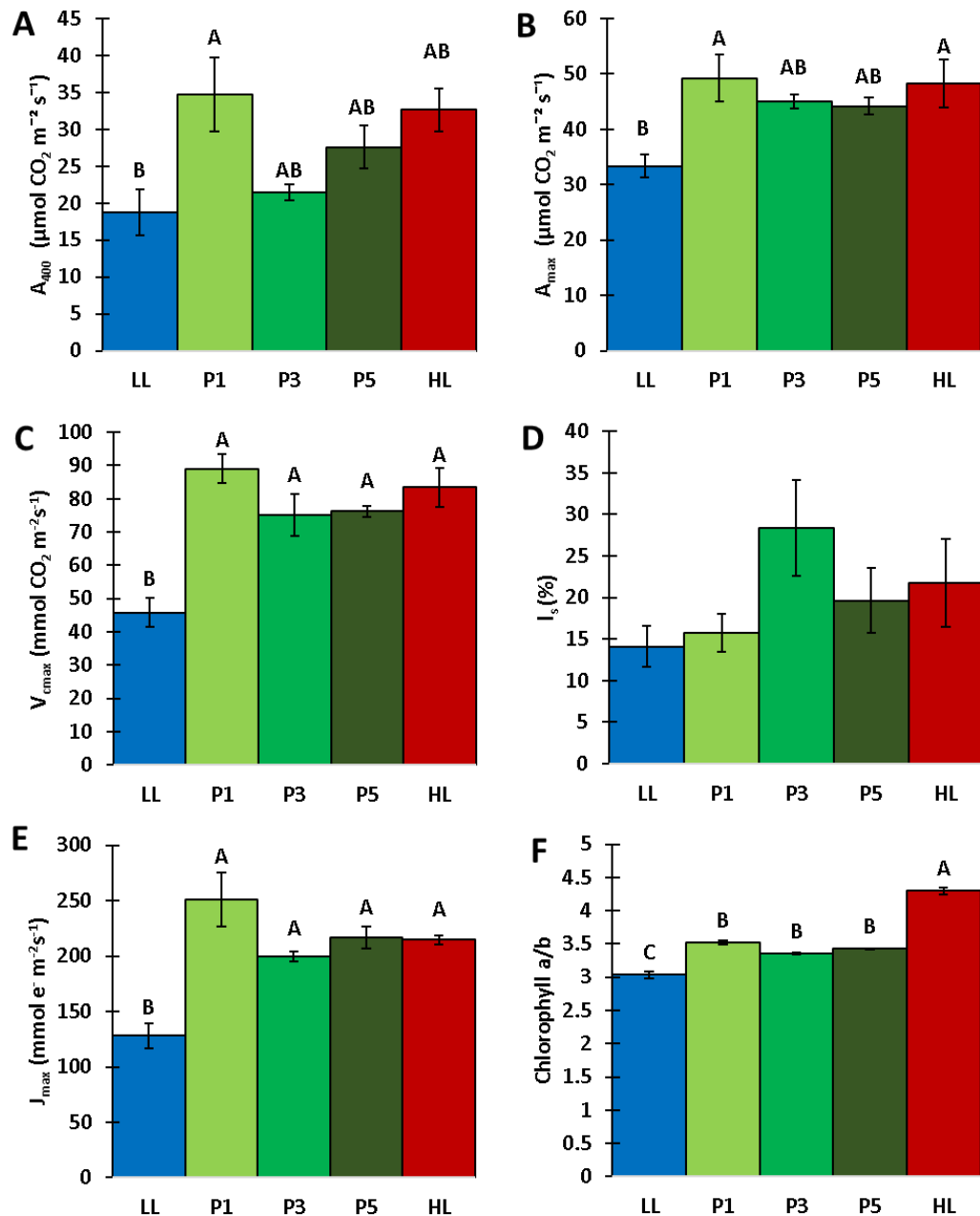


Figure 4.7

Mean assimilation rates measured at 400ppm CO₂ (ambient level, A_{400}) (**A**) and maximum assimilation rates (A_{max}) (**B**) achievable for the LL to HL transfer experiment. The measured photosynthetic rates are explained by similar trend in maximum carboxylation (V_{cmax} , **C**) whose capacity depends on CO₂ supply influenced by the relative stomatal limitation (I_s in **D**). The electron transport (J_{max} , **E**) rates also have similar trend to assimilation and the capacity is explained by the ratio of chlorophyll a/b (**F**). All means are extracted from Fig. 4.4iv. One way ANOVA followed by a post hoc Tukey's HSD test where $n=3$ with groups sharing different letters are significantly different ($p < 0.05$) and error bars represent standard error of mean.

Overall high light grown leaves undoubtedly had higher assimilation rates than LL grown leaves either measured under ambient CO₂ level (A_{400}) (Fig. 4.5A and 4.7A) or A_{max} (Fig. 4.5B and 4.7B) in both HL-LL-HL transfer directions. It is interesting to note that the rice leaf seems to have the ability to achieve A_{max} similar to the final light condition after transfer at any P-stage whereas A_{400} in general seems to follow the trend where transfer at P1 and/or P3 is the cut-off point to produce leaves with an assimilation rate similar to leaves continuously grown in the final light condition to which they are exposed.

4.4.6 Stomatal Conductance (g_s)

A series of g_s - C_i curves were also obtained from the three plants used in the previous subsection dealing with assimilation. There was a general trend for both HL and LL grown leaves (Fig. 4.8iv-HL and LL) where g_s values increased steadily in low CO₂ conditions before decreasing rapidly (HL leaves) or gradually (LL leaves) before reaching the lowest points. The key difference in overall curve shape was that HL grown leaves covered a wider range of g_s with changing CO₂ concentration, indicating a more rapid stomatal movement than LL grown leaves, which had steadier g_s values and less variation. The transfer at P1 and P3 resulted in similar overall curve pattern to LL grown leaves but, surprisingly, P5 on average (Fig. 4.8iv-P5) had the highest g_s values at any given C_i points. Fig. 4.9A shows mean g_s values at 400ppm CO₂ concentration (g_{s400}) for the individual plants while Fig.4.8B shows the mean maximum g_s values (g_{smax}) and for the same treatments. Interestingly in most cases g_{smax} values occurred before ambient CO₂ level (marked as $C_{a=400ppm}$ in Fig. 4.8). HL grown leaves on average had higher g_{s400} and g_{smax} than LL grown leaves but the leaves of P5 transfer unexpectedly had the highest overall g_s values (Fig. 4.9A and 4.9B respectively).

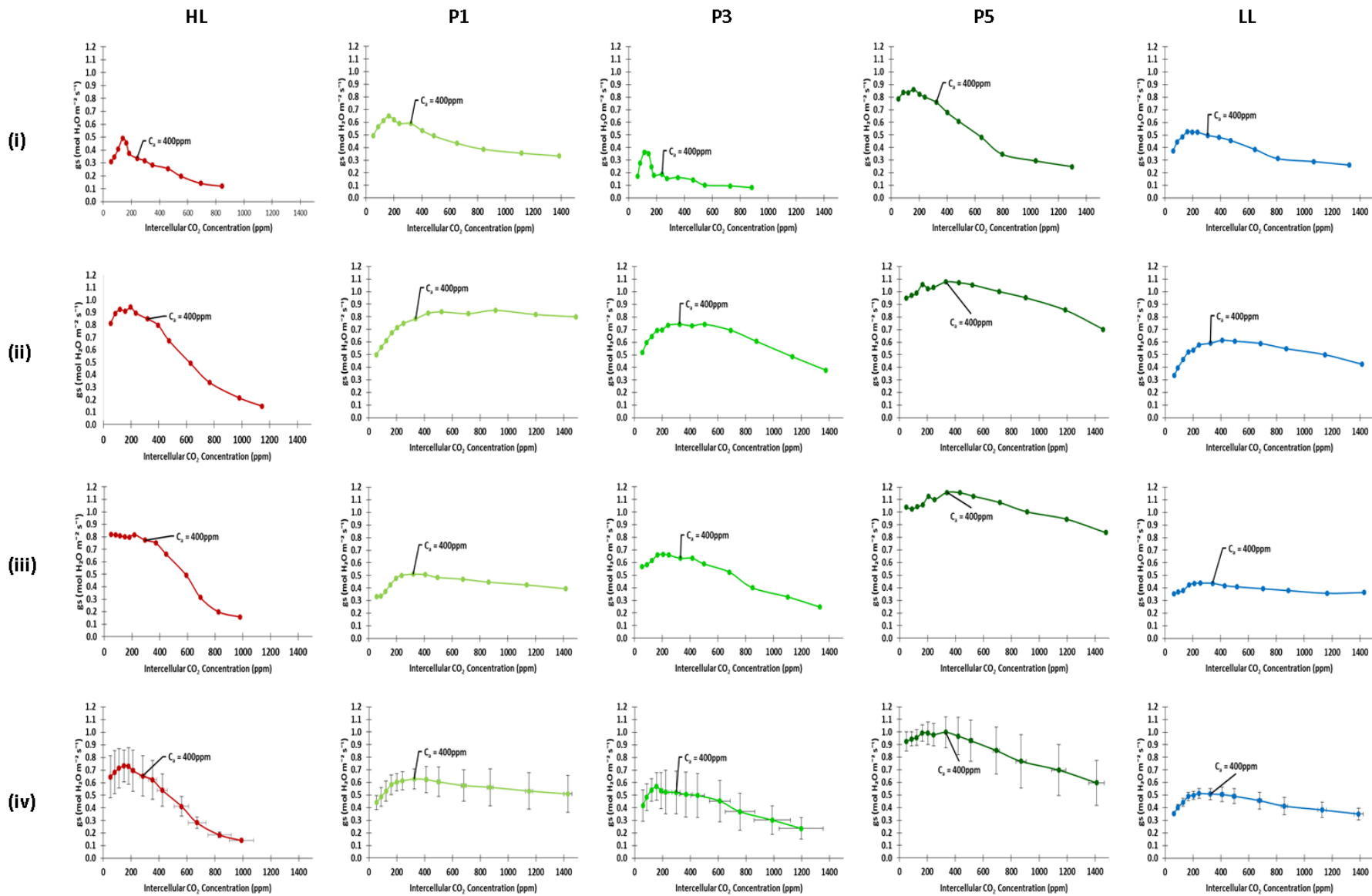


Figure 4.8

g_s - C_i curves in mature rice leaves for the transfer experiment from HL to LL. Rows (i), (ii) and (iii) represent individual curves (total $n=3$) for the corresponding treatment labelled at the top of each column. Row (iv) represents mean g_s - C_i curve for the particular treatment where the horizontal-vertical bars represent standard error of mean. Each g_s - C_i curve is marked with $C_a=400$ ppm to approximately show assimilation rate at the current ambient CO_2 level while the experiment took place.

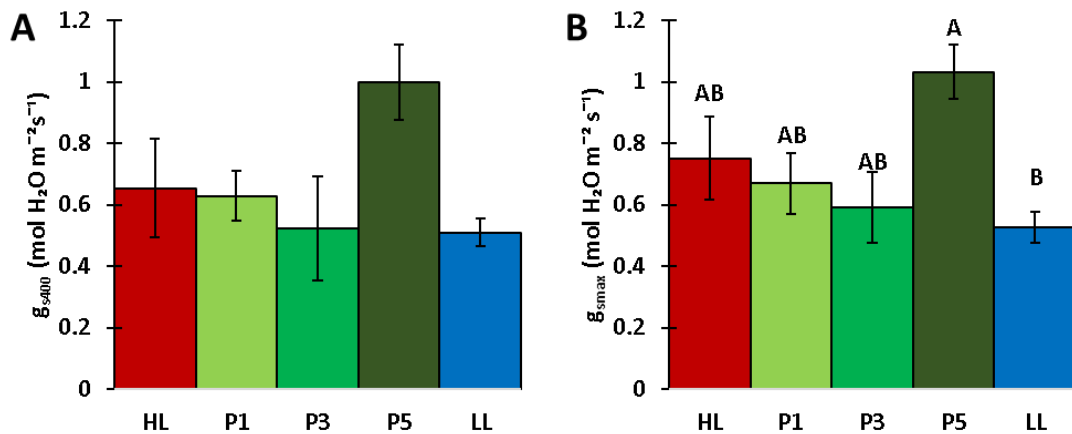


Figure 4.9

Mean stomatal conductance (g_s) rates measured at 400ppm CO_2 (ambient level, g_{s400}) (A) and maximum g_s (g_{smax}) rate (B) achievable for the HL to LL transfer experiment. The means for both g_s conditions were extracted from Fig. 4.8iv. One way ANOVA followed by a post hoc Tukey's HSD test where $n=3$ with groups sharing different letters are significantly different ($p < 0.05$) and error bars represent standard error of mean.

In the opposite transfer from LL to HL conditions, the P1 transferred leaves unexpectedly produced a similar average curve to HL grown leaves (Fig. 4.10iv-P1). The later transfer at P5 stage also produced similar average curve to LL grown leaves, indicating that overall g_s values followed the light condition to which the leaf had been the longest exposed. Mean g_{s400} and g_{smax} values showed high variation in the transfer treatments (Fig. 4.11A and 4.11B respectively). On average, g_{s400} and g_{smax} of the P1 (earliest) and P5 (latest) transfers achieved values similar to those measured in HL grown leaves.

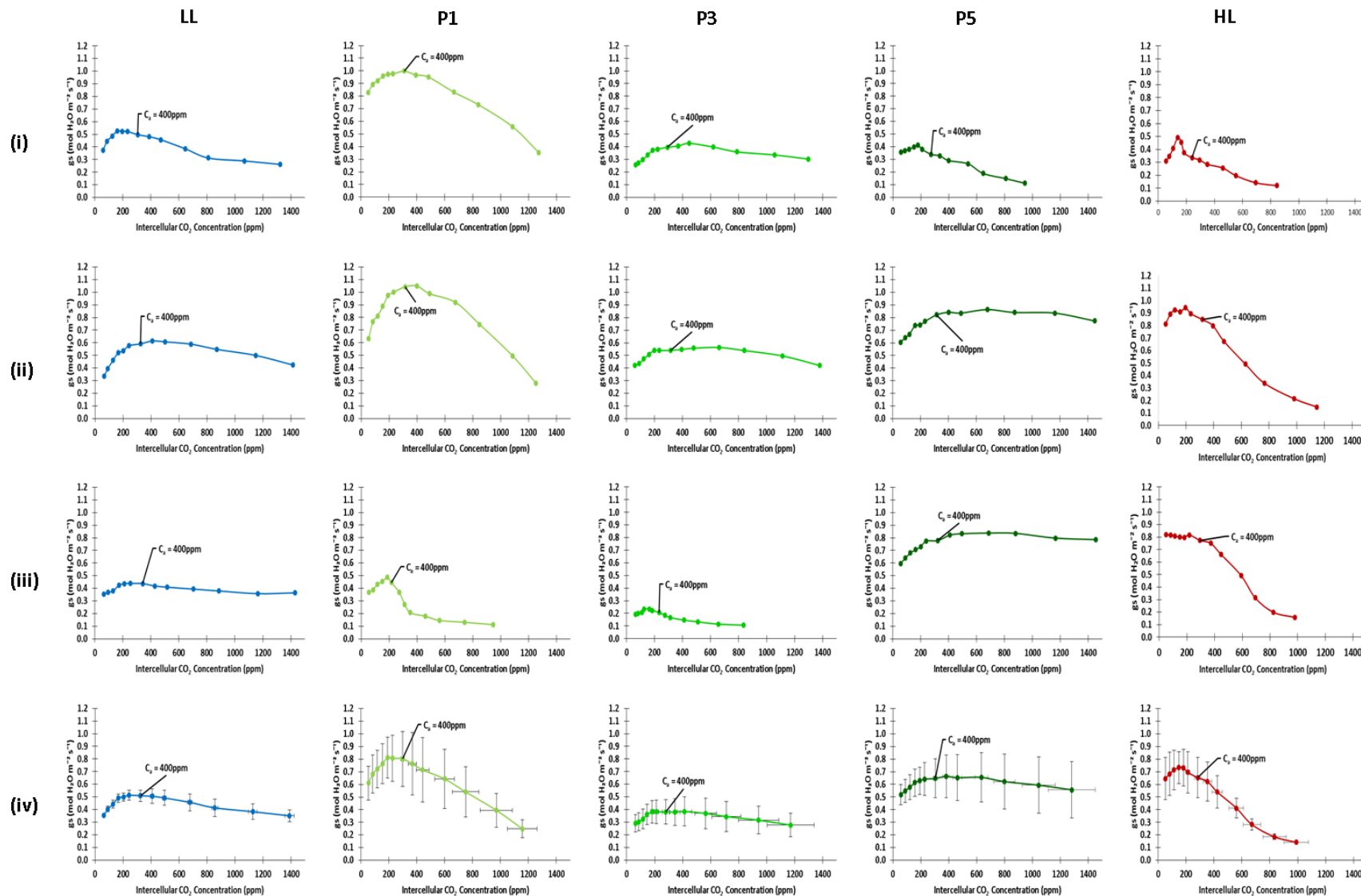


Figure 4.10

g_s - C_i curves in mature rice leaves for the transfer experiment from LL to HL. Rows (i), (ii) and (iii) represent individual curves (total $n=3$) for the corresponding treatment labelled at the top of each column. Row (iv) represents mean g_s - C_i curve for the particular treatment where the horizontal-vertical bars represent standard error of mean. Each g_s - C_i curve is marked with $C_a=400\text{ppm}$ to approximately show assimilation rate at the current ambient CO_2 level while the experiment took place.

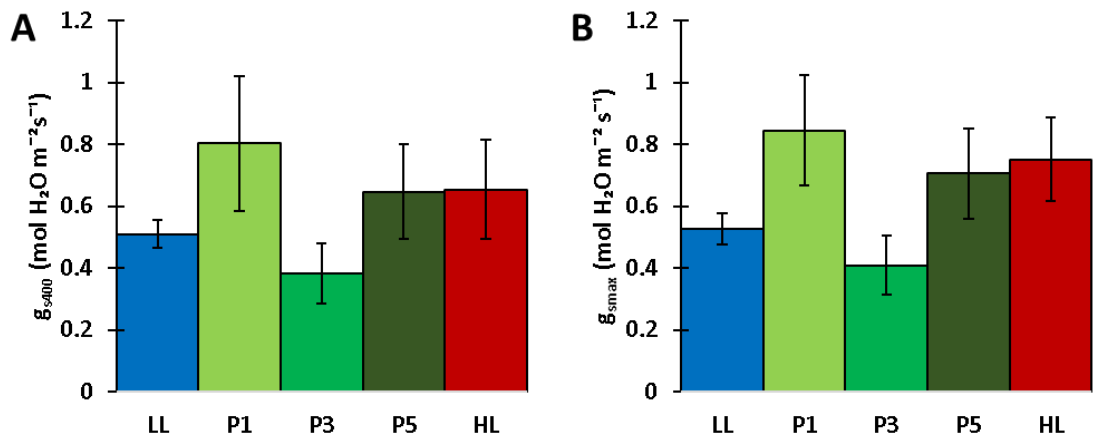


Figure 4.11

Mean stomatal conductance (g_s) rates measured at 400ppm CO_2 (ambient level, g_{s400}) (A) and maximum g_s (g_{smax}) rate (B) achievable for the LL to HL transfer experiment. The means for both g_s conditions were extracted from Fig. 4.10iv. One way ANOVA followed by a post hoc Tukey's HSD test where $n=3$ with groups sharing different letters are significantly different ($p < 0.05$) and error bars represent standard error of mean.

However the transfer at P3 stage produced a perplexing dataset where the curve had a very narrow g_s range (Fig. 4.10iii-P3) while the average g_{s400} and g_{smax} values were very low (Fig. 4.8C and 4.8D). Cross-referencing back to Fig 4.2 for the stomatal properties for these individual leaves does not indicate any unusual pattern in SCA size (Fig. 4.2A) and, in fact, SD on average was highest in this P3 transfer. The only plausible explanation for these irregular low g_s values was that the stomata were relatively closed in this particular treatment

4.4.7 Intrinsic Water Use Efficiency (iWUE)

Results from the previous two subsections were brought together to calculate the iWUE for the leaves transferred between different irradiances at particular stages of development. iWUE is defined as the ratio of CO₂ assimilation and stomatal conductance (A/g_s). At 400ppm CO₂ level (iWUE₄₀₀), HL grown leaves in general had significantly higher iWUE (value about 100) than LL grown leaves (value about 40) (Fig. 4.12A), which had similar iWUE values as leaves transferred from HL to LL at P1, P3 and P5 stages. The transfer from HL to LL in general produced minimum variation in iWUE across all treatments. As the supply of CO₂ increased so did the iWUE due to the proportional drop in g_s values, indicating stomatal closure. It is worth to note that the calculation revealed the last point of A-C_i and g_s -C_i curves always produced the highest iWUE (iWUE_{max}). HL grown leaves on average (value about 150) still had higher iWUE_{max} than LL grown leaves but surprisingly transfer at P3 stage had the highest average iWUE_{max} (value about 200) (Fig. 4.12B). This anomaly was due to the iWUE_{max} value of in one of the plants which showed a 368% increase from the iWUE₄₀₀ value. This was caused by an extremely low value of $g_{s,max}$, which in turn corresponded to an extremely low stomatal density in Fig. 4.11.

In the reverse transfer experiment from LL to HL condition, iWUE₄₀₀ values showed the same trend as seen in the other transfer mode where LL grown leaves had similar iWUE₄₀₀ with the P1, P3 and P5 transfer treatments, while HL had the highest iWUE₄₀₀ (Fig. 4.12C). There were high variations in iWUE_{max} for the transfer experiments (Fig. 4.12D) but in general transfer at P1 and P3 stage produced iWUE_{max} values most similar to HL grown leaves, while P5 transfer values were more similar to LL grown leaves (Fig. 4.12D). The occasional extremely high iWUE_{max} values measured for certain leaves were mainly caused by extremely low g_s values.

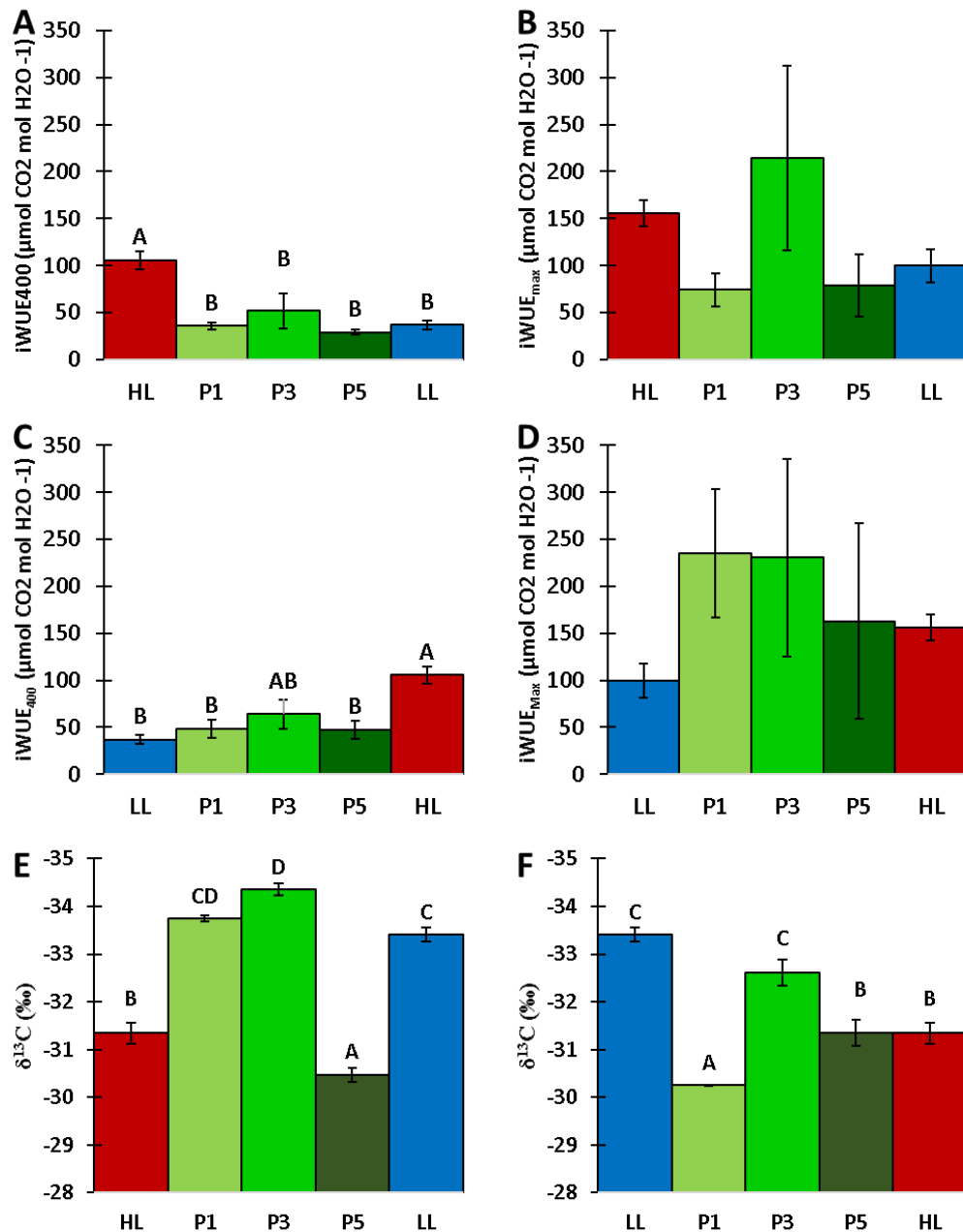


Figure 4.12

Mean intrinsic water use efficiency (iWUE) rates measured at 400ppm CO₂ (ambient level, iWUE₄₀₀) for the HL-LL (**A**) and LL-HL (**C**) transfer experiments. The maximum iWUE (iWUE_{max}) for the HL-LL (**B**) and LL-HL (**D**) transfer experiments are also calculated. iWUE is the ratio between CO₂ assimilation and stomatal conductance (A/g_s). Carbon isotope ratio (δ¹³C) is presented as per mill (‰) basis in (**E**) for HL-LL and (**F**) for LL-HL transfer experiments to validate the iWUE analyses. One way ANOVA followed by a post hoc Tukey's HSD test where n=3 with groups sharing different letters are significantly different (p < 0.05) and error bars represent standard error of mean.

Carbon isotope discrimination analysis ($\delta^{13}\text{C}$) again showed that (as in Chapter 3) HL leaves had a more positive value (about -31.3‰) compared to LL leaves (about -33.3‰) (Fig. 4.12 E and F). The same trend was observed in $\delta^{13}\text{C}$ values for the HL-LL transfer as seen in $i\text{WUE}_{400}$. The inverse LL-HL transfer revealed a generally similar trend for $i\text{WUE}_{400}$ and $\delta^{13}\text{C}$ (Fig. 4.12 C and F respectively), although it was unusual that the P5-transferred leaves had almost the same $\delta^{13}\text{C}$ as the HL leaves since the $i\text{WUE}_{400}$ value for such leaves was much lower (i.e., similar to LL leaves). This may be explained by the g_s values in these P5 leaves being similar to HL leaves but V_{cmax} values being low compared to HL leaves.

4.4.8 Correlation Between Stomatal and Physiological Properties

The previous sections that dealt individually with assimilation, stomatal conductance and water use efficiency all came from the same plants. In addition to these physio-biochemical analyses, the leaves samples from the same plants ($n=3$ for each treatment) were also used to study stomatal properties (as in the subsections 4.4.1 and 4.4.2). In this paired experiment, the correlation analysis in Table 4.2 reveals that many of the stomatal-epidermal parameters still show a significant relationship, similar to that in Table 4.1 that used a larger sample size ($n=11$).

When taken overall, the correlation matrix in Table 4.2 shows no obvious relationship between stomatal properties with assimilation and g_s values. However, a careful look at Fig. 4.1 shows that although SCA size (Fig. 4.1A) of P5 transferred leaves had similar size to LL grown leaves, the SD (Fig. 4.1I) of the three measured plants did have higher mean density among all treatments. This is consistent with Franks and Beerling (2009) who suggested (based on fossil samples) that high SD could play a role in achieving high g_{smax} . Correlation analysis between stomatal properties and $i\text{WUE}$ showed that guard cells width (GCW) and stomatal complex width (SCW) had a significantly positive relationship with $i\text{WUE}_{400}$ but SD showed almost no correlation (Table 4.2). Once again the data pooled for GCW and SCW showed significant correlation with $i\text{WUE}_{400}$ but not stomatal density (Table 4.2).

Table 4.2:

Pearson's correlation coefficients (r) among the pooled values of stomatal-epidermal against leaf physiology properties (n=3 for each parameter). Single asterisk * indicates correlations which are significant at p<0.05 confidence limit while double asterisks ** indicate correlations which are significant at p<0.01 confidence limit.

	Stomatal-Epidermal										Physiology					
	SCA	SD	GCW	SAL	SCL	SCW	CFW	SPA	%SF	A ₄₀₀	A _{max}	g _{s400}	g _{smax}	iWUE ₄₀₀	iWUE _{max}	
Stomatal-Epidermal	SCA															
	SD	-0.64**														
	GCW	0.27	0.07													
	SAL	0.74**	-0.58**	0.09												
	SCL	0.80**	-0.66**	0.15	0.91**											
	SCW	0.57**	-0.05	0.49*	0.29	0.17										
	CFW	0.28	-0.07	0.39	0.17	0.06	0.53**									
	SPA	0.65**	-0.43*	0.31	0.70**	0.65**	0.28	0.37								
	%SF	-0.37	0.73**	0.20	-0.21	-0.39	0.20	0.32	-0.15							
Physiology	A ₄₀₀	0.17	0.16	0.00	0.19	0.13	0.35	0.03	-0.17	0.22						
	A _{max}	0.18	0.32	0.21	-0.03	0.04	0.39	0.05	-0.12	0.23	0.73**					
	g _{s400}	-0.08	0.02	-0.34	0.19	0.06	-0.12	-0.10	-0.19	0.09	0.70**	0.10				
	g _{smax}	-0.05	0.01	-0.31	0.19	0.06	-0.04	-0.01	-0.20	0.11	0.72**	0.12	0.98**			
	iWUE ₄₀₀	0.34	0.12	0.59**	0.15	0.21	0.61**	0.35	0.32	0.31	0.09	0.47*	-0.51*	-0.44*		
	iWUE _{max}	0.14	0.07	0.34	0.04	0.11	0.24	0.27	0.21	0.28	-0.11	0.32	-0.64**	-0.60**	0.73**	

The question is: why did GCW not correlate with any other gas exchange parameter? Since *i*WUE gives information about both assimilation and conductance, it seems that GCW influences the CO₂ influx to fulfil carboxylation demand while at the balancing water transpired to optimise the leaf temperature.

Since GCW showed significant correlation with a number of leaf physiology parameters, a contour plot from the pooled data was prepared to see how stomatal size (GCW) and patterning (SD) might predict *i*WUE at ambient CO₂ level. The plot (Fig 4.13) suggests that a combination of GCW >4.6 μm and SD within 250-350 mm⁻² would produce 70-120 μmol CO₂ mol H₂O⁻¹ *i*WUE₄₀₀. This was the usual range observed in leaves grown in continuous HL conditions (Fig. 4.10A and 4.10C).

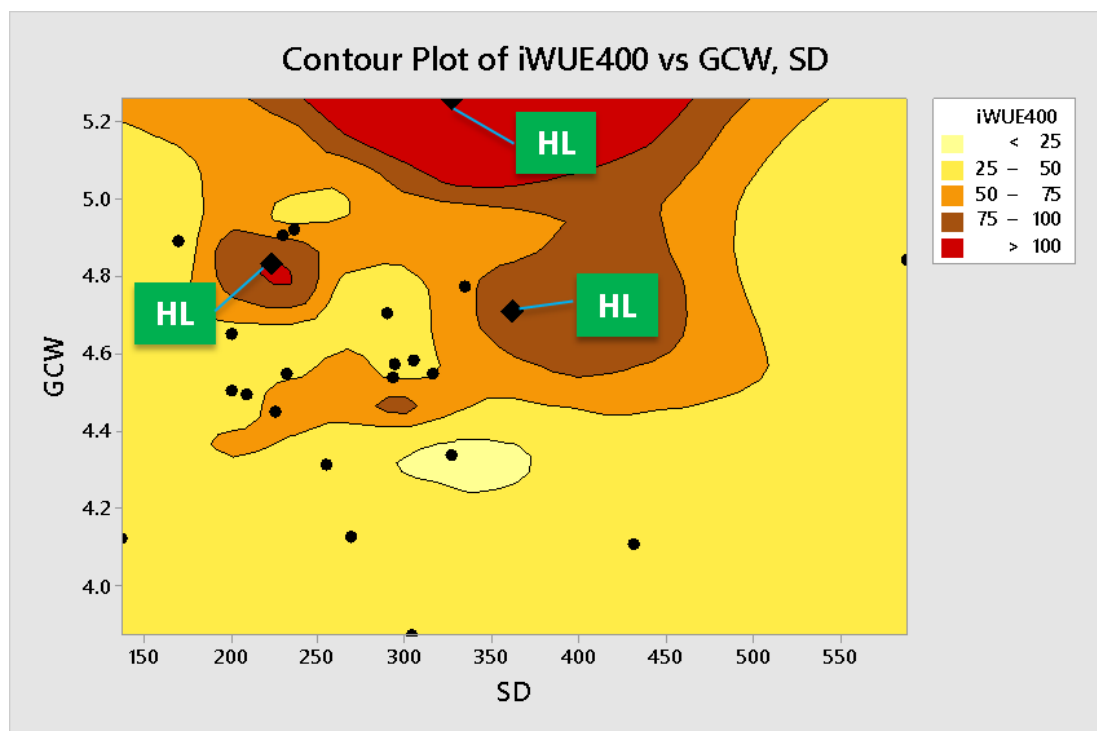


Figure 4.13

Contour plot of intrinsic water use efficiency at ambient CO₂ level (*i*WUE₄₀₀) as a function of guard cells width (GCW) and stomatal density (SD). Note that individual data point for high light (HL) grown leaves are clearly marked. The unit for the colour scale on the top right is μmol CO₂ mol H₂O⁻¹.

4.5 Discussion

The results described above indicated relatively high variation in both stomatal and cell file properties on transfer at P1 and P3 stages relative to later stages of leaf development, indicating that stomatal phenotypes are highly plastic with respect to the prevailing environmental conditions during these developmental stages. The ability of plants to acclimate to the current environment, especially irradiance, by undergoing morphological and physiological changes, has been well documented in dicots, such as *A. thaliana* (Kouřil *et al.*, 2012), and monocots, such as *Festuca arundinacea* (Wherley *et al.*, 2005). In rice, since the P1 and P3 stages are concealed within layers of outer leaf sheaths, the current light conditions signals are presumably sensed by older leaves and relayed to the actively developing primordia (known as remote long-distance signalling control, Thomas *et al.*, 2004). A number of possible signals (peptides, phytohormones, redoxes and sugars) have been postulated as the 'batons' in the signal relay from mature leaves (Coupe *et al.*, 2006; Yoshida *et al.*, 2011) which trigger response in the developing leaf, but the identity of the signal(s) remains elusive. With respect to the responding leaf, our data indicate that the leaf primordium surface up to P3 stage only comprises undifferentiated epidermal cells, suggesting that shifts in the environment during the 2-4 day developmental window prior to overt differentiation during P4 stage can have major effects on final leaf stomatal characters. Our new observations support and extend previous observations that relatively early stages in leaf development are involved in the acclimation processes which set the limits of potential performance of the mature leaf (Oguchi *et al.*, 2003; Murchie *et al.*, 2005).

The data reported here show that various stomatal size parameters are, in general, larger for HL grown leaves than LL grown leaves, in agreement with Hubbart *et al.* (2012) who also reported significantly bigger (longer) stomata on the abaxial surface in rice grown under HL condition. Since the stomatal complex in rice consists of four cells (two subsidiary cells flanking two guard cells), its area (SCA) is strongly determined by other dimensional parameters such as stomatal complex length (SCL) and stomatal complex width (SCW). Structures in the complex that play an important role in determining gas influx,

such as guard cell width (GCW) and stomatal pore area, are associated with parameters of stomatal complex size, so that when all of these stomatal size-related parameters analysed, they show a significantly correlation (Table 1). SCA and SCW must to a certain extent be set by cell file width and it is noticeable that HL leaves have wider cell files than LL leaves. Thus this parameter (cell file width), set at the level of the whole leaf, will have a significant impact on the width parameter of all stomata formed within the leaf.

After transfer from HL to LL, P1 and P3 stages of rice leaf development define a sensitivity window for various aspects of photosynthesis, (Van Campen *et al.*, 2016), and during this window the plant is able to alter stomatal size parameters in order to adjust to the prevailing LL condition. It is noticeable that stomatal size measurements made in leaves after P1 and P3 transfer consistently showed significantly higher variances compared to later P5 transferred leaves. This fits with the idea that P1-P3 stage leaves are highly plastic with respect to response to altered environment, possibly leading to over- and under-shoot in stomatal size parameters. By the P5 stage this plasticity appears to be greatly decreased, leading to a more limited response (with accompanying lower variance in the data measured). The reverse LL to HL transfer appeared to be less sensitive with respect to altered stomatal size parameters, although it is worth noting for this direction of transfer all plastochron-stages showed a significant change in GCW.

Together with size, patterning of stomata is frequently coupled to the determination of gas exchange capacity for a leaf. Similar to findings reported by Hubbart *et al.* (2012) I found that although stomatal density (SD) for HL grown leaves tended to be slightly higher than those of LL grown leaves, the difference was statistically not significant. There was a large spread of data points in the HL to LL transfer experiments, especially in P1 and P3 transfers. These data suggest that rice can respond to a change in light environment during P1 and P3 stages but this leads to a general increase in noise in the cell division process rather than directed change in overall stomatal density. As mentioned above, the number of stomata per area will be determined to some extent by the number and size of cell files within which stomata can form. Any variation in these parameters will be to some extent countered by the normal

functioning of the stomatal patterning system (leading to a normal average stomatal density) but the greater the variation in the background field of cells in which patterning occurs will, as a consequence, tend to lead to a greater variation in the densities observed.

Interestingly rice appears to show a highly consistent number of cell files that contain stomata within any single interveinal gap (maximum of four per any interveinal gap observed) and this value is independent of the actual number of cell files present in the interveinal gap. This characteristic, combined with the leaf's ability to change CFN and CFW leads to a significantly higher stomatal file percentage (%SF, Fig. 4.1G) for HL grown leaves compared to LL grown leaves. In fact this %SF parameter is another way to measure stomatal patterning (in addition to SD). It follows the trend observed for other parameters in that transfer at P3 stage appears to be the cut-off point at which alteration in final parameter observed in mature leaves can occur. Again the leaves transferred from LL to HL transfer seem to be less responsive.

The physical changes observed in leaf primordia following change in light environment are likely to be attributable to changes in gene expression. For transfer from HL to LL condition, Narawatthana (2013) reported downregulation of certain genes involved in cell and tissue morphogenesis, such as one of the of STRUBBELIG-RECEPTOR FAMILY (SUB) members (SRF8) and SCARECROW (SCR). Even though SUB is thought to be important in the control of cell division orientation plane, as well as controlling cell number shape and size (Chevalier *et al.*, 2005), no confirmed literature could be found for SR8 function except that it has been implicated in peroxidase activity and sterol biosynthesis (Eyüboğlu *et al.*, 2007). However there are numerous reports in the literature on the importance of SCR in many aspects of cell development, including the regulation of cell proliferation and guard cell expansion (Dhondt *et al.*, 2010), Kranz's anatomy establishment and asymmetric division in stomatal development (Kamiya *et al.*, 2003). Dhondt *et al.* (2012) showed in their work that the *scr* mutant had reduced cell division rate and guard cell area. Thus the changes observed in stomatal characteristics after P3 transfer could be related to altered SCR expression levels. In this analysis it was striking to see the similarity in SD between HL

and LL grown leaves. This finding is in line with other findings in rice which also found no SD difference under HL and LL systems (Hubbart *et al.*, 2013) but contrasts with the finding in *Arabidopsis* (Coupe *et al.*, 2006). These differences may be related to differences in the control of stomatal formation in monocot and dicot systems.

In the second section of this study I performed paired transfer experiments in order to investigate the relationship between stomatal phenotypes and different aspects of leaf physiology, particularly assimilation rate (A), stomatal conductance (g_s) and intrinsic water use efficiency (iWUE). In the HL to LL transfer, photosynthetic capacity measured at 400ppm CO₂ (A_{400}) increased by 25% for HL grown leaves compared to LL grown leaves. A similar trend was also observed for maximum assimilation (A_{max}) with an increase of 68.6%. HL grown leaves in general produce sun leaves with characteristics such as higher Rubisco and chlorophyll a/b ratio contents (Hubbart *et al.*, 2013), lower levels of light harvesting chlorophyll a/b proteins as well as less thylakoids stacking compared to LL grown leaves (Lichtenthaler *et al.*, 1981; Lichtenthaler *et al.*, 2007).

One important distinction between physical acclimation (e.g., stomatal size) and biochemical acclimation (e.g., carbon assimilation) is that even after relatively late P5-stage transfer the leaves were still able to modulate A_{400} and A_{max} to match leaves grown in continuously LL conditions. P5 stage is marked by the first appearance of the leaf blade from the encircling leaf sheath layers. This point onwards to the day of measurement (mature leaf, P6 stage) usually takes about 5-6 days. This relatively long period of time had minimal impact on stomatal-epidermal phenotypes but was sufficient to turn the transferred leaf into 'shade-leaf' physiologically thus resulting in $A-C_i$ curves similar to those observed in LL leaves (Fig. 4.4iv). Transfer following full leaf expansion does not change Rubisco content (Murchie *et al.* 2005), but since P-transferred leaves were still extending, this did change the Rubisco content as shown by reduced V_{cmax} values than HL leaves (Fig. 4.5C) although it was still higher compared to P1 and P5 transferred leaves. Thus the relatively higher assimilation rate by P5-transferred leaves, almost as high as HL leaves, can be explained by a correspondingly lower relative stomatal limitation (Fig. 4.5D)

which supports CO₂ diffusion, thus relatively more is available for Rubisco carboxylation. In the reverse LL to HL transfer experiment similar mean A-C_i curves (Fig. 4.5iv) were recorded for each plastochron stage transfer which practically matched the mean A- C_i curve for HL grown leaves. Analysis of A₄₀₀ and A_{max} also supports this by showing that all transfer treatments led to values that were statistically similar to the leaves grown continuously in HL. For this transfer direction, the point of P5-stage leaf emergence to the day of measurement usually takes about 3-4 days. Despite this relatively shorter acclimatization period compared to the H-L transfer discussed earlier, the resulting leaves still have a final photosynthetic ability comparable to HL grown leaves. The enhancement of assimilation can be caused to a certain extent by parallel changes in some stomatal parameters, such as higher SD and larger SCW which show a positive correlation with A_{max} (r=0.32 and r=0.39 respectively). More importantly it has been shown that even mature rice leaves have the ability to alter Rubisco and chlorophyll a/b ratio contents following transfer from LL to HL environment (Murchie *et al.*, 2005) thus rendering a high photosynthetic rate.

In addition to biochemical processes, rice leaves can also display changes in gross leaf morphology (thickness) and constituent cell size which might also influence photosynthetic performance. For example, previous work has shown that after exposure to high irradiance rice leaves are thicker (Murchie *et al.*, 2005). Work from our own group (Van Campen *et al.*, 2016) has shown that after transfer from LL to HL at P1 and P3 stages mature rice leaves have a similar thickness to leaves from plants maintained continually under HL. At later stages (P5) leaf thickness does not change appreciably after change in irradiance. Therefore for P5-transferred leaves change in mesophyll thickness cannot be the reason for the comparable A_{max} measured, suggesting a larger role for biochemical changes, potentially linked with altered stomatal performance (rather than altered stomatal characteristics of size or density).

The analysis of g_s-C_i curves also provides some interesting findings on how stomatal structures affect g_s. In doing this the curves are divided into two phases: i) stomatal opening and ii) stomatal closing. In the first phase of the curve, HL grown leaves generally have a steeper slope than LL grown leaves,

indicating rapid stomatal opening to increase CO₂ influx for active carbon assimilation activity. In all curves the entry into the second phase, that is stomatal closing, occurred before ambient CO₂ level. At this point assimilation is still in the first phase of A-C_i curve (Rubisco limited) so, theoretically, the leaf should just allow the stomata to open without any influence of water conservation (since the plants were grown hydroponically). This tight stomatal aperture regulation even in the presence of an abundance of water indicates a built-in program to maintain water use efficiency (WUE) under any water status condition. The decrease in g_s values in higher CO₂ level is normal in C₃ and C₄ plants (Osborne and Sack, 2012). Unlike the A-C_i curves pattern described in the previous section, which seems not in line with the physical measurements of stomata in the transfer experiments, g_s-C_i curves have the tendency to follow the expected trend where P1 and P3 transfer stages set the developmental window for the plant to alter and match the g_s value normally obtained in the plants grown continuously under the same light condition. However (and unexpectedly) correlation analysis failed to show any potential relationship between any stomatal phenotypes and g_s values (Table 4.2). The lack of correlation is probably due to the saturating high light conditions used during measurements, which were different from those in which the plants were grown.

It is worth to relate the P-transferred stages with the corresponding morphological development that occurs. P1, the earliest form of the developing primordium (Table 1.1,) comprises undifferentiated founder cells and is the most responsive to the altered light condition. P3 stage is marked by the initiation of epidermal specific cells, some of which will eventually form stomatal cell rows, as outlined by Liu *et al.* (2009, Fig. 1.8). Hence P3 is a critical stage during which stomatal properties such as size and density are set. Later transfer at P5 stage will not do much in altering the physical properties of stomata, thus any acclimation by the leaf at this stage (or later) will come primarily from biochemical/physiological properties. One important finding worth highlighting is that rice stomata in LL grown leaves (which are relatively small) respond minimally to changing CO₂ level, thus they do not follow the general rule that small stomata show a faster response than larger stomata in terms of opening and closing (Hetherington and Woodward, 2003;

Franks and Beerling, 2009; Lawson and Blatt, 2014). This finding warrants further investigation.

The final aspect of leaf physiology assessed in this chapter deals with iWUE, which can be regarded as an indicator of overall leaf performance. This study confirms that iWUE generally increases with high CO₂ reflecting a relatively higher A and lower g_s (Tricker *et al.*, 2005; Ainsworth and Rogers, 2007). Despite the mixed patterns observed in some of the transfer experiments, rice leaves in general seem to be very good at compensating, thus maintaining general performance. Thus, irrespective of whether the transfer takes place at the earliest (P1) or latest (P5) stage, the mature leaves still manage to adjust iWUE so that it is adapted to the final light condition. This indicates that rice has a good ability to maintain a good synchrony between A (biochemical) and g_s (structural) properties to bring about adjustment to the prevailing environment. It is interesting to observe that iWUE can be predicted essentially by one stomatal character, namely guard cell (GC) width. This is somewhat expected as previous studies have confirmed the importance of GC size in controlling stomatal movement and its positive association with photosynthesis and WUE (Xu and Zhou, 2008; Lawson and Blatt, 2014). Nevertheless, the knowledge from this study might be used to target particular parameters to generate leaves with good iWUE. Based on the predictions indicated by the contour plot using GCW and SD (Fig. 4.11) for the best iWUE at ambient CO₂ level, it seems to be always beneficial to have large guard cells but stomatal frequency must also be moderately high if rice leaves are to have a high iWUE.

CHAPTER 5

**WHOLE-MOUNT *IN SITU*
HYBRIDIZATION IN RICE**

5.1 Introduction

Studying gene expression patterns is an essential component in the characterization of gene function. Where and when a gene is expressed will limit its spatial-temporal function and provide information on the extent to which a gene can play a role in plant responses to chemical or environmental treatments. A number of strategies have been regularly employed in order to investigate gene expression patterns. These include the use of transgenic reporter constructs, gene chip technology, immunohistochemical analysis and nucleic acid, (particularly mRNA) hybridization. In reporter constructs, detectable protein products such as β -glucuronidase (Jefferson et al., 1987), green fluorescent protein (Shimomura *et al.*, 1962) and luciferase (Strehler and McElroy, 1949) are often placed under transcriptional control of specific promoters of the studied genes. A more advanced gene chip analysis using microarray technology such as Affymetrix GeneChips is also a valuable tool, especially in obtaining genome-wide expression profiling (Auer *et al.*, 2009). However these methods are often considered insufficient in providing accurate identification of gene expression and generally need to be validated against other methods involving detection of proteins and mRNA (Hejatko *et al.*, 2006). In particular, although historically most methods of gene expression analysis involved extraction of RNA and protein from whole organs, these methods lose important spatial aspects of gene expression. This is especially so if the biological target of investigation is essentially cellular in nature, as is the case for stomata. Since a protein product is often the end result of result gene expression, protein patterns can be localized and characterized using immunohistochemical techniques (Komar and Long, 2013). mRNA expression can also be visualised to cellular resolution using *in situ* hybridization techniques (Javelle *et al.*, 2011).

Classically, mRNA localization uses thinly sectioned biological samples which have been embedded in paraffin wax to preserve the structure. However this step adds more time to the entire procedure as well as being laborious and needs sufficient sectioning and mounting skills. Furthermore data comes in fragments of serial sections, sometimes providing challenges in visualising patterns in 3D. As a

result an idea to analyse whole tissues arose, originally performed on wild-type *Drosophila* fly embryos (Tautz and Pfeifle, 1989) and hence termed whole-mount *in situ* hybridization (WISH). This method has been used successfully on tissues from animals such as chicken embryos (Darnell *et al.*, 2010), zebra fish embryos (Christine and Bernard, 2008), mouse embryos (Neufeld *et al.*, 2013) and freshwater planarian, a type of flatworm (Rybak-Wolf and Solana, 2014). However WISH performed on plants has not been as successful with relatively few reports on its regular application. For plants, WISH has been most extensively optimized for *Arabidopsis* (Engler *et al.*, 1998; Brewer *et al.*, 2006; Traas, 2008) but its use has been restricted to small, transparent tissues such as roots and embryos. This narrow application of WISH in plants is probably due to several technical problems, particularly the presence of cell walls that hinder reagent permeability, relatively deeper target tissue in more mature organs, as well as naturally low mRNA levels in certain cells. Consequently the choice of tissue is restricted to simple ones and does appear as useful for more complex, denser tissues such as floral and shoot apical meristems (SAM).

To my current knowledge, there has not been any WISH protocols reported for rice so far. In this thesis the aim was to characterise the development of stomata in early leaf development. Analyses of *Arabidopsis* and grasses, including rice, have identified a series of genes involved in stomatal patterning and differentiation. With the longer term view of analysing the patterns of expression of these genes, this chapter sets out to establish a WISH protocol for rice leaves. As well as establishing a protocol for rice, a WISH method for this plant might also enable progress to be made in the analysis of spatial gene expression in other monocots.

5.1.1 The principle of WISH

The principle of WISH is shown in Fig. 5.1. An RNA probe (riboprobe or simply probe) is labelled to produce detectable signals should the hybridization with the targeted cellular mRNA (Fig. 5.1A) take place. Digoxigenin (DIG, a steroid found exclusively in *Digitalis purpurea* plant) was the probe label used in this study, although compared to radiolabelled probes it can lack similar sensitivity. However it has the advantage of convenience and has been widely used in various *in situ* hybridisation protocols.

An antisense labelled probe (Fig. 5.1B) hybridizes within the tissue of interest which has been treated to both maintain structure integrity but to allow probe permeability. If hybridization takes place, subsequent addition of an anti-digoxigenin antibody which has an alkaline phosphatase (AP) enzyme attached to it leads to a complex in which the position of the AP indicates the localisation of the target mRNA. Visualization is achieved by enzymatic reaction of AP with a colourless substrate mixture containing BCIP (5-bromo-4-chloro-3-indolyl-phosphate), and NBT (4-nitro blue tetrazolium). The reaction leads to a resultant dark blue-purple precipitate (Fig. 5.1C). Fig. 5.1D shows an example of localized dark blue precipitation in certain cells using an eFF1a (elongation factor) probe. WISH is faster than conventional *in situ* hybridization since it does not require tissue sectioning. Nevertheless, setting up the procedure involves extensive optimisation, which is described in the first part of this chapter. Apart from probe preparation, other critical steps in WISH include tissue fixation-permeation, hybridization, signal detection and imaging, as well as general experimental setup and selection of target tissue.

In theory, WISH would be a powerful tool to study stomatal development in rice given their appearance on the leaf surface. Thus deeper tissue penetration should not be an issue for the probes.

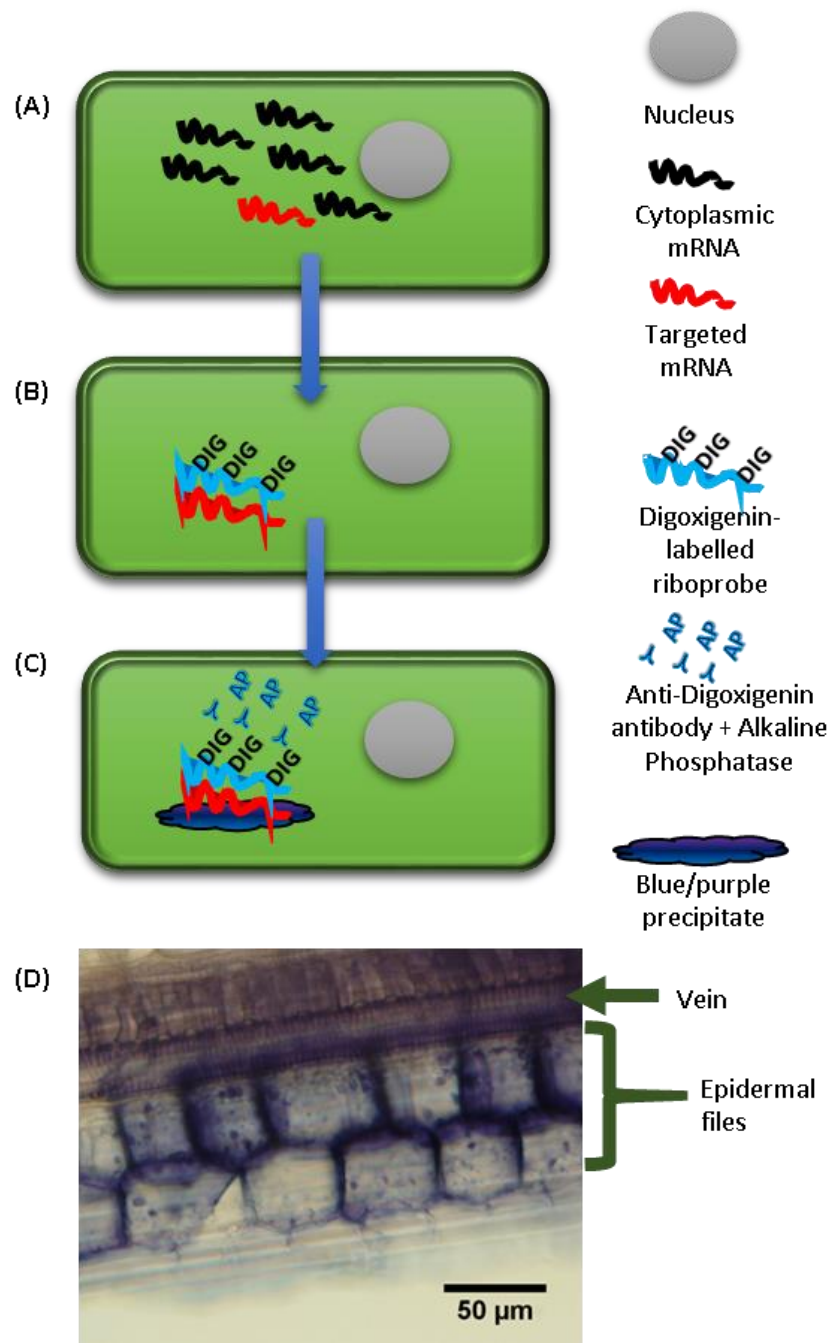


Figure 5.1

Overview of steps for *in situ* hybridization method. Tissue is treated to preserve cell structure with enhanced permeability to allow hybridization with the targeted mRNA in the cytoplasm (A). DIG-labelled riboprobe binds to the complementary mRNA (B) and allowed to react with an anti-DIG antibody that carries the alkaline phosphatase enzyme. Addition of the substrate 5-bromo-4-chloro-3-indolyl-phosphate results in a localized blue-purple precipitation (C). (D) An example of a localized detection of blue-purple precipitate in a developing P4 leaf.

Ideally I wanted to make probes for genes related to stomatal development in rice such as OsSPCH, OsMUTE and OsFAMA but due to time constraints all the probes used in this study were obtained from colleagues (Julia Van Campen and Supatthra Narawatthana). These probes (described in Table 1) belong to genes involved in different developmental processes which have been studied in rice or other orthologous plants, or whose exact functions are yet to be determined. These genes will be used to develop the WISH protocol for rice tissues. For example, the expression of histone H4 can be used as a marker for S phase of the cell cycle, thus should be expressed in some cells early in leaf development (Meshi *et al.*, 2000; Nelson *et al.*, 2002) whereas DL (DROOPING LEAF), which is known to promote midrib formation, should be expressed only within the middle region of the leaf (Ohmori *et al.*, 2011). If these genes show expected expression patterns, this provides confidence in the patterns observed for other target genes at a later stage.

5.2 Aim

1. Develop a whole mount *in situ* hybridisation method for the analysis of gene expression in rice leaves with the ultimate aim of characterising stomatal gene expression during early rice leaf development.

5.3 Methodology

In general *in situ* hybridization is sensitive to contaminants especially ribonucleases (RNases that catalyse RNA degradation) which are ubiquitous in laboratory environments. Therefore the work area was regularly cleaned using RNaseZap® (Ambion Inc.). All solutions were prepared using DEPC-treated (Diethyl pyrocarbonate) water (0.1% v/v in UHP water, shaken vigorously and incubated at 37°C before being autoclaved to inactivate DEPC). All apparatus and equipment were also treated to ensure that they were RNase free by either baking (150° for 3h) or rinsing in DEPC-treated water followed by autoclaving. All chemicals used were of the highest grade and purity possible.

The initial attempt to perform WISH on rice in this study was fundamentally based on the *Arabidopsis* protocol by Traas (2008) who adapted it from Ludevit *et al.* (1992) and Zachgo *et al.* (2000). The authors cautioned that this method is only reliable in a limited number of plant parts such as root meristems, embryos, and very young primordia. Moreover interpretation of results must be carried out with extra care. Since a number of optimisation steps were required to develop the final WISH method, this section is reported in three subsections; (i) performing WISH on rice using a protocol adapted for *Arabidopsis*, (ii) modifications of certain steps to prevent non-specific binding of either probes or antibodies, (iii) optimization of cutting of transverse sections to allow better penetration of reagents and probes into the tissue and easier interpretation of the data and (iv) the final method used for gene examining expression patterns for different probes.

All plants were grown under high light conditions using methodology described in section 2.1. In subsection (i) of this experiment, primordia at the P3 and P4 stages, which were relatively soft and small to work, with were used. Microdissection using 25G and 30G needles was performed to obtain tissue primordia. For subsection (ii) only P4 primordia were used. When the optimised method had been achieved, the plant material used was a 1 cm section of tissue from the base of the rice culm containing all layers of different plastochron stages.

This particular cutting (in stub form) had leaf no. 7 as the youngest and leaf no. 3 as the oldest leaf layer.

All riboprobes (probes) in this study were obtained from Julia Van Campen prepared using modified methods of Narawatthana, (2013) and Jane Langdale (Oxford lab, personal communication). Probe details are described in Table 5.1. Briefly, total RNA was extracted from rice leaf primordia using a TRIzol method (optimized from Narawatthana, (2013) and Van Campen, unpublished). This was used to generate cDNA and subsequently used as template in PCR amplifications. The purified PCR products were ligated to the KpnI/SacI double digested pBluescript II SK (-) plasmid which contains the promoter for T3 or T7 RNA polymerase. Primers used in this study were designed using Primer3. The recombinant plasmids were used for synthesizing sense (T7) and antisense (T3) riboprobes using the respective RNA polymerase. The digested and linearized plasmids were used for *in vitro* transcription where probes were labelled with DIG. Probe hydrolysis was carried out for probes > 500 bp since short probe fragments facilitate tissue penetration.

5.3.1 Unmodified WISH method for *Arabidopsis* performed on rice

Initially the WISH method developed for *Arabidopsis* was performed on rice to determine which aspects of the methodology worked, and which did not work on rice. Plants tissues were fixed in 4% (v/v) formaldehyde and 10% (v/v) dimethyl sulfoxide in a glass vial containing 0.1M PBS solution for 30 min. Tissues were left in fixative overnight at 4°C. Samples were then retrieved and dehydrated through an ethanol series: 30%, 60%, 70%, 85%, 95% and 100% for 30 min in each concentration. Samples were transferred to 1.5mL Eppendorf tubes and kept in 100% ethanol at -20 °C until needed. Samples were then retrieved and washed twice with 100% ethanol, then xylene for 30 min and for four washes in 100% ethanol, followed by twice in methanol. Samples were transferred to 50%

Table 5.1:

Riboprobes used for the development of the whole mount in-situ hybridization method in rice. Further gene details can be found by entering locus ID at www.rice.plantbiology.msu.edu. All antisense probes were generated using T3 RNA polymerase while T7 RNA polymerase was used for sense probes. cDNAs were cloned into the pBS vector and linearised with Kpn1 or Xho1 for T3 probes or SacI or Xba1 for T7 probes.

Riboprobe	Locus ID	Riboprobe length (bp)	Annotation
eEF1a	LOC_Os03g08010	118	Elongation factor Tu, putative, expressed
H4 (Histone-4)	LOC_Os10g39410	301	Core histone H2A/H2B/H3/H4 domain containing protein, putative, expressed
DL (Drooping Leaf)	LOC_Os03g11600	436	YABBY domain containing protein, putative, expressed
DWF7 (Delta-7-Sterol-C5)	LOC_Os01g04260	452	Fatty acid hydroxylase, putative, expressed
THF1 (Thylakoid Formation-1)	LOC_Os07g37250	343	THYLAKOID FORMATION1, chloroplast precursor, putative, expressed
CAB (Chlorophyll A-B)	LOC_Os01g41710	378	Chlorophyll A-B binding protein, putative, expressed
COV1	LOC_Os02g16880	360	Protein of unknown function DUF502 domain containing protein, expressed
CUL1 (Cullin-1)	LOC_Os05g05700	458	Cullin, putative, expressed
MON4 (MONOPTEROS)	LOC_Os04g56850	343	Auxin response factor, putative, expressed
FACKEL	LOC_Os09g39220	610	Delta14-sterol reductase, putative, expressed
CDKb2	LOC_Os08g40170	650	Cyclin-dependent kinase B2-1, putative, expressed

methanol (v/v) and 50% PBTF (0.01M PBS; 0.1% v/v Tween-20; 4% formaldehyde) solution and incubated for 5 min. The solution was changed and samples were post-fixed with 100% PBTF for 25 min then washed five times in PBT (0.01M PBS; 0.1% v/v Tween-20) for 10 min per wash. Samples were then incubated in PBTK (4% w/v Proteinase-K; PBT) for 10 min and washed four times in PBT for 5 min per wash. Samples were post-fixed again in PBTF for 25 min and washed four times in PBT for 5 min per wash. Samples were then left in PBT for 60 min.

Equal volume of PBT and WMHB (hybridisation buffer containing 50% v/v formamide; 0.5M SSC buffer; 5% w/v heparin salt; 10% w/v single-stranded salmon testes DNA; 0.1% v/v Tween-20) was used in the last wash. Samples were rinsed twice in 100% WMHB and pre-hybridized in WMHB for 3 h at 55 °C in a water bath. The buffer used for pre-hybridization was then replaced with fresh pre-warmed WMHB and 2 μ L of denatured DIG-labelled probe was added. Hybridisation was carried out for 18 h at 55 °C. Samples were gradually washed in PBT solution mixed with WMHB at 25%, 50% and 100% concentration for 20 min each. Samples were further washed in 100% PBT for 5 min. The PBT solution was replaced with new PBT solution containing antibody (diluted 1:2000) and incubated for 3 h. The antibody solution was discarded and samples were rinsed in PBT three times for 5 min each. Samples were then equilibrated for 5 min in detection buffer (0.1M Tris-HCl pH 9.5; 0.1M NaCl; 0.05M MgCl₂; water). Samples were reacted in BCIP/NBT mix (0.0075% w/v BCIP; 0.015% w/v NBT; detection buffer) in the dark at room temperature for 36 h. The enzyme reaction was stopped in TE buffer (0.1M Tris-HCl pH 9.5; 0.001M EDTA; water). Samples were dehydrated through an ethanol series (30%, 60%, 70%, 85%, 95% and 100%, 90 sec each), followed by Histoclear twice for 90 sec. Samples were mounted on a microscope slide and observed using OLYMPUS BX51 compound light microscope.

Fig. 5.2 shows results using the unmodified Arabidopsis method on the P3 and P4 rice leaf primordia. The probe used for this trial was *eEF1A*, the eukaryotic elongation factor gene, as it is constitutively expressed in developing leaves. In general the unmodified Arabidopsis method did work as there was positive signal (dark purple staining) detected for the *eEF1A* antisense probe for both P3 (Fig. 5.2 A) and P4 (Fig. 5.2 B) primordia, whereas the *eEF1A* sense probe gave no expression except for some purplish staining only in limited areas (Fig. 5.2 C). *eEF1A* abundance in cells reflects its primary roles in the synthesis of all cellular proteins, especially essential in delivering aminoacyl-tRNA (aa-tRNA) to the elongating ribosome, thus its presence is essential for cell viability (Cottrelle *et al.*, 1985; Sasikumar *et al.*, 2012). It is a good choice for an endogenous control in this study since the expression in plants should be relatively high in meristematic regions which are active in protein synthesis and lower in older, metabolically less active regions (Pokalsky *et al.*, 1989).

Despite the overwhelming positive staining observed for the antisense probe, as expected for a prolonged staining time, it was interesting to note how strongly zoned the expression pattern was in P4 primordia (Fig. 5.2 B). The staining only occurred in the mesophyll regions of the leaf rather than in the veins or bulliform cells (BC) regions. BC or motor cells are highly vacuolated and thin-walled cells (Jane and Chiang, 1991) that are responsible for leaves' ability to roll up thus conserving water content during water stress through reduced transpiration rate (Hsiao *et al.* 1984). Since BC contain large vacuoles, it was expected to see limited antisense probe signal, as reported here. Even though this method seemed to work with the antisense-probe, the result for sense probe still showed some staining in some leaf areas, especially the x-shaped silica bodies (Fig. 5.2C), thus indicating the possibility of non-specific binding of probes or the antibody used. Due to the promising results, attempts were made to optimise WISH by focusing on the blocking steps to prevent non-specific binding of probes and antibody.

5.3.2 Optimization of the blocking reagent to prevent non-specific hybridization and binding.

Non-specific binding could occur due to both probes and/or antibodies. To test the idea that the antibody was the issue, the original unmodified method as previously described was used and the P4 stage primordia was the tissue of choice. In this experiment one sample was left to hybridize without the presence of *eEF1A*-sense probe but with antibody addition, while the other sample was left to hybridize with the *eEF1A*-sense probe but without any antibody addition. The sense probe was used as a control to further confirm the finding.

Fig. 5.3 confirms this suspicion as the leaf treated with antibody only produced a similar signal pattern as before (Fig. 5.3 C) where the staining tended to take place in some leaf areas and x-shaped silica bodies (Fig. 5.3 A and 5.3 B). WISH on leaf tissue without any antibody addition resulted in a completely clear tissue (Fig. 5.3 C), thus showing that the WMHB blocking solution used was good enough to prevent non-specific probe interactions.

The next step involved the introduction of antibody blocking reagents to the protocol by introducing bovine serum albumin (BSA), a common blocking agent that would bind to charged sites (Burry, 2009). The BSA solution (1% w/v BSA; 0.3% v/v Triton X-100; 0.1M Tris-HCl and 0.15M NaCl) alone was used as a Post-WMHB solution in all the steps mentioned in sections 5.3.4.3 and 5.3.4.4. Results using the same protocol with BSA solution addition and P4 tissue as earlier, showed that although background staining still present in some leaf areas, staining on x-shaped silica bodies was absent (Fig. 5.4 A). It was hypothesized that if the antibody's affinity could be specified only for the defined epitopes, this should remove the unwanted background staining.

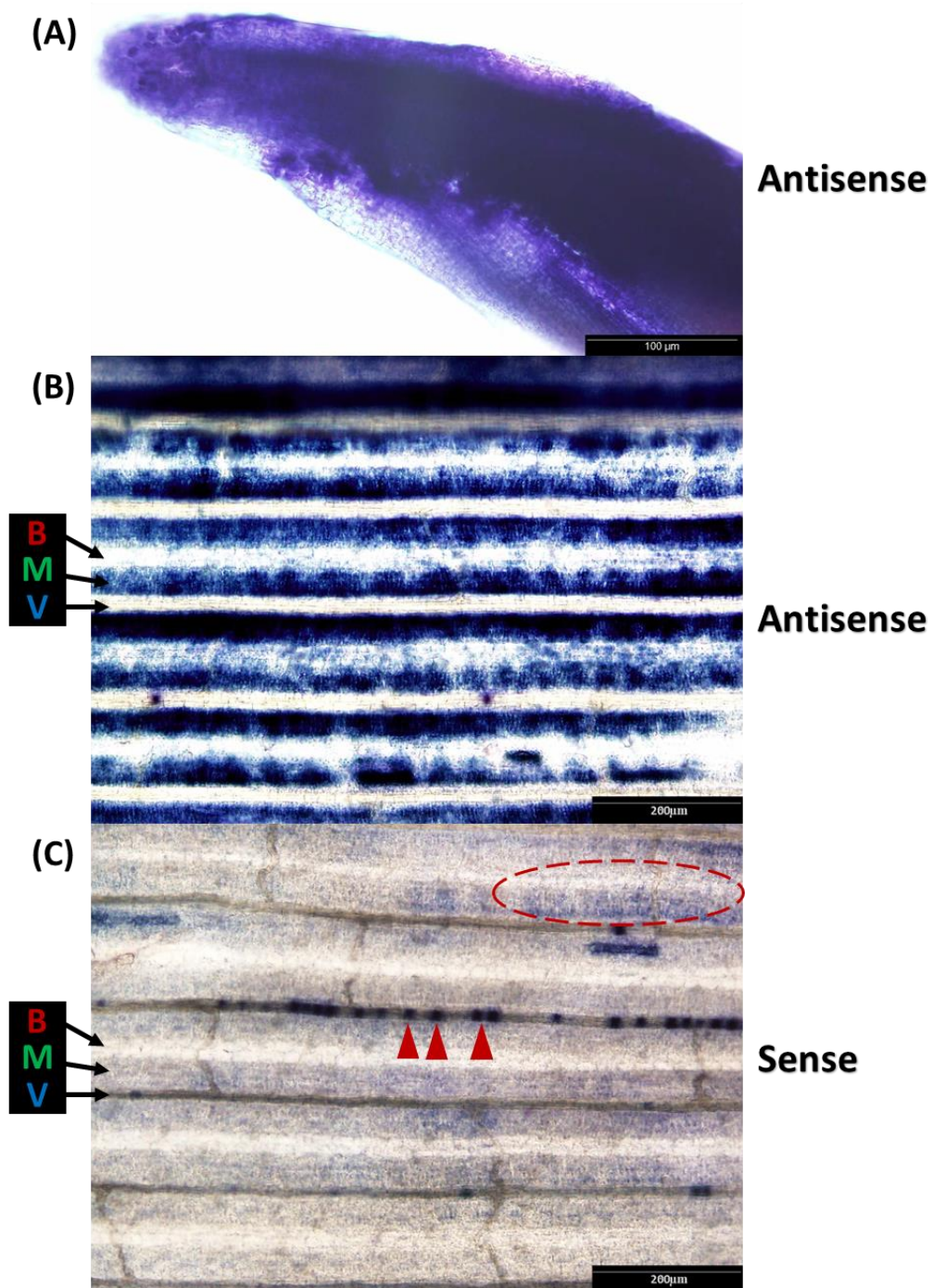


Figure 5.2
eEF1A mRNA expression pattern in rice using the unmodified WISH protocol for *Arabidopsis*. Strong antisense signal (dark purple staining following 36 h staining time) are visible in the young P3 (A) and P4 (B) leaf primordia. In general there is no signal detected for the sense probe (C) except in some interveinal gap (IG) areas (circled) and x-shaped silica bodies located on the veins (arrowheads). For any given IG area there is a vein (V), mesophyll cells (M) and bulliform cells (B) underneath the epidermis.

To further attempt to reduce the background staining acetone powder (Ace-Pow) containing preadsorbed antibody on crushed leaf tissues was prepared and a small amount added to the antibody solution. Acetone powder was prepared by grinding leaves of young rice seedlings and acetone in liquid N₂. This solution was centrifuged (10000 RPM for 2 min), decanted and left to air dry to obtain the pellet (powder). The presence of the powder in the antibody solution further reduced non-specific binding (Fig. 5.4 B). Then both BSA solution and Ace-Pow were combined in the next attempt which resulted in even greater reduction in the background staining (Fig. 5.4 C). Finally, to complement BSA as a blocking agent, sheep serum (10% v/v, Sigma) was added into the mixture (which now became the Post-WMHB solution used throughout the experiment) and together with Ace-Pow this completely prevented the background staining (Fig. 5.4 D).

5.3.3 Cutting of transverse samples for better riboprobe penetration into tissues and interpretation of results

WISH was performed using the optimized blocking reagents from the previous subsections on P3 leaf primordia (Fig. 5.5 A) but now using a probe for a histone-4 (*H4*) gene. This probe was used in all further experiments as the *eEF1A* probe ran out. H4 expression is linked to the S phase of the cell cycle, leading to localised and high levels of signal in tissue containing dividing cells, expected to be present in P3 leaves. In this experiment the staining time was reduced to about 30-45 min (checked for signals every 15 min) before stopping the reaction. In several experiments, there was no staining observed for the *H4* sense probe (Fig. 5.5 B), thus giving confidence in the blocking reagents used (as optimized in the previous subsections). The results consistently showed that the expression of *H4* antisense probe occurred in the deeper tissue layer and was concentrated near the bottom of the P3 primordium (Fig. 5.5 C).

Therefore, to improve visualisation of the H4 antisense probe deeper in the tissue a whole leaf cluster (in stub form, one cm from the culm base) was sampled for transverse sectioning as shown in Fig. 5.6. This allowed the expression pattern and localization could be better understood in leaves of different ages and stages. This way of sampling and sectioning of tissues was thus adopted for studying gene expression patterns related to leaf development throughout the rest of this study.

5.3.4 Optimised WISH for rice

Following the modifications to the Arabidopsis protocol described above, the final methodology developed for rice is described below:

5.3.4.1 Tissue selection, fixation and permeabilization

Rice leaf primordia of either P3 or P4 stage or clusters of leaf layers cut from about 1 cm from the culm base (Fig. 5.6 A) were used for this study (the former only for preliminary attempts whilst virtually all the results reported here used the latter sample source). Plants tissues that were used for some probes were slightly different in terms of age but the outermost layer (the oldest) in the leaf cluster was always leaf no. 3 (Fig. 5.6 B). Samples were cleaned, trimmed and cut using a single edged blade to produce approximately 1 cm tall stubs. Samples were fixed in Eppendorf tube containing 1000 μ l of fixative (4% v/v methanol-free formaldehyde, Sigma; 10% v/v dimethyl sulfoxide, Sigma; 0.1M PBS) overnight in a 37°C orbital shaker at 50 rpm. This is important to ensure thorough and better fixative penetration in all leaf layers. Samples were rinsed 2 x for 5 min each in PBS (pH 7.4) on a rocking table. From this step onwards all subsequent steps were done on a rocking table (at room temperature, 20-25°C) to ensure thorough reagent penetration into the tissues. Samples were dehydrated in an ethanol series of 30%, 70%, 95% and 2x 100% for 5 min each. If needed, samples could be stored in 100% ethanol for several weeks in -20°C freezer. Upon retrieval samples were brought out and left to equilibrate to room temperature before proceeding with the subsequent steps.

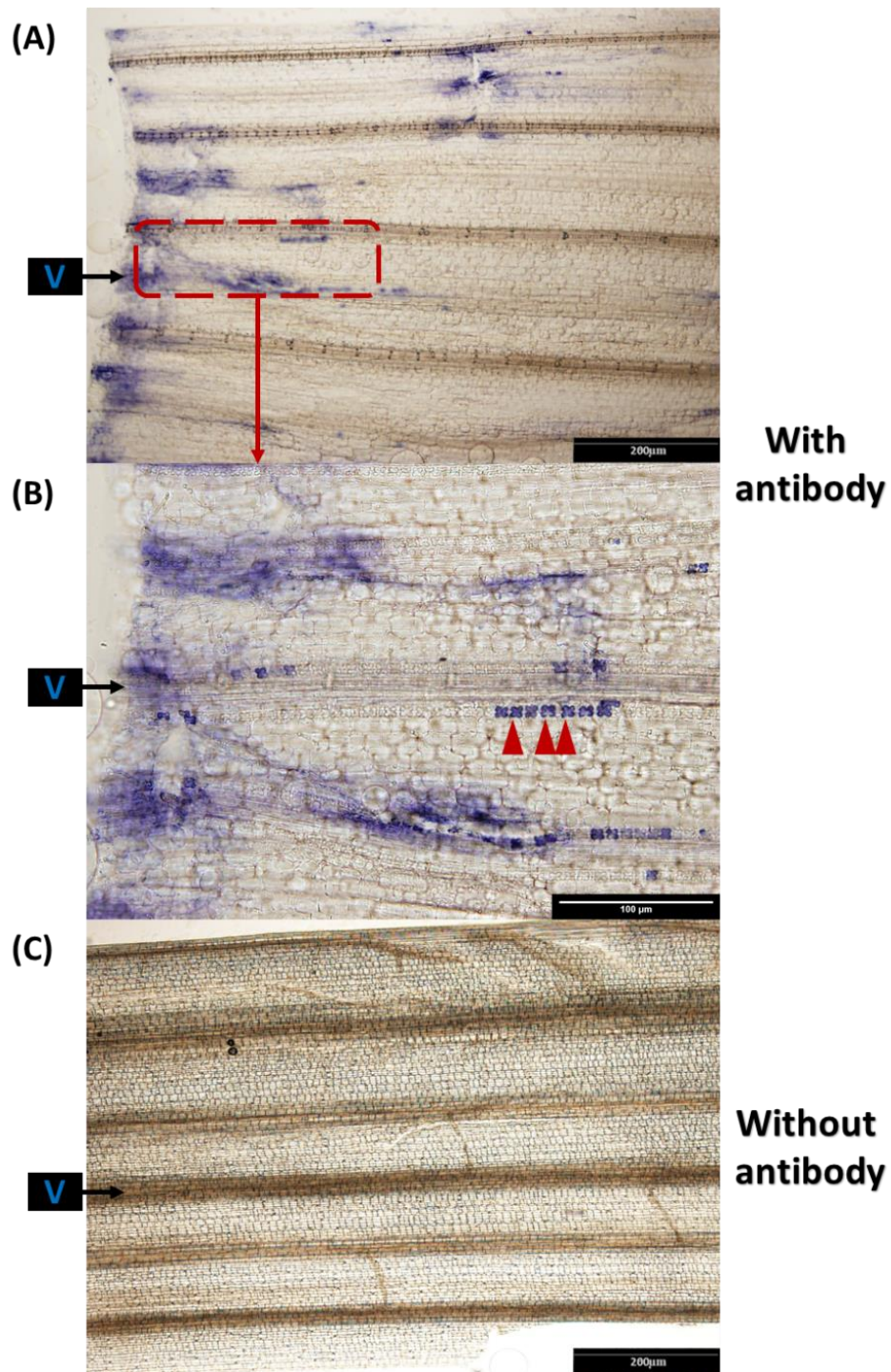


Figure 5.3

Staining pattern in P4 leaf tissue using the unmodified WISH protocol except by incorporating either *eEF1A*-sense probe or antibody only. The presence of antibody alone causes positive purple staining in some leaf regions (A) and when magnified (B) reveals staining in some interveinal gap areas and x-shaped silica bodies (arrowheads). When no antibody was added to the hybridized *eEF1A*-sense probe, no signal was obtained (C). V indicates vein.

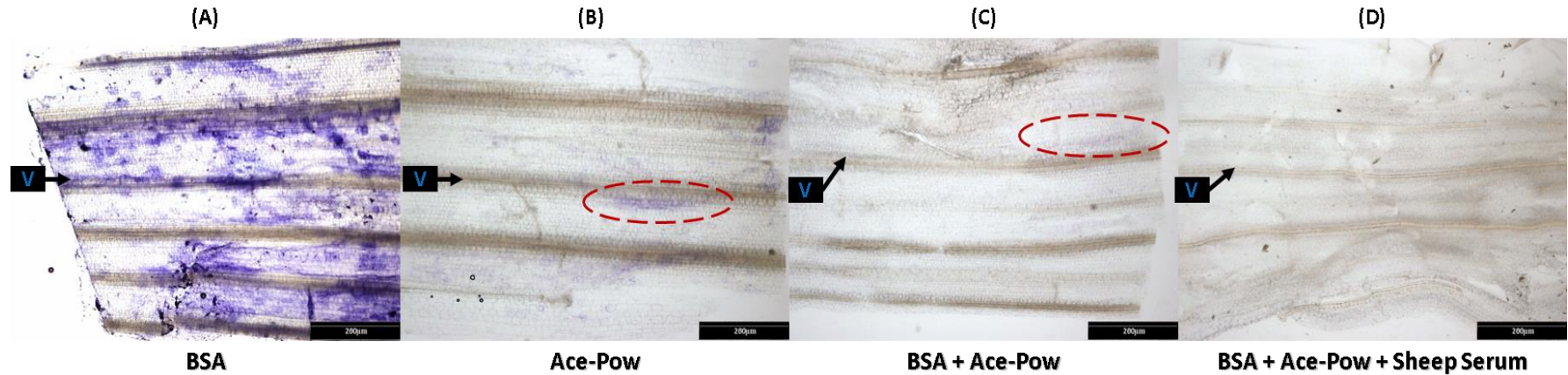


Figure 5.4:

Background staining pattern in P4 leaf tissue following the introduction of different mixtures of antibody blocking reagents in specific WISH steps. Bovine serum albumin (BSA) solution only prevents x-shaped silica bodies staining on the veins (v) but not in interveinal gap regions (**A**). Incubation of antibody in acetone powder (Ace-Pow) substantially reduce background staining (**B**, circled) and the combination of both BSA and Ace-Pow further refines the result (**C**, circled). The coupling of sheep serum and BSA together with Ace-Pow synergistically prevents background staining, thus producing a completely clear tissue (**D**).

5.3.4.2 Post-fixation and pre-hybridization treatments

Samples were post-fixed in absolute methanol (Fluka), 2 x for 2 min each, to further permeabilize the cells and precipitate remaining protein molecules. The solution was then changed to 1:1 methanol and PBTF (4% v/v methanol-free formaldehyde; 0.1M PBS; 0.1% v/v Tween-20) for 5 min and then to 100% PBTF for 30 min. Samples were rinsed in PBT (0.01M PBS; 0.1% v/v Tween-20) 4 x for 10 min each. Samples were incubated in PBTK (4% w/v Proteinase-K, Sigma; PBT) for 15 min and rinsed in PBT 4 x for 10 min each. Digestion with Proteinase-K is crucial for ensuring successful hybridization through cell lysis and inactivation of nucleases that might otherwise degrade the mRNA of interest. However, insufficient digestion will result in a reduced hybridization signal but if too long tissue integrity is compromised. This all depends on the physical nature of the tissue; the larger samples need stronger and longer Proteinase-K treatment. Samples were post-fixed again in PBTF for 30 min and rinsed in PBT 4x for 5 min each. Samples were prepared for hybridization by washing in half-strength WISH buffer (WMHB) (50% v/v formamide, Sigma; 0.5M SSC buffer; 5% w/v heparin salt, Sigma; 10% w/v single-stranded salmon testes DNA, Sigma; 0.1% v/v Tween-20) 2 x for 2 min each. Formamide is a solvent used to lower the melting point and annealing temperature of nucleic acid strands during hybridization (Betty *et al.*, 1969) together with high salt concentration provided by SSC to reduce stringency thus promoting hybridization (Schildkraut, 1965). The rate and quality of hybridization is further achieved by incorporating anionic macromolecules such as single-stranded salmon sperm DNA that prevents non-specific probe interactions (Bancroft and Marilyn, 2008) while heparin salt in general reduces background for DIG-labelled probes (James *et al.*, 1994). Samples were then prehybridized in new full strength WMHB for 3 h at 55°C in a water bath. This is important to equilibrate samples with the WMHB solutions thus blocking sites of non-specific interactions before the addition of probes.

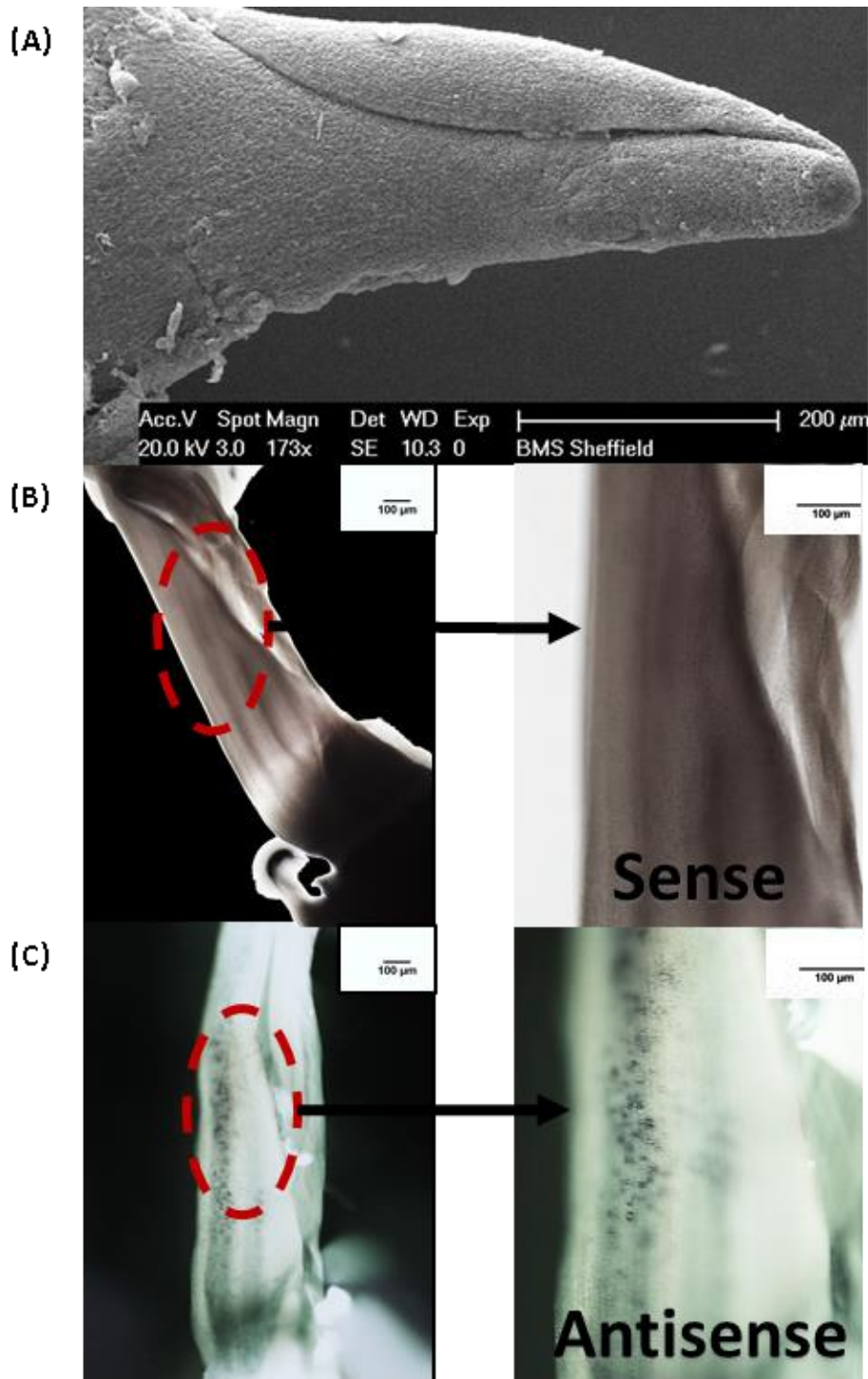
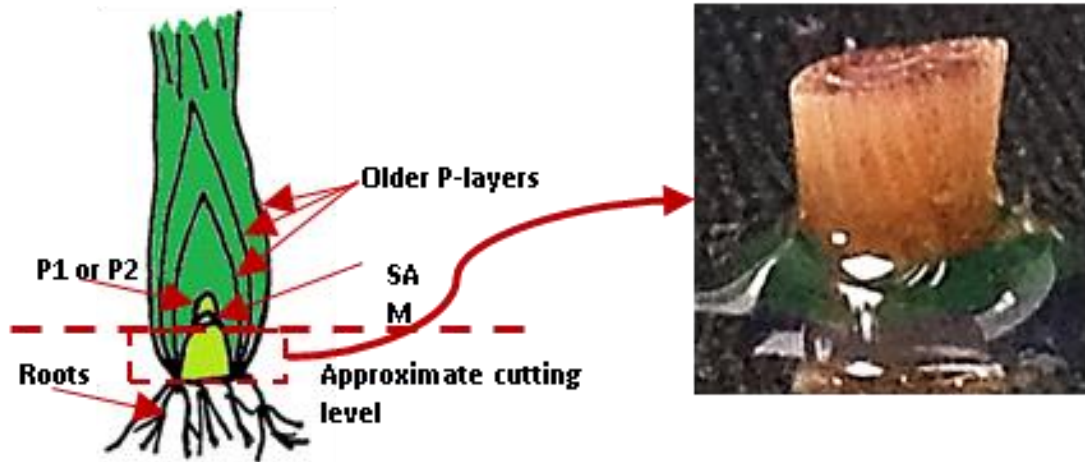


Figure 5.5:

mRNA expression pattern of the rice *Histone-4* gene in P3 leaf primordia. WISH was performed on the P3 tissue was dissected out. SEM micrograph (A) shows the whole structure of P3. The sense probe yielded no signals (B) and looks clear under magnification. The antisense probe produced signals (C) concentrated near the bottom of primordium and when magnified reveals dotted/streaked staining pattern.

(A)



(B)

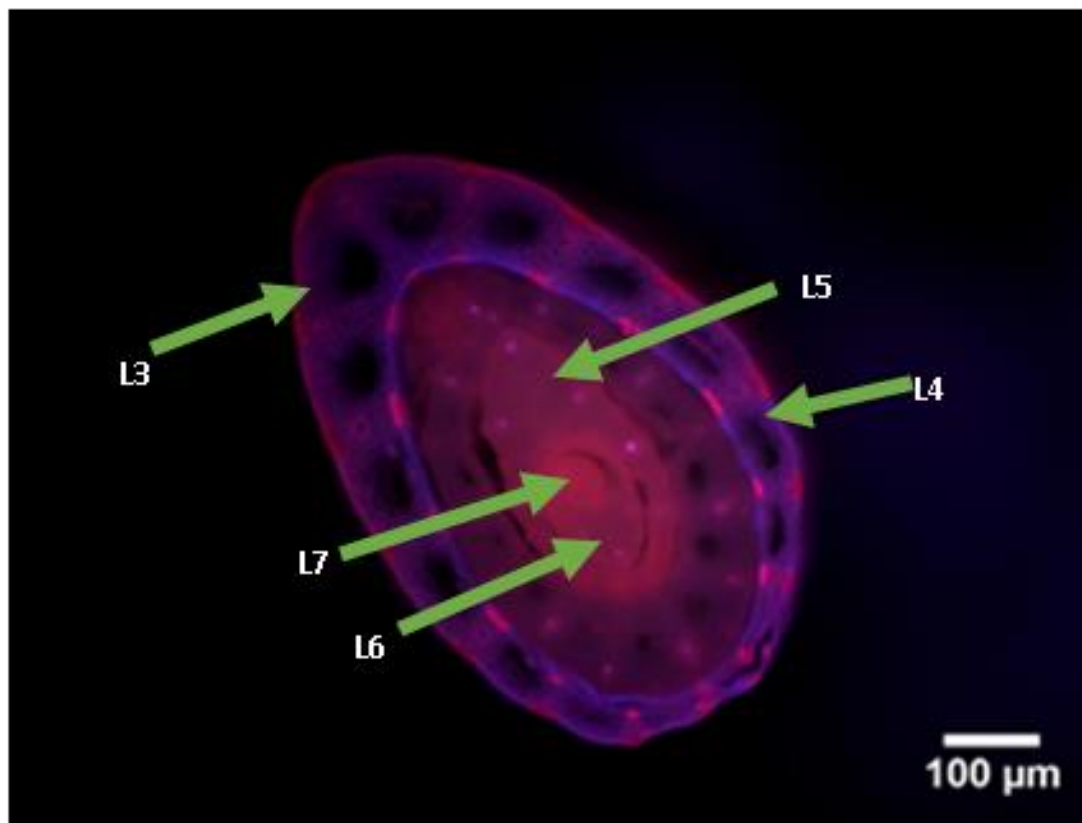


Figure 5.6:

Longitudinal section of a typical rice culm at the base (A), exposing leaf layers of different plastochron (P) stages and shoot apical meristem (SAM). Dashed line indicates a typical cutting level (about 1cm from the culm base) used for the whole mount *in-situ* to reveal the most number of leaf layers when being viewed from the top. The magnified image is the resultant stub cut (Image by Ahmad Nazrin Zakaria). When the stub is viewed from the top (B), it always shows leaf no. 3 (L3) as the outermost and oldest leaf layer.

5.3.4.3 Hybridization and antibody incubations

Samples were replaced with pre-warmed (55°C) WMHB. 2 µL of 1/10 dilution DIG-labelled probe was added per reaction. Samples were hybridized for 20 h at 55° in a water bath. Samples were then thoroughly washed using fresh WMHB 5 x for 25 min each. Post-WMHB solution (10% v/v sheep serum, Sigma; 1% w/v bovine serum albumin, Sigma; 0.08M Tris-HCl, Sigma; 0.12M NaCl; 0.24% v/v Triton X-100, Sigma) was gradually introduced to the samples (Post-WMHB: WMHB) at 25%, 50% and 100% for 20 min each. Samples were further washed in Post-WMHB 3 x for 5 min each. Post-WMHB solution is a mix containing proteins (sheep and bovine serums) that coat any membranes/surfaces in the samples that have high affinity for proteins so that the antibody used to bind with the DIG-labelled probes will not bind everywhere non-specifically thus reducing background staining (Otto, 1993). Samples were then incubated for at least 3 h on ice in an antibody solution (0.1% v/v Anti-Digoxigenin-AP Fab fragments, Roche; Acetone powder from young leaves; Post-WMHB) which had been prepared one day earlier and kept in dark at 4°C.

5.3.4.4 Colorimetric signal detection and imaging

The antibody solution was discarded and samples were rinsed in Post-WMHB 3 x for 5 min each. Samples were equilibrated for 5 min in detection buffer (0.1M Tris-HCl pH 9.5; 0.1M NaCl; 0.05M MgCl₂; water). Samples were reacted in BCIP/NBT mix (0.0075% w/v BCIP, Roche; 0.015% w/v NBT, Roche; detection buffer) in the dark at room temperature until sufficient colour development was detected for antisense probes. The mechanism for colour development has been described in section 5.1.1. This step varied depending on the probes used so during incubation period the signal was checked every 10-15 min until the staining produced was deemed satisfactory. Successfully hybridized mRNA was detected as dark blue-purple staining within cells. To a certain extent background staining could be present but normally a lighter blue-purple colour. Reactions were stopped in TE buffer (0.1M Tris-HCl pH 9.5; 0.001M EDTA; water) 2 x for 10 min each. Samples were carefully manipulated using fine tweezers and placed onto glass slides and constantly hydrated as necessary using the TE buffer while being viewed and photographed under a OLYMPUS BX51 compound light microscope. Images were captured and processed using a OLYMPUS DP71 camera and built-in CELL-A software.

5.4 Results

Once the WISH protocol for rice had been optimised it was used to explore the expression patterns of the genes listed in Table 5.1.

The *H4* gene is linked to the S phase of the cell cycle. The *H4* antisense probe was clearly observed as dotted purple stain in the younger leaf (leaf no. 5 - 7) cluster and young axillary leaf cluster (Fig. 5.7 A) indicating tissue containing actively dividing cells. The same localized expression pattern was absent in older leaves (L3 and L4) which had reached maturity. Signals were completely absent when the sense probe was used (Fig. 5.7 B) again showing the effectiveness of the blocking reagents used in this method. Furthermore, it only took 45 min for the staining to be clearly perceived, thus a great time saving compared to the original method. However, artefact staining was also present, although it appeared as brownish stains and usually occur in lignified dermal layers. Nevertheless this view of the transversely cut leaf cluster in general gave a clear view of expression localization, thus was employed as a way of cutting for the subsequent attempts with different probes, described below.

Five of the nine other genes probes examined (*CDKb2*, *DL*, *MON4*, *COV1* and *DWF7*) showed positive results with staining only observed for the antisense probes (Fig. 5.8 – 5.12). Interestingly the probe for CYCLIN-DEPENDENT-KINASE (*CDKb2*) gene had a similar expression pattern as in *H4* probe earlier which was dotted in appearance and only in the youngest leaf layers (Fig. 5.8 A, L6 and L7). In a younger L5, expression was only observed in vascular region but no expression at all was seen in older leaf layers (L3 and L4) or samples hybridized with the sense probe (Fig. 5.8 B). The antisense probe for the *DL* (*DROOPING LEAF*) gene was specifically expressed in dark vertical bands within the middle region of the leaf that would become the midrib in mature leaf (Fig. 5.9 A). Furthermore the expression only happened in the two youngest leaf blades (L6 and L7) with no expression in older leaf layers (L5-L3, which were basically leaf sheaths thus had no midribs) or in the sense probes (Fig. 5.9 B).

Probe: *Histone-H4*
Staining time: 45 min

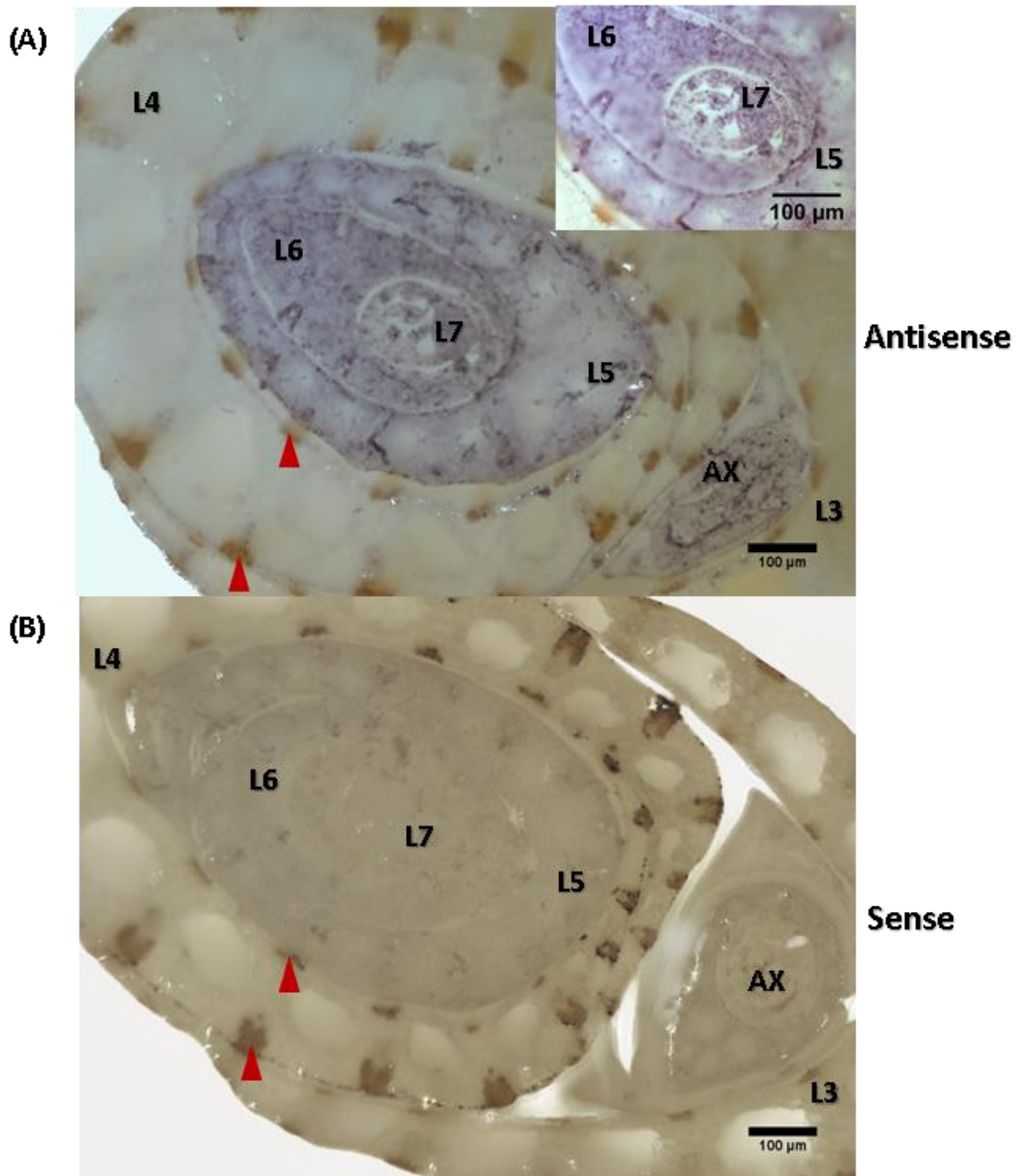


Figure 5.7:

mRNA expression pattern of rice *Histone-4* gene in a transversely cut culm containing a cluster of leaf layers. The outermost and oldest layer is leaf no. 3 (L3) and the leaf layers gets progressively smaller and younger towards the cluster centre. (A) shows positive expression pattern (dotted purple stain) for antisense probe in relatively younger leaf layers (L5-7) and the inset image is the magnified centre region of the cluster. No signal is detected anywhere for the sense probe in (B). Axillary leaf cluster (AX) that will give rise to a new tiller are also present. Artefact staining (non-purple) is present in lignified dermal layers (arrowheads).

The antisense probe for the *MONOPTEROS (MON4)* gene also showed a specific expression localized in vascular bundle regions (Fig. 5.10 A), consistent with a role in vascular differentiation and patterning, especially in developing and relatively younger leaf layers (L5-L7). Such expression was absent in more mature leaf sheath layers (L3 and L4) and in the sense probe samples (Fig. 5.10 B). The expression of the *CONTINUOUS VASCULAR RING (COV1)* gene was highest in the youngest leaf sheath layer (L4) and it persisted in the oldest L3 sheath layer where staining was observed in the septum region between lacuna in which vascular bundles could be found in the adaxial part (Fig. 5.11 A). Staining was much paler in the youngest leaves (L5 and L6) and completely absent for the sense probe (Fig. 5.11 B). The expression of the *DELTA-7-STEROL-C5-6-DESATURASE (DWF7)* gene also showed the same pattern as in *COV1* where it occurred highly in the youngest leaf sheath layer (L4) particularly around lacuna edges, in the septum regions of mature L3 sheath layer but much paler in the youngest L6 and L7 (Fig. 5.12 A) and no expression in samples hybridized with the sense probe (Fig. 5.12 B).

The expression of the *CHLOROPHYLL A-B BINDING PROTEIN (CAB)* was only high in the mesophyll areas of developing leaf layers (L5 and L6) but in areas that would give rise to lacuna and vascular bundles, the purplish signal was much paler (Fig. 5.13 A). The expression was also weaker in the youngest L7 samples and the more mature leaf sheath layers (L3 and L4) that contained fully formed lacuna and vascular bundles, whereas sense probe yielded no signal (Fig. 5.13 B). *CULLIN-1 (CUL1)* also showed some positive expression for the antisense probe, especially around the lacuna edges (Fig. 5.14 A). Even though the staining intensity was not as prominent as with the other probes reported before, it was higher than that observed with the sense probe which produced essentially clear tissue (Fig. 5.14 B).

Despite the promising results produced by the optimised WISH on the majority of the probes tested, certain probes yielded unsatisfactory results. They were probes for THYLAKOID FORMATION FACTOR (THF1) and DELTA-14-STEROL REDUCTASE (FACKEL) genes. Both THF1 (Fig. 5.15 A and B) and FACKEL (Fig. 5.16 A and B) produced signal not only with the antisense probes but with the sense probes as well.

Probe: *CDKb2*
Staining time: 30 hours
(antisense); 8 hours (sense)

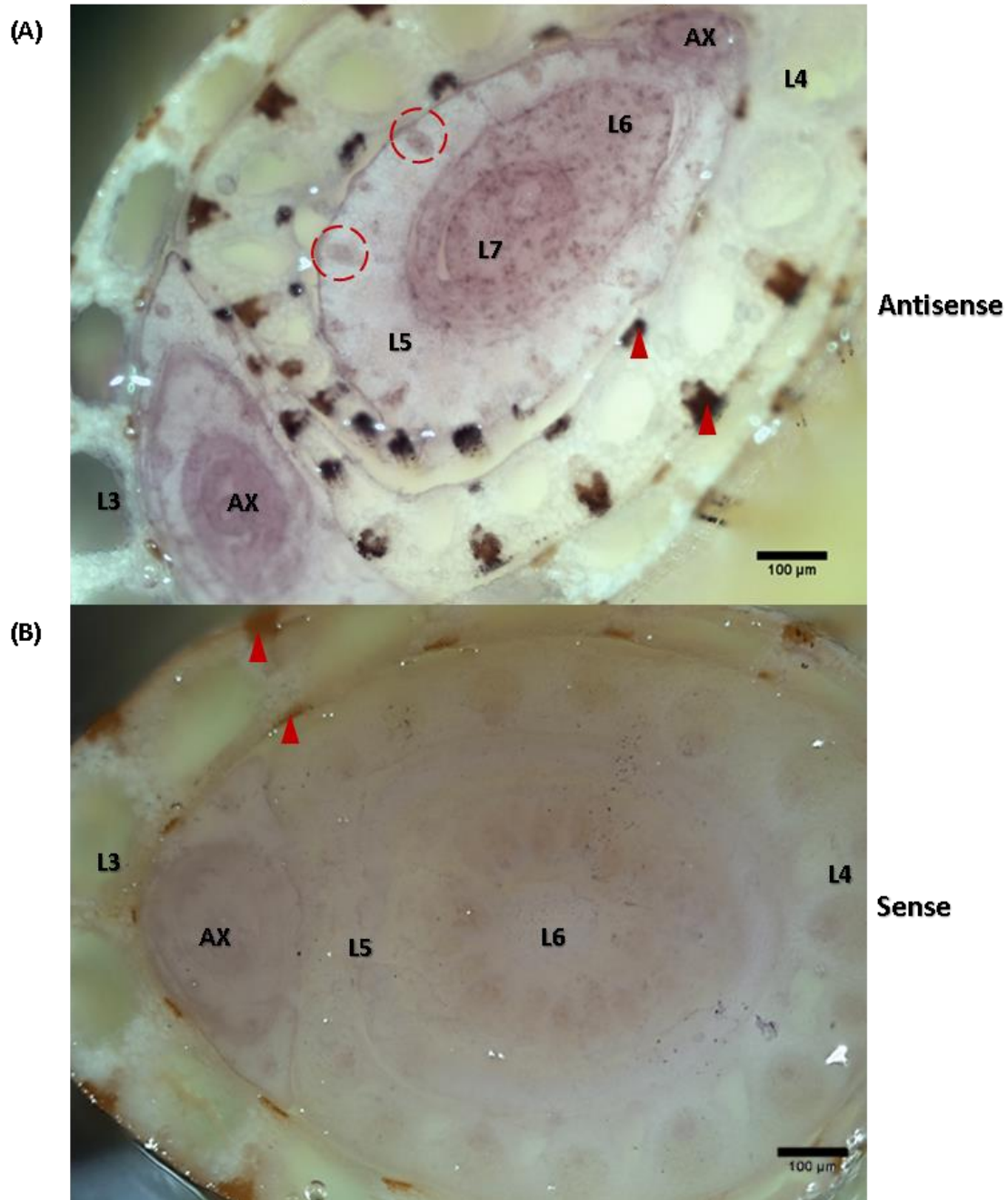


Figure 5.8:

mRNA expression pattern of rice *Cyclin-dependent kinase B2-1 (CDKb2)* gene. The outermost and oldest layer is leaf no. 3 (L3) and the leaf layer gets progressively smaller and younger towards the cluster centre. (A) shows positive expression pattern (dotted purplish-crimson stain) for antisense probe in the youngest leaf layers (L6 and 7) and in the axillary leaf clusters (AX). Expression also localized within vascular bundle regions (circled). No equivalent staining is detected anywhere for the sense probe in (B). Artefact staining (non-purplish) is present in lignified dermal layers (arrowheads).

Probe: *DL*
Staining time: 3 hours 45 min

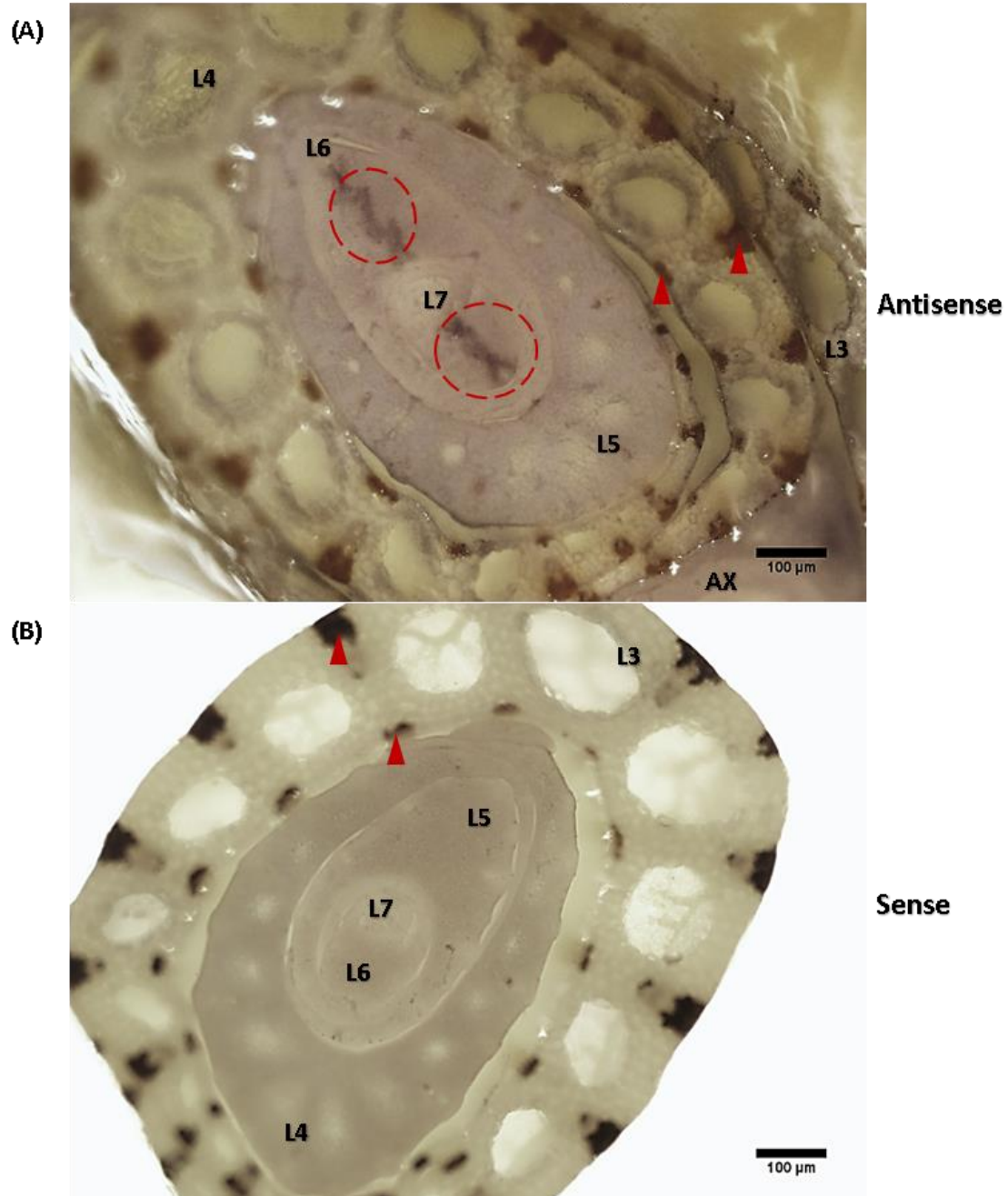


Figure 5.9:

mRNA expression pattern of rice *Drooping Leaf* (*DL*) gene. The outermost and oldest layer is leaf no. 3 (L3) and the leaf layer gets progressively smaller and younger towards the cluster centre. (A) shows positive expression pattern (dark vertical bands) for antisense probe in the youngest leaf layers (L6 and 7) which localized within presumptive midrib regions. No equivalent staining is detected anywhere for the sense probe in (B). Axillary leaf cluster (AX) that will give rise to a new tiller are also present. Artefact staining (non-purple) is present in lignified dermal layers (arrowheads).

Probe: *MON4*
Staining time: 30 hours
(antisense); 8 hours (sense)

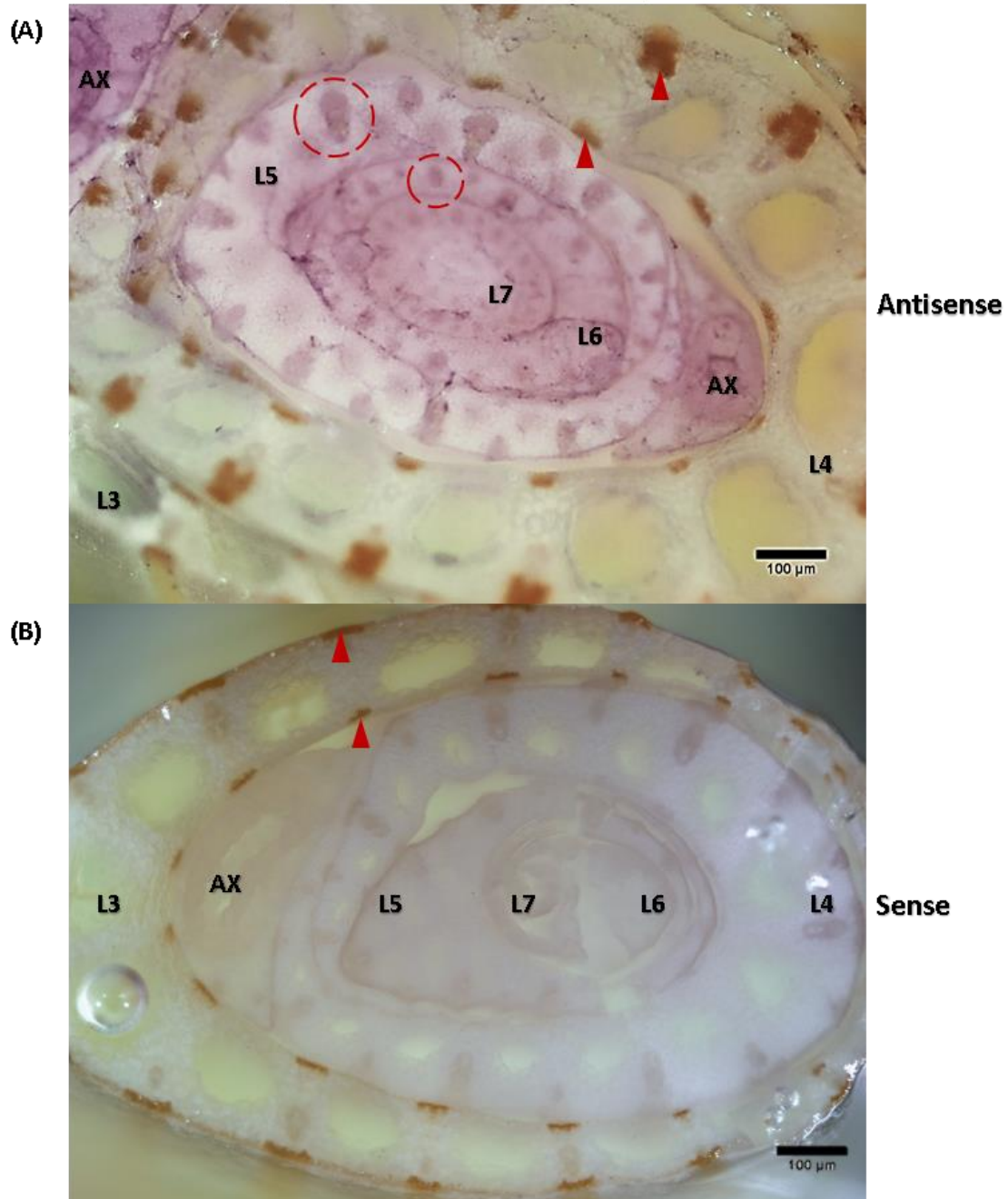


Figure 5.10:

mRNA expression pattern of rice *MONOPTEROS* (*MON4*) gene. The outermost and oldest layer is leaf no. 3 (L3) and the leaf layer gets progressively smaller and younger towards the cluster centre. (A) shows positive expression localization for antisense probe in the three youngest leaf layers (L5 - 7) within vascular bundle regions (circled) and in axillary leaf cluster (AX). No equivalent staining is detected anywhere for the sense probe in (B). Artefact staining (non-purple) is present in lignified dermal layers (arrowheads).

Probe: *COV1*
Staining time: 2 hours 15 min

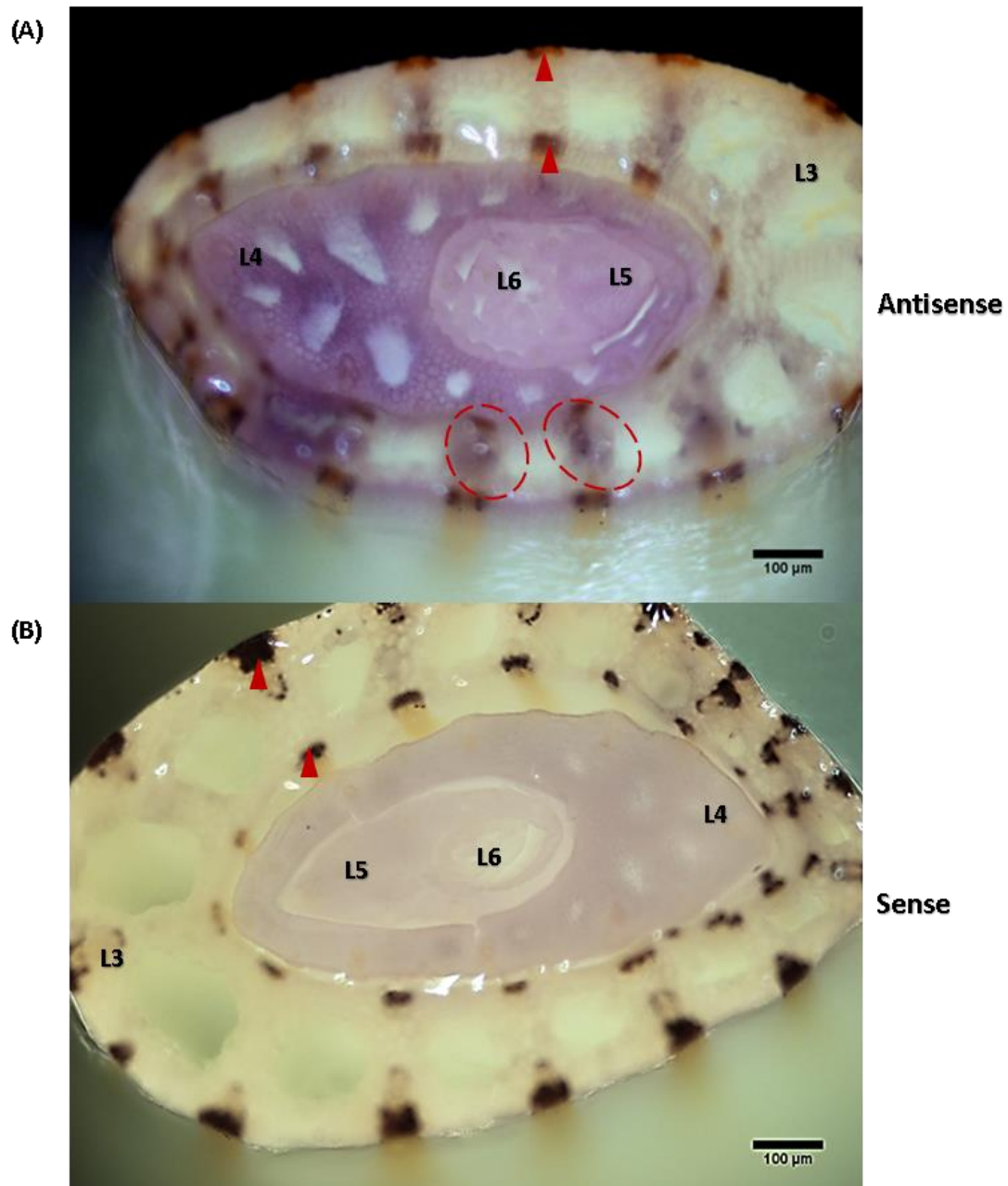


Figure 5.11:

mRNA expression pattern of rice *CONTINUOUS VASCULAR RING (COV1)* gene. The outermost and oldest layer is leaf no. 3 (L3) and the leaf layers gets progressively smaller and younger towards the cluster centre. (A) shows high positive expression (purple stain) for antisense probe in the youngest leaf sheath layer (L4) and also localized in the septum regions between lacuna (circled) in the older sheath layer (L3). No equivalent staining is detected anywhere for the sense probe in (B). Artefact staining (non-purple) is present in lignified dermal layers (arrowheads).

Probe: *DWF7*
Staining time: 4 hours 55 min

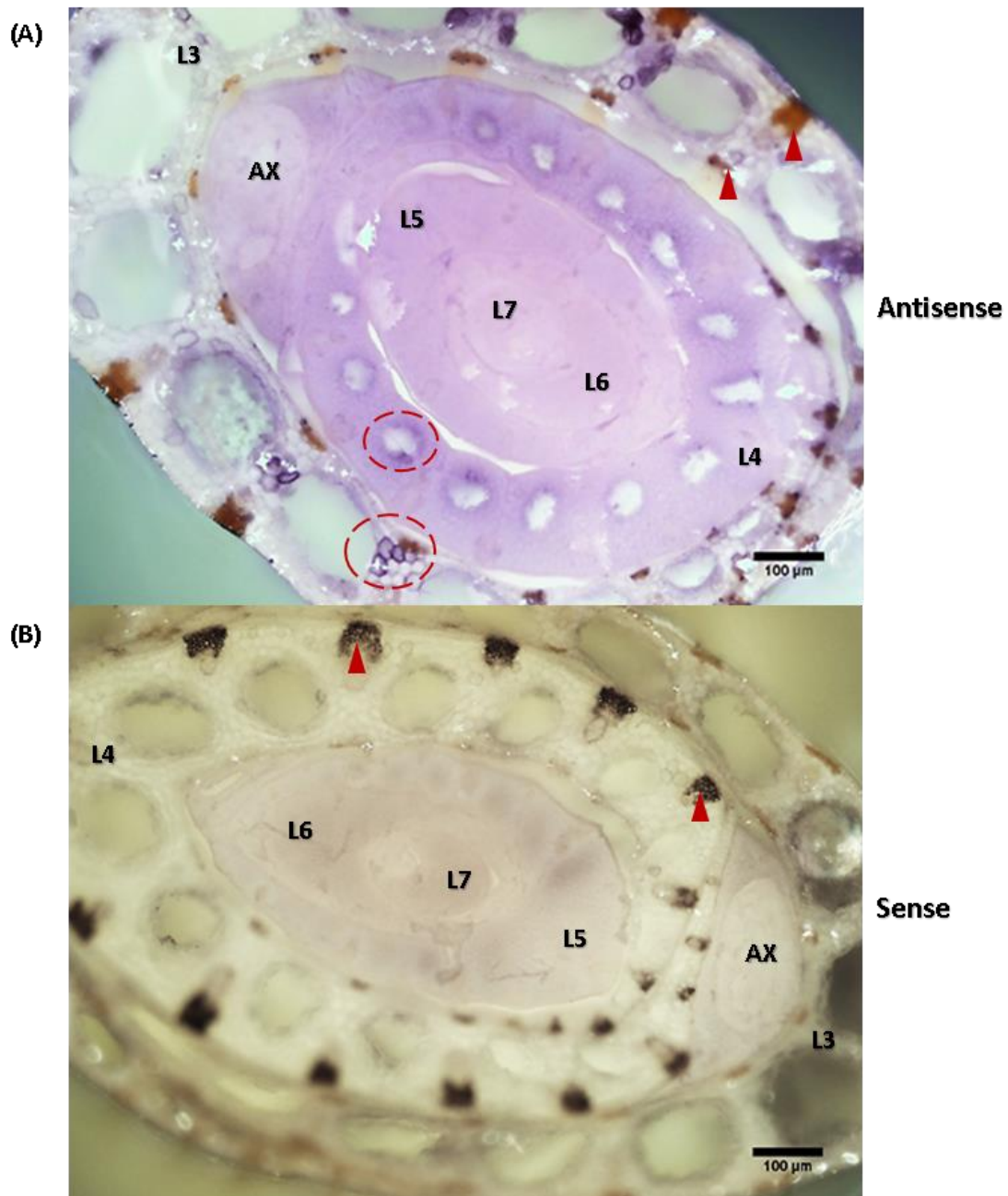


Figure 5.12

mRNA expression pattern of rice *DELTA-7-STEROL-C5* (*DWF7*) gene. The outermost and oldest layer is leaf no. 3 (L3) and the leaf layers get progressively smaller and younger towards the cluster centre. (A) shows high positive expression (purple stain) for antisense probe in the youngest leaf sheath layer (L4) especially at the edge of lacuna (circled in L4) and also localized in the septum regions between lacuna in the older sheath layer (circled in L3). No equivalent staining is detected anywhere for the sense probe in (B). (AX) is the axillary leaf cluster and non-purple artefact staining is present in lignified dermal layers (arrowheads).

Probe: **CAB**
Staining time: 9 hours 45 min

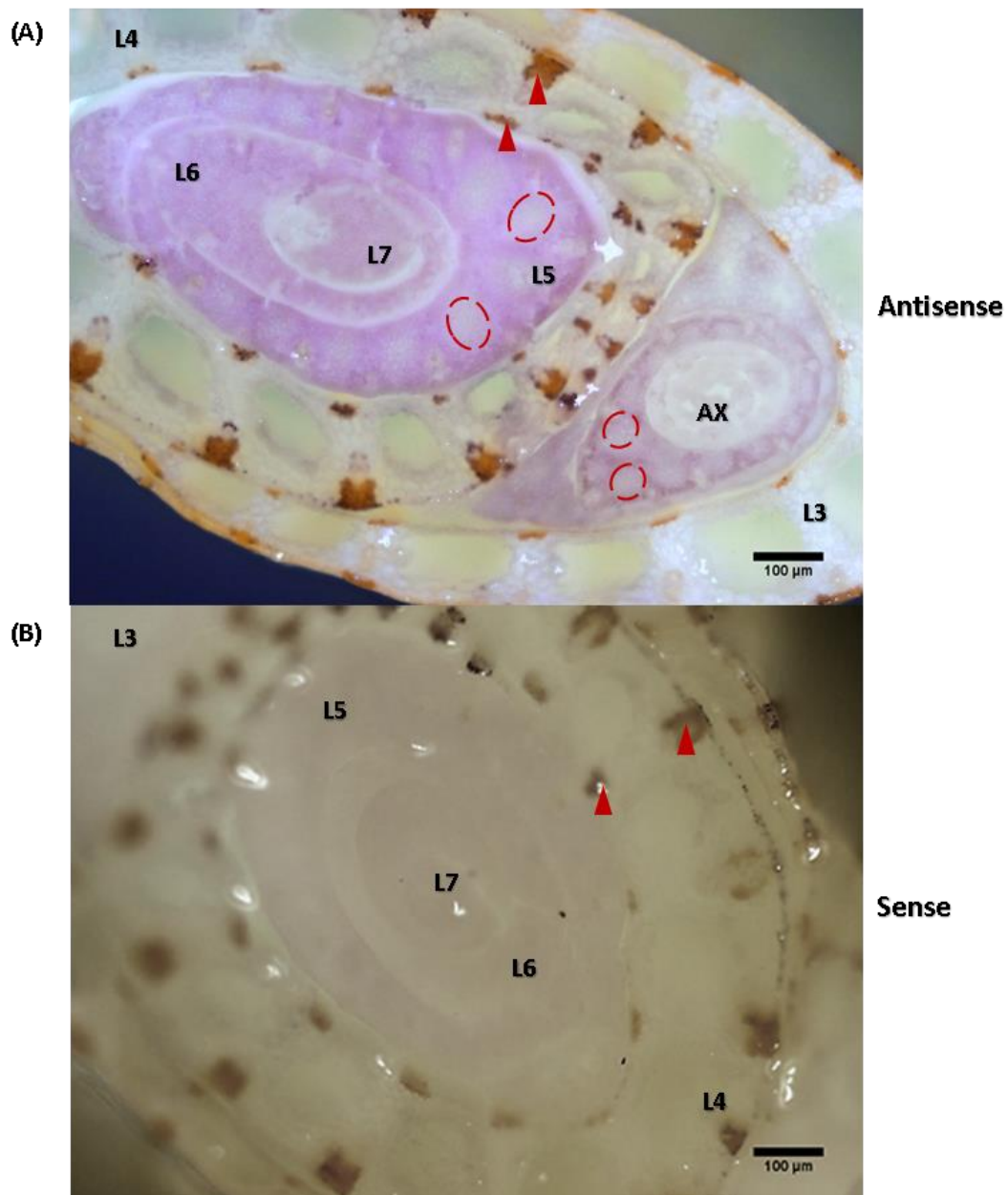


Figure 5.13:

mRNA expression pattern of rice *CHLOROPHYLL A-B* (*CAB*) gene. The outermost and oldest layer is leaf no. 3 (L3) and the leaf layer gets progressively smaller and younger towards the cluster centre. (A) shows high positive expression (purple stain) for antisense probe in the mesophyll areas of developing leaf layers (L5 and L6). Expression is much paler in the presumptive lacuna (circled) and vascular bundle (VB) areas, and this is true for axillary cluster (AX) region as well. No equivalent staining is detected in the youngest L7, the more mature leaf sheath layers (L3 and L4) that contained fully formed lacuna and VB and also for the sense probe in (B). Non-purple artefact staining is present in lignified dermal layers (arrowheads).

Probe: *CUL1*
Staining time: 2 hours 15 min

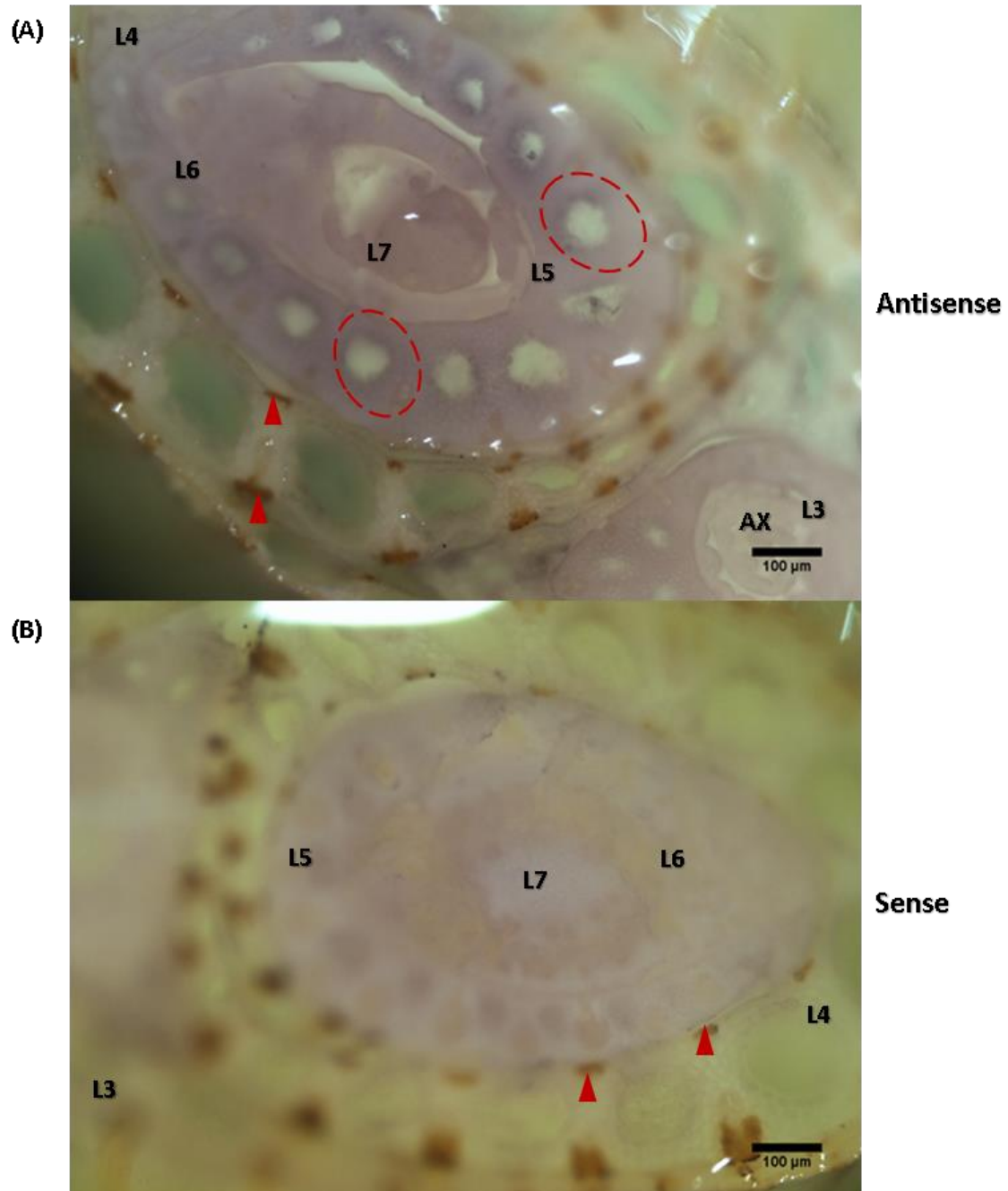


Figure 5.14:

mRNA expression pattern of rice *CULLIN-1* (*CUL1*) gene. The outermost and oldest layer is leaf no. 3 (L3) and the leaf layer gets progressively smaller and younger towards the cluster centre. (A) shows positive expression (slight dark stain) for antisense probe in the youngest leaf sheath layer (L4) especially at the edge of lacuna (circled). No equivalent staining is detected anywhere for the sense probe in (B). (AX) is the axillary leaf cluster and non-purplish artefact staining is present in lignified dermal layers (arrowheads).

Probe: *THF1*
Staining time: 4 hours 55 min

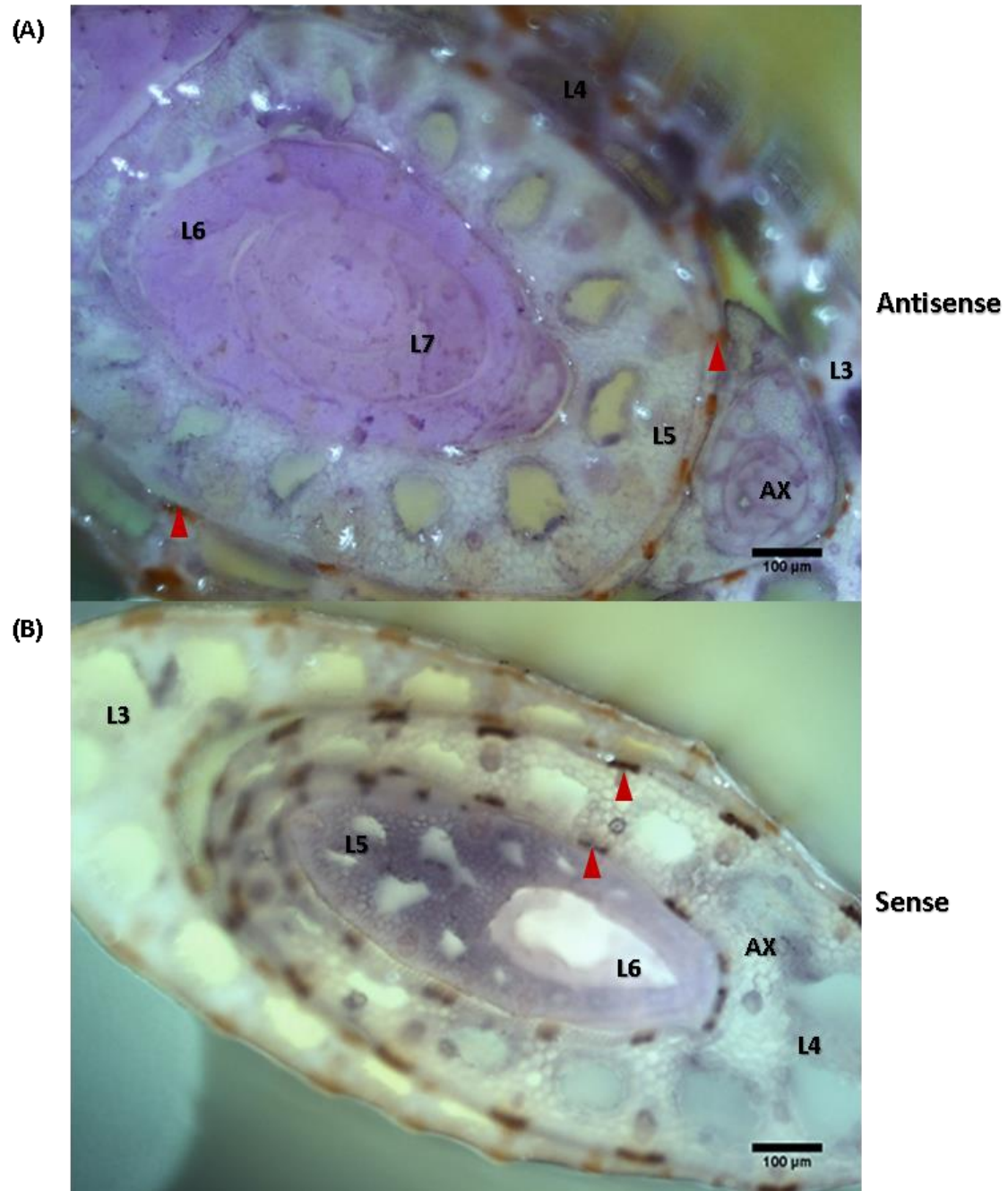


Figure 5.15:

False-positive mRNA expression pattern of rice *THYLAKOID FORMATION FACTOR* (*THF1*) gene. The outermost and oldest layer is leaf no. 3 (L3) and the leaf layer gets progressively smaller and younger towards the cluster centre. (A) shows positive staining (purple) for antisense especially in the youngest leaves (L6 and L7) . Similar purple staining is detected in L5 and L6 for the sense probe in (B). (AX) is the axillary leaf cluster and non-purple artefact staining is present in lignified dermal layers (arrowheads).

Probe: *FACKEL*
Staining time: 30 hours

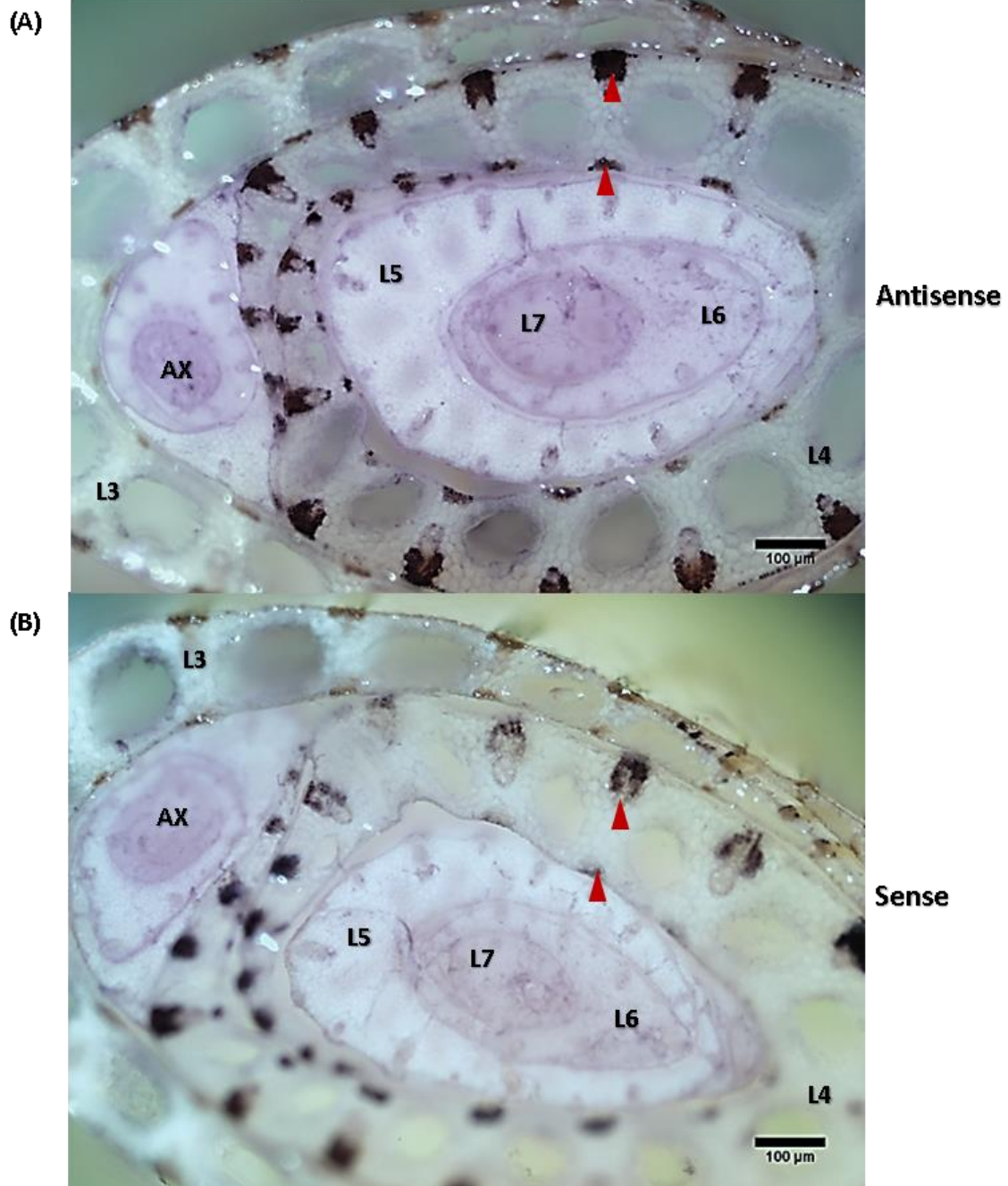


Figure 5.16:

False-positive mRNA expression pattern of rice *DELTA-14-STEROL REDUCTASE* (*FACKEL*) gene. The outermost and oldest layer is leaf no. 3 (L3) and the leaf layer gets progressively smaller and younger towards the cluster centre. (A) shows positive staining (purple) for antisense especially in the youngest leaves (L5-L7). Similar purple staining pattern is detected in L5-L7 for the sense probe in (B). (AX) is the axillary leaf cluster and non-purple artefact staining is present in lignified dermal layers (arrowheads).

5.5 Discussion

The aim of the results reported in this chapter was to establish a whole mount *in situ* hybridisation (WISH) procedure for the analysis of gene expression in rice leaves, particularly for future studies of stomatal development in the epidermis. Due to time restrictions, it was not possible to extend the analysis to stomata-related genes but for the first time a WISH protocol that worked in a reliable fashion for a number of genes was developed for rice.

WISH experiments using *Histone-4* revealed an interesting finding. Using P3 leaf primordia, the signal for the antisense probe was concentrated near the base of the primordium and seemed to be in the deeper tissue layer (Fig. 5.5 C). This pattern of signal fits with the expected localisation of cell division towards the leaf base and to *Histone-H4* being expressed only during the S phase of the cell cycle, thus leading to a spotty pattern (Nelson *et al.*, 2002). In addition, transverse cutting of an intact leaf cluster allowed better tissue penetration of the reagents and probes allowing gene expression patterns deeper in the tissue to be more easily visualised since chronologically each primordium is at a unique differentiation or maturity stage, each having particular tissues or structures (Fig. 5.6 B). For example the experiment using the *H4* antisense probe showed that *Histone-4* expression was zoned in the youngest leaf layers in the cluster (Fig. 5.7 A).

In traditional *in situ* hybridization methods thin tissue sections (2-dimensional) are taken while the WISH method uses whole tissues (3-dimensional) allowing better interpretation of gene expression patterns as well as taking a significantly shorter amount of time to perform (3 days vs. one week). Comparison of the traditional *in situ* hybridisation of the *H4* gene probe to leaf cross-sections (Van Campen, unpublished) and WISH, showed that the expression patterns were highly comparable. This suggests that the pattern obtained using WISH reflected the endogenous pattern of *Histone-H4* expression. Thus for all other gene probes reported in this chapter, the optimized WISH on transverse cut leaf clusters (WISH-TC) was employed.

Experiments using WISH-TC with the probes for other genes of various functions yielded convincing and reliable results for seven out of the nine tested (limited staining when hybridized with the sense probes, signal observed with anti-sense probe). When compared with the control *H4* expression (Fig. 5.7 A), cyclin-dependent kinase (CDK) had the most similar expression localization and appearance in which the spotty staining patterns were detected in the youngest leaf layers and in the axillary leaf cluster (Fig. 5.8 A). This finding is similar to the previously reported work using *Arabidopsis* (Segers *et al.*, 1996; Andersen *et al.*, 2008). In these reports Segers *et al.* (1996) summarize that the second type of CDK gene (*CDKb2*, as used in this study) shows expression in the cell cycle (thus can be a candidate endogenous control besides *H4*) while Andersen *et al.* (2008) highlight the general importance of CDK genes in ensuring normal cell cycle progression and for meristem organization, with high *CDKb2* genes expression in the SAM during the cell cycle essential to prevent meristematic defects.

WISH-TC has also proven to be useful in detecting gene expression which is tightly confined in a very specific leaf area, as in *DL* (DROOPING LEAF) expression (Fig. 5.9 A). *DL* expression appears as dark vertical bands in a presumptive midrib location in the leaf blade. This result is similar to the expression reported by Ohmori *et al.*, (2011) who also worked with rice. *DL* plays two important roles in rice, namely leaf midrib formation and flower carpel specification (Yamaguchi *et al.*, 2004). Since *DL* is thought to promote a larger midrib, it plays a role in the formation of erect leaves, thus can be a target in rice leaf engineering. Leaf erectness is undoubtedly a useful agronomic trait in rice because erect leaves perceive more sunlight even for lower leaves and require smaller growing area than those with floppier leaves. In fact it has been proven to increase biomass production since erect rice plants can be fitted into a more densely spaced crop (Sakamoto *et al.*, 2006).

Positive expression was also detected using probes for genes that have roles in leaf vasculature. *MONOPTEROS* (*MON4*) is a type of auxin response factor (ARF) and in this study its expression was highly localized in actively developing vascular bundle systems (Fig. 5.10 A) and this agrees with the localization found abundantly in emerging veins of *Arabidopsis* (Wenzel *et al.*, 2007). ARF transcription factors

bind on promoter regions of genes and regulate expression with respect to auxin level. Auxin itself is a phytohormone whose role is essential in vascular patterning since its high level is detected in procambial cells in *Arabidopsis* (Mattson *et al.*, 2003) whilst local application promotes vascular strand formation (Sachs, 1981). Meanwhile *CONTINUOUS VASCULAR RING (COV1)* product is a putative integral membrane protein and is likely to play a role in the maintenance or the initiation of a defined vascular bundle (Parker *et al.*, 2003). WISH-TC supports this hypothesis by showing even *COV1* expression in the younger leaf sheaf layer (vascular bundles yet to develop) while in the mature leaf sheath layer expression is concentrated only in the septum space between lacunas where a continuous ring of vascular cambium is located (Fig. 5.11 A). To a certain extent, the expression of *DELTA-7-STEROL-C5-DESATURASE (DWF7)* is similar to *COV1* (Fig. 5.12). Comparison of these results with published data show that in *Arabidopsis* *DWF7* protein localization (linked to oleosin formation) is also detected in leaf vascular tissue (Silvestro, 2013). It is interesting that *DWF7* expression is concentrated around the edges of the lacuna. If oleosin is present in rice it could reflect a role in desiccation in this region (Hsieh and Huang, 2007).

Genes associated with photosynthesis were also tested using WISH-TC, namely *CHLOROPHYLL A-B BINDING PROTEIN (CAB)*. The observed expression pattern (Fig. 5.13) agrees with Vainstein *et al.* (1989) who reported that *CAB* expression is abundant in both bundle sheath cells and mesophyll cells of maize leaves. The lack of expression in the mature leaf sheath layers is consistent with the idea that *CAB* levels decline in relatively older leaves as reported in barley leaves (Humbeck and Krupinska, 2003). A higher expression pattern for this probe might have been expected, but since the protein is encoded for a gene family more work is needed to investigate whether different members of the family show differential expression during leaf development. Final positive expression, although not as pronounced as other probes discussed earlier, was obtained using a probe for a *CULLIN-1 (CUL1)* gene. This was similar to *DWF7* expression in that was concentrated at the edges of lacuna (Fig. 5.9). Plants produce three primary types of CULLIN and *CUL1* is one of them that assembles the CULLIN-RING E3 ubiquitin ligase complex which controls many aspects of plant adaptation and development (Hua and Vierstra, 2011). The

functional interpretation of this expression pattern requires more work but is an example of how WISH can reveal interesting patterns.

Despite the reliability and versatility of the WISH-TC method presented so far, it is still not entirely perfect since it can give data which are difficult to interpret (e.g. with the *THYLAKOID FORMATION FACTOR (THF1)* and *DELTA-14-STEROL REDUCTASE (FACKEL)* probes (Fig. 5.15 and 5.16). Further optimization steps may be necessary so that the existing WISH-TC work as well with these probes. For example it may be necessary to reduce the probe length, especially for FACKEL (610 bp, Table 5.1), since it is a general practice to have probe length <500 bp to ensure good tissue penetration. Staining time and ambient temperature are factors that need to be taken into account as well since the staining times are rather long for these probes (almost 5hours for *THF1* and 30hours for *FACKEL*). Since the colour development is an enzymatic reaction, performing it in a constant temperature environment (23-25°C) in an incubator rather than on the bench will give a more moderate staining speed thus more power at stopping the reaction once sufficient signal has been detected. It may also be good to further enhance the blocking power, for example by adding 5% non-fat dry milk powder. As pointed out earlier, no single protein mixture can be a universal blocker for all probes. Finally in order to overcome one persistent shortcoming in WISH-TC (non-purple artefact staining of the lignified dermal layers) a number of approaches could be used to solubilize the lignin, such as microwave-assisted alkali treatment and liquid ammonia (Janker-Obermeier *et al.*, 2012; Strassberger *et al.*, 2015). Nevertheless these additional steps for further optimization of WISH should be done with great care and one at a time so that the general robustness of the method on rice is not compromised.

The optimized WISH method presented in this study has been shown to work on nine out of eleven probes for genes of various roles and functions. Taken as a whole, the optimization of WISH for rice is important since it opens the door to the more rapid analysis of the spatial control of gene expression in leaves compared to, for example, traditional *in situ* hybridisation on leaf sections. A main challenge in rice (and plant) biology is to understand the function of the thousands of genes expressed in the plant at any one time. Determining when and where a gene is

expressed provides important information on the potential function of that gene. Developing an atlas of rice gene expression using WISH is something that could be explored in the future. The application of WISH on the relatively complex and challenging leaf tissue paves the way to adapt this method for use on other organs in rice, such as floral parts and seed development. However, it is clear from the analysis reported here that it is possible that different tissues might show different problems in terms of background, so further optimisation of the procedure will be possible. It is also clear that the success of the approach is probe dependent. Although the results showing here are encouraging, the probes selected for analysis represent genes which are relatively highly expressed (Van Campen, unpublished data). The method needs to be further tested using probes for genes which are expressed at lower levels to judge the sensitivity of the approach. The protocol reported here was developed with the aim of investigating the expression of genes involved in stomatal differentiation. Unfortunately time limitations mean that these experiments have not yet been performed. Since stomata only form in a few cells in one layer of tissue (the epidermis) during a limited time of leaf development, it will be interesting to see if the sensitivity of WISH is sufficient to visualise these expression patterns.

Despite this caution, the WISH method described here provides encouraging results that it can be used to provide important data on gene expression patterns during early leaf development in rice.

CHAPTER 6

GENERAL DISCUSSION

6.1 Sun and shades characteristics of rice leaves

Leaves that grow in either high light or low light environments are known to be different in terms of leaf thickness (Terashima *et al.*, 2001), chloroplast structure (Lichtenthaler, *et al.*, 1981), pigment contents (Anderson *et al.*, 1995) and assimilation rates (Boardman, 1977). The initial aim of the work reported here was to characterise sun and shade type leaves in rice with a special emphasis on stomatal properties. Previous work on the effects of irradiance level on stomata and photosynthesis were generally conducted using *Arabidopsis* (Coupe *et al.*, 2006; Bussis *et al.*, 2006) with more limited analysis of grass leaves, such as rice. A deeper understanding of stomatal development in rice and its relationship to leaf function under different environmental conditions will provide a better understanding of rice leaf function.

In rice, guard cells are flanked by a pair of subsidiary cells, thus producing a stomatal complex (Fig. 3.6). With respect to length and width properties, many size measurements can be derived from this stomatal complex structure but for the sun-shade comparison, only stomatal complex and pore areas (SCA and SPA respectively) were analysed. Approximation of pore area was obtained using a formula for elongated hexagon and its derivation has been described in section 2.3.3.3. Other studies such as Dow *et al.* (2014) assume pore area is an ellipse, which is reasonable for *Arabidopsis* guard cells which are kidney-shaped but in rice they are dumbbell-shaped, thus a long hexagon is proposed to be more appropriate for the area assessment (Fig. 2.2). This pore area formula for rice might be useful for other related grass crops such as maize and wheat.

HL conditions in general produced larger stomatal dimensions compared to LL grown leaves, thus supporting other published work on rice (Hubbart *et al.*, 2012) and *Arabidopsis* (Coupe *et al.*, 2005). However this is not a universal phenomenon since other plant species, such as tobacco, produce stomata of similar size in either high or low irradiance level (Thomas *et al.*, 2003). SCA and SPA in HL grown rice are generally bigger in interveinal gaps (IGs) across the leaf width from midrib to the leaf margin (Fig. 3.5 A and B) compared to LL leaves, thus confirming previous work on rice (Hubbart *et al.*, 2012). This

detailed way of measuring stomata reveals that there is a tendency for stomata to be big (for HL leaves) in the first IG (immediately next to midrib) and the last IGs close to the leaf margin. This is more pronounced for SPA measurements. Middle IGs further away from midrib and margin seem to show more representative values for the entire leaf width, thus were the region chosen for analyses reported in chapter 4. The data reported here indicate that the sampling method does matter in stomatal studies in grasses such as rice. Care must be taken where stomata are sampled with respect to veins and leaf margin.

In general stomatal density (SD) was not different between HL and LL leaves across all IGs, although the last IG (in HL) certainly showed a higher SD than LL leaves (Fig. 3.5 C). This comparison scheme is purely based on an 'IG to IG' basis and since HL and LL produce different number of IGs in total, the last IG in HL is actually the 3rd last IG in LL, i.e. is not equivalent. As pointed out earlier, it is important to sample stomata in the most representative IGs, usually in the middle of the leaf width, and this approach has been explained in Fig. 3.8A and 3.8B. Besides SD, it is also possible to express patterning in rice using stomatal file percentage (%SF). Rice stomata only occur in certain epidermal files bound by two veins. %SF can vary because the number of "pure" epidermal cell files (without stomata) is not fixed and this parameter is used in Chapter 4 for further patterning analysis. In this work it is noticeable to see how in rice in almost all the leaves, independent of any treatments given, the stomatal file number (epidermal file that contains at least one stoma) varied only from two to four. This 'maximum four stomatal files' rule is only violated when the IG is next to the mid vein (Fig. 6.1 A) and close to the leaf margin (Fig. 6.1 C), otherwise the rule is true in all other IGs (Fig. 6.1 B).

Gas exchange analysis revealed that, as expected, HL leaves consistently had higher assimilation rates compared to LL leaves under varying CO₂ levels, reflecting the expected sun-type photosynthetic apparatus and agreeing with many previously reported works (Murchie *et al.*, 2005; Hubbart *et al.*, 2013; Narawatthana, 2013). Especially at high CO₂ levels in the A-C_i experiments, the carboxylation activity of Rubisco is highly elevated. Increasing CO₂ concentration around Rubisco by 1000 ppm (and beyond) would almost eliminate all oxygenase activity (von Caemmerer, 2000), explaining the

invariably higher assimilation rates obtained than under ambient CO₂ level (around 400ppm).

However the curve fitting tool used in this study only focuses on the two primary limitations, namely V_{cmax} and J_{max} . In the second phase of the curve the assimilation data points usually stay relatively flat, but sometimes when the C_a given is high enough, they can drop, as seen in HL leaves (Fig. 3.9). This phenomenon can be associated with the third phase of the curve, namely triose-phosphate utilization limitation (TPU) (von Caemmerer, 2000; Long and Bernacchi, 2003). Favouring carboxylation over oxygenase activity undoubtedly enhances carbon assimilation, which in turn produces a lot of 3-carbon sugars, namely triose-phosphate (3-phosphoglyceraldehyde). This is utilized either by transporting triose-phosphate from the chloroplast to cytosol or utilized in the chloroplast (Leegood, 1996). In the chloroplast, triose-phosphate is converted to starch, thus releasing the inorganic phosphate groups that can be reutilized in photophosphorylation (producing ATP needed to regenerate RuBP) (Sharkey, 1985; Leegood and Furbank, 1986). Thus, when TPU takes place other processes are affected, leading to a plateau in assimilation or even a decrease (in the case discussed here). This could be a mechanism employed to maintain photosynthesis to an optimum level (Sharkey *et al.*, 2004) within the given overall HL leaf characteristics.

Stomatal conductance (g_s) measured in these experiments showed that LL grown leaves have higher g_s values compared to HL leaves in both oxygen conditions. This is a perplexing result because a number of works using rice (Narawatthana, 2013) and other species (Gross *et al.*, 2008; Guidi *et al.*, 2008) reported that sun leaves tend to have higher g_s than shade leaves. Experimental set up could be the source of discrepancies, such as light and relative humidity levels. However, based on the g_s modelling using a formula by Franks and Farquhar (2001), high g_s is expected when stomata are relatively smaller (thus leading to higher density). But as discussed earlier, stomatal density is similar between HL and LL leaves, thus leaving the high g_s to be explained by the third component of the formula, namely stomatal pore depth (SPD). I do not have the measurements for this parameter but there

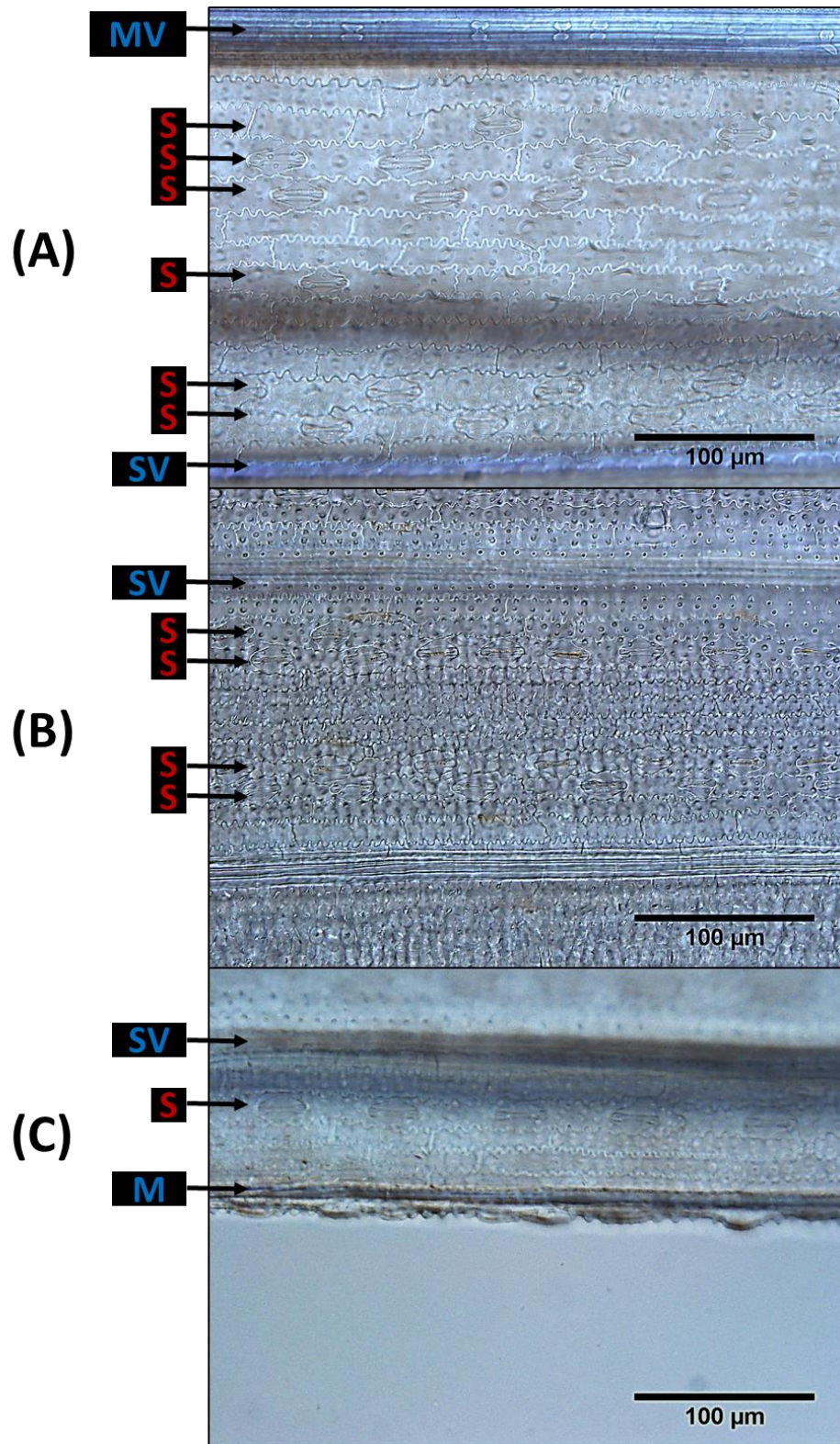


Figure 6.1:

Relative positions of stomatal files (S) with respect to midvein (MV), small vein (SV) or leaf margin (M). There are usually more than four stomatal files in the interveinal gap (IG) next to a MV (A). In IGs in the middle of the leaf width (B), stomatal files always follow the ‘maximum four rule’ The last IG next to margin (C) usually has only one stomatal file and a high in stomatal density.

might be a good connection between SPD and general leaf thickness because the thin LL leaves (Narawatthana, 2013) may also have a relatively shallow SPD that facilitates gas movement. The difference of g_s between HL and LL leaves could also possibly be explained by differential stomatal opening. If each stoma had a different capacity in controlling aperture due to its location (with respect to the vein) or natural solute contents, the cumulative effects could lead to the unusual varying g_s responses reported in this study, which opens an opportunity for further investigation.

Pigment quantification revealed that rice leaves follow the general view that HL leaves contain a higher chlorophyll a/b ratio (Kitajima and Hogan, 2003) than LL leaves because of relatively lower chlorophyll-b content (Fig. 3.12G). LL leaves invest more in making chlorophyll-b (hence more LHCII as well) as a predominant pigment molecule to capture and channel quantum energies. As showed by Evans and Seeman (1989), in terms of leaf nitrogen partitioning, sun and shade leaves invest almost similar amount of N to make light harvesting components, but HL leaves spend more N to make enzymes associated with carbon reduction, thus indicating LL leaves commitment to capture photons energy in shady environments. However it is worth noting that a number of Amazonian tree species have been shown to do the opposite by investing more in chlorophyll-a (Morais *et al.*, 2007). Other photosynthetic organisms, such as diatoms and brown algae, are also known not to invest in chlorophyll-b (Northrop and Connor, 2008) under similar conditions.

Besides being photosynthetically active, HL leaves are also efficient at managing water, made evident by a higher intrinsic water use efficiency (iWUE) than LL leaves (Fig. 3.13A) The analysis of carbon isotope ratio also showed that HL leaves had more positive values, thus showing a higher discrimination against the heavier ^{13}C compared to LL leaves (Fig. 3.13B). This happens when CO_2 demand at the carboxylation site is relatively high due to the abundance and activity of Rubisco. During such a situation Rubisco becomes less stringent in assimilating CO_2 from the heavier ^{13}C isotope, although in normal conditions the lighter ^{12}C is always the choice. Stomatal aperture can also be minimal since the rapid drawdown at the carboxylation site creates a strong gradient drives CO_2 influx, thus resulting in lower g_s . This

is translated into a higher water use efficiency (Franks *et al.*, 2015), which is a desirable quality in crop plants.

6.2 Leaf development, stomatal patterning and leaf performance

Stomatal differentiation occurs during relatively early stages of leaf development, yet this pattern of stomata is likely to significantly influence the photosynthetic performance of the mature leaf. Plants have thus evolved mechanisms by which stomatal patterning in the early phase of leaf development is attuned to the prevailing environmental conditions, including light. A second part of this thesis aimed to investigate the relationship of leaf developmental stage to the ability to respond to the light environment by altering aspects of stomatal differentiation.

To perform such an investigation one first has to have a robust means of assigning leaf developmental stage. It has been 6 decades since Ralph Erickson and Francis Michelini proposed the idea of plastochron index for studying plant stem development (Erickson and Michelini, 1957). Historically, the plastochron itself is not a new concept since the term was coined by Askenasy in 1880, referring to the elapsed time between initiation of two successive internode cells of *Nitella* algae. Esau (Esau, 1965) highlighted that this general definition by Askenasy could be applied to leaf primordium initiation, apical growth, internodes or axillary buds or floral organs development, as well as similar stages of shoot vascularization. Thus in terms of leaf development Schmidt (1924) was regarded by Esau as the first author to specifically used plastochron as the period of time between the initiation of two successive individual, pairs, or whorls of leaf primordia by shoot apical meristem (SAM).

In the first part of chapter 4, I established a plastochron index system for rice which allowed me to robustly assign leaf developmental stage. Importantly, due to the robust patterning of leaf initiation over time, this system allowed me to accurately assess the developmental stage of very young primordia (hidden from view), thus facilitating transfer experiments where leaf primordia at specific stages of development were transferred from one light regime to another. Thus, a series of transfer experiments were performed on rice

growing initially under HL or LL conditions. When the leaf no. 5 (which is hidden in layers of outer leaf sheath) had reached plastochron (P) stage 1,3 or 5 (using leaf no. 3 length as a proxy for estimation) the plant was transferred to the opposite light condition. The idea behind this experiment was that although leaf no. 5 is not directly exposed to the new light condition, it can still undergo acclimation to adjust the developing leaf to the new light condition by means of systemic signalling originating from mature leaves (Fig. 6.2). There are a number of mobile signals that can be transduced via the vascular system from mature leaves to the developing primordia such as sugars, peptides and phytohormones (Coupe *et al.*, 2006; Yoshida *et al.*, 2011). The focus of this investigation was on the leaf response to the systemic signal rather than the signal itself, the nature of which remains a mystery and which deserves further investigation. With a prolonged exposure of the plant to a new light condition, leaf no. 5 is expected to adapt both physiologically and morphologically, including changes to stomatal phenotype (a major focus of this investigation). The main question was whether the developmental stage of leaf 5 had a major influence on the ability of the leaf to respond to these systemic signals.

In the transfer experiments reported here, the primordia at stages P1 and P3 generally showed an ability to respond to exposure of the plant to a new light regime by altering aspects of epidermal patterning, whereas by the P5 stage this was lost. Even in some parameters not showing a significant shift in mean value, there was a significant difference in variation when transfer was performed at the early (P1, P3) stages of leaf development. Taken together, these data indicate that the epidermis of rice leaves retains a significant plasticity up to the P3 stage, but that this plasticity is lost by the P5 stage of development. There thus appears to be a sensitivity window for rice leaves to alter stomatal phenotypes in response to altered new light conditions. Published data from our group suggests that various photosynthetic-related properties are also alterable in these P-stages (Van Campen *et al.*, 2016). For

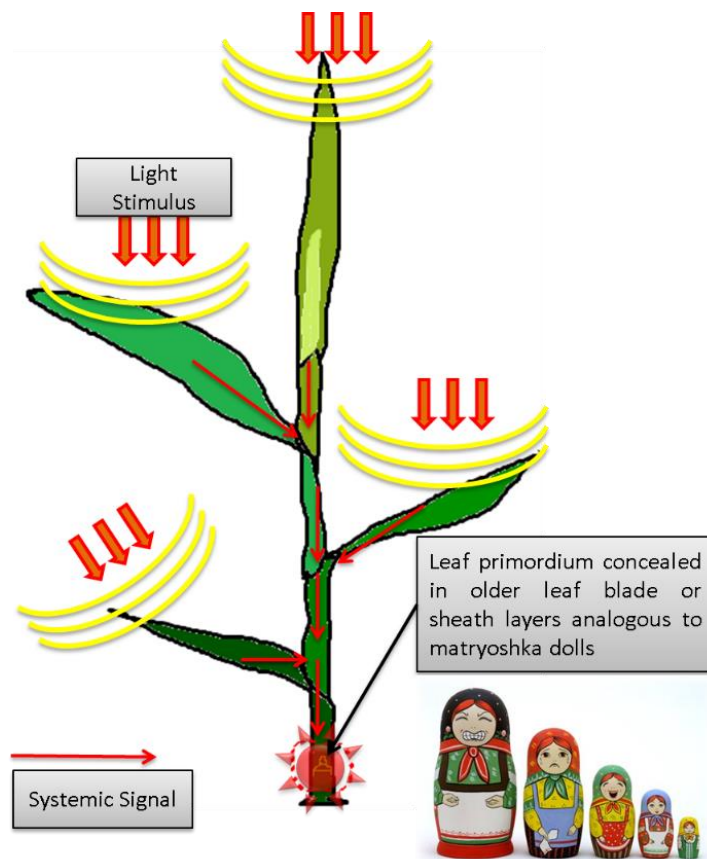


Figure 6.2:

Schematic illustration of potential systemic signaling relay system via vascular system perceived by older leaves that influence leaf acclimatization in developing and concealed leaf primordium.

both dicot (Gonzalez *et al.*, 2012) and monocot (Fournier *et al.*, 2005) leaves, virtually all cells are actively dividing at the beginning of leaf primordia development from the SAM. As development advances, cells at the leaf apex stop dividing and starts expanding while cells at the base are still in a phase of division. It is worth nothing that low light extends the duration of cell production, particularly in grass species growing with an abundance of nutrients (Sugiyama and Gotoh, 2010). Therefore in the transfer experiments from HL to LL conditions, it is expected that the number of epidermal cells will increase, consistent with the since P1 and P3-transferred leaves having the highest values for cell file number (Fig. 4.3F). However the increased number of dividing cells under LL conditions also tends to come with higher variation in cell number, as reported by Sugiyama and Gotoh (2010) using *Festuca arundinacea*, and a similar trend is reported here with the P1 and P3-transferred leaves. Thus the high variation in some parameters following

transfer at early P stages to LL conditions might be explained by an increased rate of cell division. The higher number of cells which have the potential to undergo differentiation to, for example, stomata, might simply lead to more noise in the system, thus higher variation.

It is interesting that transfer from LL to HL conditions generally led to less dramatic shifts in patterns of epidermal characteristics (Fig. 4.5). This might relate to the mechanism of systemic signalling from mature to young leaves which is thought to underpin the regulation of epidermal properties in the developing leaf primordia. The nature of this signal is unknown, but if it is related to metabolic/photosynthetic activity in the mature leaves (Hou *et al.*, 2015) it might be that the shift to $750 \mu\text{mol m}^{-2} \text{s}^{-1}$ (HL under our conditions) was not sufficient to generate a strong signal. A shift to higher irradiance (e.g., $1000 \mu\text{mol m}^{-2} \text{s}^{-1}$) might be required to trigger a stronger response. The nature of the systemic-signal generating mechanism remains a major unknown. Efforts are emerging in understanding Target of Rapamycin (TOR, a highly conserved protein kinase) signaling network in multicellular plants (Xiong and Sheen, 2015) and sugars derived from photosynthesis, such as sucrose, seems to be the most likely signals involved in activating plant TOR kinase (Ren *et al.*, 2013; Xiong *et al.*, 2013). Studies have revealed that the TOR pathway is an essential controller for cytoplasmic growth, cellular development and proliferation (Zhang *et al.*, 2013; Sablowski and Dornelas, 2014). Future work might explore the role of TOR activity in the source leaf response to altered irradiance, as well as the potential role of TOR signaling in modulating the cellular response in the target leaves.

An interesting observation from the transfer experiments is that guard cell width is the only parameter that is significantly altered following any P-stage transfer. This degree of plasticity implies GCW is not especially restricted by stomatal complex width. Guard cells in rice are sandwiched between pair of subsidiary cells whose partial collapse is required for guard cells to swell. A deeper understanding of the functional relationship of the guard cells and subsidiary cells may reveal insight into the plasticity of grass (rice) stomatal response to environmental change (Lawson, 2009).

Although stomatal density in HL and LL leaves was similar there was a higher spread of data in the HL to LL transfer experiment, especially in the P1 and P3 transfers (Fig. 4.3I). This suggests that the rice epidermis can respond to the LL environment during these P-stages by initiating longitudinal cell divisions (resulting in higher number of cell files, Fig. 4.3F) and varying the cell file width (Fig. 4.3H). These cellular changes are associated with more irregular stomatal differentiation, resulting in the higher variation in the SD values obtained. Besides density, stomatal patterning in rice can also be expressed in terms of stomatal file percentage (%SF). Since the IG used for this study has been selected based on the scheme in Fig. 3.5A and 3.5B, the number of cell files that contain stomata within any single interveinal gap always lies between two and four (Fig. 6.1B). This property, combined with the leaf's ability to change CFN and CFW, leads to a significantly higher percentage of cell files containing stomata in HL grown leaves compared to LL grown leaves. This %SF parameter follows the trend in which P3 transfer appears to be the cut-off point to produce significant alteration in final stomatal properties in the mature leaf in response to altered irradiance. These data thus fit to a general cell division response being possible in P1 and P3 stages but not in P5 leaves, i.e., the systemic signalling system is not stomata specific but may alter the entire field of cells within which the stomata patterning system functions.

Since the experiments summarised above led to changes in stomatal properties, I investigated the extent to which this led to altered photosynthetic performance in the target leaves. To do this, a paired experiment was performed in which measurements of physiological parameters such as assimilation rate (A), stomatal conductance (g_s) and intrinsic water use efficiency ($iWUE$) were associated with the stomatal phenotypes observed in the same leaf.

In the transfer experiment (HL to LL condition), transfer at the latest P5 stage, marked by the first appearance of the leaf blade from the sheath, conferred no significant changes in the stomatal parameters measured. However even there was no change in the stomatal parameters at maturity (P6-stage) in the LL condition, the relatively long period of time (5-6 days) from P5 to P6 allowed the leaves to acclimate physiologically (Fig. 4.16iv). However, the acclimation

was only partial since the leaves only achieved A_{\max} values similar to LL grown leaves after transfer at any P-stage (Fig. 4.7B) whereas A_{400} in general followed the trend where transfer at P1 and/or P3 was the cut-off point to produce leaves with an assimilation rate similar to LL grown leaves (Fig. 4.7A). Among the photosynthetic components analysed, only V_{cmax} of the P-transferred leaves showed comparable values to the LL grown leaves (Fig. 4.7C), suggesting a leaf's ability to change Rubisco content continues to a relatively later developmental stage.

The opposite transfer from LL to HL conditions generally revealed less plasticity in the stomatal parameters measured (Fig. 4.5B). However the measured A_{400} and A_{\max} values for the P-5 transferred leaves were similar to HL grown leaves (Fig 4.9A and B). Analysis also revealed that leaves transferred at any P-stages were able to increase V_{cmax} (Fig 4.9C), J_{\max} (Fig. 4.9E) and chlorophyll a/b ratio (4.9F) to match those observed in HL grown leaves. Taking all the physiological data together, it seems that stomata (despite not changing much either in size or density) are able to 'work more' under some conditions, i.e., they can open more to allow for more CO_2 diffusion, thus allowing an increase in photosynthesis. This is possible since the measured (operational) g_s results from partially open stomatal aperture. When the need arises (e.g, low CO_2 levels, high RH, blue-red light and possibly high photosynthetic capacity, as in this study), stomata have the capacity to increase their aperture (Dow *et al.*, 2014), thus overriding their normal, submaximal aperture size.

The analysis of $g_s\text{-}C_i$ curves also revealed some interesting findings about g_s responses in rice. In this entire study rice was always grown hydroponically, therefore access to water was never an issue. Thus, theoretically, when CO_2 is steadily increasing from low concentrations, stomata should open to allow more rapid gas exchange without any danger of increased transpiration having a negative outcome on their ability to maintain turgor pressure and water potential. However in all the $g_s\text{-}C_i$ curves analyzed, stomatal closing occurred before ambient CO_2 level (400ppm). This tight g_s response seems to be pre-programmed, indicating the ability of rice to maintain optimum water use efficiency in any given water status condition.

C_i concentrations in leaves have long been known to regulate g_s (Mott, 1988) and are determined by cellular respiration, photosynthesis rate and atmospheric CO_2 levels (C_a) (Lawson *et al.*, 2014). However the role of photosynthesis in g_s regulation has been a matter of debate for many years since two photosynthetic cells, namely mesophyll (via mesophyll-derived signals, Mott *et al.* (2014)) and guard cells (via osmotic adjustment, Lawson *et al.*, (2003); Lawson *et al.*, (2014)) make contributions to stomatal aperture control in response to CO_2 changes. However recent findings have shown that starch biosynthesis in guard cells is required for proper stomatal closure under high C_a condition, while starch biosynthesis in mesophyll cells makes a negligible contribution to the process (Azoulay-Shemer *et al.*, 2016). Moreover elevated CO_2 levels also enhance anion channel activity in guard cells, inducing stomatal closure via the action of the SLAC1 protein that regulates gates for anion transport (Yamamoto *et al.*, 2016). But why did stomatal closure always occur before the ambient CO_2 level in this present study? As mentioned, starch accumulation in guard cells is required for stomatal closure. During the increase in C_a levels, photosynthesis rate increases progressively so that where sugars such as sucrose, fructose and glucose accumulate, helping to drive stomatal opening (Antunes *et al.*, 2012). Sugar accumulation, at sub-ambient C_a level, leads to conversion to starch that which helps drive stomatal closure. In addition, there is no need to widely open stomata at high C_a levels since CO_2 will readily diffuse across the concentration gradient into substomatal chamber. The plant thus has a variety of mechanism to achieve optimal balance between CO_2 uptake and water-loss over a range of ideal and sub-optimal growth conditions (Haworth *et al.*, 2015). A recent finding has confirmed this, showing that plants grown under elevated CO_2 condition produce less responsive stomata (poor aperture control), causing the leaves to become more vulnerable to water stress and high temperature (Haworth *et al.*, 2016).

Among all the physiological parameters analysed in this study, iWUE at ambient CO_2 is the only one that showed significant correlation with one stomatal phenotype, namely guard cell width. As discussed earlier, it is noteworthy that GCW is the only parameter that significantly altered in the generally less responsive LL-HL transfer experiment. It seems that GCW is

also indicative of the plants iWUE. This is consistent with the widely observed importance of guard cells in stomatal control, which in turn affects general leaf performance. (Lawson and Blatt, 2014). Although the mechanistic link of GCW and iWUE is not entirely clear, this information could be exploited by crop breeders in the search for useful traits for drought prone areas or for general water conservation in agricultural crops. Effective stomatal control is crucial to the plant stress response (Killi *et al.*,2017) and the identification of any physical parameter which could be used as a proxy for iWUE would be very useful in screening programs.

6.3 Optimization of a tool for studying gene expression in rice

In the final part of this thesis I developed a technique with the ultimate aim to examine the expression of genes involved in stomatal differentiation and how these might respond to altered environment. The whole-mount in situ hybridisation (WISH) technique was chosen as a tool to study gene expression in rice. Due to time limitations I could not prepare the probes for stomata-related genes but was fortunate enough to obtain probes for various genes from colleagues which were used to optimise the procedure. WISH is a very useful tool in studying gene expression because it saves time and is less laborious compared to the commonly used in situ hybridization technique that involves embedding and sectioning of biological tissues.

WISH in this study was based on the protocol by Traas (2008) who optimized it for use on young, soft *Arabidopsis*, such as embryos and leaf primordia. Without any modification of the original protocol, hybridisation of the control probe (for the *eEF1A* gene) already yielded promising results, especially since the bulliform cells were completely stain-free with the antisense probes (Fig. 5.3). However it was still not perfect because some background and non-specific staining also occurred in some interveinal gap areas and x-shaped silica bodies. I then performed an intensive optimization of WISH for rice, starting by formulating a blocker concoction to prevent non-specific interactions of antibody with the tissue that can lead to false staining. The results showed that no single protein mixture could be a universal blocker because I had to

combine three reagents, namely bovine albumin serum, sheep serum and antibody pre-adsorbed to acetone powder, in order to obtain a satisfactorily clear and stain-free leaf tissue indicating the absence of non-specific antibody binding (Fig 5.5). Further optimization was also made in terms of tissue preparation by making a transverse cut on intact leaf clusters to promote tissue penetration. At the same time this sectioning approach allowed signal detection in leaves of different ages which have distinct structures associated with them due to their different maturity levels, such as undifferentiated epidermal cells, lignified dermal layers, vascular systems and lacuna (Fig.5.2). Staining time is also an important factor in WISH, so for each probe tested the enzymatic reaction in the colour development was stopped as soon as sufficient signal was detected. This combined WISH reagent optimization and transverse cutting are termed WISH-TC.

Comparison of the results reported here with other work on similar genes shows that WISH-TC manages to produce a highly comparable result, suggesting that it is a reliable technique to be used on other probes. These highly similar results included probes for the genes Histone-H4 (Fig. 5.7: compare with Van Campen, unpublished) and DROOPING LEAF (Fig. 5.9: compare with Ohmori *et al.*, 2011) where both comparisons are with rice. Some probes compared against data from *Arabidopsis* (a different species) still yielded positive and similar gene expression patterns, such as probes for the genes *MONOPTEROS* (Fig. 5.10: Compared Wenzel *et al.*, 2007) and *DELTA-7-STEROL-C5-DESATURASE (DWF7)* (Fig. 5.12: compare with Silvestro, 2013). Some of these genes are either putative or of unknown functions in rice, such as *DWF7* and *CUL1*. It is interesting to see *DW7* expression is concentrated around the edges of lacuna since in *Arabidopsis* it is linked to oleosin formation, thus if oleosin is present in rice this could mean it is involved in the desiccation of lacuna regions (Hsieh and Huang, 2007). While *CUL1* protein function is putative in rice, in *Arabidopsis* its role is known to be a component of a protein complex, namely CULLIN-RING E3 ubiquitin ligase complex which controls many aspects of plant development (Hua and Vierstra, 2011). Observation of *CUL1* expression in rice using WISH-TC suggests concentration around lacuna edges (like *DW7*) which could lead to a functional interpretation via more confirmative work.

In this study WISH-TC has been shown to work in a reliable fashion but it is still not a universal method since it sometimes gives data which are uncertain and difficult to interpret, for example with the *THYLAKOID FORMATION FACTOR (THF1)* and *DELTA-14-STEROL REDUCTASE (FACKEL)* probes (Fig. 5.15 and 5.16). This suggests further optimization has to take place with certain probes, including probe hydrolysis (ensuring probe length <500bp to promote tissue penetration), the use of additional protein blockers such as non-fat dry milk powder, and possibly further tissue digestion to promote probe penetration using cellulase enzymes which can be particularly useful in complex tissue (Rozier *et al.*, 2014). Staining time and ambient temperature are also very important because, as mentioned earlier, the colour develops enzymatically. A constant ambient temperature would certainly be helpful in giving more power to be precise in stopping the reactions once sufficient signals have been detected for the antisense probes. For future development of WISH it is advisable to have an incubator so that temperature can be kept constant at all stages of the experiment, especially providing more reliability in the reaction time during the final staining step.

6.4 Concluding remarks and future work

Very early stages in rice leaf development (up to P3) have been identified as a very dynamic phase in which the leaf primordium is responsive to the systemic signals generated in the mature leaves which indicate the overall light regime of the plant. The transfer from HL to LL indicated that the rice leaf is more responsive in terms of physical and physiological acclimation for this transfer compared to transfer from LL to HL. Acclimatisation during the P3 stage is a co-ordinated processes involving stomatal differentiation and biochemical alteration to better prepare the leaf to the current light conditions. As pointed out by Van Campen *et al* (2016), stages prior to P4 can be manipulated since photosynthetic competence is being established during this early stage. Even though transfer at the late P5 stage is insufficient to confer significant stomatal changes, the time from P5 to maturity (about 5 days) is enough for the leaf to alter the physiological photosynthetic machinery, thus compensating for limited stomatal adaptation. It is interesting that the guard cells width (GCW)

parameter kept cropping up as the most plastic parameter during the transfer experiments, and in the paired experiments of stomatal structure and leaf physiology. It is the only stomatal parameter that had significant correlation with leaf water use efficiency.

The optimization of the WISH method for rice has shown reliability and superiority in terms of time and general workload compared to the traditional *in situ* hybridisation method. As has been pointed out earlier, the main eventual aim of this technique optimisation was to study the control of stomatal development in rice, but due to long time taken for optimization it could only be performed using the available control probes. This work certainly opens up the opportunity to try WISH using stomatal related genes such as *OsSPCH*, *OsMute* and *OsFama*. The level of mRNA for these genes might be low so further optimization on the WISH method might be needed. Future work might include the use of fluorimetric WISH instead of the regular colorimetric staining so that multiple probes labelled with different fluorescent signals could be introduced at the same time, yielding a more comprehensive picture regarding different gene expression and localization in the same tissue.

In conclusion, the work reported in this thesis provides an insight into the differentiation of stomata in rice, in particular how it responds to altered irradiance at particular stages of leaf development. Understanding the genetic mechanism by which this response occurs will provide a better understanding of how rice leaves adapt to the environment, which may help in the selection of plants for improved crop performance.

REFERENCES

- Aasamaa K, Sober A, Rahi M** (2001) Leaf anatomical characteristics associated with shoot hydraulic conductance, stomatal conductance and stomatal sensitivity to changes of leaf water status in temperate deciduous trees. *Funct Plant Biol* **28**: 765–774
- Adachi M, Hasegawa T, Fukayama H, Tokida T, Sakai H, Matsunami T, Nakamura H, Sameshima R, Okada M** (2014) Soil and water warming accelerates phenology and down-regulation of Leaf photosynthesis of rice plants grown under free-air CO₂ enrichment (FACE). *Plant Cell Physiol* **55**: 370–380
- Andersen SU, Buechel S, Zhao Z, Ljung K, Novák O, Busch W, Schuster C, Lohmann JU** (2008) Requirement of B2-type cyclin-dependent kinases for meristem integrity in *Arabidopsis thaliana*. *Plant Cell* **20**: 88–100
- Anderson JM, Chow WS, Park Y-II** (1995) The grand design of photosynthesis: Acclimation of the photosynthetic apparatus to environmental cues. *Photosynth Res* **46**: 129–139
- Antunes WC, Provart NJ, Williams TCR, Loureiro ME** (2012) Changes in stomatal function and water use efficiency in potato plants with altered sucrolytic activity. *Plant Cell Environ* **35**: 747–759
- Apel K, Hirt H** (2004) Reactive oxygen species: Metabolism, oxidative stress, and signal transduction. *Annu Rev Plant Biol* **55**: 373–399
- Askenasy E** (1880) Über eine neue methode, um die vertheilung der wachsthumsintensitat in wachsenden theilen zu bestimmen. *Naturhistorisch-Medizinischer Verein, Heidelb Verhandlungen, Neue Ser* **2**: 70–153
- Athanasiou K, Dyson BC, Webster RE, Johnson GN** (2010) Dynamic acclimation of photosynthesis increases plant fitness in changing environments. *Plant Physiol* **152**: 366–73
- Auer H, Newsom DL, Kornacker K** (2009) Expression profiling using Affymetrix GeneChip microarrays. *Methods Mol Biol* **509**: 35–46
- Azoulay-Shemer T, Bagheri A, Wang C, Palomares A, Stephan AB, Kunz H-H, Schroeder JI** (2016) Starch biosynthesis in guard cells but not in mesophyll cells is involved in CO₂-induced stomatal closing. *Plant Physiol* **171**: 788–98
- Bailey S, Walters RG, Jansson S, Horton P** (2001) Acclimation of *Arabidopsis thaliana* to the light environment: The existence of separate low light and high light responses. *Planta* **213**: 794–801
- Balsamo RA, Bauer AM, Davis SD, Rice BM** (2003) Leaf biomechanics, morphology, and anatomy of the deciduous mesophyte *Prunus serrulata* (*Rosaceae*) and the

evergreen sclerophyllous shrub *Heteromeles arbutifolia* (Rosaceae). *Am J Bot* **90**: 72–77

Bancroft JD, Gamble M (2008) Theory and practice of histological techniques, Sixth. Elsevier Health Sciences, Philadelphia

Bassham JA, Benson AA, Calvin M (1950) The path of carbon in photosynthesis. *J Biol Chem* **185**: 781–7

Bergmann DC (2004) Integrating signals in stomatal development. *Curr Opin Plant Bio* **7**: 26–32

Bernacchi CJ, Rosenthal DM, Pimentel C, Long SP, Farquhar GD (2009) Modeling the temperature dependence of C₃ photosynthesis. *In* A Laisk, L Nedbal, L Govindjee, eds, *Photosynth. silico Underst. Complex. from Mol. to Ecosyst.* Springer, Dordrecht, pp 231–246

Brewer PB, Heisler MG, Hejatko J, Friml J, Benková E (2006) In situ hybridization for mRNA detection in Arabidopsis tissue sections. *Nat Protoc* **1**: 1462–7

Burry RW (2009) Immunocytochemistry: A practical guide for biomedical research. Springer Science & Business Media, New York

Caemmerer S (2000) Biochemical models of leaf photosynthesis. CSIRO Publishing, Victoria

Chazdon RL, Pearcy RW (1991) The importance of sunflecks for forest understory plants. *Bioscience* **41**: 760–766

Cookson SJ, Van Lijsebettens M, Granier C (2005) Correlation between leaf growth variables suggest intrinsic and early controls of leaf size in *Arabidopsis thaliana*. *Plant, Cell Environ* **28**: 1355–1366

Cottrelle P, Cool M, Thuriaux P, Price VL, Thiele D, Buhler J-M, Fromageot P (1985) Either one of the two yeast EF-1 alpha genes is required for cell viability. *Curr Genet* **9**: 693–697

Coupe SA, Palmer BG, Lake JA, Overy SA, Oxborough K, Woodward FI, Gray JE, Quick WP (2006) Systemic signalling of environmental cues in Arabidopsis leaves. *J. Exp. Bot.* pp 329–341

Darnell DK, Stanislaw S, Kaur S, Antin PB (2010) Whole mount in situ hybridization detection of mRNAs using short LNA containing DNA oligonucleotide probes. *RNA* **16**: 632–7

Dow GJ, Bergmann DC, Berry JA (2014) An integrated model of stomatal development and leaf physiology. *New Phytol* **201**: 1218–1226

Eberwine JH, Valentino KL, Barchas JD (1994) In situ hybridization in neurobiology: Advances in methodology. Oxford University Press, New York

- Ehleringer J, Hall A, Farquhar G** (1993) Stable isotopes and plant carbon-water relations. Academic Press, San Diego, CA
- Elert E** (2014) Rice by the numbers: A good grain. *Nature* **514**: S50–S51
- Engler J de A, Montagu M Van, Engler G** (1998) Whole-mount in situ hybridization in plants. *In* JM Martinez-Zapater, J Salinas, eds, Arab. Protoc. Humana Press, New York City, pp 373–384
- Erickson RO, Michelini FJ** (1957) The plastochron index. *Am J Bot* **44**: 297
- Esau K** (1965) Plant Anatomy, 2nd ed. John Wiley, New York, New York, USA
- Ethier, G.J. and Livingston, N.J.** (2004). On the need to incorporate sensitivity to CO₂ transfer conductance into the Farquhar-von Caemmerer-Berry leaf photosynthesis model. *Plant, Cell Environ.* **27**: 137–153.
- Farquhar GD, Ehleringer JR, Hubick KT** (1989) Carbon isotope discrimination and photosynthesis. *Annu Rev Plant Physiol Plant Mol Biol* **40**: 503–537
- Farquhar GD, Caemmerer S** (1981) Some relationships between the biochemistry of photosynthesis and the gas exchange of leaves. *Planta* **153**: 376–387
- Farquhar GD, von Caemmerer S, Berry JA, Caemmerer S, Farquhar GD, Berry JA** (1980) A biochemical model of photosynthetic CO₂ assimilation in leaves of C₃ species. *Planta* **149**: 78–90
- Farquhar GD, Sharkey TD** (1982) Stomatal conductance and photosynthesis. *Annu Rev* **33**: 317–345
- Field CB, Behrenfeld MJ, Randerson JT, Falkowski P** (1998) Primary production of the biosphere: integrating terrestrial and oceanic components. *Science* (80-) **281**: 237–240
- Fleming AJ** (2005) The control of leaf development. *New Phytol* **166**: 9–20
- Fournier C, Durand JL, Ljutovac S, Schaufele R, Gastal F, Andrieu B** (2005) A functional-structural model of elongation of the grass leaf and its relationships with the phyllochron. *New Phytol* **166**: 881–894
- Franks PJ, Beerling DJ** (2009) Maximum leaf conductance driven by CO₂ effects on stomatal size and density over geologic time. *Proc Natl Acad Sci U S A* **106**: 10343–7
- Gonzalez N, Vanhaeren H, Inze D** (2012) Leaf size control: Complex coordination of cell division and expansion. *Trends Plant Sci* **17**: 332–340
- Granier C, Tardieu F** (1999) Water deficit and spatial pattern of leaf development. Variability in responses can be simulated using a simple model of leaf development. *Plant Physiol* **119**: 609–620

- Guo W, Li B, Zhang X, Wang R** (2007) Architectural plasticity and growth responses of *Hippophae rhamnoides* and *Caragana intermedia* seedlings to simulated water stress. *J Arid Environ* **69**: 385–399
- Haworth M, Killi D, Materassi A, Raschi A** (2015) Coordination of stomatal physiological behavior and morphology with carbon dioxide determines stomatal control. *Am J Bot* **102**: 677–688
- Haworth M, Killi D, Materassi A, Raschi A, Centritto M** (2016) Impaired stomatal control is associated with reduced photosynthetic physiology in crop species grown at elevated CO₂. *Front Plant Sci* **7**: 1568
- Hejátko J, Blilou I, Brewer PB, Friml J, Scheres B, Benková E** (2006) *In situ* hybridization technique for mRNA detection in whole mount Arabidopsis samples. *Nat Protoc* **1**: 1939–46
- Horton P, Ruban A** (2005) Molecular design of the photosystem II light-harvesting antenna: photosynthesis and. *J Exp Bot* **56**: 365–373
- Hou F, Jin L-Q, Zhang Z-S, Gao H-Y** (2015) Systemic signalling in photosynthetic induction of *Rumex* K-1 (*Rumex patientia* × *Rumex tianschaious*) leaves. *Plant Cell Environ* **38**: 685–692
- Hsiao TC, O'toole JC, Yambao EB, Turner NC** (1984) Influence of osmotic adjustment on leaf rolling and tissue death in rice (*Oryza sativa* L.). *Plant Physiol* **75**: 338–41
- Hsieh K, Huang AHC** (2007) Tapetosomes in *Brassica tapetum* accumulate endoplasmic reticulum-derived flavonoids and alkanes for delivery to the pollen surface. *Plant Cell* **19**: 582–96
- Hua Z, Vierstra RD** (2011) The cullin-RING ubiquitin-protein ligases. *Annu Rev Plant Biol* **62**: 299–334
- Hubbart S, Bird S, Lake J a, Murchie EH** (2013) Does growth under elevated CO₂ moderate photoacclimation in rice? *Physiol Plant* **148**: 297–306
- Humbeck K, Krupinska K** (2003) The abundance of minor chlorophyll a/b-binding proteins CP29 and LHCl of barley (*Hordeum vulgare* L.) during leaf senescence is controlled by light. *J Exp Bot* **54**: 375–383
- Itoh J-I, Nonomura K-I, Ikeda K, Yamaki S, Inukai Y, Yamagishi H, Kitano H, Nagato Y** (2005) Rice plant development: From zygote to spikelet. *Plant Cell Physiol* **46**: 23–47
- James SA, Bell DT** (2000) Influence of light availability on leaf structure and growth of two *Eucalyptus globulus* ssp. *globulus* provenances. *Tree Physiol* **20**: 1007–1018

- Jane W-N, Chiang S-HT** (1991) Morphology and development of bulliform cells in *Arundo formosana* Hack. *Taiwania* **36**: 85–97
- Janker-Obermeier I, Sieber V, Faulstich M, Schieder D** (2012) Solubilization of hemicellulose and lignin from wheat straw through microwave-assisted alkali treatment. *Ind Crops Prod* **39**: 198–203
- Javelle M, Marco CF, Timmermans M** (2011) *In situ* hybridization for the precise localization of transcripts in plants. *J Vis Exp* e3328
- Jefferson RA, Kavanagh TA, Bevan MW** (1987) GUS fusions: beta-glucuronidase as a sensitive and versatile gene fusion marker in higher plants. *EMBO J* **6**: 3901–7
- Kalt-Torres W, Kerr PS, Usuda H, Huber SC** (1987) Diurnal changes in maize leaf photosynthesis I. Carbon exchange rate, assimilate export rate, and enzyme activities. *Plant Physiol* **83**: 283–288
- Kamiya N, Itoh J-I, Morikami A, Nagato Y, Matsuoka M** (2003) The SCARECROW gene's role in asymmetric cell divisions in rice plants. *Plant J* **36**: 45–54
- Karp G** (2010) Photosynthesis and the chloroplast. *Cell Mol. Biol. Concepts Exp.*
- Karpinski S** (1999) Systemic signalling and acclimation in response to excess excitation energy in *Arabidopsis*. *Science* (80-) **284**: 654–657
- Killi D, Bussotti F, Raschi A, Haworth M** (2017) Adaptation to high temperature mitigates the impact of water deficit during combined heat and drought stress in C₃ sunflower and C₄ maize varieties with contrasting drought tolerance. *Physiol Plant* **159**: 130–147
- Kitajima K, Hogan KP** (2003) Increases of chlorophyll a/b ratios during acclimation of tropical woody seedlings to nitrogen limitation and high light. *Plant Cell Environ* **26**: 857–865
- Koch K** (2004) Sucrose metabolism: regulatory mechanisms and pivotal roles in sugar sensing and plant development. *Curr Opin Plant Biol* **7**: 235–46
- Komar CM, Long MJ** (2013) Immunohistochemical techniques to identify and localize proteins of interest in paraffin embedded tissue sections. *Methods Mol Biol* **952**: 197–206
- Kouřil R, Wientjes E, Bultema JB, Croce R, Boekema EJ** (2013) High-light vs. low-light: effect of light acclimation on photosystem II composition and organization in *Arabidopsis thaliana*. *Biochim Biophys Acta* **1827**: 411–9
- Kubínová L** (1991) Stomata and mesophyll characteristics of barley leaf as affected by light: Stereological analysis. *J Exp Bot* **42**: 995–1001

- Lake JA, Woodward FI, Quick WP** (2002) Long-distance CO₂ signalling in plants. *J Exp Bot* **53**: 183–193
- Lalonde S, Tegeder M, Throne-Holst M, Frommer WB, Patrick JW** (2003) Phloem loading and unloading of sugars and amino acids. *Plant Cell Environ* **26**: 37–56
- Lawson T, Oxborough K, Morison JIL, Baker NR** (2003) The responses of guard and mesophyll cell photosynthesis to CO₂, O₂, light, and water stress in a range of species are similar. *J Exp Bot* **54**: 1743–1752
- Lawson T** (2009) Guard cell photosynthesis and stomatal function. *New Phytol* **181**: 13–34
- Lawson T, Blatt MR** (2014) Stomatal size, speed, and responsiveness impact on photosynthesis and water use efficiency. *Plant Physiol* **164**: 1556–1570
- Lawson T, Simkin AJ, Kelly G, Granot D** (2014) Mesophyll photosynthesis and guard cell metabolism impacts on stomatal behaviour. *New Phytol* **203**: 1064–1081
- Leegood RC** (1996) Primary photosynthate production: Physiology and metabolism. *In* AAS E. Zamski, ed, *Photoassimilate Distrib. Plants Crop. SourceSink Relationships*. Dekker Inc., New York, pp 21–41
- Leegood RC, Furbank RT** (1986) Stimulation of photosynthesis by 2% oxygen at low temperatures is restored by phosphate. *Planta* **168**: 84–93
- Leong T-Y, Anderson JM** (1984) Adaptation of the thylakoid membranes of pea chloroplasts to light intensities. I. Study on the distribution of chlorophyll-protein complexes. *Photosynth Res* **5**: 105–115
- Lichtenthaler HK, Buschmann C, Döll M, Fietz HJ, Bach T, Kozel U, Meier D, Rahmsdorf U** (1981) Photosynthetic activity, chloroplast ultrastructure, and leaf characteristics of high-light and low-light plants and of sun and shade leaves. *Photosynth Res* **2**: 115–141
- Lichtenthaler HK, Kubn G, Prenzel UU, Meier D, Kuhn G, Prenzel UU, Meier D** (1982) Chlorophyll-protein levels and degree of thylakoid stacking in radish chloroplasts from high-light, low-light and bentazon-treated plants. *Physiol Plant* **56**: 183–188
- Long SP, Bernacchi CJ** (2003) Gas exchange measurements, what can they tell us about the underlying limitations to photosynthesis? Procedures and sources of error. *J Exp Bot* **54**: 2393–401
- Ludevid D, Hofte H, Himmelblau E, Chrispeels MJ** (1992) The expression pattern of the tonoplast intrinsic protein -TIP in *Arabidopsis thaliana* is correlated with cell enlargement. *Plant Physiol* **100**: 1633–1639

- Mahan JR, Upchurch DR** (1988) Maintenance of constant leaf temperature by plants—I. Hypothesis-limited homeothermy. *Environ Exp Bot* **28**: 351–357
- Makino A** (2011) Photosynthesis, grain yield, and nitrogen utilization in rice and wheat. *Plant Physiol* **155**: 125–9
- Makino A** (2003) Rubisco and nitrogen relationships in rice: Leaf photosynthesis and plant growth. *Soil Sci Plant Nutr* **49**: 319–327
- Makino A, Mae T, Ohira K** (1988) Differences between wheat and rice in the enzymic properties of ribulose-1,5-bisphosphate carboxylase/oxygenase and the relationship to photosynthetic gas exchange. *Planta* **174**: 30–38
- Makino A, Mae T, Ohira K** (1987) Variations in the contents and kinetic properties of ribulose-1,5-bisphosphate carboxylases among rice species. *Plant Cell Physiol* **28**: 799–804
- Marshall, B. and Biscoe, P. V.** (1980). A model for C₃ leaves describing the dependence of net photosynthesis on irradiance. *J. Exp. Bot.* **31**: 29–39.
- Masle J, Gilmore SR, Farquhar GD** (2005) The ERECTA gene regulates plant transpiration efficiency in Arabidopsis. *Nature* **436**: 866–870
- Mattsson J, Ckurshumova W, Berleth T** (2003) Auxin signalling in Arabidopsis leaf vascular development. *Plant Physiol* **131**: 1327–39
- McConaughy BL, Laird CD, McCarthy BJ** (1969) Nucleic acid reassociation in formamide. *Biochemistry* **8**: 3289–3295
- McDonald MS** (2003) Photobiology of higher plants. John Wiley & Sons, West Sussex
- Melis A** (1999) Photosystem-II damage and repair cycle in chloroplasts: What modulates the rate of photodamage in vivo? *Trends Plant Sci* **4**: 130–135
- Meshi T, Taoka KI, Iwabuchi M** (2000) Regulation of histone gene expression during the cell cycle. *Plant Mol Biol* **43**: 643–57
- Mohammady, Shahram Khazaei H, Reisi F** (2006) The study of stomatal characteristics in Iranian wheat wild accessions and land races. *Wheat Inf Serv* **103**: 5–12
- Morais RR de, Gonçalves JF de C, Santos Júnior UM dos, Dünisch O, Santos ALW dos** (2007) Chloroplastid pigment contents and chlorophyll a fluorescence in Amazonian tropical three species. *Rev Árvore* **31**: 959–966
- Mott KA, Berg DG, Hunt SM, Peak D** (2014) Is the signal from the mesophyll to the guard cells a vapour-phase ion? *Plant Cell Environ* **37**: 1184–1191

- Murchie EH, Hubbart S, Peng S, Horton P** (2005) Acclimation of photosynthesis to high irradiance in rice: gene expression and interactions with leaf development. *J Exp Bot* **56**: 449–60
- Murchie EH, Horton P** (1997) Acclimation of photosynthesis to irradiance and spectral quality in British plant species: chlorophyll content, photosynthetic capacity and habitat preference. *Plant Cell Environ* **20**: 438–448
- Murchie EH, Lawson T** (2013) Chlorophyll fluorescence analysis: A guide to good practice and understanding some new applications. *J Exp Bot* **64**: 3983–3998
- Murchie EH, Hubbart S, Chen Y, Peng S, Horton P** (2002) Acclimation of rice photosynthesis to irradiance under field conditions. *Plant Physiol* **130**: 1999–2010
- Nelson DM, Ye X, Hall C, Santos H, Ma T, Kao GD, Yen TJ, Harper JW, Adams PD** (2002) Coupling of DNA synthesis and histone synthesis in S phase independent of cyclin/cdk2 activity. *Mol Cell Biol* **22**: 7459–72
- Northrop RB, Connor AN** (2008) Introduction to molecular biology, genomics and proteomics for biomedical engineers. CRC Press, Boca Raton
- Ogren E, Evans JR** (1993) Photosynthetic light-response curves. *Planta* **189**: 182–190
- Oguchi R, Hikosaka K, Hirose T** (2005) Leaf anatomy as a constraint for photosynthetic acclimation: Differential responses in leaf anatomy to increasing growth irradiance among three deciduous trees. *Plant, Cell Environ* **28**: 916–927
- Oguchi R, Hikosaka K, Hirose T** (2003) Does the photosynthetic light-acclimation need change in leaf anatomy? *Plant, Cell Environ* **26**: 505–512
- Ohmori Y, Toriba T, Nakamura H, Ichikawa H, Hirano H-Y** (2011) Temporal and spatial regulation of DROOPING LEAF gene expression that promotes midrib formation in rice. *Plant J* **65**: 77–86
- Oka HI** (1958) Intervarietal variation and classification of cultivated rice. *Indian J Genet Plant Breed* **18**: 79–89
- Otto JJ** (1993) Immunoblotting. *Antibodies Cell Biol*. Academic Press, p 452
- Palevitz BA** (1981) The structure and development of stomatal cells. *In* PG Jarvis, TA Mansfield, eds, *Stomatal Physiol*. Cambridge University Press, Cambridge, pp 1–23
- Parker G** (2003) Isolation of COV1, a gene involved in the regulation of vascular patterning in the stem of Arabidopsis. *Development* **130**: 2139–2148
- Paul M** (2007) Trehalose 6-phosphate. *Curr Opin Plant Biol* **10**: 303–9

- Pokalsky AR, Hiatt WR, Ridge N, Rasmussen R, Houck CM, Shewmaker CK** (1989) Structure and expression of elongation factor 1 alpha in tomato. *Nucleic Acids Res* **17**: 4661–73
- Raschke K** (1975) Stomatal Action. *Annu Rev Plant Physiol* **26**: 309–340
- Ren M, Venglat P, Qiu S, Feng L, Cao Y, Wang E, Xiang D, Wang J, Alexander D, Chalivendra S, et al** (2013) Target of rapamycin signalling regulates metabolism, growth, and life span in arabidopsis. *Plant Cell Online* **24**:
- Roche D** (2015) Stomatal conductance is essential for higher yield potential of C3 crops. *CRC Crit Rev Plant Sci* **34**: 429–453
- Rolland F, Baena-Gonzalez E, Sheen J** (2006) Sugar sensing and signalling in plants: Conserved and novel mechanisms. *Annu Rev Plant Biol* **57**: 675–709
- Rozier F, Mirabet V, Vernoux T, Das P** (2014) Analysis of 3D gene expression patterns in plants using whole-mount RNA *in situ* hybridization. *Nat Protoc* **9**: 2464–75
- Rybak-Wolf A, Solana J** (2014) Whole-mount *in situ* hybridization using DIG-labeled probes in planarian. *Methods Mol Biol* **1211**: 41–51
- Sablowski R, Carnier Dornelas M** (2014) Interplay between cell growth and cell cycle in plants. *J Exp Bot* **65**: 2703–2714
- Sachs T** (1981) Advances in botanical research. *Adv Bot Res*. doi: 10.1016/S0065-2296(08)60351-1
- Sakamoto T, Morinaka Y, Ohnishi T, Sunohara H, Fujioka S, Ueguchi-Tanaka M, Mizutani M, Sakata K, Takatsuto S, Yoshida S, et al** (2006) Erect leaves caused by brassinosteroid deficiency increase biomass production and grain yield in rice. *Nat Biotechnol* **24**: 105–9
- Sasikumar AN, Perez WB, Kinzy TG** (2012) The many roles of the eukaryotic elongation factor 1 complex. *Wiley Interdiscip Rev RNA* **3**: 543–55
- Scarpella E, Rueb S, Meijer AH** (2003) The RADICLELESS1 gene is required for vascular pattern formation in rice. *Development* **130**:
- Schildkraut C** (1965) Dependence of the melting temperature of DNA on salt concentration. *Biopolymers* **3**: 195–208
- Schmidt A** (1924) Histologische studien an phanerogamen vegetationspunkte. *Bot Arch* **8**: 345–404
- Schultz HR, Matthews MA** (1993) Xylem development and hydraulic conductance in sun and shade shoots of grapevine (*Vitis vinifera* L.): Evidence that low light uncouples water transport capacity from leaf area. *Planta* **190**: 393–406

- Schymanski SJ, Or D, Zwieniecki M** (2013) Stomatal control and leaf thermal and hydraulic capacitances under rapid environmental fluctuations. *PLoS One* **8**: e54231
- Segers G, Gadisseur I, Bergounioux C, Engler J, Jacquard A, Montagu M, Inze D** (1996) The *Arabidopsis* cyclin-dependent kinase gene *cdc2bAt* is preferentially expressed during S and G2 phases of the cell cycle. *Plant J* **10**: 601–612
- Sharkey TD** (1985) Photosynthesis in intact leaves of C³ plants: Physics, physiology and rate limitations. *Bot Rev* **51**: 53–105
- Shimomura O, Johnson FH, Saiga Y** (1962) Extraction, purification and properties of aequorin, a bioluminescent protein from the luminous hydromedusan, *Aequorea*. *J Cell Comp Physiol* **59**: 223–239
- Shimshi D, Ephrat J** (1975) Stomatal behaviour of wheat cultivars in relation to their transpiration, photosynthesis, and yield. *Agron J* **67**: 326
- Silvestro D, Andersen TG, Schaller H, Jensen PE** (2013) Plant sterol metabolism. $\Delta(7)$ -Sterol-C5-desaturase (STE1/DWARF7), $\Delta(5,7)$ -sterol- $\Delta(7)$ -reductase (DWARF5) and $\Delta(24)$ -sterol- $\Delta(24)$ -reductase (DIMINUTO/DWARF1) show multiple subcellular localizations in *Arabidopsis thaliana* (Heynh) L. *PLoS One* **8**: e56429
- Sims DA, Pearcy RW** (1991) Photosynthesis and respiration in *Alocasia macrorrhiza* following transfers to high and low light. *Oecologia* **86**: 447–453
- Singh J, Pandey P, James D, Chandrasekhar K, Achary VMM, Kaul T, Tripathy BC, Reddy MK** (2014) Enhancing C₃ photosynthesis: an outlook on feasible interventions for crop improvement. *Plant Biotechnol J* **12**: 1217–1230
- Smillie IRA, Pyke KA, Murchie EH** (2012) Variation in vein density and mesophyll cell architecture in a rice deletion mutant population. *J Exp Bot* **63**: 4563–4570
- Spínola MC, Pérez-Ruiz JM, Pulido P, Kirchsteiger K, Guinea M, González M, Cejudo FJ** (2008) NTRC new ways of using NADPH in the chloroplast. *Physiol Plant* **133**: 516–524
- Stadler R, Wright KM, Lauterbach C, Amon G, Gahrtz M, Feuerstein A, Oparka KJ, Sauer N** (2005) Expression of GFP-fusions in *Arabidopsis* companion cells reveals non-specific protein trafficking into sieve elements and identifies a novel post-phloem domain in roots. *Plant J* **41**: 319–331
- Strassberger Z, Prinsen P, Klis F van der, Es DS van, Tanase S, Rothenberg G** (2015) Lignin solubilisation and gentle fractionation in liquid ammonia. *Green Chem* **17**: 325–334
- Strauss-DeBenedetti S, Berlyn GP** (1994) Leaf anatomical responses to light in 5 tropical *Moraceae* of different successional status. *Am J Bot* **81**: 1582–1591

- Strehler BL, McElroy WD** (1949) Purification of firefly luciferin. *J Cell Comp Physiol* **34**: 457–466
- Sugiyama SI, Gotoh M** (2010) How meristem plasticity in response to soil nutrients and light affects plant growth in four *Festuca* grass species. *New Phytol* **185**: 747–758
- Sugiyama S, Gotoh M** (2010) How meristem plasticity in response to soil nutrients and light affects plant growth in four *Festuca* grass species. *New Phytol* **185**: 747–758
- Sultan SE** (1995) Phenotypic plasticity and plant adaptation. *Acta Bot Neerl* **44**: 363–383
- Sun D, Liddle MJ** (1991) Field occurrence, recovery, and simulated trampling resistance and recovery of two grasses. *Biol Conserv* **57**: 187–203
- Taiz L, Zeiger E** (2010) *Plant physiology*, Fifth. Sinauer Associates Inc., Massachusetts, USA
- Taiz L, Zeiger E** (2010) Photosynthesis: Physiological and ecological considerations. *Plant Physiol*. Fifth Ed., 5th ed. Sinauer Associates Inc., Massachusetts, USA, pp 243–270
- Takahashi S, Badger MR** (2011) Photoprotection in plants: a new light on photosystem II damage. *Trends Plant Sci* **16**: 53–60
- Tanaka Y, Kumagai E, Tazoe Y, Adachi S, Homma K, Homma K** (2014) Leaf photosynthesis and its genetic improvement from the perspective of energy flow and CO₂ diffusion. *Plant Prod Sci* **17**: 111–123
- Tautz D, Pfeifle C** (1989) A non-radioactive *in situ* hybridization method for the localization of specific RNAs in *Drosophila* embryos reveals translational control of the segmentation gene hunchback. *Chromosoma* **98**: 81–5
- Taylor SH, Franks PJ, Hulme SP, Spriggs E, Christin P a, Edwards EJ, Woodward FI, Osborne CP** (2012) Photosynthetic pathway and ecological adaptation explain stomatal trait diversity among grasses. *New Phytol* **193**: 387–96
- Terashima I, Araya T, Miyazawa S-I, Sone K, Yano S** (2005) Construction and maintenance of the optimal photosynthetic systems of the leaf, herbaceous plant and tree: An eco-developmental treatise. *Ann Bot* **95**: 507–519
- Terashima I, Miyazawa S-I, Hanba YT** (2001) Why are sun leaves thicker than shade leaves? — Consideration based on analyses of CO₂ diffusion in the leaf. *J Plant Res* **114**: 93–105
- Thisse C, Thisse B** (2008) High-resolution *in situ* hybridization to whole-mount zebrafish embryos. *Nat Protoc* **3**: 59–69

- Thompson G, Schulz A** (1999) Macromolecular trafficking in the phloem. *Trends Plant Sci* **4**: 354–360
- Thornley, J. and Johnson, I.** (1990). *Plant and crop modelling* (Oxford University Press).
- Timm S, Florian A, Arrivault S, Stitt M, Fernie AR, Bauwe H** (2012) Glycine decarboxylase controls photosynthesis and plant growth. *FEBS Lett* **586**: 3692–3697
- Traas J** (2008) Whole-mount *in situ* hybridization of RNA probes to plant tissues. *CSH Protoc* **2008**: pdb.prot4944
- Turgeon R** (2006) Phloem loading: How leaves gain their independence. *Bioscience* **56**:
- Turgeon R, Wolf S** (2009) Phloem transport: cellular pathways and molecular trafficking. *Annu Rev Plant Biol* **60**: 207–221
- Turner JS, Brittain EG** (1962) Oxygen as a factor in photosynthesis. *Biol Rev* **37**: 130–170
- Vainstein A, Ferreira P, Peterson CC, Verbeke JA, Thornber JP** (1989) Expression of the major light-harvesting chlorophyll a/b-protein and its import into thylakoids of mesophyll and bundle sheath chloroplasts of maize. *Plant Physiol* **89**: 602–9
- Valladares F, Martinez-Ferri E, Balaguer L, Perez-Corona E, Manrique E** (2000) Low leaf-level response to light and nutrients in Mediterranean evergreen oaks: A conservative resource-use strategy? *New Phytol* **148**: 79–91
- van Campen J, Yaapar MN, Narawatthana S, Lehmeier C, Wanchana S, Thakur V, Chater C, Kelly S, Rolfe SA, Quick WP, et al** (2016) Combined chlorophyll fluorescence and transcriptomic analysis identifies the P3/P4 transition as a key stage in rice leaf photosynthetic development. *Plant Physiol* **170**: 1655–74
- Venora G, Calcagno F** (1991) Study of stomatal parameters for selection of drought resistant varieties in *Triticum durum* DESF. *Euphytica* **57**: 275–283
- Vilaine F, Palauqui J-C, Amselem J, Kusiak C, Lemoine R, Dinant S** (2003) Towards deciphering phloem: a transcriptome analysis of the phloem of *Apium graveolens*. *Plant J* **36**: 67–81
- Vincent JF V** (1982) The mechanical design of grass. *J Mater Sci* **17**: 856–860
- Vogelmann TC, Martin G** (1993) The functional significance of palisade tissue: penetration of directional versus diffuse light. *Plant Cell Environ* **16**: 65–72
- von Caemmerer S, Evans JR** (2010) Enhancing C₃ Photosynthesis. *Plant Physiol* **154**: 589–592

- Wang L, Ruan Y-L** (2013) Regulation of cell division and expansion by sugar and auxin signalling. *Front Plant Sci* **4**: 163
- Wentworth M, Murchie EH, Gray JE, Villegas D, Pastenes C, Pinto M, Horton P** (2006) Differential adaptation of two varieties of common bean to abiotic stress: II. Acclimation of photosynthesis. *J Exp Bot* **57**: 699–709
- Wenzel CL, Schuetz M, Yu Q, Mattsson J** (2007) Dynamics of MONOPTEROS and PIN-FORMED1 expression during leaf vein pattern formation in *Arabidopsis thaliana*. *Plant J* **49**: 387–98
- Wherley BG, Gardner DS, Metzger JD** (2005) Tall Fescue photomorphogenesis as influenced by changes in the spectral composition and light intensity. *Crop Sci* **45**: 562
- Whitney SM, Kane HJ, Houtz RL, Sharwood RE** (2009) Rubisco oligomers composed of linked small and large subunits assemble in tobacco plastids and have higher affinities for CO₂ and O₂. *Plant Physiol* **149**: 1887–1895
- Wobus U, Weber H** (1999) Sugars as signal molecules in plant seed development. *Biol Chem* **380**: 937–944
- Wuyts N, Massonnet C, Dautat M, Granier C** (2012) Structural assessment of the impact of environmental constraints on *Arabidopsis thaliana* leaf growth: a 3D approach. *Plant Cell Environ* **35**: 1631–1646
- Xiong Y, McCormack M, Li L, Hall Q, Xiang C, Sheen J** (2013) Glucose-TOR signalling reprograms the transcriptome and activates meristems. *Nature* **496**: 181–186
- Xiong Y, Sheen J** (2015) Novel links in the plant TOR kinase signalling network. *Curr Opin Plant Biol* **28**: 83–91
- Xu Z, Zhou G** (2008) Responses of leaf stomatal density to water status and its relationship with photosynthesis in a grass. *J Exp Bot* **59**: 3317–3325
- Yamaguchi T, Nagasawa N, Kawasaki S, Matsuoka M, Nagato Y, Hirano H-Y** (2004) The YABBY gene DROOPING LEAF regulates carpel specification and midrib development in *Oryza sativa*. *Plant Cell* **16**: 500–9
- Yamamoto Y, Negi J, Wang C, Isogai Y, Schroeder JI, Iba K** (2016) The transmembrane region of guard cell SLAC1 channels perceives CO₂ signals via an ABA-independent pathway in *Arabidopsis*. *Plant Cell Online* **28**: 557–567
- Yamori W, Evans JR, Von Caemmerer S** (2010) Effects of growth and measurement light intensities on temperature dependence of CO₂ assimilation rate in tobacco leaves. *Plant Cell Environ* **33**: 332–343

- Zachgo S, Perbal M-C, Saedler H, Schwarz-Sommer Z** (2000) *In situ* analysis of RNA and protein expression in whole mounts facilitates detection of floral gene expression dynamics. *Plant J* **23**: 697–702
- Zhang G-H, Xu Q, Zhu X-D, Qian Q, Xue H-W** (2009) SHALLOT-LIKE1 Is a KANADI transcription factor that modulates rice leaf rolling by regulating leaf abaxial cell development. *Plant Cell* **21**: 719–735
- Zhang Y, Persson S, Giavalisco P** (2013) Differential regulation of carbon partitioning by the central growth regulator target of rapamycin (TOR). *Mol Plant* **6**: 1731–3
- Zunzunegui M, Ain-Lhout F, Barradas MCD, Álvarez-Cansino L, Esquivias MP, García Novo F** (2009) Physiological, morphological and allocation plasticity of a semi-deciduous shrub. *Acta Oecologica* **35**: 370–379

Combined Chlorophyll Fluorescence and Transcriptomic Analysis Identifies the P3/P4 Transition as a Key Stage in Rice Leaf Photosynthetic Development^{1[OPEN]}

Julia C. van Campen, Muhammad N. Yaapar, Supathtra Narawatthana², Christoph Lehmeier³, Samart Wanchana, Vivek Thakur, Caspar Chater, Steve Kelly, Stephen A. Rolfe, W. Paul Quick, and Andrew J. Fleming*

Department of Animal and Plant Sciences, University of Sheffield, Sheffield S10 2TN, United Kingdom (J.C.v.C., M.N.Y., S.N., C.L., C.C., S.A.R., A.J.F.); International Rice Research Institute, DAPO Box 7777, Metro Manila, The Philippines (S.W., V.T., W.P.Q.); National Center for Genetic Engineering and Biotechnology, Khlong Luang, Pathum Thani 12120, Thailand (S.W.); Departamento de Biología Molecular de Plantas, Instituto de Biotecnología, Universidad Nacional Autónoma de México, Mexico (C.C.); and Department of Plant Sciences, University of Oxford, Oxford OX1 3RB, United Kingdom (S.K.)

ORCID IDs: 0000-0002-7016-1366 (J.C.v.C.); 0000-0003-4551-0920 (S.N.); 0000-0002-8567-5802 (C.L.); 0000-0003-2058-2020 (C.C.); 0000-0001-8583-5362 (S.K.); 0000-0003-2141-4707 (S.A.R.); 0000-0002-9703-0745 (A.J.F.).

Leaves are derived from heterotrophic meristem tissue that, at some point, must make the transition to autotrophy via the initiation of photosynthesis. However, the timing and spatial coordination of the molecular and cellular processes underpinning this switch are poorly characterized. Here, we report on the identification of a specific stage in rice (*Oryza sativa*) leaf development (P3/P4 transition) when photosynthetic competence is first established. Using a combined physiological and molecular approach, we show that elements of stomatal and vascular differentiation are coordinated with the onset of measurable light absorption for photosynthesis. Moreover, by exploring the response of the system to environmental perturbation, we show that the earliest stages of rice leaf development have significant plasticity with respect to elements of cellular differentiation of relevance for mature leaf photosynthetic performance. Finally, by performing an RNA sequencing analysis targeted at the early stages of rice leaf development, we uncover a palette of genes whose expression likely underpins the acquisition of photosynthetic capability. Our results identify the P3/P4 transition as a highly dynamic stage in rice leaf development when several processes for the initiation of photosynthetic competence are coordinated. As well as identifying gene targets for future manipulation of rice leaf structure/function, our data highlight a developmental window during which such manipulations are likely to be most effective.

Rice (*Oryza sativa*) is a C₃ grass whose seeds are the single most important staple food, providing one-fifth of the world's dietary energy supply (Elert, 2014).

The source of all carbon in these seeds is photosynthesis, and there is significant interest in improving this fundamental process through the alteration of several morphological, biochemical, and physiological traits in leaves (Long et al., 2006; Hibberd et al., 2008). However there are still large gaps in our knowledge of leaf development and the ontogeny of photosynthesis, in both rice and other species. For example, although we have a deep and detailed understanding of the mechanism of photosynthesis, it is still unclear at exactly which stage in development a rice leaf first gains the capacity to capture light energy for carbon fixation. Linked to this, although it is well established that leaves in many species (including rice) can undergo morphological and photosynthetic acclimation to the environment (Hikosaka and Terashima, 1995; Murchie and Horton, 1997; Oguchi et al., 2003) and it is known that the cellular processes underpinning this acclimation occur during relatively early stages of leaf development (Jurik et al., 1979; Sims and Pearcy, 1992; Murchie et al., 2005), the point when developmental plasticity is lost has not been defined precisely.

¹ This work was supported by the Biotechnology and Biological Sciences Research Council (grant no. BB/J004065 to C.L., S.A.R., and A.J.F. as well as CASE studentship no. BB/J012610/1 to J.C.v.C. in collaboration with the International Rice Research Institute), by a Malay Government studentship to M.N.Y., and by a Thai Government studentship to S.N.

² Present address: Rice Department, Ministry of Agriculture and Cooperatives, Bangkok 10900, Thailand.

³ Present address: Kansas Biological Survey, University of Kansas, Lawrence, KS 66047.

* Address correspondence to a.fleming@sheffield.ac.uk.

The author responsible for distribution of materials integral to the findings presented in this article in accordance with the policy described in the Instructions for Authors (www.plantphysiol.org) is: Andrew J. Fleming (a.fleming@sheffield.ac.uk).

A.J.F. and W.P.Q. designed the research; J.C.v.C., M.N.Y., and S.N. performed research; S.A.R. contributed new analytic tools; S.K. contributed new computational tools; S.K., V.T., S.W., J.C.v.C., C.C., and M.N.Y. analyzed data; A.J.F. and J.C.v.C. wrote the article, with all authors contributing to the final version.

^[OPEN] Articles can be viewed without a subscription.

www.plantphysiol.org/cgi/doi/10.1104/pp.15.01624

Rice leaves are initiated by a coordinated process of cell growth and division that leads to the formation of a protrusion on the shoot apical meristem (Itoh et al., 2005). The primordium (enclosed within the encircling sheaths of older leaves) then undergoes further development to form a mature leaf that consists of a flattened blade and a sheath encompassing the younger leaves, which develop sequentially from the shoot apical meristem. The young plant thus consists of a series of concentric leaves all of which originate from the meristem and are produced in a series separated by a time period, termed the plastochron (P). The definition of leaves by their sequential order of formation (L1, L2, L3...) and plastochron age (P1, P2, P3...) allows the comparison of leaves from different plants at equivalent developmental stages. P1 stage is characterized by a small protrusion forming on the flank of the shoot apical meristem. This protrusion then forms a hood-shaped structure around the shoot apical meristem (P2 stage) before completely enclosing the shoot apical meristem and taking on an elongated conical shape (P3 stage; Itoh et al., 2005). The subsequent P4 stage is characterized by a phase of rapid elongation of the leaf blade and visible greening of the tissue. Due to the degree of elongation that occurs during P4, the stage can be subdivided into stages (1–12) defined by particular blade lengths (Kusumi et al., 2010). At P5 stage, the distal tip of the leaf starts to protrude from the sheaths of older leaves, being pushed up by rapid elongation of the more proximal sheath, before growth stops as the leaf reaches maturity (P6 stage).

In addition to distinct developmental stages over time, individual grass leaves (such as rice) show a clear gradient of development along the longitudinal axis (Li et al., 2010). This has been successfully exploited in a number of investigations to allow comparisons of transcriptomes, proteomes, and metabolomes in cells undergoing different stages of differentiation. These analyses have revealed key pathways and fundamental regulators of photosynthesis in rice and also in maize (*Zea mays*; Li et al., 2010; Majeran et al., 2010; Pick et al., 2011; Wang et al., 2014). These patterning events at the base of mature leaves reflect a template set by the more mature differentiated tissue, distinct from the processes that must occur within a new leaf primordium, where the pattern arises *de novo*. Thus, studying the morphology, physiology, and gene expression dynamics of rice leaf primordia has the potential to provide novel insights that may not be evident in studies of mature leaf gradients.

With respect to the analysis of the very earliest stages of grass leaf development, previous work has successfully used laser microdissected portions of maize shoot apical meristem domains to identify transcripts associated with leaf initiation (Ohtsu et al., 2007). This work was restricted to the extremely early processes of leaf determination and initiation (up to P1) and did not encompass subsequent stages of leaf development. This was achieved by Wang et al. (2013b), who recently provided a detailed transcriptomic analysis of early leaf development in maize using dissected primordia.

These data provided the first analysis of a monocot leaf at this developmental resolution. To date, a similar analysis has not been reported for rice.

Most of the work on early leaf development (in both monocots and dicots) has focused on changes in the transcriptome, yet relating these data to the physiological function of the leaf is often problematic. Gene expression at the transcript level does not necessarily imply biochemical or physiological function (Amiour et al., 2012; Fernie and Stitt, 2012; Lan et al., 2012). In the case of photosynthesis, chlorophyll fluorescence has developed as a routine technique for the measurement of photosynthetic function (Krause and Weis, 1991; Maxwell and Johnson, 2000; Meng et al., 2001; Baker, 2008); however, most equipment is designed for measurements in leaves that can be clamped within a chamber, greatly restricting the minimum size of the material that can be analyzed. Microfluorescence techniques have been developed that provide the appropriate resolution for the analysis of small leaf primordia; however, these have generally been applied to the analysis of plant-microbe interactions (for review, see Berger et al., 2007) and plant stress response (for review, see Baker and Rosenqvist, 2004) rather than used in the context of leaf development.

A significant body of work has shown that many plants have the ability to acclimate their leaves to the light environment, leading to the formation of sun or shade leaves (Kubinova, 1991; Murchie and Horton, 1997; Oguchi et al., 2003; Kim et al., 2005; Terashima et al., 2006). The ambient environment is sensed by mature leaves, leading to the formation of an as yet uncharacterized signal that influences the morphogenesis of developing leaves at a distance from the mature leaves. It is clear that this systemic signaling system exists in rice and that responding leaves are young (Murchie et al., 2005), but the precise developmental stage during which this developmental plasticity exists is not known, nor is whether this developmental window of sensitivity to acclimation correlates with the expression of particular sets of genes associated with specific elements of leaf differentiation.

Here, we report on a combined physiological and transcriptomic analysis of the early stages of rice leaf development. These data provide a description of the gene expression changes occurring during the earliest phase of acquisition of photosynthetic competence. In addition, by exploiting a series of transfer experiments between high- and low-irradiance regimes at distinct leaf stages, we identify the P3/P4 transition as a key stage in rice leaf development where a coordinated differentiation of photosynthetic tissue, vasculature, and stomata occurs.

RESULTS

Photosynthetic Function in Rice Leaves Is Established at the P3/P4 Transition

The first three leaves of a rice plant (P1–P3) are already initiated in the embryo prior to germination. Following germination, additional leaves are produced

at regular intervals by the shoot apical meristem (Itoh et al., 2005). Leaf 5 showed a typical and reproducible growth pattern (Fig. 1A) and was chosen for use in all subsequent analyses. Observing developing leaves in rice is complicated by the fact that they are hidden from view by the sheaths of older leaves. Therefore, we characterized a plastochron index (Erickson and Michelini, 1957; Hill and Lord, 1990; Fournier et al., 2005; Fig. 1C), which allowed us to use the length of leaf 3 to robustly assess the developmental stage of leaf 5 without destruction of the plant. Plants could thus be selected and treated at specific plastochron stages of leaf 5 without invasive manipulations. Figure 1, B and D, show the P1 to P6 (mature) stages of leaf 5 growth, and Supplemental Figure S1 provides an overview of the histology of the different stages of rice leaf development.

To investigate at exactly which developmental stage and where within the leaf the ability to generate electron flow via the absorption of light energy occurred, we used chlorophyll fluorescence microscopy. Figure 2 shows a series of example images from leaves at P3, P4, and P5 stages as well as mature leaf blades. Due to their relative size, only portions of the P5 and mature leaf blades are shown. For each sample, the raw

fluorescence output is shown adjacent to the calculated values and distribution of ϕ PSII, which provides a measure of the quantum efficiency of electron transport. P3 stage primordia occasionally displayed measurable electron transport (Fig. 2A), but this was very weak and tightly localized to the distal tip of the primordia. Four out of nine P3 primordia analyzed did not display any measurable signal. Early P4 stage leaves showed a much more robust ability to generate electron transport, with all (10 out of 10) samples analyzed showing detectable signal. The signal was again restricted to the distal tip of the leaves but was higher than that observed in P3 samples (Fig. 2B). For comparison, all P5 stage leaves analyzed (which were all visibly green) and all mature leaves analyzed showed a more uniform and very high signal (Fig. 2, C and D).

These physiological data suggested that the ability of rice leaf tissue to perform a basic function of photosynthesis (absorption of light energy to generate an electron flow) develops at the very end of the P3 stage at the distal tip but that there is then a rapid transition to photosynthetic competence during early P4 stage. Analysis of the ultrastructure of plastids during leaf 5 development supported this interpretation. Plastids in P3 primordia lacked any obvious granal structure

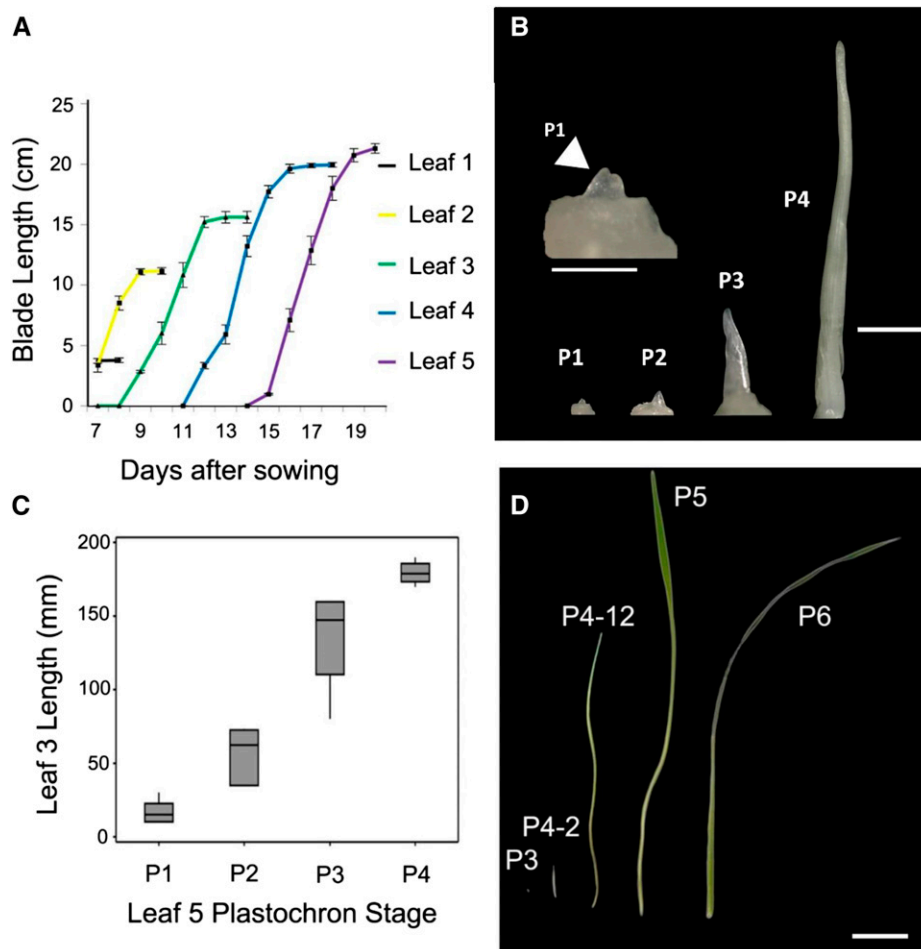


Figure 1. Analysis of leaf growth. A, Leaf blade elongation over time for the first five leaves of IR64 rice. Error bars show SD ($n = 10$). B, Dissected apices to reveal leaf primordia at P1 (greater magnification in inset), P2, P3, and P4-1 (less than 1 cm) stages. Bars = 0.25 mm (P1, P2, and P3) and 1 mm (P4-1). C, Plastochron index showing the relationship between the length of leaf 3 and developmental stage (P1, P2, P3, and P4) of leaf 5 ($n = 7$). D, Leaf primordia at stages P3, P4-2 (less than 2 cm), P4-12 (less than 12 cm), P5, and P6 stages. Bar = 1 cm.

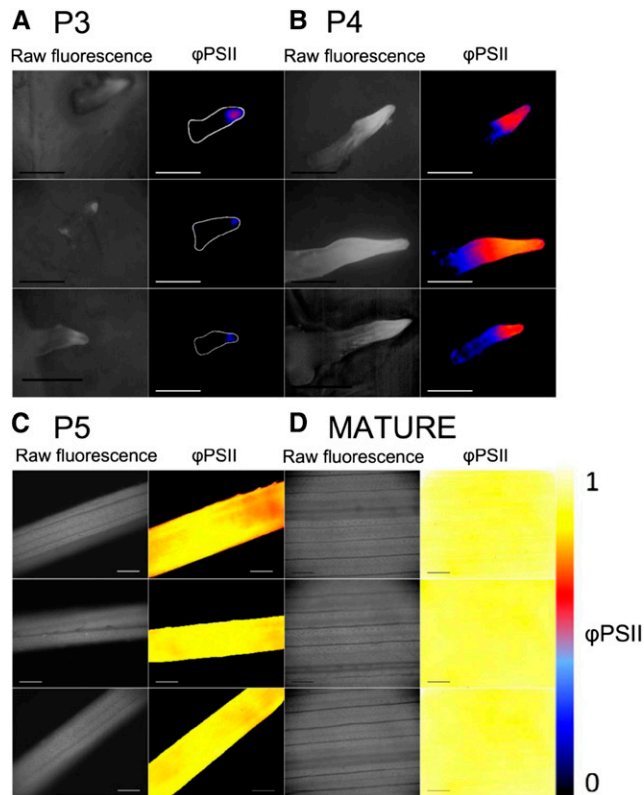


Figure 2. Chlorophyll fluorescence and photosynthetic efficiency during early leaf development. Raw chlorophyll fluorescence (left images) and ϕPSII (right images) are shown at $50 \mu\text{mol m}^{-2} \text{s}^{-1}$ in P3 (A), P4 (B), P5 (C), and mature (D) leaves. Images are shown for three biological replicates for each leaf stage. ϕPSII value is indicated by the scale adjacent to D. Bars = 0.25 mm.

(Fig. 3A), whereas by P4 stage, plastids with occasional grana were observed (Fig. 3B). In contrast, P5 plastids had distinct grana (Fig. 3C), which looked very similar to those in mature leaves (Fig. 3D). It was noticeable that, even in the P3 stage plastids (i.e. in leaves in which we infer photosynthesis was not occurring or was very limited), distinct starch grains were observed (Fig. 3A). We also investigated the developmental phase of the acquisition of potential photosynthetic capability by examining the pattern of chlorophyll autofluorescence using confocal microscopy. In P4 stage primordia, a clear maximum of signal intensity was observed near the tip of the leaf, with more proximal regions displaying a striated pattern of chlorophyll fluorescence (Fig. 3E).

We did not extract and measure the chlorophyll content of P3 and P4 stage leaves, due to technical difficulties and the oversimplification of the spatial differences in chlorophyll content in P3 and P4 stage leaves this would represent. However, chlorophyll content was around 593 mg m^{-2} in mature leaf blades ($n = 5$; $\text{SD} = 177 \text{ mg m}^{-2}$) and 335 mg m^{-2} in P5 stage leaves ($n = 5$; $\text{SD} = 54.9 \text{ mg m}^{-2}$). The average raw fluorescence signal in regions of P3 and P4 stage leaves

where it was detectable was around 10% to 20% (P3 stage) or 10% to 60% (P4 stage) of the raw fluorescence signal observed in mature leaves. Thus, we estimate the average chlorophyll content of these regions of P3 and P4 stage leaves to be around 60 to 120 mg m^{-2} (P3 stage leaves) or 60 to 360 mg m^{-2} (P4 stage leaves), depending on the sampling location.

To further investigate the nature of the biochemical and physiological events underpinning the very early stages of the acquisition of photosynthetic potential, we analyzed the induction kinetics of ϕPSII : $\phi\text{PSII} = (F_m' - F_s)/F_m'$, where F_m' is maximum PSII fluorescence in the light-adapted state and F_s is steady-state fluorescence (Maxwell and Johnson, 2000; Fig. 4, A–D). Data were extracted from up to seven regions of interest (ROIs) along the length of three of the five P3 stage primordia

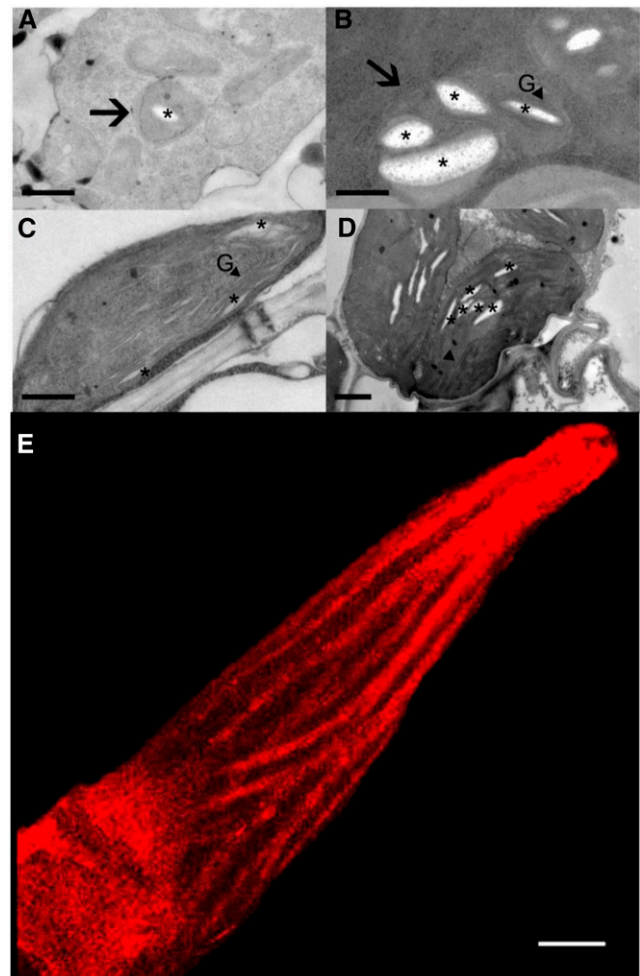


Figure 3. Plastid differentiation during early leaf development. A to D, Transmission electron micrographs of plastids in leaves at P3 stage (A), P4 stage (B), P5 stage (C), and mature leaves (D). E, Chlorophyll autofluorescence in a P4 stage leaf. G, Stacked grana. Asterisks indicate starch grains, and arrows indicate plastids. The locations that sections were taken from are shown in Supplemental Figure S1C. Bars = $0.5 \mu\text{m}$ (A–C), $1 \mu\text{m}$ (D), and $100 \mu\text{m}$ (E).

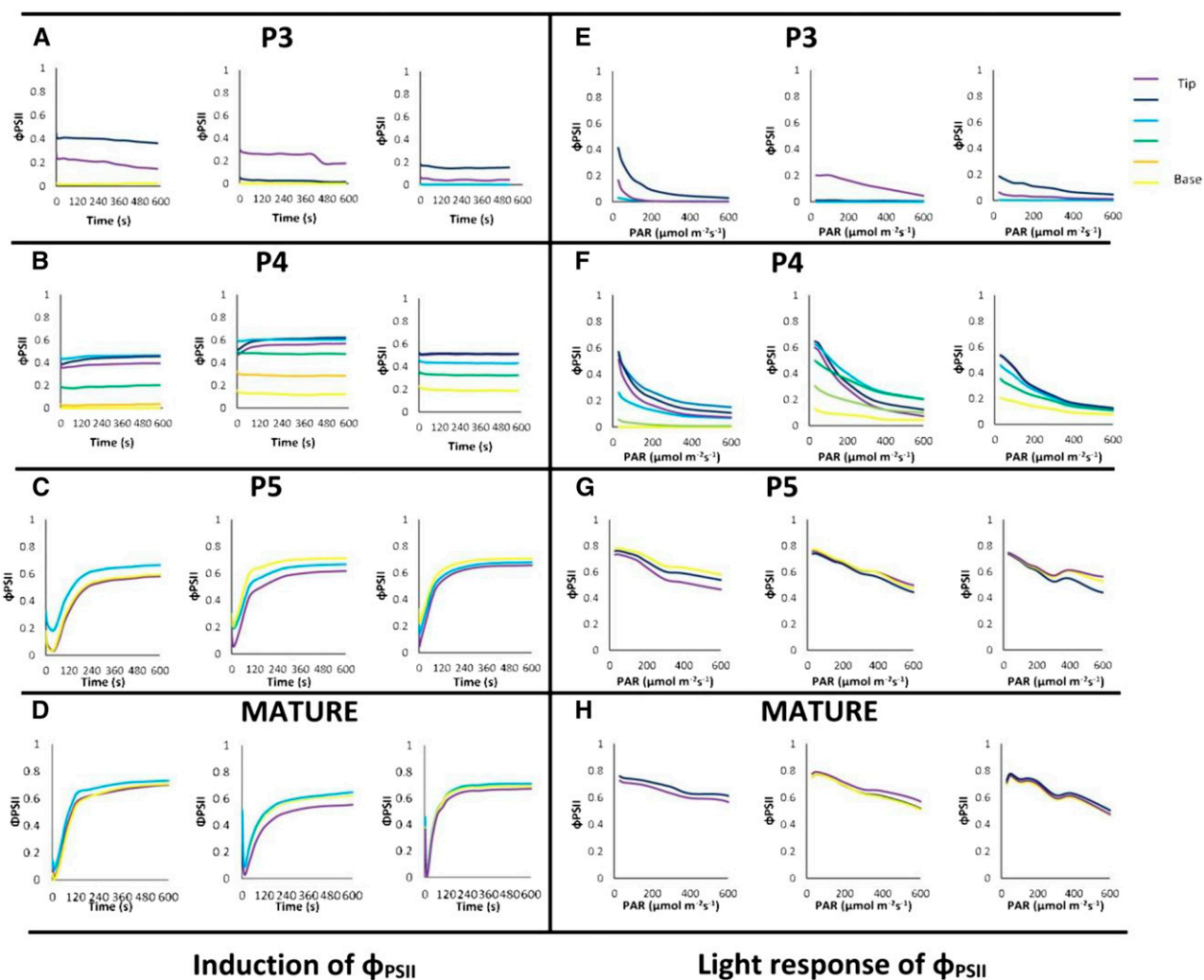


Figure 4. Induction kinetics of photosynthesis during early leaf development. A to D, Induction of ϕ_{PSII} at $50 \mu\text{mol m}^{-2} \text{s}^{-1}$ in different regions of P3 stage (A) and P4 stage (B) leaves and at $200 \mu\text{mol m}^{-2} \text{s}^{-1}$ in P5 stage (C) and mature (D) leaves. E to H, Light response of ϕ_{PSII} in different regions of P3 stage (E), P4 stage (F), P5 stage (G), and mature (H) leaves. Images are shown for three biological replicates for each leaf stage. Regions of measurement, from tip to base, are indicated by the color legend adjacent to E. PAR, Photosynthetically active radiation.

in which ϕ_{PSII} was measurable (Fig. 4A) as well as three P4 stage primordia (Fig. 4B). The results indicated a high degree of variation both along individual primordia (from base to tip) and between primordia, both at the P3 and P4 stages, consistent with the idea that rapid changes were occurring in the capacity for electron transport around this transition. Very fast induction rates were observed in the P3 samples, consistent with P3 leaves being developing sink tissues with high levels of reduced metabolites (Turgeon, 1989; Meng et al., 2001). Slightly slower rates of ϕ_{PSII} induction were observed in tip regions of P4 stage primordia, consistent with our proposal that the generation of Calvin cycle intermediates, the activation of Calvin cycle enzymes, and possibly stomatal opening require more time in this tissue at this stage of leaf development. These data can be compared with those

observed in P5 stage and mature leaves, which showed slower induction kinetics but much higher values of ϕ_{PSII} and, overall, more robust patterns of induction despite the higher irradiance used (Fig. 4, C and D). These patterns are characteristic of source leaves in which photosynthetic function has been fully established (Makino et al., 2002).

After leaf primordia at different developmental stages had undergone induction and reached a steady state of electron transport, they were exposed to a series of increasing irradiances (Fig. 4, E–H). At each irradiance, steady-state ϕ_{PSII} images were collected and data were extracted from regions along the length of leaf primordia, as described for ϕ_{PSII} induction. In P3 stage leaf primordia, a light response of ϕ_{PSII} was measurable only in the regions nearest the distal tip, and ϕ_{PSII} dropped rapidly to very low levels as the irradiance

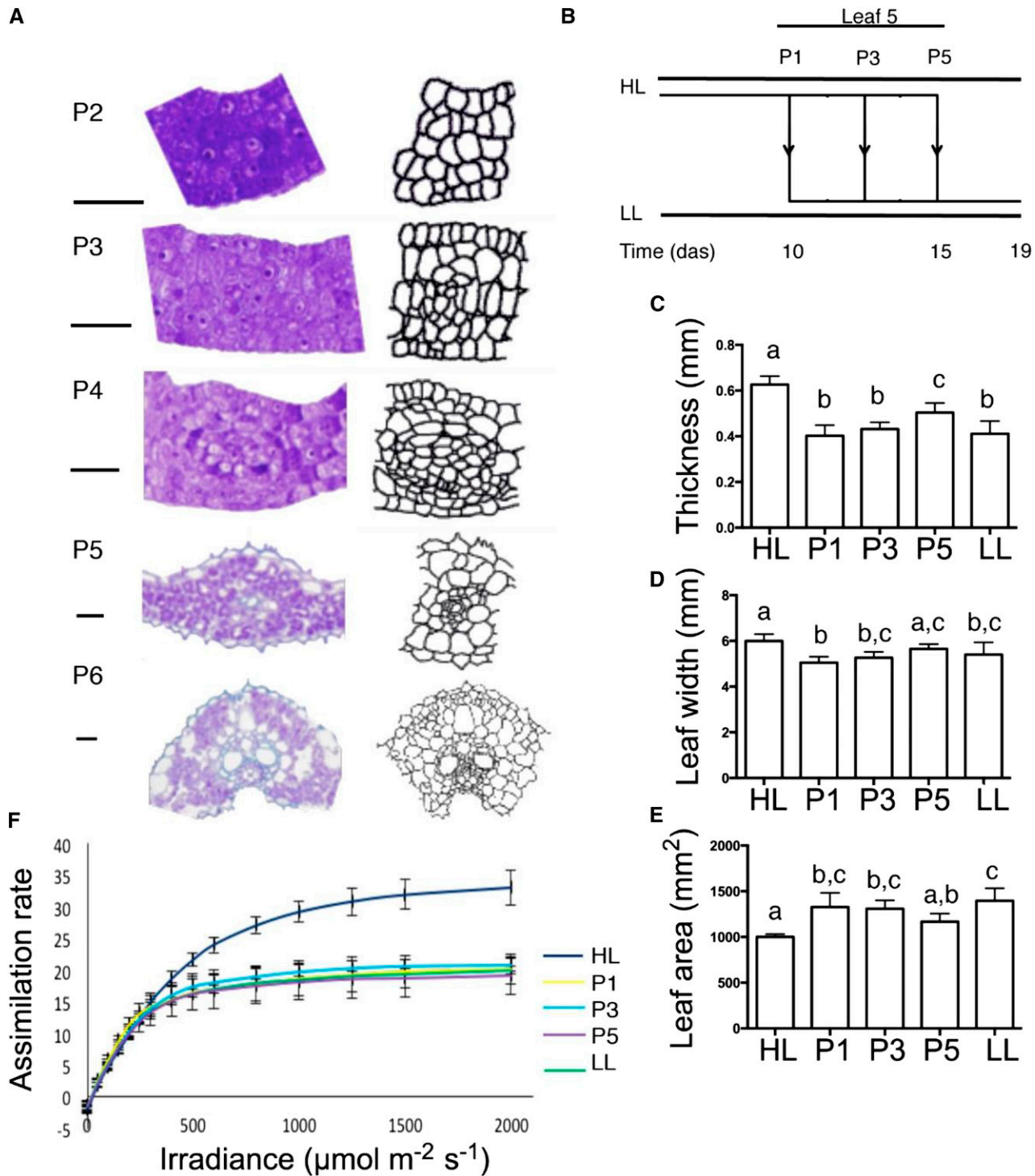


Figure 5. Leaf morphogenesis in response to altered irradiance during early leaf development. A, Vein differentiation in primordia at P2, P3, P4, and P5 stages and at maturity. The locations that sections were taken from are shown in Supplemental Figure S1C. Bars = 0.05 mm. B, Schematic of irradiance transfer experiments. Plants grown under HL conditions were either maintained under HL conditions or transferred to LL conditions when leaf 5 had achieved specific developmental stages (P1, P3, and P5), then maintained under LL conditions until analysis. C to E, Measurements of thickness (C), width (D), and area (E) in leaves grown under HL conditions and transferred to LL conditions at P1, P3, or P5 stage of leaf 5 development. Error bars show *se* (*n* = 7). Different letters indicate statistically significant differences (Tukey's honestly significant difference test, *P* < 0.05). F, Light response curves for assimilation rates in leaf 5 of plants as described in B. Error bars show *sd* (*n* ≥ 4).

increased (Fig. 4E). In P4 stage leaf primordia, a light response of ϕ PSII was measurable in regions farther away from the tip than in P3 primordia, and all 10 primordia analyzed still showed a ϕ PSII of 0.2 to 0.1 in regions nearest the tip at the highest irradiance used (Fig. 4F). Generally, the heterogeneity seen in steady-state ϕ PSII values after induction was also seen in the light response of ϕ PSII in P3 stage leaves (Fig. 4, A and E). This can be compared with the pattern of light induction seen in P5 and mature leaf samples (Fig. 4, G and H), which showed relatively consistent induction kinetics along the length of the leaves analyzed and high consistency between different samples. Nonphotosynthetic quenching was also measured during induction and at a range of irradiances, but slight movement of the samples between recording of the F_m and F_m' in P3 and P4 stage leaves limited the interpretation of these data (Supplemental Fig. S3).

A Loss of Leaf Developmental Plasticity Occurs after the P3 Stage

The above data highlighted the P3/P4 transition as a key stage in the transition to photosynthetic competence during rice leaf development. To investigate to what extent this physiological transition correlated with specific elements of leaf differentiation, we performed a histological analysis of leaf 5 from P2 through P6. At P2 stage, there was little overt cellular differentiation to indicate the future position of vascular tissue across the leaf blade (Fig. 5A; Supplemental Fig. S1). By P3 stage, coordinated patterns of cell division indicated regions of vascular formation that became more pronounced during P4, so that by P5 stage and the mature P6 stage, a classical pattern of vascular differentiation into xylem and phloem was apparent (Fig. 5A).

It has long been established that rice leaves grown under different irradiances undergo a process of acclimation to yield distinct leaf morphologies (Murchie et al., 2005). To investigate the degree of developmental plasticity in this system and to define when this plasticity is lost, we performed a series of experiments in which plants containing leaf 5 at particular developmental stages (P1, P3, and P5) were transferred from a high-light (HL; $700 \mu\text{mol m}^{-2} \text{s}^{-1}$) to a low-light (LL; $250 \mu\text{mol m}^{-2} \text{s}^{-1}$) environment and the structure and photosynthetic function of the mature leaves were measured (Fig. 5, B–F). As shown in Figure 5C, leaf 5 grown continuously under an HL environment had a mean thickness of 0.63 mm, whereas leaf 5 grown continuously under an LL environment was significantly thinner (0.41 mm; $P < 0.05$, Tukey's honestly significant difference test). When plants were transferred from HL to LL conditions when leaf 5 was at P1 or P3 stage, the mature leaves attained an appropriate thickness for the new LL environment (0.4 mm when transferred at P1 stage and 0.43 mm when transferred at P3 stage). However, when the transfer occurred at the P5 stage, the mature leaf was of intermediate thickness

(0.5 mm), indicating that at the P5 stage, leaves were no longer able to morphologically acclimate fully to the new light environment, consistent with previous work (Murchie et al., 2005). Measurement of leaf blade width (Fig. 5D) and area (Fig. 5E) revealed that growth in the surface plane of the blade showed a similar pattern of determination by the P5 stage with respect to light environment as leaf thickness.

Combined gas-exchange/chlorophyll fluorescence analysis indicated that leaf 5 of plants grown under continual HL conditions had a higher assimilation rate at ambient CO_2 than the equivalent leaf grown under LL conditions (Fig. 5F). When leaf 5 was transferred from HL to LL conditions at the P1, P3, or P5 stage, it was able to physiologically acclimate at all stages so that the measured leaf assimilation rate in the mature leaf was similar to a leaf maintained continuously under LL conditions. These data indicated that photosynthetic capacity could acclimate post-P5 via altered biochemistry, consistent with previous observations (Murchie et al., 2002, 2005).

Having established that rice leaves were showing an appropriate acclimation response at the gross morphological level, we set out to investigate the light response at the cellular level, with particular emphasis on stomatal patterning, since one might expect this to relate to the acquisition of photosynthetic function. Stomata in rice leaves form in specific epidermal cell files (Fig. 6A; Luo et al., 2012). Epidermal cell files are formed in a series of IVGs defined by parallel vascular strands along the long axis of the leaf. SD within each IVG at the midpoint along mature leaf 5 was measured in plants grown under HL and LL conditions (Fig. 6B). Under HL conditions, leaves had a maximum of 16 IVGs, whereas under LL conditions, up to 18 IVGs formed. Values of SD were found to be reasonably constant across all IVGs under both treatments, with the exception of the IVGs at the leaf margin, which tended to have a relatively high SD. With respect to IVD, these were generally smaller in LL conditions across all regions of the leaf (Fig. 6C). Again, the IVD values at the leaf margin for both HL and LL leaves tended to be different from the rest, with the margin IVD being relatively small, mirroring the relatively high SD values observed in this IVG (Fig. 6B).

As in other grass leaves, stomata in rice are formed via an intricate but stereotypical series of cell divisions leading to the development of a stomatal complex consisting of a pair of guard cells and supporting cells (Fig. 6E; Luo et al., 2012). When SCA was measured in mature HL-grown leaves, a relatively consistent value was observed in all IVGs (Fig. 6D). When leaves were grown under continual LL conditions, a much smaller SCA was measured in all IVGs (Fig. 6D). To further investigate the nature of this difference in SCA and to identify the developmental window during which SCA was set, we analyzed stomata in a series of plants that had been transferred from HL to LL conditions at specific stages of development of leaf 5 (as described

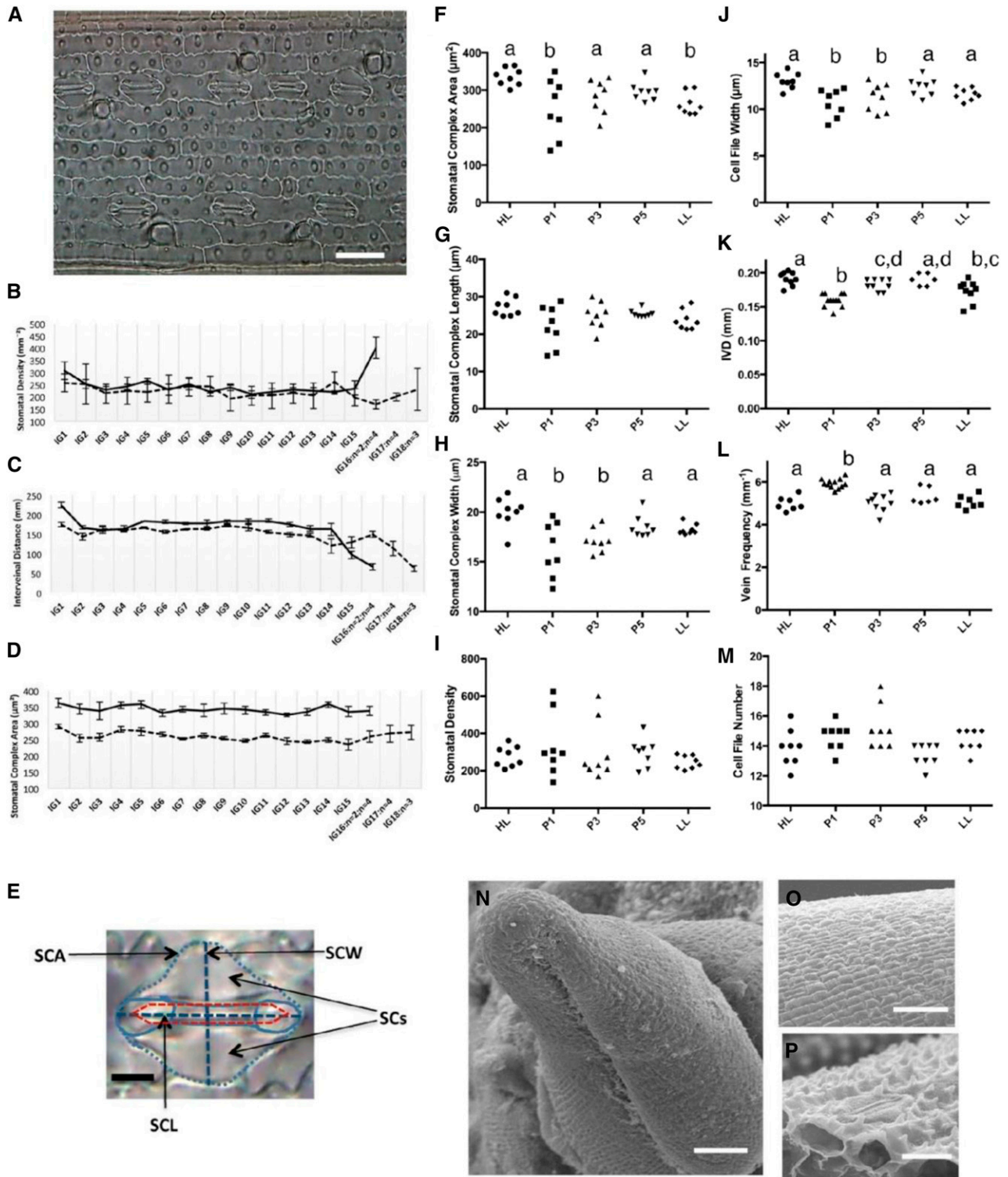


Figure 6. Stomatal size and density after leaf transfer between different irradiances. A, Epidermis showing an interveinal gap (IVG) with cell files containing stomatal complexes. Bar = 30 μm . B to D, Measurements of stomatal density (SD; B), interveinal distance (IVD; C), and stomatal complex area (SCA; D) in IVGs (IG) across mature rice leaves grown under HL (solid lines) and LL (broken lines) conditions. Under LL conditions, more IVGs were generated, leading to the observation of IG17 and IG18 in a few LL leaves (number indicated by value n). Error bars indicate se; $n = 5$ except where indicated. E, Individual stomatal complex indicating the supporting cells (SC) and the dimensions taken for SCA, stomatal complex length (SCL), and stomatal complex length (SCW). Bar = 5 μm . F to M, Measurements of SCA (F), SCL (G), SCW (H), SD (I), cell file width (CFW; J), IVD (K), vein

in Fig. 5B). These data displayed a startling significant difference in variance between samples transferred at different developmental stages (Brown-Forsythe test, $P < 0.001$), with leaves transferred at P1 and P3 stages showing very high variances (Fig. 6F). A nonparametric analysis of the data (Kruskal-Wallis test with posthoc Dunn's multiple comparison) indicated that the median SCA values for P1-transferred and LL samples were significantly different from the other treatments ($P < 0.05$), suggesting a fluidity in the setting of stomatal size in early rice leaf development that is later lost.

To investigate the cause of this variation in SCA, we measured SCL and SCW. A similar pattern was observed to that recorded for SCA, suggesting that the variation observed in SCA reflected changes in both SCL and SCW (Fig. 6, G and H). Comparison of the different SCL samples revealed a significant difference in variance (Brown-Forsythe test, $P < 0.01$), with P1- and P3-transferred samples showing the highest variances, but a nonparametric test did not distinguish any of the samples for SCL. The SCW data also showed a significant variation in variance (Brown-Forsythe test, $P < 0.05$), and the median values obtained from leaves transferred at P1 and P3 stages could be distinguished from the other treatments (Kruskal-Wallis test with Dunn's multiple comparison, $P < 0.05$).

Interestingly, although comparison of the mean values of SD in the transferred leaves indicated no difference between the different treatments, the data indicated a higher variance in SD in the P1- and P3-transferred leaves compared with the other samples (Fig. 6I), with some transferred leaves showing very low (fewer than 150 stomata mm^{-2}) or very high (more than 600 stomata mm^{-2}) values (Supplemental Fig. S4). Thus, a plasticity in the setting of various stomatal parameters was observed during very early leaf development that seemed to be lost later.

An analysis of stomatal differentiation by scanning electron microscopy supported the interpretation that early stage primordia (P1 and P3) show greatest flexibility in the light response of SCA. At P3 stage, epidermal cell files were clearly visible along the surface of the primordium, but no overt signs of stomatal differentiation were apparent (Fig. 6, N and O). By late P4 stage, differentiated stomata were clearly visible (Fig. 6P), consistent with the P4 stage being a phase of rapid stomatal differentiation, subsequent to patterning events during P3.

Since stomata in rice form along epidermal cell files, we also investigated the extent to which the

parameters of stomatal size and density might be set by the overall parameters of epidermal CFN and CFW within IVGs and the relationship of these parameters to whole-leaf values of vein number and IVD. The overall pattern of CFW was similar to that observed for SCA (Fig. 6, F and J). The differences in variance for CFW were less than for SCA, and the P1- and P3-transferred samples had a significantly lower CFW than the other treatments (ANOVA with posthoc Tukey's honestly significant difference test, $P < 0.05$).

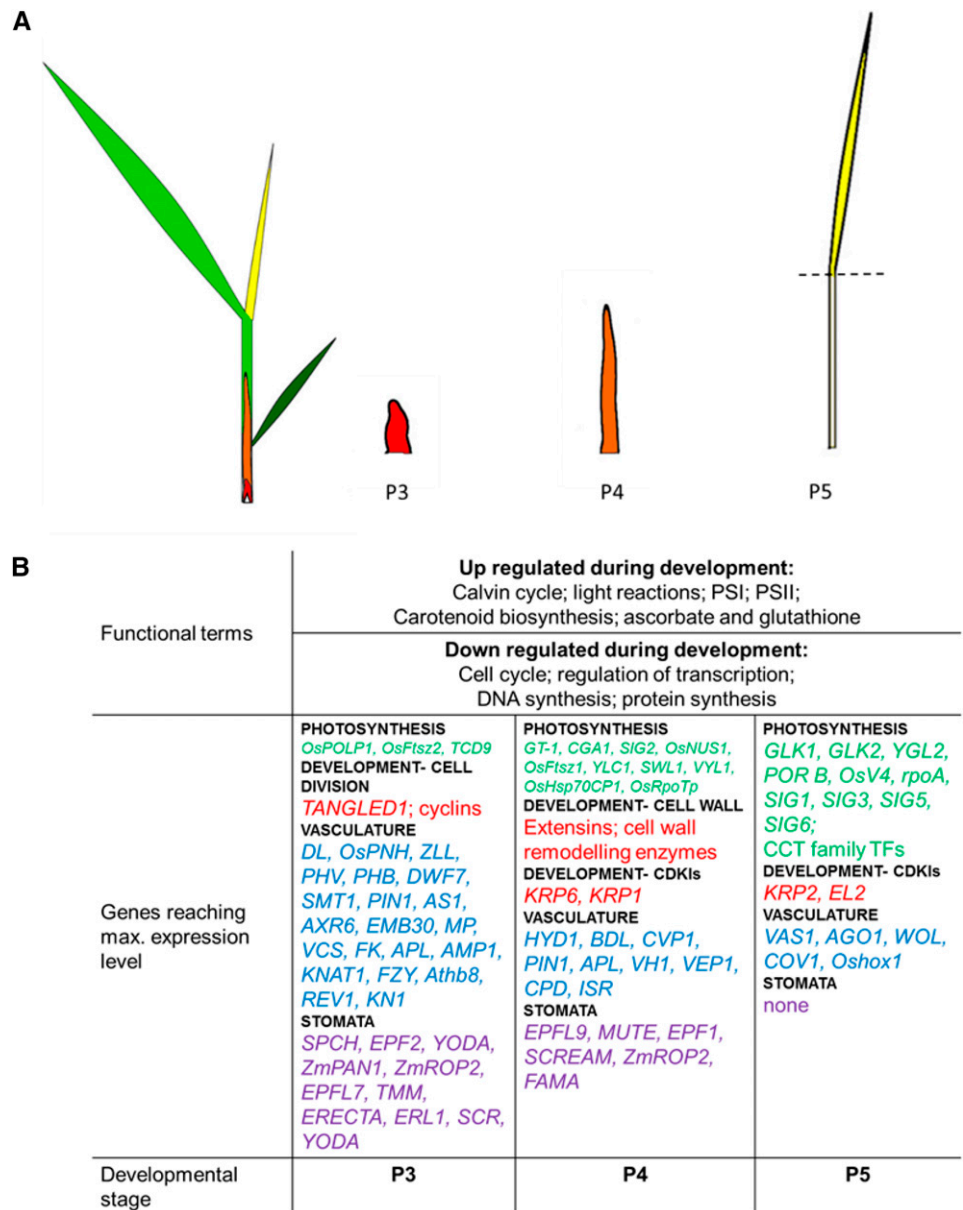
The differences in CFW were accompanied by differences in IVD (Fig. 6K). Most notably, the P1-transferred leaves had a significantly smaller IVD compared with HL leaves ($P < 0.005$), and LL leaves also had smaller average IVD ($P < 0.01$). A decrease in IVD is predicted to lead to an increase in the frequency of veins across the leaf blade (since veins set the boundaries for IVD). This was observed for the P1-transferred leaves, which showed a significantly higher vein frequency than the other treatments ($P < 0.05$; Fig. 5L). It is interesting that, although under HL conditions IVD was higher than under LL conditions and CFN was essentially unchanged (Fig. 6M), vein frequency across the blade of HL and LL leaves was very similar (Fig. 6L). This apparent discrepancy was resolved by the observation that, under HL conditions, the width of the vascular bundles was smaller than under LL conditions. Thus, there appeared to be a compensation process between IVD and vascular bundle width that acted to maintain vein frequency and a relatively constant number of intervening epidermal cell files.

In addition to investigating the outcome on leaf development of transitions from HL to LL conditions, we also analyzed the reverse situation, where leaf primordia at specific plastochron stages from plants grown under LL conditions were transferred to HL conditions. For this analysis, we focused on those traits that showed the most marked differences in the high- to low-irradiance experiments described above. As shown in Supplemental Figure S5A, leaves grown under LL conditions and then transferred to HL conditions at P5 stage did not attain a typical HL thickness at maturity, whereas leaves transferred at the P3 stage achieved a thickness that could not be discriminated from leaves continually kept under HL conditions. Interestingly, P1 stage leaves transferred to HL conditions remained relatively thin at maturity, suggesting that, under some conditions, very early stage primordia can remain fixed with respect

Figure 6. (Continued.)

frequency (L), and cell file number (CFN; M) in leaves either grown continually under HL or LL conditions or transferred from HL to LL conditions at P1, P3, or P5 stage. Where appropriate, identical letters in a graph indicate samples that could not be distinguished from each other by statistical analysis (see text). N to P, Scanning electron microscopy images of a P3 primordium (N), a higher magnification of the surface of a P3 primordium (no stomatal complexes visible; O), and a mature stomatal complex in a P4 primordium (P). Bars = 30 μm (N and O) and 10 μm (P).

Figure 7. Key changes in gene expression during early rice leaf development. A, Leaf developmental stages used for RNAseq analysis and their positions on the plant (not to scale; colors added for clarity). B, Key functional terms up-regulated and down-regulated during development and selected genes reaching their maximum expression levels at P3, P4, or P5 stage. Where a gene name is shown twice, rice has two orthologs of the Arabidopsis gene of interest. See also Supplemental Tables S2 to S7 and Supplemental Figure S7.



to final leaf thickness. When SCA was analyzed, a similar pattern was observed, with the P5-transferred leaves displaying a mean SCA that was similar to that observed under LL conditions and distinct from that observed under HL conditions (Supplemental Fig. S5B), with P1- and P3-transferred leaves showing a more intermediate phenotype. There was no difference in mean SD between the different treatments (Supplemental Fig. S5C), but there was a trend for higher variance in the leaves transferred at P3 and P5 stages, with densities of over 500 stomata mm⁻² being observed. Similarly, the various treatments did not lead to a significant difference in final CFW, although there was a trend again for higher variance in leaves transferred at P3 and P5 stages (Supplemental Fig. S5D).

Gene Expression Patterns Underpinning the P3/P4 Transition

Our analysis of both physiology and structure identified the P3/P4 transition as an important stage in rice leaf development with respect to the acquisition of photosynthetic capability and associated cellular differentiation, as well as the ability to respond to environmental signals by altering aspects of cellular differentiation. To investigate the gene expression changes underpinning this transition, we performed RNA sequencing (RNAseq) analysis on leaf 5 at P3 stage and P4 stage and on the leaf blade at P5 stage (Supplemental Data S1). Overall, 14,502 genes were identified that were differentially expressed during early leaf development (out of a total of 25,768 for

Table 1. Expression patterns of rice genes known to be involved in photosynthetic development

Locus	Gene Name(s)	Reference	Cluster
LOC_Os09g38980	TCD9	Jiang et al. (2014b)	down 1
LOC_Os05g37160	OsFtsz2	Vitha et al. (2001)	down 1
LOC_Os06g07210	RNRL1	Yoo et al. (2009)	down 3
LOC_Os06g14620	RNRS1	Yoo et al. (2009)	down 3
LOC_Os02g56100	RNRL2	Yoo et al. (2009)	down 3
LOC_Os06g03720	RNRS2	Yoo et al. (2009)	down 3
LOC_Os08g07840	OsPOLP1	Takeuchi et al. (2007)	down 3
LOC_Os03g20460	OsGKpm, VIRESCENT2	Sugimoto et al. (2007)	neutral
LOC_Os03g16430	SIG2B	Kasai et al. (2004)	neutral
LOC_Os02g39340	OsDG2	Jiang et al. (2014a)	neutral
LOC_Os03g45400	NUS1, VIRESCENT1	Kusumi et al. (1997); Kusumi et al. (2011)	peak
LOC_Osp1g00240	rpoB	Hanaoka et al. (2005)	peak
LOC_Osp1g00250	rpoC1	Hanaoka et al. (2005)	peak
LOC_Osp1g00260	rpoC2	Hanaoka et al. (2005)	peak
LOC_Os11g26160	SIG2A	Kasai et al. (2004)	peak
LOC_Os06g44230	OsRpoTp	Kusumi et al. (2004)	peak
LOC_Os09g21250	YLC1	Zhou et al. (2013)	peak
LOC_Os05g23740	OsHsp70CP1	Kim and An (2013)	peak
LOC_Os03g29810	VYL, OsClp6	Dong et al. (2013)	peak
LOC_Os05g32680	PAC	Meurer et al. (1998)	peak
LOC_Os04g56970	OsFtsz1	Vitha et al. (2001)	peak
LOC_Os04g42030	SNOW-WHITE LEAF1	Hayashi-Tsugane et al. (2014)	peak
LOC_Os08g06630	SIG1	Kasai et al. (2004)	up 1
LOC_Osp1g00660	rpoA	Hanaoka et al. (2005)	up 2
LOC_Os05g51150	SIG3	Kasai et al. (2004)	up 2
LOC_Os04g39970	OsV4	Gong et al. (2014)	up 2
LOC_Os05g50930	SIG5	Kasai et al. (2004)	up 3
LOC_Os08g14450	SIG6	Kasai et al. (2004)	up 3
LOC_Os06g40080	YGL2	Chen et al. (2013)	up 3
LOC_Os10g35370	PORB	Kang et al. (2015)	up 3
Not found in rice	SIG4	Kasai et al. (2004)	Not applicable

which expression was detected). Having validated the RNAseq data (Supplemental Fig. S6), we interrogated the data sets to identify patterns of gene expression during early leaf development that might underpin the key processes identified by our morphological and physiological analysis. These results are summarized in Figure 7 and described below.

Since our analysis indicated that photosynthetic electron transport first develops at the P3/P4 stage transition, we first investigated the pattern of transcript accumulation for those genes annotated as photosynthetic (MapMan bin PS).

Our results indicated that 40 genes involved in photosynthesis (out of 351 rice genes annotated with MapMan bin PS) were already at 50% or more of their mature leaf expression level at the earliest developmental stage studied, P3 (Supplemental Table S2), suggesting that a small number of genes involved in the photosynthetic process are already transcriptionally expressed in tissues that are not yet photosynthetically active. The most common expression pattern of genes annotated as involved in photosynthesis was an increase in expression from P3 to P4 and from P4 to P5 stages (159 genes; Supplemental Table S3A). Broadly, functional groups of genes up-regulated from P3 to P5 stage were found to include those involved in the Calvin-Benson cycle,

photosynthetic light reactions, and subunits of both PSI and PSII. These expression changes were accompanied by the up-regulation of photoprotective mechanisms such as carotenoid biosynthesis (18 of 21 annotated genes; Supplemental Table S3B) and around half of genes involved in ascorbate and glutathione metabolism (49 of 106 annotated genes; Supplemental Table S3C).

A range of expression patterns was seen in genes identified previously through rice mutant studies as playing a role in photosynthetic development (Table I). A small number of these were most highly expressed at P3 stage. However, many other genes with known rice photosynthetic mutant phenotypes showed a peak in expression at P4 stage, as well as several genes with *Arabidopsis* (*Arabidopsis thaliana*) photosynthetic mutant phenotypes. A further group of genes with rice photosynthetic mutant phenotypes were maximally expressed at P5 stage. Genes showing this expression pattern also included orthologs of those known to play a role in photosystem assembly in *Arabidopsis*. Only a small number of genes that have known mutant phenotypes involved with photosynthesis in rice showed a neutral expression pattern in these early stages of leaf development.

To investigate the control of expression of these photosynthesis-associated genes at the P3/P4 stages,

we also analyzed transcription factors showing similar patterns to these known photosynthetic genes during rice leaf development, which led to the identification of 30 genes with increasing expression patterns during early leaf development and 21 genes whose transcripts peaked at P4 stage (for full selection criteria, see "Materials and Methods"; Supplemental Table S4A). This list included genes shown previously to play a role in regulating chloroplast development (e.g. *GLK1* and *GLK2*; Fitter et al., 2002; Wang et al., 2013a), supporting the notion that the other transcription factor genes in this list may also play a role in facilitating or regulating the onset of photosynthesis. Notably, there are also several CCT family transcription factors in our list of potential regulators of photosynthetic development.

The setting of aspects of CFW, SCA, and vein frequency, as well as the overall parameters of leaf width and thickness, prior to the P5 stage suggested that genes involved in cell growth and division at the P3/P4 transition play an important role in determining morphological parameters linked to photosynthesis and acclimation. In line with this, functional groups of genes down-regulated from P3 to P5 stage included those involved in the cell cycle (24 genes, including *ARF75*, *TANGLED1*, and many cyclins), regulation of transcription (270 genes, including transcription factors and chromatin-remodeling factors), DNA synthesis (97 genes, including histones and DNA polymerase subunits), and protein synthesis (both plastid and nonplastid; 108 genes, mostly involved in ribosome biogenesis). Notably, the P3/P4 transition was associated with an increase in the expression of genes associated with the inhibition of progress through the cell cycle (*KRP1* and *KRP6*) and an increased relative expression of genes associated with cell wall differentiation and remodeling.

The P3/P4 transition is associated with vascular differentiation and patterning (Fig. 5A), and of the 36 rice genes identified as vascular development regulators or orthologs of vascular development regulators in Arabidopsis (Scarpella and Meijer, 2004; Supplemental Table S5), 22 reached their highest level of expression by P3 stage, nine peaked at P4 stage, and only five were expressed most highly at P5 stage (Fig. 7B). Thus, most of these putative vascular development regulators showed a decrease in expression from P3 to P5. Of the few genes known to have a vascular mutant phenotype in rice, several were most highly expressed at P3 stage, including *OsKn3*, *OsAGO7*, and *NARROW AND ROLLED LEAF1* (Postma-Haarsma et al., 1999; Shi et al., 2007; Hu et al., 2010). However, a neutral expression pattern across the three stages studied was observed for the *NARROW LEAF1*, *NARROW LEAF2*, and *NARROW LEAF3* genes (Qi et al., 2008; Cho et al., 2013). As auxin has long been known to be involved in vascular development, we also studied the expression patterns of *OsPIN* genes found previously to be expressed in the vasculature (Wang et al., 2009). These genes showed a mixture of expression patterns, with *OsPIN1a* most highly expressed at P3 stage, *OsPIN5b* showing a

neutral expression pattern, *OsPIN10a* peaking at P4 stage, and *OsPIN5a* and *OsPIN1b* reaching maximal expression at P5 stage. The expression of *OsPIN2* was not detected.

Finally, since our results indicated that the P3 stage was characterized by a plastic response in terms of stomatal size in response to altered light environment (Fig. 6) but that this plasticity was lost by P5 stage, we interrogated our data to identify which rice genes and orthologs of maize and Arabidopsis genes linked with stomatal differentiation and patterning were expressed during P3 and P4 stages. Of the 17 genes identified as putative stomatal development regulators in rice, 11 were most highly expressed at P3 stage (Fig. 7B; Supplemental Table S6). This included orthologs of *SPEECHLESS*, *TOO MANY MOUTHS*, *EPF2*, *EPFL7*, and *YODA* (Bergmann et al., 2004; Liu et al., 2009; Rychel et al., 2010). A further five reached their highest expression level at P4 stage, including rice orthologs of *SCREAM1*, *EPFL9*, and *MUTE* (Liu et al., 2009; Hunt et al., 2010). The expression of all stomatal differentiation genes was less in P5 than in earlier stages.

DISCUSSION

Despite the importance of leaves as the basic engine for photosynthesis-derived nutrition, aspects of our understanding of how these organs develop in monocots are incomplete. In this article, we set out to address this knowledge gap by addressing some specific questions. When does a rice leaf gain capacity for light capture to generate reducing power for carbon fixation? How well does this acquisition of physiological capability correlate with morphological aspects of leaf differentiation and with underlying patterns of gene expression? How flexible are these developmental processes, and when is developmental plasticity lost?

The P3/P4 Transition Is When Photosynthetic Competence Is Initiated

By creating a plastochron index, we were able to stage rice leaf development in a robust fashion, enabling comparison of equivalent leaves. Although the main structural and anatomical changes that occur during rice leaf development have been characterized (Itoh et al., 2005), our results provide an analysis of how this structure relates to function (i.e. when a leaf actually gains the capacity to perform an essential element of photosynthesis, such as absorption of light energy to generate an electron flow).

Although the microfluorescence technique used for this analysis places some constraints on data interpretation (e.g. no absolute measures of electron transport rate or photosynthetic capacity were calculated, since absorbance was found to be variable [Supplemental Fig. S2], and other assumptions made in the comparison of these very different tissues may not be met), we are confident that true quenching of chlorophyll

fluorescence was occurring in our primordia and that our ϕ PSII measurements are valid. We cannot rule out the presence of some cyclic electron flow, reduction of the plastoquinone pool in the dark (Corneille et al., 1998), or the presence of a small proportion of light-harvesting complexes not connected to reaction centers. However, we did not observe the very high raw fluorescence signal that might be observed if a large proportion of light-harvesting complexes were uncoupled and the reasonable F_v/F_m (maximum photochemical efficiency of PSII in the dark-adapted state) values observed indicate nonzero amounts of quenching. Furthermore, the light response of ϕ PSII observed in primordia shows the expected pattern of decreasing ϕ PSII at increasing irradiances, consistent with a functioning electron transport chain.

Our results indicate that the ability to absorb light energy to generate an electron flow is gained at the very end of the P3 stage of development at the distal tip of the primordium, followed by a very rapid transition to photosynthetic competence during early P4. Electron transport efficiency does not reach the level of that of a mature leaf until the P5 stage, while little additional photosynthetic electron transport efficiency is gained between P5 stage and the mature leaf. The high variability of the light response of ϕ PSII between samples and between regions is consistent with P3 and P4 stage primordia undergoing rapid photosynthetic development, with different leaves having widely differing abilities to use increasing amounts of light to drive electron transport. This interpretation was supported by a structural analysis of plastid differentiation. Plastids prior to P3 stage lacked obvious grana, whereas by P4 stage, plastids had internal structure consistent with a capacity for photosynthetic activity. P3 plastids frequently contained starch granules, suggesting that the plastids were importing carbon from source leaves and that starch grains were being used as a temporary carbon store, potentially enabling rapid growth during the fundamental biochemical switch from sink to source metabolism. Recently, Kusumi et al. (2010) used a similar structural analysis of plastid differentiation alongside chlorophyll fluorescence imaging to show that, in rice, leaves at the P4-2 stage (around 2 cm long; before emergence) have measurable ϕ PSII. Other than that of Kusumi et al. (2010), there are few studies reporting photosynthetic measurements on very young leaves. Meng et al. (2001) showed that, in the developmental gradient present in a developing tobacco (*Nicotiana tabacum*) leaf (the youngest used was 3.9 cm long), even regions at the base have a measurable rate of electron transport. Peterson et al. (2014) reported changes in the relative abundance of PSI and PSII along maize leaves (the third leaf of 12-d-old seedlings was used) and concluded that redox mediation of chlorophyll biosynthesis may regulate photosystem assembly and thus ensure the development of a suitable PSI/PSII excitation balance. In the most immature (basal) leaf segment studied, Peterson et al. (2014) also reported a larger nonvariable component of fluorescence, which

they attribute to a moderate accumulation of incompletely assembled, nonfunctional PSII complexes. However, no detailed measurements of ϕ PSII kinetics at different developmental stages of the leaf were reported in those studies. Our data agree with those of Kusumi et al. (2010), but we also show that the first detectable electron transport occurs before this in the tip of P3 stage leaves and that the development of photosynthetic function occurs basipetally thereafter. Thus, the large longitudinal developmental gradient in the acquisition of ϕ PSII in P3 and P4 stage primordia can be visualized to a high spatial resolution using our approach.

These physiological data can be compared with our mRNA analysis. In particular, we addressed two questions. Which photosynthetic genes become transcriptionally active at the onset of the physiological process? Is there a core set of early photosynthetic genes in rice?

Analysis of gene expression in the very earliest stage of leaf initiation in maize indicated that there is no significant difference in the expression of photosynthesis-related genes between the shoot apical meristem proper and leaves at the P0/P1 stages (Brooks et al., 2009), whereas in tomato (*Solanum lycopersicum*; a dicot), a gene encoding the small subunit of Rubisco was already expressed at P1 stage but not expressed in the shoot apical meristem (Fleming et al., 1993). In another study, it was found that, in older intact maize seedlings, 39 photosynthesis-related genes were up-regulated compared with shoot apical meristems (Ohtsu et al., 2007). However, both studies in maize used microarrays enriched in probes reflecting specific subsets of tissues, limiting the extent to which the results can be compared with our RNAseq-based analysis (Ohtsu et al., 2007; Brooks et al., 2009). In rice, we found that, by the P3 stage, 40 genes involved in photosynthesis (out of 351 rice genes annotated as photosynthetic) were already at 50% or more of their mature leaf expression levels. These data suggest that over one-tenth of genes involved in photosynthesis are already highly expressed before a leaf can actually utilize the encoded enzymatic machinery. Since light is required for the final step in chlorophyll biosynthesis, and our analysis indicated a wave of acquisition of chlorophyll fluorescence from the primordium tip toward the base at the P3/P4 transition, our data suggest that the basic machinery for photosynthetic electron transport is developmentally set prior to the late P3 stage by a core set of genes, with a light-related trigger initiating the actual capability for photosynthetic electron flow. Analysis of P2 stage primordia would allow further testing of this hypothesis; however, we found the dissection of such young primordia in rice to be technically very challenging.

Many of the genes that are maximally expressed at P4 stage are known to have chloroplast biogenesis mutant phenotypes, emphasizing the importance of this stage for the development of photosynthetic capability. Transcripts for most genes encoding the core

photosynthetic machinery (including those for most electron transport chain components and Calvin-Benson cycle enzymes) increase from both P3 to P4 and P4 to P5, showing that bulk production of these vital components of autotrophy occurs over a relatively longer developmental time. Kusumi et al. (2010) split photosynthetic development in rice into three stages: DNA replication and plastid division (late P3/early P4 stage); activation of the chloroplast genetic system (particularly the transcription/translation machinery; early P4 stage); and activation of the photosynthetic machinery (late P4 stage to P5 stage and beyond). Our results are largely consistent with their findings. However, we also pinpoint a varied set of photosynthesis-related genes that are already expressed at the very early P3 stage, we add more genes with known mutant phenotypes into the expression picture, and we identify a novel set of transcription factors that show expression changes accompanying those of these known genes. This diverse list of transcription factors contains known regulators of photosynthetic development as well as many CCT family genes. In Arabidopsis, the CCT family gene *CIA2* was found to regulate chloroplast protein synthesis and import (Sun et al., 2009). Thus, this list of transcription factors may provide a useful toolbox for future modification of photosynthetic function in rice.

The developmental stages in which we have studied the transcriptomic dynamics are directly comparable to those studied previously in maize (Wang et al., 2013b). In these maize primordia, key photosynthetic genes, such as those encoding Calvin cycle enzymes and PSII reaction center subunits, are already expressed at low levels and are up-regulated in later developmental stages. In maize primordia, the chlorophyll biosynthetic enzyme *PORB* seems not to be expressed until later developmental stages (equivalent to rice P4/P5), which is also when tetrapyrrole biosynthesis shows a peak of activity. Other available data sets on monocot developmental transcriptomics are from segments along the maize leaf developmental gradient (Li et al., 2010; Tausta et al., 2014; the third leaf of 9-d-old seedlings was used). Although it is more difficult to directly compare these studies of leaf segments with our entire (but much younger) primordia, the general pattern of photosynthetic genes already being expressed in the youngest segments at the base of the leaf (before the sink-source transition) is consistent with our findings.

Major Patterning Events Linked to Photosynthesis Occur in the Leaf at the P3/P4 Transition

In addition to the appropriate biochemical apparatus for light capture and carbon fixation, photosynthesis requires the integrated supply and export of material, including CO₂, water, carbon, and nitrogen. Since our physiological analysis indicated that the P3/P4 transition is key to the acquisition of photosynthetic

competence, we investigated whether associated elements of leaf differentiation, including vasculature and stomata, were coordinated with this phase. Our data indicate that this is the case and identify a series of genes whose expression is likely to be involved in the appropriate spatial and temporal differentiation of these elements. Undoubtedly, the development of morphological characteristics is affected by the longitudinal developmental gradient existing within rice leaf primordia, as visualized in our chlorophyll fluorescence imaging analysis. We captured precisely positioned snapshots along this gradient that demonstrate major changes in morphological development at the P3, P4, and P5 developmental stages. This provides guidance for the interpretation of our stage-specific gene expression data.

Stomatal differentiation occurs during P4 stage, and our analysis revealed the expression during this phase of a number of genes associated in other systems with processes of stomatal patterning and differentiation. Previous attempts to detect the expression of some of these genes in rice (e.g. *OsSPCH1* and *OsSPCH2*) have failed (Liu et al., 2009), suggesting that the highly targeted and staged RNAseq approach taken here was essential for the detection of these transcripts. The overall pattern of stomata-associated gene expression was consistent with the observed limitation of stomatal differentiation to the P3/P4 stage. Expression of most of these genes was minimal in P5 stage leaves, and the others tended to show a gradual decline in expression from P3 to P5, with some showing a peak in expression at P4 (e.g. *OsMUTE*, *OsSCREAM1*, and *OsEPFL9*). In light of the role of these genes in controlling stomatal patterning and differentiation in other systems, these rice genes likely play a vital role in setting parameters of stomatal pattern and number.

Since there is significant interest in modifying aspects of rice leaf structure for crop improvement, we thought it would be informative to explore the limits of flexibility of the normal process of leaf differentiation, since this would both inform on the boundaries of the system and identify whether particular stages of development should be targeted for modification. To do this, we exploited the knowledge that transfer of rice plants from high to low irradiance leads to an acclimation process in developing leaves so that morphology appropriate to the new light environment is generated. Focusing on stomata, these experiments supported and extended previous observations that this morphological acclimation process occurs prior to the P5 stage, whereas photosynthetic capacity can acclimate post-P5 stage through altered biochemistry (Murchie et al., 2005). Our data indicate that stomata in high-irradiance-grown rice are larger than those grown under low irradiance but with no significant shift in mean stomatal density. Most strikingly, they indicate that at the P1 and P3 stages, the process of stomatal patterning is highly plastic and can respond to a shift in irradiance to generate mature leaves with high variation in stomatal density and size. Thus, rice leaves do possess an

inherent plasticity in the stomatal patterning mechanism that is subject to environmental regulation, but this is limited to the P1 to P3 stages. This is clearest in leaves transferred from HL to LL conditions but is also apparent in leaves transferred in a reciprocal fashion from LL to HL conditions. The situation here is slightly more complex, but again, it is the P3 stage that appears to be the key developmental phase in terms of the plasticity of response to the external environment. Although well documented in eudicots, the mechanism of systemic control of leaf development by environmental factors remains unclear (Lake et al., 2001, 2002; Murchie et al., 2005; Coupe et al., 2006). Our results suggest that manipulation of this system could allow the generation of rice leaves with very distinct stomatal properties and, thus, water relations. We suggest that targeting the P3/P4 stage of development would be most appropriate for such manipulations.

Due to the anatomy of rice leaves, the width of a stomatal complex will be influenced by the width of the epidermal cell file within which it arises. Coupled to the number of cell files within an IVG and the number of IVGs in a leaf (which will be set by the number of veins and the overall width of a leaf), a complex interaction of cellular and leaf-scale patterning and differentiation events will influence the final number and size of stomata. Our data show that transfer of a rice leaf from an HL to an LL environment at a very early stage of development (P1) leads to narrower leaves with an increased number of (but smaller) IVGs. The absolute number of cell files within these narrower IVGs remains relatively constant, but the width of the cell files tends to be smaller (i.e. the leaf acclimates to the new environment at the cellular level). At the level of gene expression, genes involved in cell division processes tend to decrease in transcript level from P3 through P5, but it is interesting that some members of the *KRP* gene family (associated with the termination of cell division; De Veylder et al., 2001; Barrôco et al., 2006) show peaks of relative transcript level at the P3 and P5 stages. Modulation of expression of these genes may play a role in determining the number and size of cells as leaves enter the P5 stage of rice leaf maturation.

Our data indicate that changes in epidermal cell file number and size were linked with changes in vein number and size. As in maize, the midvein is initiated early (by rice P2 stage, maize P1/P2 stage), with the development of lateral veins occurring at the next developmental stage (rice P3 stage, maize P3/P4 stages; Wang et al., 2013a). However, in maize, foliar leaves develop the spacing (by P4 stage) and characteristic Kranz anatomy (by P5 stage) of C_4 plants, which does not occur in our C_3 rice leaves. The venation pattern that develops in rice is instead broadly similar to that of many other C_3 grasses (Sakaguchi and Fukuda, 2008; Sage and Sage, 2009; for review, see Nelson and Dengler, 1997).

To investigate the regulation of vascular development in rice further, we studied the developmental

timing of expression in rice of a number of genes previously linked with the control of vascular development in rice, Arabidopsis, and maize (Scarpella and Meijer, 2004). Most of these genes reached maximal expression at the P3 stage followed by a general decrease by P5. The general decline in the number of highly expressed vascular-linked genes from P3 to P5 coincides with the decrease in the rate of differentiation seen at these later stages, suggesting that this loss of gene expression may limit the ability of older stages to initiate new vascular tissue. Mutation in some of these genes has been shown to lead to altered vascular differentiation in rice (Nishimura et al., 2002; Yamaguchi et al., 2004), suggesting that they represent a panel of relevance for the future investigation of rice leaf vascular development. However, the number of rice vein patterning mutants described at the molecular level is very limited, and many of those mentioned here show pleiotropic developmental defects, including a strong link between vein patterning and leaf width (Qi et al., 2008). Thus, suitable targets for the manipulation of rice vascular patterning remain elusive.

How the differentiation of vascular and surrounding photosynthetic tissue is organized has been much debated (Berleth et al., 2000; Scarpella et al., 2003). Chlorophyll fluorescence arose in stripes along the developing leaf, consistent with the idea that, already by the early P4 stage, leaf tissue was set on a developmental trajectory setting apart nonphotosynthetic vascular and photosynthetic intervening mesophyll tissue. The differentiation of photosynthetic tissue may be organized in reference to the network of developing vascular tissue, which provides a scaffold from which positional signals inform the differentiation of the mesophyll. Conversely, Andriankaja et al. (2012) showed that the exit from proliferation of Arabidopsis leaf cells may be regulated by their photosynthetic differentiation, and Scarpella et al. (2004) demonstrated in Arabidopsis that mesophyll differentiation terminates the iterative process of vascular initiation. Which of these processes is at play in monocots, and rice specifically, is unclear. However, we provide evidence that vascular development and the initiation of photosynthetic differentiation are temporally and spatially coordinated in rice, with both occurring around the P3/P4 stages. In addition, the striated pattern of chlorophyll autofluorescence observed in P4 stage primordia (Fig. 3) is reminiscent of vascular patterning. Direct evidence for positional signals from the vasculature informing photosynthetic development in rice is not available; however, in plants with very clear compartmentalization of photosynthetic and nonphotosynthetic function, such as the C_4 plant maize, such positional information is known to be key (Nelson and Langdale, 1989). The molecular nature of positional information derived from the vasculature has begun to be pinned down in root development (Sabatini et al., 1999; Nakajima et al., 2001; Wu et al., 2014), suggesting that this is a tractable problem.

CONCLUSION

The results reported here identify the P3/P4 transition as a highly dynamic stage in rice leaf development where initial competence for photosynthesis is achieved. This is coordinated with processes of vascular and stomatal differentiation, and we identify sets of genes involved in the setting of each of these processes. As well as identifying targets for future manipulation, our results suggest that such manipulations should target stages prior to P4 to exploit the endogenous plasticity of differentiation exhibited by rice leaves during this phase of development.

MATERIALS AND METHODS

Plant Material and Growth Conditions

Rice (*Oryza sativa* var *indica*; IR64) plants were grown in hydroponics as described (Makino et al., 1997). Plants were grown in a growth chamber (Conviron; www.conviron.com) at high light ($700 \mu\text{mol m}^{-2} \text{s}^{-1}$) or low light ($250 \mu\text{mol m}^{-2} \text{s}^{-1}$) with a 12-h/12-h light/dark cycle, 50% humidity, ambient CO_2 , and a temperature of 28°C .

Histology

For leaf thickness measurements, 1-cm sections were cut from mature fifth leaf blades, fixed in 4:1 ethanol:acetic acid for 24 h, and embedded in Technovit 7100 (TAAB; www.taab.co.uk). Samples were sectioned at $2 \mu\text{m}$ thickness using a Leica RM2145 microtome (www.leica-microsystems.com), stained with Toluidine Blue (Sigma-Aldrich; www.sigmaaldrich.com), and imaged using an Olympus DP71 microscope (www.olympus-lifescience.com). Line drawings of vascular development were rendered manually in Adobe Photoshop CS5. Thickness was measured at the bulliform cells using Adobe Photoshop version 12.0. For transmission electron microscopy, primordia at different developmental stages were dissected into 3% (v/v) glutaraldehyde (Sigma-Aldrich) in 0.1 M phosphate buffer. Further fixation and processing were as described (Wallace et al., 2015). For confocal microscopy, P4 stage leaf primordia were dissected, mounted in water, and imaged using an inverted LSM510 Meta confocal microscope (Zeiss; www.zeiss.co.uk). Excitation was with a 488-nm argon laser. Emitted light was detected at 650 to 710 nm. Noise in the image background only was removed using Adobe Photoshop.

Scanning Electron Microscopy

Rice leaf primordia were fixed for 6 h on a 2-rpm orbital shaker in glass vials containing 4% (w/v) paraformaldehyde (Thermo Fisher Scientific), 2.5% (w/v) glutaraldehyde (Agar Scientific), 0.5% (v/v) Tween 20 (Sigma-Aldrich), and 0.2 M phosphate-buffered saline, pH 7.4 (Sigma-Aldrich), all prepared using ultrahigh purified water. Fixative was replaced with two changes of phosphate-buffered saline for 30 min each. Samples were dehydrated in acetone (Fisher Scientific) series of 5%, 10%, 25%, 40%, 55%, 70%, 85%, 95%, and two times 100% (v/v) for 1 h each. Samples were dried with liquid CO_2 using a Polaron critical point dryer (Agar Scientific). Samples were then mounted onto aluminum stubs using black carbon stickers (Agar Scientific) and sputter coated with gold (Edwards S150B gold sputter coater) in an argon gas atmosphere. Images were obtained using a scanning electron microscope (Philips XL-20) and processed with embedded XL-20 software.

Light Response Curves

Light response curves were recorded on mature fifth leaves in which blade elongation was no longer occurring. Gas exchange was recorded using an LI-6400 portable photosynthesis system (LICOR Biosciences; www.licor.com) at irradiances of 50, 100, 150, 200, 250, 300, 400, 500, 600, 800, 1,000, 1,250, 1,500, and $2,000 \mu\text{mol m}^{-2} \text{s}^{-1}$ using a constant air flow rate of $200 \mu\text{mol m}^{-2} \text{s}^{-1}$, a sample CO_2 concentration of $400 \mu\text{mol m}^{-2} \text{s}^{-1}$, a block temperature of 28°C , and a relative humidity of 50%. Plants were allowed to acclimate to each

subsequent irradiance level for 3 min. The average of up to 54 photosynthetic assimilation rate measurements recorded at 5-s intervals was taken at each irradiance level.

Chlorophyll Fluorescence Microscopy

P3 and P4 stage leaf primordia were dissected, mounted on cooled set agarose in a humid environment, and imaged using a modified Olympus BX50WI microscope (Rolfe and Scholes, 2002). After exposing leaf primordia to an initial dark period of 5 min, the minimal level of fluorescence was recorded (F_0) and a saturating pulse was applied ($3,000 \mu\text{mol m}^{-2} \text{s}^{-1}$) to measure the initial maximum fluorescence (F_m). Subsequently, an actinic light was switched on, and F_s/F_m' was recorded every 30 s over a period of 20 min as primordia went through induction. Optimal induction irradiances to avoid photodamage of $50 \mu\text{mol m}^{-2} \text{s}^{-1}$ for P3 and P4 stage leaves and $200 \mu\text{mol m}^{-2} \text{s}^{-1}$ for P5 stage and mature leaves were determined through pilot experiments. For light response curves, primordia were exposed to irradiances of 30, 50, 100, 150, 200, 300, 400, and $600 \mu\text{mol m}^{-2} \text{s}^{-1}$ after undergoing induction. Plants were allowed to acclimate to each subsequent irradiance level for 5 min, after which four F_s/F_m' measurements were taken at 30-s intervals. For induction and light response curves, data were extracted from several circular ROIs, each with a diameter of $40 \mu\text{m}$. ROIs were evenly spaced along the entire length of the primordium (P3 and P4 stage leaves; up to seven ROIs) or positioned at the base, midpoint, and tip of P5 or mature leaf blades (three ROIs per leaf blade), with positioning over the midvein or major veins avoided (Supplemental Fig. S1C). Where no signal was recorded in multiple ROIs throughout the course of the induction or light response experiment, plotted traces may overlap. Absorbance was imaged using the red/far-red light method (Rolfe and Scholes, 2010).

Chlorophyll Content Analysis

Chlorophyll was extracted and chlorophyll content was quantified using the method described by Lichtenthaler and Wellburn (1983). Briefly, two leaf discs (each 4 mm in diameter) were collected from the middle of the P5 or mature leaf blade ($n = 5$ per stage) and ground up in 10 mL of cold 80% (v/v) acetone using a pestle and mortar. Chlorophyll *a* and *b* concentrations were measured using a spectrophotometer (Perkin Elmer), with the following calculations used: chlorophyll *a* ($\mu\text{g mL}^{-1}$) = $12.21 (A_{663}) - 2.81 (A_{646})$; chlorophyll *b* ($\mu\text{g mL}^{-1}$) = $20.13 (A_{646}) - 5.03 (A_{663})$.

Analysis of Stomatal and Vein Patterning

For each rice leaf, a 1-cm segment at the midpoint was cut and fixed in ethanol:acetic acid (7:1, v/v) for 2 to 3 d at room temperature, then bleached (25% [v/v] economic bleach; Ottimo Supplies) for 1 d. Samples were cleared using two to three drops of chloral hydrate solution (10 g of chloral hydrate in 2.5 mL of water and 1 g of glycerol) for 1 h at room temperature. One to two drops of modified Hoyer's solution (10 g of chloral hydrate from Riedel-de Haen, 1 g of glycerol from Sigma-Aldrich, and 3 g of 20% [w/v] gum arabic solution from Minerals-Water) was employed as mountant, and samples were placed on glass slides. Samples were observed with an Olympus BX51 light microscope using Nomarski differential interference contrast optics. Photomicrographs were taken with an Olympus DP71 camera (12.5 megapixels) using an Olympus U-TVO.63XC camera adapter, both mounted on the microscope. Images were captured and processed using CELL-B version 2.7 and ImageJ software for stomata, IVC, and vein counting as well as measuring. The areas of stomatal complexes, aperture length, and guard cell width were measured using a Bamboo Pen Tablet from Wacom. Statistical analysis was done using Minitab16 and Graphpad Prism6.

RNA Extraction and Sequencing

For P3 stage leaves, 240 primordia were used per RNA sample; for P4 stage leaves, five primordia were used per sample (P4 stage leaves around 1 cm in length); and for P5 stage leaves, three leaves were used per sample (blade tissue down to the collar only). Samples were harvested between 3 and 5 h into the photoperiod to minimize the potential influence of circadian factors, and the analysis was performed with three biological replicates. RNA was extracted using TriZol (Invitrogen) and cleaned up and DNase1 treated using the Sigma Plant Total RNA kit (Sigma-Aldrich). The quality of the resulting RNA was assessed using the Agilent 2100 BioAnalyzer (www.genomics.agilent.com), and

all RNA integrity number values were found to be above 8. RNAseq was carried out at the Liverpool Centre for Genomic Research (www.liv.ac.uk/genomic-research) using RiboZero-treated RNA with library construction following the Illumina TruSeq stranded mRNA protocol (www.illumina.com). Sequencing (Illumina HiSeq 2000) produced paired-end reads with a read length of 100 bp.

Transcript Quantification and Differential Gene Expression Analysis

Paired-end reads were subjected to quality trimming and adaptor filtering using Trimmomatic (Bolger et al., 2014) using the settings LEADING:10, TRAILING:10, SLIDINGWINDOW:5:15, and MINLEN:50. The quality-filtered paired-end reads were then mapped to the complete set of coding sequences from version 7.0 of the *japonica* rice Michigan State University Release 7 using bowtie2 (Langmead and Salzberg, 2012), and transcript abundances were estimated using RSEM (Li and Dewey, 2011). All pairwise comparisons between developmental stages were made using DESeq (Anders and Huber, 2010), using the default normalization method and identifying differentially expressed genes as those with a Benjamini-Hochberg corrected $P \leq 0.05$ (Benjamini and Hochberg, 1995). A principal component analysis plot of all count data by replicate was generated using SIMCA-P+ (version 12).

Validation of RNAseq Data by Quantitative Reverse Transcription-PCR

After RNA analysis by Illumina sequencing, both in silico quality control and quantitative PCR (qPCR) validation of the expression patterns of selected genes were used to assess the quality of the data (Supplemental Fig. S6; Supplemental Table S1). These indicated a low variance between biological replicates and verified that the patterns of expression identified by bioinformatic analysis were reflected at the level of qPCR quantification. Validation of RNAseq data was carried out using RNA retained from the original samples submitted for RNAseq. Moloney murine leukemia virus reverse transcriptase (Invitrogen; www.lifetechnologies.com) was used for complementary DNA (cDNA) synthesis following the manufacturer's protocol. cDNA from each of three biological replicates for each developmental stage was used, except for P3 stage, where two biological replicates were used. Primers were designed using QuantPrime (Arvidsson et al., 2008; for details, see Supplemental Table S1B). PCR amplification was carried out in an ABI StepOne Plus qPCR system using SYBR Green Master Mix (Invitrogen). Two technical replicates from two separate cDNA synthesis reactions were averaged for each biological replicate, and relative fold changes in expression between developmental stages were calculated using the $\Delta\Delta CT$ method (Schmittgen and Livak, 2008).

Functional Term Enrichment Analysis and Identification of Genes of Interest

The direction of the \log_2 (fold change) in expression between stages and its Benjamini-Hochberg-corrected significance ($P < 0.05$) were used to cluster all loci into 11 expression clusters (Supplemental Fig. S7). Custom Perl scripts were used to group genes into clusters. Loci for which there were fewer than 10 fragment alignments were not clustered. The 11 clusters were used to identify the stage at which individual genes reached their maximum expression level.

For MapMan (version 3.5.1R2; Usadel et al., 2005) term enrichment analysis testing, significantly enriched gene groups were identified as those with a Benjamini-Hochberg-corrected $P < 0.05$ following Wallenius approximation and length normalization of uncorrected P values using GSeq (Young et al., 2010). Up-regulated functional terms were those overrepresented in clusters of genes that were up-regulated between at least two developmental stages and not down-regulated between any two developmental stages. Down-regulated functional terms were those overrepresented in clusters of genes that were down-regulated between at least two developmental stages and not up-regulated between any two developmental stages.

Potential novel regulators of photosynthetic development (Supplemental Table S4A) were identified by applying the following rules: genes must be transcription factors; they must be in cluster up 2 (significantly up-regulated from P3 to P4, no significant change from P4 to P5), up 3 (significantly up-regulated from P3 to P4 and from P4 to P5), or peak (significantly up-regulated from P3 to P4, significantly down-regulated P4 to P5); \log_2 (fold change) for P3-P4 ≥ 2 ; level of expression in P4 stage ≥ 5 ; level

of expression in mature leaves ≥ 5 (not for genes in the peak cluster; data from Davidson et al., 2012); and level of expression in rice endosperm ≤ 5 (Davidson et al., 2012).

For genes putatively involved in vascular and stomatal development, genes of interest from Arabidopsis (*Arabidopsis thaliana*) and maize (*Zea mays*) were identified from the literature (Scarpella and Meijer, 2004; Liu et al., 2009; Supplemental Tables S5 and S6). Rice orthologs of these genes were identified using conditional orthology assignment as described by Aubry et al. (2014).

Sequence data from this article can be found in the GenBank/EMBL data libraries under accession number SRP062323.

Supplemental Data

The following supplemental materials are available.

Supplemental Figure S1. Anatomy of the rice shoot apical meristem and developing leaves.

Supplemental Figure S2. Absorbance of developing leaves.

Supplemental Figure S3. Induction and light response of nonphotosynthetic quenching.

Supplemental Figure S4. Stomatal density extremes.

Supplemental Figure S5. Leaf and stomatal characteristics after transfer from LL to HL conditions.

Supplemental Figure S6. RNAseq quality control.

Supplemental Figure S7. Enrichment analysis of gene expression clusters.

Supplemental Table S1. Verification of RNAseq results by qPCR and qPCR primer details.

Supplemental Table S2. Genes annotated with MapMan bin PS that reach 50% or greater maximal expression by P3 stage.

Supplemental Table S3. Genes annotated with MapMan bins PS, Carotenoids, or Ascorbate and Glutathione and their expression patterns during rice early leaf development.

Supplemental Table S4. Transcription factors that are potential regulators of photosynthetic development.

Supplemental Table S5. Arabidopsis and maize genes known to regulate vascular development and their putative rice orthologs, and expression patterns of other rice genes known to be involved in vascular development.

Supplemental Table S6. Putative regulators of stomatal development in rice and their expression patterns during early leaf development.

Supplemental Data S1. All rice RNAseq count data, median normalized.

ACKNOWLEDGMENTS

We thank Dr. Nicola Green at the Kroto Research Institute for assistance with confocal imaging, Chris Hill for assistance with transmission electron microscopy, and Marion Bauch and the staff at the NERC Biomolecular Analysis Facility in Sheffield for technical assistance.

Received November 3, 2015; accepted January 22, 2016; published January 26, 2016.

LITERATURE CITED

- Amiour N, Imbaud S, Clément G, Agier N, Zivy M, Valot B, Balliau T, Armengaud P, Quilleré J, Cañas R, et al (2012) The use of metabolomics integrated with transcriptomic and proteomic studies for identifying key steps involved in the control of nitrogen metabolism in crops such as maize. *J Exp Bot* **63**: 5017–5033
- Anders S, Huber W (2010) Differential expression analysis for sequence count data. *Genome Biology*, **11**: R106

- Andriankaja M, Dhondt S, De Bodt S, Vanhaeren H, Coppens F, De Milde L, Mühlenbock P, Skirycz A, Gonzalez N, Beemster GTS, et al (2012) Exit from proliferation during leaf development in *Arabidopsis thaliana*: a not-so-gradual process. *Dev Cell* 22: 64–78
- Arvidsson S, Kwasiński M, Riano-Pachon DM, Mueller-Roeber B (2008) QuantPrime – a flexible tool for reliable high-throughput primer design for quantitative PCR. *BMC Bioinformatics*, 9: DOI: 10.1186/1471-2105-9-465
- Aubry S, Kelly S, Kuempers BMC, Smith-Unna RD, Hibberd JM (2014) Deep evolutionary comparison of gene expression identifies parallel recruitment of trans-factors in two independent origins of C-4 photosynthesis. *PLoS Genetics* 10: e1004365
- Baker NR (2008) Chlorophyll fluorescence: a probe of photosynthesis in vivo. *Annu Rev Plant Biol* 59: 89–113
- Baker NR, Rosenqvist E (2004) Applications of chlorophyll fluorescence can improve crop production strategies: an examination of future possibilities. *J Exp Bot* 55: 1607–1621
- Barróco RM, Peres A, Droual AM, De Veylder L, Nguyen SL, De Wolf J, Mironov V, Peerbolte R, Beemster GTS, Inzé D, et al (2006) The cyclin-dependent kinase inhibitor *Orysa*;KRP1 plays an important role in seed development of rice. *Plant Physiol* 142: 1053–1064
- Benjamini, Y, Hochberg, Y (1995) Controlling the false discovery rate – a practical and powerful approach to multiple testing. *J R Stat Soc Ser B*, 57: 289–300
- Berger S, Sinha AK, Roitsch T (2007) Plant physiology meets phytopathology: plant primary metabolism and plant-pathogen interactions. *J Exp Bot* 58: 4019–4026
- Bergmann DC, Lukowitz W, Somerville CR (2004) Stomatal development and pattern controlled by a MAPKK kinase. *Science* 304: 1494–1497
- Berleth T, Mattsson J, Hardtke CS (2000) Vascular continuity and auxin signals. *Trends Plant Sci* 5: 387–393
- Bolger, AM, Lohse M, Usadel B (2014) Trimmomatic: a flexible trimmer for Illumina sequence data. *Bioinformatics* 30: 2114–2120
- Brooks L III, Strable J, Zhang X, Ohtsu K, Zhou R, Sarkar A, Hargreaves S, Elshire RJ, Eudy D, Pawlowska T, et al (2009) Microdissection of shoot meristem functional domains. *PLoS Genet* 5: e1000476
- Chen H, Cheng Z, Ma X, Wu H, Liu Y, Zhou K, Chen Y, Ma W, Bi J, Zhang X, et al (2013) A knockdown mutation of YELLOW-GREEN LEAF2 blocks chlorophyll biosynthesis in rice. *Plant Cell Rep* 32: 1855–1867
- Cho SH, Yoo SC, Zhang H, Pandeya D, Koh HJ, Hwang JY, Kim GT, Paek NC (2013) The rice narrow leaf2 and narrow leaf3 loci encode WUSCHEL-related homeobox 3A (*OsWOX3A*) and function in leaf, spikelet, tiller and lateral root development. *New Phytol* 198: 1071–1084
- Corneille S, Courmac L, Guedeny G, Havaux M, Peltier G (1998) Reduction of the plastoquinone pool by exogenous NADH and NADPH in higher plant chloroplasts: characterization of a NAD(P)H-plastoquinone oxidoreductase activity. *Biochim Biophys Acta* 1363: 59–69
- Coupe SA, Palmer BG, Lake JA, Overy SA, Oxborough K, Woodward FI, Gray JE, Quick WP (2006) Systemic signalling of environmental cues in *Arabidopsis* leaves. *J Exp Bot* 57: 329–341
- Davidson RM, Gowda M, Moghe G, Lin H, Vaillancourt B, Shiu SH, Jiang N, Buell CR (2012) Comparative transcriptomics of three Poaceae species reveals patterns of gene expression evolution. *Plant J* 71: 492–502
- De Veylder L, Beeckman T, Beemster GTS, Krols L, Terras F, Landrieu I, van der Schueren E, Maes S, Naudts M, Inzé D (2001) Functional analysis of cyclin-dependent kinase inhibitors of *Arabidopsis*. *Plant Cell* 13: 1653–1668
- Dong H, Fei GL, Wu CY, Wu FQ, Sun YY, Chen MJ, Ren YL, Zhou KN, Cheng ZJ, Wang JL, et al (2013) A rice virescent-yellow leaf mutant reveals new insights into the role and assembly of plastid caseinolytic protease in higher plants. *Plant Physiol* 162: 1867–1880
- Elert E (2014) Rice by the numbers: a good grain. *Nature* 514: S50–S51
- Erickson RO, Michelini FJ (1957) The plastochron index. *Am J Bot* 44: 297–305
- Fernie AR, Stitt M (2012) On the discordance of metabolomics with proteomics and transcriptomics: coping with increasing complexity in logic, chemistry, and network interactions scientific correspondence. *Plant Physiol* 158: 1139–1145
- Fitter DW, Martin DJ, Copley MJ, Scotland RW, Langdale JA (2002) GLK gene pairs regulate chloroplast development in diverse plant species. *Plant J* 31: 713–727
- Fleming AJ, Mandel T, Roth I, Kuhlemeier C (1993) The patterns of gene expression in the tomato shoot apical meristem. *Plant Cell* 5: 297–309
- Fournier C, Durand JL, Ljutovac S, Schäufele R, Gastal F, Andrieu B (2005) A functional-structural model of elongation of the grass leaf and its relationships with the phyllochron. *New Phytol* 166: 881–894
- Gong X, Su Q, Lin D, Jiang Q, Xu J, Zhang J, Teng S, Dong Y (2014) The rice *OsV4* encoding a novel pentatricopeptide repeat protein is required for chloroplast development during the early leaf stage under cold stress. *J Integr Plant Biol* 56: 400–410
- Hanaoka M, Kanamaru K, Fujiwara M, Takahashi H, Tanaka K (2005) Glutamyl-tRNA mediates a switch in RNA polymerase use during chloroplast biogenesis. *EMBO Rep* 6: 545–550
- Hayashi-Tsugane M, Takahara H, Ahmed N, Himi E, Takagi K, Iida S, Tsugane K, Maekawa M (2014) A mutable albino allele in rice reveals that formation of thylakoid membranes requires the SNOW-WHITE LEAF1 gene. *Plant Cell Physiol* 55: 3–15
- Hibberd JM, Sheehy JE, Langdale JA (2008) Using C4 photosynthesis to increase the yield of rice: rationale and feasibility. *Curr Opin Plant Biol* 11: 228–231
- Hikosaka K, Terashima I (1995) A model of the acclimation of photosynthesis in the leaves of C-3 plants to sun and shade with respect to nitrogen use. *Plant Cell Environ* 18: 605–618
- Hill JP, Lord EM (1990) A method for determining plastochron indexes during heteroblastic shoot growth. *Am J Bot* 77: 1491–1497
- Hu J, Zhu L, Zeng D, Gao Z, Guo L, Fang Y, Zhang G, Dong G, Yan M, Liu J, et al (2010) Identification and characterization of NARROW AND ROLLED LEAF 1, a novel gene regulating leaf morphology and plant architecture in rice. *Plant Mol Biol* 73: 283–292
- Hunt L, Bailey KJ, Gray JE (2010) The signalling peptide EPFL9 is a positive regulator of stomatal development. *New Phytol* 186: 609–614
- Itoh J, Nonomura K, Ikeda K, Yamaki S, Inukai Y, Yamagishi H, Kitano H, Nagato Y (2005) Rice plant development: from zygote to spikelet. *Plant Cell Physiol* 46: 23–47
- Jiang Q, Ma X, Gong X, Zhang J, Teng S, Xu J, Lin D, Dong Y (2014a) The rice *OsDG2* encoding a glycine-rich protein is involved in the regulation of chloroplast development during early seedling stage. *Plant Cell Rep* 33: 733–744
- Jiang Q, Mei J, Gong XD, Xu JL, Zhang JH, Teng S, Lin DZ, Dong YJ (2014b) Importance of the rice *TCD9* encoding α subunit of chaperonin protein 60 (*Cpn60 α*) for the chloroplast development during the early leaf stage. *Plant Sci* 215-216: 172–179
- Jurik TW, Chabot JF, Chabot BF (1979) Ontogeny of photosynthetic performance in *Fragaria virginiana* under changing light regimes. *Plant Physiol* 63: 542–547
- Kang SJ, Fang YX, Zou GX, Ruan BP, Zhao J, Dong GJ, Yan MX, Gao ZY, Zhu L (2015) White-green leaf gene encoding protochlorophyllide oxidoreductase B is involved in chlorophyll synthesis of rice. *Crop Sci* 55: 284–293
- Kasai K, Kawagishi-Kobayashi M, Teraishi M, Ito Y, Ochi K, Wakasa K, Tozawa Y (2004) Differential expression of three plastidial sigma factors, *OsSIG1*, *OsSIG2A*, and *OsSIG2B*, during leaf development in rice. *Biosci Biotechnol Biochem* 68: 973–977
- Kim GT, Yano S, Kozuka T, Tsukaya H (2005) Photomorphogenesis of leaves: shade-avoidance and differentiation of sun and shade leaves. *Photochem Photobiol Sci* 4: 770–774
- Kim SR, An G (2013) Rice chloroplast-localized heat shock protein 70, *OsHsp70CP1*, is essential for chloroplast development under high-temperature conditions. *J Plant Physiol* 170: 854–863
- Krause GH, Weis E (1991) Chlorophyll fluorescence and photosynthesis: the basics. *Annu Rev Plant Physiol Plant Mol Biol* 42: 313–349
- Kubinova L (1991) Stomata and mesophyll characteristics of barley leaf as affected by light: stereological analysis. *J Exp Bot* 42: 995–1001
- Kusumi K, Chono Y, Shimada H, Gotoh E, Tsuyama M, Iba K (2010) Chloroplast biogenesis during the early stage of leaf development in rice. *Plant Biotechnol* 27: 85–90
- Kusumi K, Mizutani A, Nishimura M, Iba K (1997) A virescent gene *V-1* determines the expression timing of plastid genes for transcription/translation apparatus during early leaf development in rice. *Plant J* 12: 1241–1250
- Kusumi K, Sakata C, Nakamura T, Kawasaki S, Yoshimura A, Iba K (2011) A plastid protein *NUS1* is essential for build-up of the genetic system for early chloroplast development under cold stress conditions. *Plant J* 68: 1039–1050
- Kusumi K, Yara A, Mitsui N, Tozawa Y, Iba K (2004) Characterization of a rice nuclear-encoded plastid RNA polymerase gene *OsRpoTp*. *Plant Cell Physiol* 45: 1194–1201

- Lake JA, Quick WP, Beerling DJ, Woodward FI (2001) Plant development: signals from mature to new leaves. *Nature* **411**: 154
- Lake JA, Woodward FI, Quick WP (2002) Long-distance CO₂ signalling in plants. *J Exp Bot* **53**: 183–193
- Lan P, Li W, Schmidt W (2012) Complementary proteome and transcriptome profiling in phosphate-deficient Arabidopsis roots reveals multiple levels of gene regulation. *Mol Cell Proteomics* **11**: 1156–1166
- Langmead B, Salzberg SL (2012) Fast gapped-read alignment with Bowtie 2. *Nat Methods* **9**: p. 357–359
- Li B, Dewey CN (2011) RSEM: accurate transcript quantification from RNA-Seq data with or without a reference genome. *BMC Bioinformatics* **12**: DOI: 10.1186/1471-2105-12-323
- Li P, Ponnala L, Gandotra N, Wang L, Si Y, Tausta SL, Kebrom TH, Provart N, Patel R, Myers CR, et al (2010) The developmental dynamics of the maize leaf transcriptome. *Nat Genet* **42**: 1060–1067
- Lichtenthaler HK, Wellburn AR (1983) Determinations of total carotenoids and chlorophylls *a* and *b* of leaf extracts in different solvents. *Biochem Soc Trans* **11**: 591–592
- Liu T, Ohashi-Ito K, Bergmann DC (2009) Orthologs of Arabidopsis thaliana stomatal bHLH genes and regulation of stomatal development in grasses. *Development* **136**: 2265–2276
- Long SP, Zhu XG, Naidu SL, Ort DR (2006) Can improvement in photosynthesis increase crop yields? *Plant Cell Environ* **29**: 315–330
- Luo L, Zhou WQ, Liu P, Li CX, Hou SW (2012) The development of stomata and other epidermal cells on the rice leaves. *Biol Plant* **56**: 521–527
- Majeran W, Friso G, Ponnala L, Connolly B, Huang M, Reidel E, Zhang C, Asakura Y, Bhuiyan NH, Sun Q, et al (2010) Structural and metabolic transitions of C4 leaf development and differentiation defined by microscopy and quantitative proteomics in maize. *Plant Cell* **22**: 3509–3542
- Makino A, Miyake C, Yokota A (2002) Physiological functions of the water-water cycle (Mehler reaction) and the cyclic electron flow around PSI in rice leaves. *Plant Cell Physiol* **43**: 1017–1026
- Makino A, Sato T, Nakano H, Mae T (1997) Leaf photosynthesis, plant growth and nitrogen allocation in rice under different irradiances. *Planta* **203**: 390–398
- Maxwell K, Johnson GN (2000) Chlorophyll fluorescence: a practical guide. *J Exp Bot* **51**: 659–668
- Meng QW, Siebke K, Lippert P, Baur B, Mukherjee U, Weis E (2001) Sink-source transition in tobacco leaves visualized using chlorophyll fluorescence imaging. *New Phytol* **151**: 585–595
- Meurer J, Grevelding C, Westhoff P, Reiss B (1998) The PAC protein affects the maturation of specific chloroplast mRNAs in Arabidopsis thaliana. *Mol Gen Genet* **258**: 342–351
- Murchie EH, Horton P (1997) Acclimation of photosynthesis to irradiance and spectral quality in British plant species: chlorophyll content, photosynthetic capacity and habitat preference. *Plant Cell Environ* **20**: 438–448
- Murchie EH, Hubbart S, Chen Y, Peng S, Horton P (2002) Acclimation of rice photosynthesis to irradiance under field conditions. *Plant Physiol* **130**: 1999–2010
- Murchie EH, Hubbart S, Peng S, Horton P (2005) Acclimation of photosynthesis to high irradiance in rice: gene expression and interactions with leaf development. *J Exp Bot* **56**: 449–460
- Nakajima K, Sena G, Nawy T, Benfey PN (2001) Intercellular movement of the putative transcription factor SHR in root patterning. *Nature* **413**: 307–311
- Nelson T, Dengler N (1997) Leaf vascular pattern formation. *Plant Cell* **9**: 1121–1135
- Nelson T, Langdale JA (1989) Patterns of leaf development in C4 plants. *Plant Cell* **1**: 3–13
- Nishimura A, Ito M, Kamiya N, Sato Y, Matsuoka M (2002) OsPNH1 regulates leaf development and maintenance of the shoot apical meristem in rice. *Plant J* **30**: 189–201
- Oguchi R, Hikosaka K, Hirose T (2003) Does the photosynthetic light-acclimation need change in leaf anatomy? *Plant Cell Environ* **26**: 505–512
- Ohtsu K, Smith MB, Emrich SJ, Borsuk LA, Zhou R, Chen T, Zhang X, Timmermans MCP, Beck J, Buckner B, et al (2007) Global gene expression analysis of the shoot apical meristem of maize (*Zea mays* L.). *Plant J* **52**: 391–404
- Peterson RB, Oja V, Eichelmann H, Bichele I, Dall'Osto L, Laisk A (2014) Fluorescence F0 of photosystems II and I in developing C3 and C4 leaves, and implications on regulation of excitation balance. *Photosynth Res* **122**: 41–56
- Pick TR, Bräutigam A, Schlüter U, Denton AK, Colmsee C, Scholz U, Fahnenstich H, Pieruschka R, Rascher U, Sonnewald U, et al (2011) Systems analysis of a maize leaf developmental gradient redefines the current C4 model and provides candidates for regulation. *Plant Cell* **23**: 4208–4220
- Postma-Haarsma AD, Verwoert II, Stronk OP, Koster J, Lamers GEM, Hoge JHC, Meijer AH (1999) Characterization of the KNOX class homeobox genes Oskn2 and Oskn3 identified in a collection of cDNA libraries covering the early stages of rice embryogenesis. *Plant Mol Biol* **39**: 257–271
- Qi J, Qian Q, Bu Q, Li S, Chen Q, Sun J, Liang W, Zhou Y, Chu C, Li X, et al (2008) Mutation of the rice *Narrow leaf1* gene, which encodes a novel protein, affects vein patterning and polar auxin transport. *Plant Physiol* **147**: 1947–1959
- Rolfe SA, Scholes JD (2002) Extended depth-of-focus imaging of chlorophyll fluorescence from intact leaves. *Photosynth Res* **72**: 107–115
- Rolfe SA, Scholes JD (2010) Chlorophyll fluorescence imaging of plant-pathogen interactions. *Protoplasma* **247**: 163–175
- Rychel AL, Peterson KM, Torii KU (2010) Plant twitter: ligands under 140 amino acids enforcing stomatal patterning. *J Plant Res* **123**: 275–280
- Sabatini S, Beis D, Wolkenfelt H, Murfett J, Guilfoyle T, Malamy J, Benfey P, Leyser O, Bechtold N, Weisbeek P, et al (1999) An auxin-dependent distal organizer of pattern and polarity in the Arabidopsis root. *Cell* **99**: 463–472
- Sage TL, Sage RF (2009) The functional anatomy of rice leaves: implications for refixation of photorespiratory CO₂ and efforts to engineer C4 photosynthesis into rice. *Plant Cell Physiol* **50**: 756–772
- Sakaguchi J, Fukuda H (2008) Cell differentiation in the longitudinal veins and formation of commissural veins in rice (*Oryza sativa*) and maize (*Zea mays*). *J Plant Res* **121**: 593–602
- Scarpella E, Francis P, Berleth T (2004) Stage-specific markers define early steps of procambium development in Arabidopsis leaves and correlate termination of vein formation with mesophyll differentiation. *Development* **131**: 3445–3455
- Scarpella E, Meijer AH (2004) Pattern formation in the vascular system of monocot and dicot plant species. *New Phytol* **164**: 209–242
- Scarpella E, Rueb S, Meijer AH (2003) The RADICLELESS1 gene is required for vascular pattern formation in rice. *Development* **130**: 645–658
- Schmittgen TD, Livak KJ (2008) Analyzing real-time PCR data by the comparative C-T method. *Nat Protocols* **3**: 1101–1108
- Shi Z, Wang J, Wan X, Shen G, Wang X, Zhang J (2007) Over-expression of rice OsAGO7 gene induces upward curling of the leaf blade that enhanced erect-leaf habit. *Planta* **226**: 99–108
- Sims DA, Percy RW (1992) Response of leaf anatomy and photosynthetic capacity in *Alocasia macrorrhiza* (Araceae) to a transfer from low to high light. *Am J Bot* **79**: 449–455
- Sugimoto H, Kusumi K, Noguchi K, Yano M, Yoshimura A, Iba K (2007) The rice nuclear gene, VIRESCENT 2, is essential for chloroplast development and encodes a novel type of guanylate kinase targeted to plastids and mitochondria. *Plant J* **52**: 512–527
- Sun CW, Huang YC, Chang HY (2009) CIA2 coordinately up-regulates protein import and synthesis in leaf chloroplasts. *Plant Physiol* **150**: 879–888
- Takeuchi R, Kimura S, Saotome A, Sakaguchi K (2007) Biochemical properties of a plastidial DNA polymerase of rice. *Plant Mol Biol* **64**: 601–611
- Tausta SL, Li P, Si Y, Gandotra N, Liu P, Sun Q, Brutnell TP, Nelson T (2014) Developmental dynamics of Kranz cell transcriptional specificity in maize leaf reveals early onset of C4-related processes. *J Exp Bot* **65**: 3543–3555
- Terashima I, Hanba YT, Tazoe Y, Vyas P, Yano S (2006) Irradiance and phenotype: comparative eco-development of sun and shade leaves in relation to photosynthetic CO₂ diffusion. *J Exp Bot* **57**: 343–354
- Turgeon R (1989) The sink-source transition in leaves. *Annu Rev Plant Physiol Plant Mol Biol* **40**: 119–138
- Usadel B, Nagel A, Thimm O, Redestig H, Blaessing OE, Palacios-Rojas N, Selbig J, Hannemann J, Piques MC, Steinhauser D, et al (2005) Extension of the visualization tool MapMan to allow statistical analysis of arrays, display of corresponding genes, and comparison with known responses. *Plant Physiology* **138**: 1195–1204
- Vitha S, McAndrew RS, Osteryoung KW (2001) FtsZ ring formation at the chloroplast division site in plants. *J Cell Biol* **153**: 111–120

- Wallace S, Chater CC, Kamisugi Y, Cuming AC, Wellman CH, Beerling DJ, Fleming AJ (2015) Conservation of Male Sterility 2 function during spore and pollen wall development supports an evolutionarily early recruitment of a core component in the sporopollenin biosynthetic pathway. *New Phytologist* **205**: 390–401
- Wang JR, Hu H, Wang GH, Li J, Chen JY, Wu P (2009) Expression of PIN genes in rice (*Oryza sativa* L.): tissue specificity and regulation by hormones. *Mol Plant* **2**: 823–831
- Wang L, Czedik-Eysenberg A, Mertz RA, Si Y, Tohge T, Nunes-Nesi A, Arrivault S, Dedow LK, Bryant DW, Zhou W, et al (2014) Comparative analyses of C₄ and C₃ photosynthesis in developing leaves of maize and rice. *Nat Biotechnol* **32**: 1158–1165
- Wang P, Fouracre J, Kelly S, Karki S, Gowik U, Aubry S, Shaw MK, Westhoff P, Slamet-Loedin IH, Quick WP, et al (2013a) Evolution of GOLDEN2-LIKE gene function in C₃ and C₄ plants. *Planta* **237**: 481–495
- Wang P, Kelly S, Fouracre JP, Langdale JA (2013b) Genome-wide transcript analysis of early maize leaf development reveals gene cohorts associated with the differentiation of C4 Kranz anatomy. *Plant J* **75**: 656–670
- Wu S, Lee CM, Hayashi T, Price S, Divol F, Henry S, Pauluzzi G, Perin C, Gallagher KL (2014) A plausible mechanism, based upon Short-Root movement, for regulating the number of cortex cell layers in roots. *Proc Natl Acad Sci USA* **111**: 16184–16189
- Yamaguchi T, Nagasawa N, Kawasaki S, Matsuoka M, Nagato Y, Hirano HY (2004) The YABBY gene DROOPING LEAF regulates carpel specification and midrib development in *Oryza sativa*. *Plant Cell* **16**: 500–509
- Yoo SC, Cho SH, Sugimoto H, Li J, Kusumi K, Koh HJ, Iba K, Paek NC (2009) Rice *Virescent3* and *Stripe1* encoding the large and small subunits of ribonucleotide reductase are required for chloroplast biogenesis during early leaf development. *Plant Physiol* **150**: 388–401
- Young MD, Wakefield MJ, Smyth GK, Oshlack A (2010) Gene ontology analysis for RNA-seq: accounting for selection bias. *Genome Biol* **11**: R14
- Zhou K, Ren Y, Lv J, Wang Y, Liu F, Zhou F, Zhao S, Chen S, Peng C, Zhang X, et al (2013) Young Leaf Chlorosis 1, a chloroplast-localized gene required for chlorophyll and lutein accumulation during early leaf development in rice. *Planta* **237**: 279–292